LIGHT WATER REACTOR FUEL RESPONSE DURING REACTIVITY INITIATED ACCIDENT EXPERIMENTS

TOSHIO FUJISHIRO   ROGER L. JOHNSON
PHILIP E. MACDONALD   RICHARD K. McCARDELL

August 1978

EG&G Idaho, Inc.

IDAHO NATIONAL ENGINEERING LABORATORY

DEPARTMENT OF ENERGY

7809260200

ERRATA

NUREG/CR-0269, TREE-1237 DISTRIBUTION

Errata to NUREG/CR-0269, TREE-1237, "Light Water Reactor Fuel Response
During Reactivity Initiated Accident Experiments", August 1978, T. Fujishiro,
R. L. Johnson, P. E. MacDonald, and R. K. McCardell.
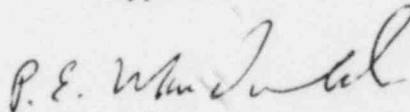
On page v, paragraph 2, last sentence, change "...with pressures to
1.2 MPa, ..." to " ... with pressures to 12 MPa, ...".

NUREG/CR-0269
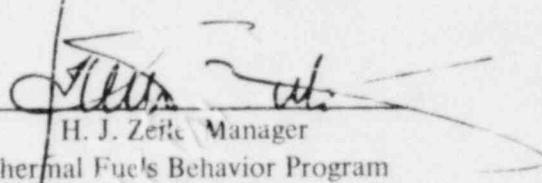
TREE 1237

LIGHT WATER REACTOR FUEL RESPONSE DURING

REACTIVITY INITIATED ACCIDENT EXPERIMENTS

Approved:

P. E. Whindald

P. E. MacDonald, Manager
LWR Fuel Research Division

H. J. Zeile

H. J. Zeile, Manager
Thermal Fuels Behavior Program

L. J. Ybarrondo

L. J. Ybarrondo, Director
Water Reactor Research

LIGHT WATER REACTOR FUEL RESPONSE DURING

REACTIVITY INITIATED ACCIDENT EXPERIMENTS

Toshio Fujishiro[a]
Roger L. Johnson[b]
Philip E. MacDonald
Richard K. McCardell

Date Published: August 1978

Idaho National Engineering Laboratory
Idaho Falls, Idaho 83401
Operated by
EG&G Idaho, Inc.
for the
U.S. Department of Energy
Idaho Operations Office

[a]   Japan Atomic Energy Research Institute.

[b]   STAFCO, Inc.

ACKNOWLEDGMENTS

ABSTRACT

This report presents a summary of existing test results, data correlations, and interpretations relevant to the current understanding of light water reactor fuel behavior under conditions of a reactivity initiated accident. Experimental data are included from test programs previously carried out in the Capsule Driver Core (SPERT Project) and TREAT facilities at the Idaho National Engineering Laboratory and currently ongoing in the Japanese Nuclear Safety Research Reactor. Test results are summarized and presented, primarily as derived from the literature, in terms of the thresholds, modes, and consequences of fuel rod failure. The effects of fuel rod design variations, environmental variations, elevated burnup, and fuel waterlogging are described. The data are correlated and analyzed to illustrate trends and salient features. Where possible, interpretations are made in terms of basic fuel properties and capsule environment.

SUMMARY

Most of the applicable experimental data on the behavior of light water reactor fuel rods during a simulated reactivity initiated accident (RIA) have been obtained from programs conducted in the Capsule Driver Core (SPERT Project) and TREAT facilities at the Idaho National Engineering Laboratory (INEL) and from the Nuclear Safety Research Reactor (NSRR) of the Japan Atomic Energy Research Institute. Similar ongoing test programs at the Power Burst Facility at the INEL, and at the NSRR are providing additional applicable data.

In each of these facilities, a driver core with encapsulated test fuel in a central flux trap was operated to produce a power excursion. The magnitude and time duration of these excursions were comparable to those of severe, hypothesized RIAs in light water reactors (LWRs). The experiments were performed with single fuel rods (or a small cluster of rods) composed of oxide fuel with metal cladding. The several designs tested were generally representative of those used in LWRs. The test capsules contained stagnant water at atmospheric pressure and room temperature.

Energy deposition, and consequent enthalpy increase, in the test fuel was the single most important independent variable. The threshold for failure of unirradiated fuel was generally about 240 to 265 cal/g UO_2, and was relatively insensitive to cladding material, cladding heat treatment, fuel form, fuel material, and gap width. Correlation of the cladding temperature and failure behavior data for several test rod designs indicates that the incipient failure threshold has a stronger dependence on the energy deposition near the fuel surface than on the radial average energy deposition. Reduction of the water/fuel ratio through the use of shroud enclosures caused a reduction in the failure threshold. Single, unirradiated NSRR fuel rods with small-diameter shrouds (water/fuel ratio of 0.71) failed at about 211 to 247 cal/g UO_2, compared with about 244 to 264 cal/g UO_2 for similar NSRR rods without shrouds. A similar reduction in the failure threshold was indicated from the results of scoping tests with five-rod clusters (both with and without shrouds). Prepressurization of NSRR fuel rods caused a reduction in the failure threshold for internal pressures $\geqslant 1.2$ MPa. Rods prepressurized to 2.9 MPa failed in the range of 150 to 160 cal/g UO_2.

Cladding melting during the power excursion or cracking of embrittled cladding during cooldown were the apparent causes of failure of unirradiated fuel rods for tests in which the fuel rods received a total energy deposition of 350 cal/g UO_2 or less. Shrouds were found to have little effect on the maximum cladding temperatures, but did cause a significant increase in the duration of film boiling on the cladding surface. Prepressurized fuel rods ($\geqslant 1.2$ MPa) failed by cladding rupture prior to the attainment of cladding melting.

Radial and axial deformation of both the fuel and cladding were found in fuel rods which did not fail during testing. Radial cladding deformation was apparently directly related to thermal expansion of the fuel, whereas axial elongation of the cladding was apparently caused by fuel stack growth following radial gas gap closure.

Unirradiated fuel rods subjected to energy depositions in excess of about 350 cal/g UO_2 failed by cladding rupture prior to the attainment of cladding melting, and significant fragmentation of the rods occurred. Internal pressure from UO_2 vaporization was shown to be the likely cause of these failures.

The consequences of unirradiated fuel rod failures were insignificant below about 300 cal/g UO_2. In the 300 to 500 cal/g range, fuel rods were broken up and fragmented, but pressures did not exceed a few MPa and nuclear-to-mechanical energy conversions did not exceed 1%. Metal-water reaction was first detectable at about 200 cal/g UO_2 and increased to about 50% at 500 cal/g UO_2. Tests at over 600 cal/g UO_2 had more severe consequences, with pressures to 1.2 MPa, energy conversions to nearly 3%, and metal-water reaction to nearly 100%.

In tests with preirradiated fuel rods, having burnups to 32 000 MWd/t, rod failures occurred at lower energy depositions in some cases than similar unirradiated fuel rods, with little sensitivity attributable to the degree of burnup. The lower failure threshold was not statistically established because only a few preirradiated rods were tested. The preirradiated rods apparently failed as a result of internal pressure or fuel-cladding interaction, or both, at energy depositions at which unirradiated rods failed from cladding melting or cracking of embrittled cladding. Pressure and mechanical energy generation were detected at lower energy depositions ($\geqslant 200$ cal/g UO_2) for preirradiated rods; however, the observed magnitudes were relatively insignificant.

Numerous tests were performed with waterlogged fuel rods. Waterlogging, or absorbing water within oxide fuel, could result during shutdown conditions in a fuel rod with damaged cladding. The failure threshold of waterlogged fuel was strongly dependent on cladding material and cladding heat treatment. Zircaloy clad waterlogged rods were found to fail by cladding rupture at energy depositions as low as 60 cal/g UO_2. Although failure often produced high transient pressures (in the tens of MPa) in the test capsule, the pressure pulses were very narrow and did not contain sufficient energy to damage adjacent rods. Large radial cladding expansion and small, or negative, axial cladding expansion occurred.

The experimental programs to date have provided significant information to aid in understanding fuel behavior under RIA conditions and in preparing preliminary models of such behavior. To further develop and verify these models, additional experimental data are required with preirradiated fuel under conditions more nearly typical of power reactor environments (high temperature, pressure, flow, and initial power). The reactor safety research programs of the Nuclear Regulatory Commission and the Japan Atomic Energy Research Institute are structured to provide such additional data.

CONTENTS

FIGURES

xi

TABLES

LIGHT WATER REACTOR FUEL RESPONSE DURING

REACTIVITY INITIATED ACCIDENT EXPERIMENTS

I. INTRODUCTION

Commercial nuclear power reactors are designed with multiple barriers to prevent the release of fission products. These barriers include the fuel rod cladding, the primary system pressure vessel and associated piping, and the containment. The rapid, inadvertent insertion of reactivity into a light water reactor (LWR) core has long been recognized as a potential mechanism for failure of the fuel rod cladding. Extensive cladding failure and dispersal of fuel could disrupt the core such that cooling capability would be significantly impaired and could damage and conceivably breach the coolant pressure boundary.

Understanding the performance of LWR fuel under normal and accident conditions is a major objective of the United States Nuclear Regulatory Commission's (NRC) Reactor Safety Research Program[1,2]. The extensive examination of the results of out-of-pile and in-pile experiments and associated analyses that are currently underway will result in a better understanding of the physical response of reactor fuels to various postulated accidents. These experiments will provide basic information for evaluating current modeling techniques to predict the consequences of a wide range of accidents during the normal useful life of a fuel rod.

To minimize the possibility of damage from potential reactivity initiated accidents (RIAs) in commercial LWRs, NRC design requirements have been imposed on reactivity control systems to limit "the potential amount and rate of reactivity increase to assure that the effects of postulated reactivity accidents can neither (a) result in damage to the reactor coolant pressure boundary greater than limited local yielding nor (b) sufficiently disturb the core, its support structure, or other reactor pressure vessel internals to impair significantly the capability to cool the core. These postulated reactivity accidents shall include consideration of rod ejection (unless prevented by positive means), rod dropout, steam line rupture, changes in reactor coolant temperature and pressure, and cold water addition"[3]. Worst-case RIAs in commercial LWRs are postulated to result from the rapid removal of control rod elements from the reactor core. In a pressurized water reactor (PWR), the RIA is a result of the hypothesized mechanical rupture of a control rod drive mechanism housing or control rod drive nozzle, which results in the coolant system pressure ejecting an inserted control rod from the core. In a boiling water reactor (BWR), the worst-case RIA (rod drop) results from (a) the separation (complete rupture, breakage, or disconnection) of an inserted control rod drive from its cruciform control blade at or near the coupling, (b) the sticking of the control blade in the inserted position as the rod drive is withdrawn, and (c) the rapid falling of the control blade to the withdrawn rod drive position.

Acceptable analytical methods and assumptions that may be used to evaluate the consequences of rod ejection accidents in PWRs to assure that the aforementioned NRC requirements have been met are identified in NRC Regulatory Guide 1.77[4]. Similar methods and assumptions are used in the evaluation of BWR rod drop accidents. By using the recommended methods and assumptions of Reference 4, or by acceptable alternate methods, the applicant (or licensee) is expected to show that:

"(1) Reactivity excursions will not result in a radial average fuel enthalpy greater than 280 cal/g at any axial location in any fuel rod.

(2) Maximum reactor pressure during any portion of the assumed transient will be less than the value that will cause stresses to exceed the Emergency Condition stress limits as defined in Section III of the ASME Code.

(3) Offsite dose consequences will be well within the guidelines of 10 CFR 100."

The recommended fuel enthalpy limitation (< 280 cal/g) is based on a Regulatory staff review of fuel behavior experimental data available prior to 1974. Their findings indicated that the failure consequences were insignificant below 300 cal/g for both irradiated and unirradiated UO_2 fuel rods subjected to rapid power excursions. Therefore, 280 cal/g was considered a conservative maximum limit to ensure minimal core damage and maintenance of both short-term and long-term core cooling capability. The assumption applied is that the recommended guidelines regarding reactor coolant pressure boundary stresses and offsite dose consequences would also likely be met if compliance with the enthalpy limitation is satisfactorily demonstrated.

Complex analysis techniques are used to estimate the effects of postulated RIAs in LWRs. These techniques generally couple the transient neutronics behavior, fuel rod thermal and mechanical response, and the coolant hydrodynamic response. Typical examples of such analysis methods are provided in References 5, 6, and 7. Verification of these analytical models is incomplete, however, due to limitations of existing fuel behavior data. Much of the applicable RIA experimental data were obtained several years ago in the SPERT (Capsule Driver Core) and TREAT test programs, which investigated the behavior of single or small clusters of fuel rods under ambient conditions, no forced coolant flow, and zero initial power. Cooperative test programs currently underway in the Japanese Nuclear Safety Research Reactor (NSRR)[8] and plans for the Power Burst Facility (PBF) at the Idaho National Engineering Laboratory are expected to provide RIA fuel behavior data under conditions more nearly typical of power reactor operation, thus allowing further verification and development of analytical models.

The experiments to determine the behavior of LWR fuels under RIA conditions in the Capsule Drive Core (CDC) facility at SPERT and in the TREAT facility were primarily carried out between 1965 and 1970. Following termination of testing activities in the CDC

in 1970, funding limitations precluded the preparation and publication of report(s) summarizing and evaluating the test results. Thus, much of the CDC data were reported only piecemeal in progress and interim reports and were not made generally available to the technical community in a comprehensive form convenient for safety analysis and model verification purposes. Likewise, comparisons of CDC and TREAT results, where applicable, were not generally documented. With the recent resumption of RIA fuel behavior testing in the NSRR and plans for such testing in the PBF, it has been deemed desirable to remedy this deficiency. Therefore, a first objective of this report is to present an organized summary of test results from the CDC, TREAT, and NSRR facilities relevant to fuel behavior under RIA conditions.

The CDC, TREAT, and NSRR test results are presented in Section II, basically as derived from the literature. Results of experiments with fuel rods having similar design features and properties are grouped and discussed in Section II-1. These test results form a baseline data set, which is defined to include results from tests conducted in capsules with stagnant water at ambient temperature and atmospheric pressure with single, unirradiated, pelletized UO_2, cold-worked zircaloy clad fuel rods with radial dimensions typical of or scaled to approximate commerical reactor fuel. Data from these tests are used to establish the behavior of typical LWR fuels under RIA conditions primarily in terms of the thresholds, modes, and consequences of fuel failure. In Sections II-2 through II-5, the results of tests performed to evaluate the effects of fuel rod design variations, local environmental variations, fuel burnup, and fuel waterlogging are discussed. For each design or parametric variation, test results are compared with the behavior of the baseline test fuels. Differences and similarities in observed behavior are noted and discussed to illustrate the influence of specific design or parametric variations on the response of the test fuel under RIA conditions.

A second, albeit important, objective of this report is to present selected correlations and interpretations of the RIA test data that have been developed to date. In Section III, the test measurements are systematically correlated to establish trends and illustrate salient features of the data. Wherever possible, interpretations are made in terms of basic properties and characteristics of the test fuel and environment. Maximum cladding temperatures, cladding deformation, and fuel deformation are discussed relative to fuel rod characteristics and the test environment in Sections III-1 and III-2. The mode of failure near the failure threshold and the high energy failure modes and mechanisms associated with unirradiated UO_2 fuel rods are discussed in Sections III-3 and III-4, respectively.

Section IV itemizes those conclusions that have been formulated regarding the current understanding of fuel behavior under RIA conditions. Limitations of existing data and important unresolved issues are included. The appendices provide pertinent supporting information. Appendix A describes the test facilities, environments, fuels, instrumentation, and measurments. Appendices B and C organize and summarize test data from the NSRR and from the CDC.

II. TEST RESULTS

Significant results from the SPERT, TREAT, and NSRR test programs are presented in this section. The test programs previously completed by the SPERT and TREAT projects have provided much of the applicable experimental fuel behavior data under RIA conditions. These programs were primarily designed to provide data on the thresholds, modes, and consequences of failure of LWR fuels subjected to rapid power excursions. Such data have been used by reactor vendors and the Nuclear Regulatory Commission in the performance and evaluation of LWR safety analyses. These test facilities have the capability to subject single test fuel rods to energy deposition rates and magnitudes equivalent to and beyond those postulated for RIAs in commercial reactors. Several fuel design and parametric variations were investigated over a wide range of energy depositions. Test facility limitations, however, prevented the conduct of experiments with initial coolant and power level conditions representative of commercial reactor operation. The facilities were also incapable of tests with fuel rod clusters large enough to provide information on potential fuel failure propagation and interaction effects. A similar test program is presently being conducted at the Japan Atomic Energy Research Institute in the NSRR, which has testing capabilities approximating those of the CDC and TREAT facilities. The NSRR experimental program is developing a more comprehensive understanding of the results previously obtained by the SPERT and TREAT programs, using similarly designed LWR test fuel. RIA testing in the NSRR is being coordinated with planned RIA tests in the Power Burst Facility, which can accommodate larger test fuel arrays under conditions more nearly representative of power reactor operation.

The CDC, TREAT, and NSRR test facilities are characterized by a driver core normally operated in a transient mode with a centrally located flux trap. Encapsulated fuel rods positioned in the central flux trap space were subjected to power excursions simulating the magnitude and time duration of severe RIAs in LWRs. Minimum reactor period capabilities of the driver cores were approximately 35, 3, and 2 ms for TREAT, the CDC at SPERT, and the NSRR, respectively. Capsule environments were comprised of stagnant water at atmospheric pressure and room temperature. Test specimens were single or small clusters of metal clad, oxide fuel rods of several designs, generally representative of those used in LWRs. The facilities, capsule environments and hardware, and test fuels are described further in Appendix A.

Pretest, dynamic, and posttest measurements, also described in Appendix A, were made to obtain information on experimental variables of interest. The pretest characteristics of test fuel rods were determined from measurements made during and following fabrication and included determination of physical properties, weights, dimensions, and radiographic inspection. Dynamic measurements made directly during tests typically included cladding and coolant temperatures, fuel rod internal and capsule pressures, fuel and cladding deformations, capsule water column velocity, and, in TREAT, high speed motion pictures of the test fuel during excursions. Energy deposition in the test fuel, the independent variable of principal interest in RIA tests, was usually derived indirectly from calibrations based on

4

radiochemical fission product analyses. The energy deposition for a particular experimental configuration was dependent on the characteristics of the test fuel and was generally controlled by variations of the initial period of the driver core power excursion. Metal-water reaction extent and nuclear-to-mechanical energy conversion were also determined indirectly for some tests. Metal-water reaction extents were determined on the basis of posttest hydrogen evolution measurements, whereas nuclear-to-mechanical energy conversion determinations were based on measurements of capsule water column velocity. Posttest examination of the test fuel generally included visual inspection, photography, and measurement of dimensions. Detailed metallurgical examinations were only performed in isolated cases.

The dynamic effects of interest in RIA experiments usually occur within tens of milliseconds to a few seconds following test initiation. Examples of the behavior of several variables during a typical RIA experiment are shown in Figure 1. These variables are representative of the behavior of a test rod subjected to a nondestructive energy deposition.

In addition to those tests performed to obtain RIA data on LWR fuels, numerous transient tests for other purposes were conducted in the CDC and TREAT. In the CDC, for example, experiments were performed to measure the UO_2-water reaction, to evaluate the effects of fissile particle size in mixed oxide rods, and to proof test CDC and Power Burst Facility (PBF) driver core fuel. In TREAT, a major part of the test program has been devoted to liquid metal fast breeder reactor fuels and metal-water reaction tests. The results of these experiments in the CDC and TREAT are documented in the literature and are not included in this report.

The test results discussed in the following sections are categorized to first establish a baseline data set and then delineate the effects of fuel design variations, environmental variations, burnup, and waterlogging on the thresholds, modes, and consequences of fuel failure. Only highlights and conclusions are presented, basically as derived from the references listed in Section V and Appendix B. Data specific to individual CDC and NSRR tests are organized and summarized in Appendices B and C.
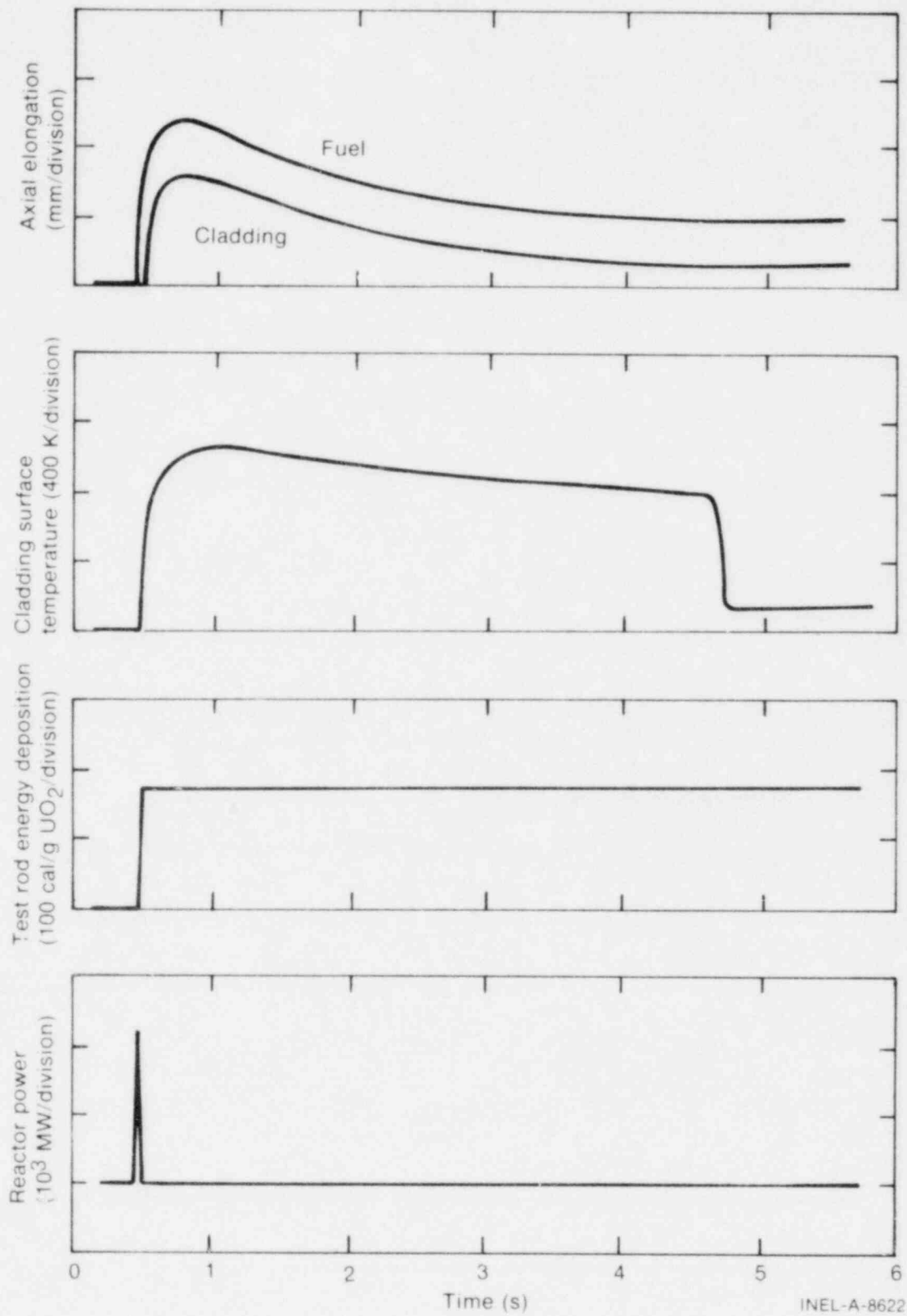
Fig. 1 Typical behavior of a test rod during a nondestructive RIA experiment.

6

1. BASELINE TEST RESULTS

Numerous experiments have been conducted with single, unirradiated test fuel rods having similar design features and properties. The results of these tests form a baseline data set with which the results of the tests with fuel rod design variations, environmental variations, elevated burnup, and waterlogged fuel are subsequently compared and evaluated. The baseline tests are defined to include those tests conducted in capsules with stagnant water at ambient temperature and atmospheric pressure with single, unirradiated, unpressurized[a] pelletized UO_2, cold-worked zircaloy clad fuel rods with radial dimensions typical of or scaled to approximate commercial reactor fuel. Test rods of this type include the SPX, SPXM, GEX, and GEP rods used in the CDC experiments, the NSRR-STD and JPDR-II rods used in NSRR experiments, and certain of the UO_2 pellet rods used in the TREAT experiments. As may be noted from the fuel rod characteristics listed in Table I, which contains information on all the test rods discussed in this report, some of the aforementioned test rod designations are generally used to describe rods with several design variations. However, only those rods meeting the specified baseline test fuel criteria are considered in this section.

1.1 Failure Thresholds

The initial failure threshold (defined as loss of cladding integrity) was determined by conducting tests with energy depositions both below and above the failure threshold, such that the failure threshold for a particular rod type was generally established in terms of an energy deposition range. The lower bound of the range was the highest energy deposition that did not result in failure, and the upper bound of the range was the lowest energy deposition that resulted in failure. Failure thresholds for several baseline fuel types are given in Table II.

Fuel types shown in Table II are those for which an adequate number of tests were conducted near the failure threshold to permit reasonable estimation of the energy depositon required for failure. The enrichment of the JPDR-II fuel rods, 2.6%, was too low to allow attainment of energy depositions sufficient to cause failure, and the SPX rods tested near the failure threshold were clad with annealed, rather than cold-worked zircaloy.

The information sources for the failure thresholds cited are indicated in Table II. Only single threshold values are shown for the GEP and TREAT rods because:

(1) The failure threshold for GEP pellet rods was reported in Reference 9 to be between 201 and 243 cal/g UO_2. Subsequent investigations and tests showed that a failure observed at 205 cal/g UO_2 was probably strongly influenced by carbon impurities ($\sim$51 ppm) in the fuel pellets. Test rods with reduced

---

[a] A test rod with an internal pressure of one atmosphere or less.

7

TABLE I

NOMINAL CHARACTERISTICS OF TEST FUEL RODS[a]

Fuel Rod Type	F-type	SPX	SPXM	GEX	GEP	GEXPR	GEXPR-CH	TREAT	NSRR-STD	NSRR-WG	JPDR-II
Overall length (cm)	106	53	19.5	22.6/71	22.1/71	21.1	21.1	21.1	26.5	26.5	26.5
Active length (cm)	91	46	12.7	13.2/61	13.2/61	12.7	13.0	14.0	13.5	13.5	13.5
Cladding material	304-SS	304-SS/Zr-2	304-SS/Zr-2	Zr-2	Zr-2	Zr-2	Zr-2	Zr-2	Zr-4	Zr-4	Zr-4
Cladding heat treatment	AN	AN/CW	AN/CW	10% CW	10% CW	10% CW	10% CW	--	CW	CW	CW
Cladding outside diameter (cm)	1.184	0.635	0.635	0.794	1.43	0.794	0.794	1.422	1.072	1.072	1.223
Cladding thickness (mm)	0.508	0.356	0.356	0.508	0.813	0.508	0.508	0.71	0.62	0.62	0.70
Fuel material	UO_2	UO_2	UO_2	UO_2	UO_2	PuO_2-UO_2	PuO_2-UO_2	UO_2	UO_2	UO_2	UO_2
Fuel form	PL	PL	PL	PL/PW	PL/PW	PL	PL[b]	PL/PW	PL	PL	PL
Fuel density (% TD)	92	95	95	94/84	94/84	91	92	95/82	95	95	95
Enrichment (%)	4.8	3/5/10.5	5/10.5	5/7	5/7	7(wt% Pu)	7(wt% Pu)	5	5/10/20	10	2.6
Pellet diameter (cm)	1.067	0.559	0.559	0.681	1.23	0.683	0.688	1.260	0.929	0.909	1.066
Pellet length (cm)	1.52	1.14	1.14	1.20	2.20	0.711	0.615	--	1.0	1.0	1.5
Pellet end shape	FL	FL	FL	FL/D	FL/D	FL	FL	FL	CH	CH	FL
Radial gas gap (mm)[c]	0.076	0.025	0.025	0.038	0.102	0.051	0.051	0.102	0.095	0.195	0.085
Peak-to-average radial power density[d]	1.136	1.05/1.07/1.17	1.07/1.17	-/1.13(PL) -/1.12(PW)	1.19/1.27(PL) -/1.24(PW)	1.20	1.20	--	1.16/1.23/ 1.63	1.23	1.08

[a] Abbreviations used in this table are are follows:

AN - annealed	D - dished	PW - powder
CH - chamfered	FL - flat	SS - stainless steel
CW - cold-worked	PL - pellet	Zr - zircaloy

[b] GEXPR-CH rods had a 2.92-mm hole axially through the center of the fuel pellets.

[c] Gas gap and plenum fill gas was helium at one atmosphere for all test rods.

[d] Multiple values correspond to enrichment or fuel form variations, or both.

8

TABLE II

INITIAL FAILURE THRESHOLDS
(Single, Cold-Worked Zircaloy Clad, Pellet Fueled Rods)

Fuel Rod Type	Active Length (cm)	Cladding Outside Diameter (cm)	UO_2 Enrichment (%)	Failure Threshold (cal/g UO_2)[a]
GEX	13.2	0.794	7	223 to 256[9]
GEP	13.2	1.430	7	~240[9]
SPXM	12.7	0.635	10.5	240 to 257[9]
NSRR-STD	13.5	1.072	10	214 to 264[8,10,11]
TREAT	14.0	1.422	5	~270[12]

[a] Failure threshold energy depositions are radial averages at the axial flux peak.

carbon impurities (<1 ppm) withstood energy depositions of 238 and 240 cal/g UO_2 without failure. The effects of carbon impurities are further discussed in Section II-2.4.2.

(2) Three TREAT rods tested near the failure threshold showed failure at both 266 and 274 cal/g UO_2, but did not fail at 269 cal/g UO_2. On the basis of these results, Freshley and Harrison[12] estimated the failure threshold to be ~270 cal/g UO_2.

The slightly higher failure threshold observed for the TREAT rods may have been due, in part, to greater heat losses prior to completion of the energy deposition than was the case for the other rod types. The particular TREAT tests from which these results were obtained had reactor periods of 60 to 70 ms, whereas the CDC tests (GEX, GEP, SPXM rods) had reactor periods of 3 to 8 ms, and the NSRR tests (NSRR-STD rods,) had reactor periods about 2 ms. Energy depositions were completed in about 500 ms for the TREAT tests, whereas only 10 to 50 ms were required for the energy depositions to be completed in the CDC and NSRR tests. The effects of these differences in energy deposition rates have not been quantitatively evaluated. In any case, the slightly higher failure thresholds observed for the TREAT rods are statistically insignificant because of the uncertainty (on the order of ±12%) of the energy deposition values for the various fuel rod types.

1.2 Failure Modes

Energy depositions in the range of 120 to 150 cal/g UO_2 resulted in departure from nucleate boiling (DNB) for the baseline tests rods. The occurrence of DNB caused cladding surface oxidation, the extent of which increased with increasing energy depositions. For energy depositions near or slightly in excess of the initial failure threshold, cladding melting and extensive cladding oxidation were evident from posttest inspections of the test rods. Several of the test rods were subjected to detailed postirradiation metallurgical examinations, which indicated the following with respect to the cladding:

(1) GEP pellet rods[9]: Metallographic and electron microprobe examinations were performed on two GEP pellet rods tested at 201 and 243 cal/g UO_2. Cladding failure did not occur for the test at 201 cal/g UO_2. Photomicrographs of the cladding from a transverse cross section at the center of the active fuel length showed the formation of zirconium oxide on both the outer and inner surfaces of the cladding. The oxidation layers were thin, on the order of 5 μm on the outer surface and less on the inner surface, with negligible oxygen diffusion into the cladding.

The test at 243 cal/g UO_2 resulted in cladding melting near the top of the active fuel length and significant cladding swelling over the active length. Cladding photomicrographs in the vicinity of the cladding breach and near the axial center of the rod showed both internal and external oxidation. In the breached region, both surfaces had layers of zirconium oxide about 50 μm thick on the outside and about 25 μm on the inside. Underneath these oxide layers were layers of oxygen-stabilized alpha-phase zirconium of similar thicknesses. Adjacent to each oxygen-rich layer was a region of acicular structure believed to be the precipitation of alpha platelets from oxygen-enriched beta-zirconium. Oxygen was diffused into this region from the oxide. The cladding sample from the nonbreached section of the rod showed less oxidation and no evidence of the acicular structure.

(2) TREAT pellet rod[12]: The cladding of a TREAT pellet rod tested at 274 cal/g UO_2 was metallurgically examined. Cladding failure occurred near the axial center of this rod from melting and deterioration due to reaction with water vapor. The cladding in a region of the rod that did not melt, but which reached a temperature in excess of 1270 K, exhibited zirconium oxide layers on the outside and inside of 40 and 10 μm in thickness, respectively. Under the zirconium oxide were layers of oxygen-stabilized alpha-phase zirconium.

In the region of cladding melting, the zirconium oxide layer on the external surface was over 100 μm thick and contained an intermediate ZrO_{2-x} region. An oxygen-stabilized alpha-zirconium layer of comparable thickness, about 100 μm, formed beneath the zirconium oxide layer. Intimate fuel-cladding contact and reaction occurred on the inner surface in the region of cladding melting, and the inner surface zirconium oxide layer was consumed by the high temperature cladding. The region of fuel where the fuel-cladding reaction occurred was probably oxygen deficient. A reaction layer having the appearance of oxygen-stabilized alpha-zirconium, but which may have been uranium-zirconium solid solution, formed at the fuel-cladding interface in the reaction zone. In the once-molten cladding region, significant cladding thickness variations occurred. There were regions where the zirconium metal phase was completely consumed and only a zirconium oxide layer remained on the UO_2 fuel.

These metallurgical analyses indicate increasing oxygenation, and consequent embrittlement of the zircaloy cladding with increasing energy depositions. Significant nonuniformities in the extent of oxidation were noted where partial or complete cladding melting occurred.

Figures 2, 3, and 4 show typical posttest photographs of GEX, SPXM, and NSRR-STD fuel rods, respectively. For tests with energy depositions slightly above the initial failure threshold, failure appeared to have resulted from melting or cracking of embrittled cladding, or both (for example, the GEX rod at 257 cal/g UO_2 in Figure 2, the SPXM rod at 287 cal/g UO_2 in Figure 3, and the NSRR-STD rod at 270 cal/g UO_2 in Figure 4). Cladding cracks were generally evident in the failed rods; however, the time of occurrence of these cracks relative to cladding melting, which also occurred in most cases, could not be determined. Because cracking of the type observed required extensive cladding embrittlement, most of the cracks probably occurred after several seconds of film boiling on the cladding surface, perhaps during the quenching or cooling cycle (quenching is illustrated at about 5 s in the cladding temperature trace of Figure 1). The cracks observed in once-molten cladding also appeared to have occurred during cooldown, because they tended to be rugged and sharp-edged. In the TREAT tests[12], the zirconium oxide layer tended to contain the molten cladding, since no evidence was present of zirconium running down or dripping away from the test rods. Further, considerable plasticity was reported to have occurred in the zirconium oxide layers at temperatures above 770 K, but the films were brittle at room temperature. Posttest disassembly and handling operations represented another potential sources of cladding cracking. Rods tested in the vicinity of and beyond the failure threshold tended to be fragile; thus, handling fractures occasionally occurred, some of which may not have been identified as such.

Energy
deposition
(cal/g UO₂)

342

257

69-3513

Fig. 2 Posttest photographs of GEX pellet rods tested in the CDC.

12
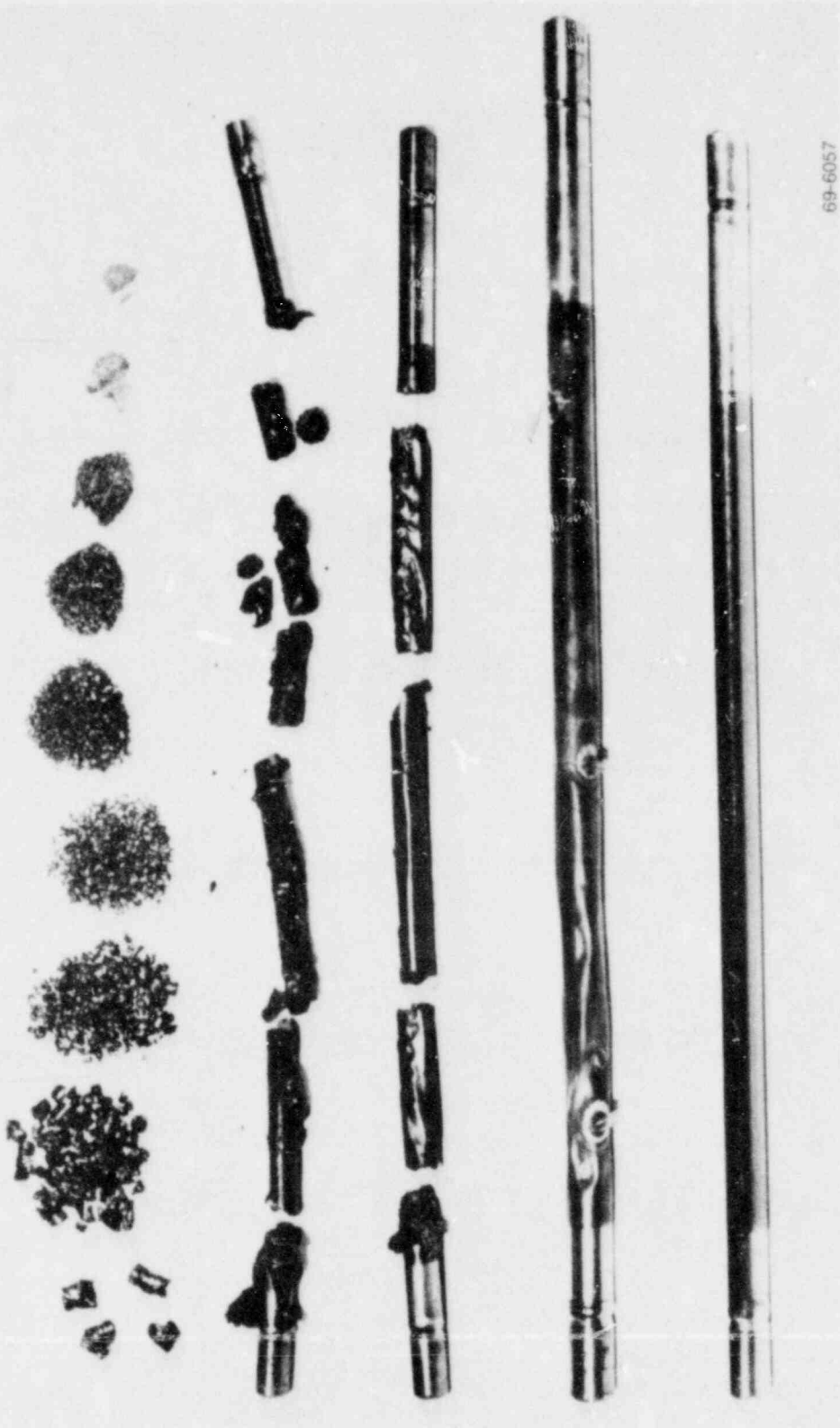
Fig. 3 Posttest photographs of SPXM rods tested in the CDC.

69-6057

Energy deposition
(cal/g UO₂)

378

338

287

240

168

13
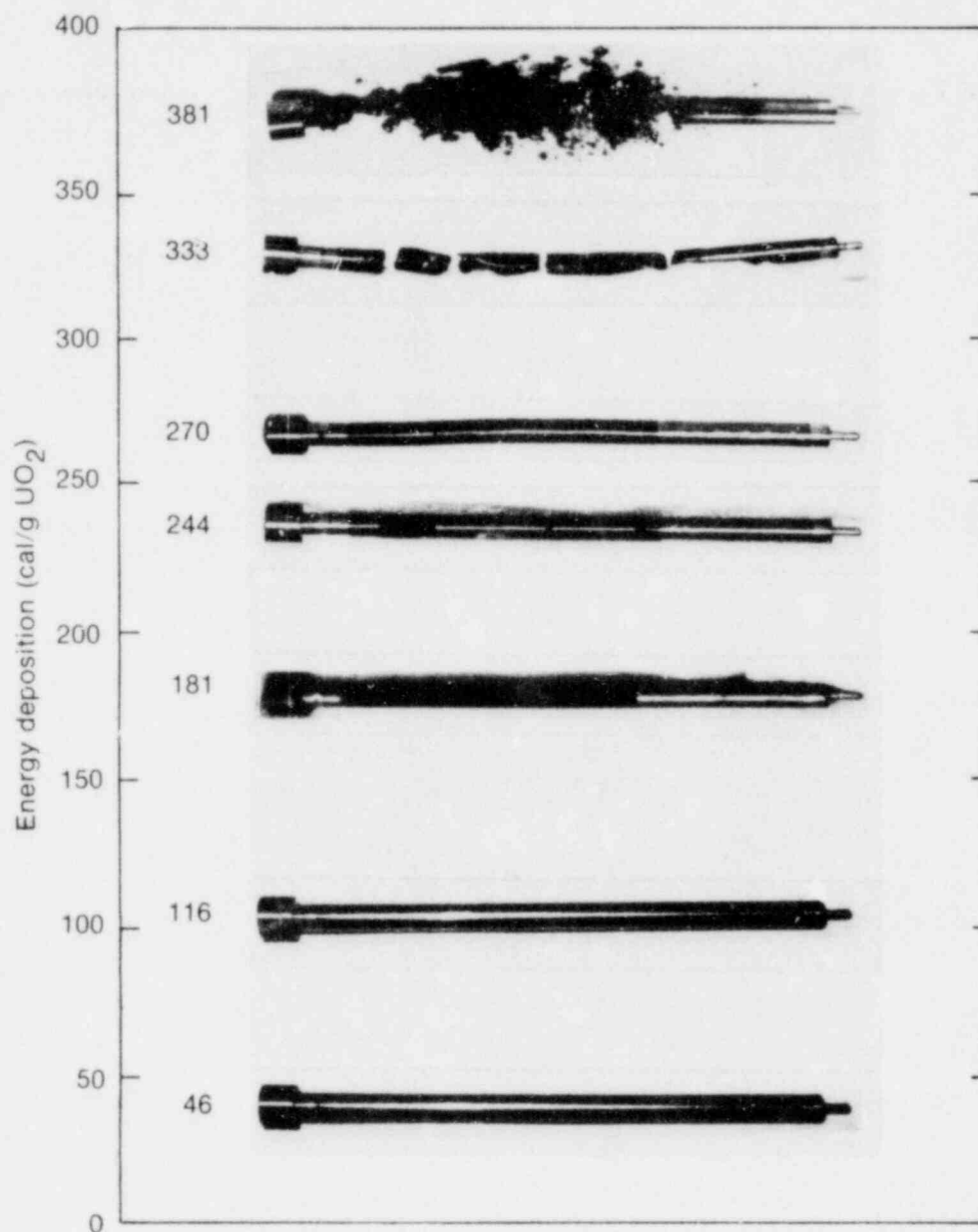
Fig. 4 Posttest photographs of NSRR-STD rods tested in the NSRR.

GEX[9], SPX[13], SPXM[9], and NSRR-STD[11] rods were tested to energy depositions in excess of 400 cal/g UO_2. For energy depositions from the initial failure threshold to about 350 cal/g UO_2, the extent of cladding melting and oxidation increased with increasing energy deposition and caused the fuel rods to break up into progressively smaller pieces. Energy depositions in excess of about 350 cal/g UO_2 caused fragmentation of the rods into fine particles. Examples of fragmented rods are shown in Figure 3 (test at 378 cal/g UO_2) and in Figure 4 (test at 381 cal/g UO_2).

For energy depositions greater than about 350 cal/g UO_2, cladding surface temperatures at the time of failure were below the cladding melting temperature and generally declined with increasing energy depositions. Thus, failure by internal rod pressure was indicated, with consequent increased rod fragmentation. Analysis of the particle size distributions from fragmented GEX, SPXM, and SPX rods[14] showed that the mean particle diameter decreased with increasing energy deposition, but asymptotically approached a lower limit of about 5 mils for energy depositions exceeding about 500 cal/g UO_2.

1.3 Failure Consequences

The consequences of single-rod failures were evaluated primarily on the basis of pressure generated within the capsule coolant, nuclear-to-mechanical energy conversion, and the extent of cladding-water reaction, all as a function of test fuel energy deposition. (The methods used to determine nuclear-to-mechanical energy conversion and cladding-water reaction are discussed in Appendix A.) For the baseline fuel types, the specific consequences were as detailed in the following subsections.

1.3.1 Pressure. Pressures generated following rod failure were not generally detectable for energy depositions less than 300 cal/g UO_2. In the 300 to 500 cal/g UO_2 range, maximum measured pressures generally increased with increasing energy depositions, but were no more than a few MPa. Severe fragmentation of two SPXM rods, each tested at about 650 cal/g UO_2, resulted in maximum measured pressures of 11 and 12 MPa[9]. It should be noted that in both the CDC and NSRR tests, capsule pressure measurements were made by a transducer located at the bottom of the capsules, which caused doubling of the indicated pressure magnitudes. The doubling effect was clearly illustrated in a waterlogged fuel rod test in the NSRR[10] (Test 401-4C) in which the measured peak pressure at the capsule bottom was about 6 MPa, whereas several other pressure transducers located within the capsule in the vicinity of the test rod showed peak pressures of about 3 MPa.

1.3.2 Nuclear-to-Mechanical Energy Conversion. Nuclear-to-mechanical energy conversions, determined from measured capsule water column velocities, were not detected for energy depositions less than about 300 cal/g UO_2. In the 300 to 500 cal/g range, conversion ratios were always less than 1%. Energy depositions over 600 cal/g UO_2 for SPXM test rods produced conversion ratios near 2%[9], apparently as a result of severe fragmentation. Figure 5 shows energy conversion plotted as a function of total test fuel energy deposition for SPXM rods tested in the CDC[a].

---

[a] The solid line curve shown in the figure is an approximation to the data points drawn by the authors to illustrate the trend of the data. Such curves are used frequently in this report, particularly where several sets of data are shown in the same figure. Unless otherwise noted, these curves represent neither mathematical fits to the data nor analytical calculations of behavior.
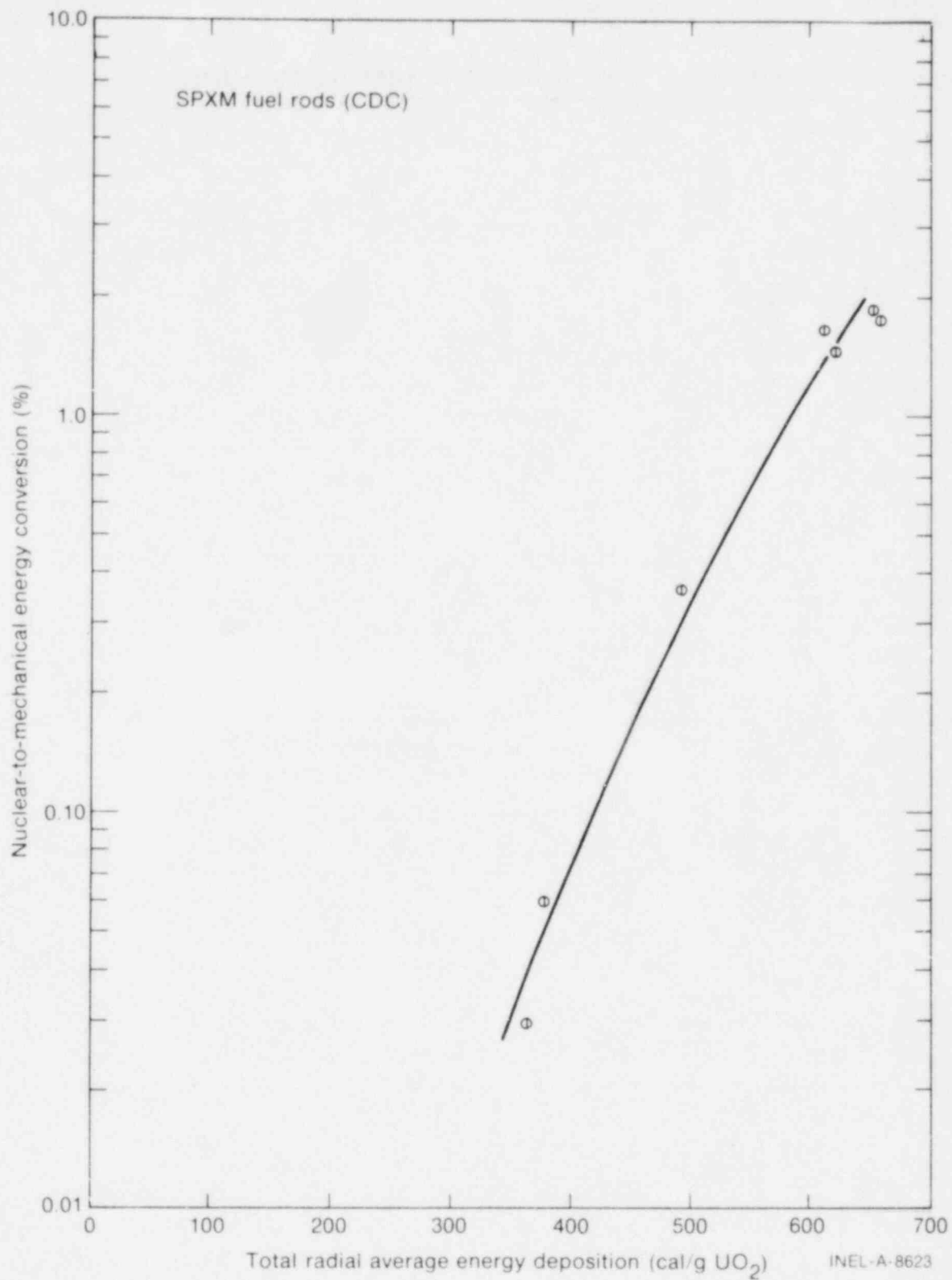
Fig. 5 Nuclear-to-mechanical energy conversion as a function of total energy deposition for SPXM fuel rods tested in the CDC.

1.3.3 Metal-Water Reaction. Metal (cladding)-water reactions were determined from posttest hydrogen evolution measurements (Appendix A). Figure 6 shows reaction extents as a function of total energy deposition for SPXM and GEX rods[9]. As shown, reactions were first detected for energy depositions exceeding about 160 cal/g UO_2, which approximately corresponded to the energy deposition for which film boiling became prominent. Similar reaction extents were measured for both SPXM and GEX rods up to about 350 cal/g UO_2. Above 350 cal/g, significantly higher reaction extents were measured for the SPXM rods, reaching indicated values of approximately 100% for energy depositions exceeding 600 cal/g UO_2. As shown in Figure 6, data from the GEX rod tests that resulted in fuel spillage into the coolant were corrected for hydrogen evolution from radiolysis and UO_2-water reaction. This correction significantly lowered the reaction extents for the higher energy tests. The high energy deposition SPXM data would be similarly lowered by correction for radiolysis and UO_2-water reaction; however, the SPXM rods would likely still show higher reaction extents than the GEX rods.

These results have led to the conclusion that unirradiated single rods produce insignificant failure consequences for energy depositions below about 300 cal/g UO_2. Capsule pressures and nuclear-to-mechanical energy conversion ratios become noticeable in the 300 to 500 cal/g UO_2 range, with increased severity observed beyond 500 cal/g UO_2.
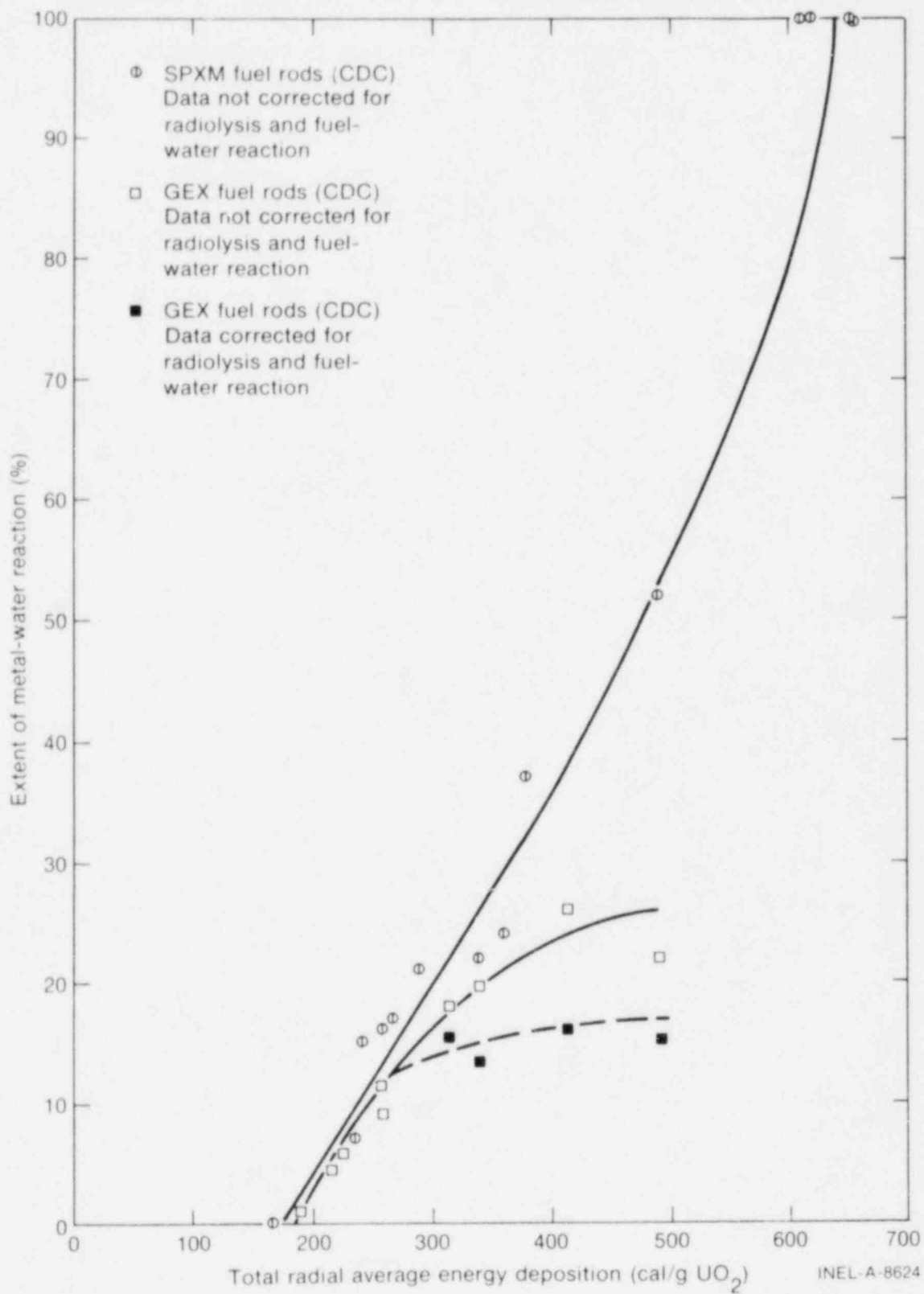
Fig. 6 Extent of metal-water reaction as a function of total energy deposition for SPXM and GEX fuel rods tested in the CDC.

2. EFFECTS OF TEST FUEL DESIGN VARIATIONS

Tests in the CDC and NSRR have been conducted to evaluate the effects of several fuel rod design variations. The effects of these design variations have been determined by comparison with the behavior of the baseline fuels. Significant differences and similarities in behavior attributable to specific design variations are summarized in this section.

2.1 Cladding Material

SPX and F-type fuel rods clad with Type-304 annealed stainless steel were tested in the CDC. Maximum measured cladding temperatures as a function of energy deposition were lower for stainless steel than for zircaloy clad rods, apparently because of the higher heat capacity of stainless steel. However, because of the lower melting temperature of stainless steel, cladding melting occurred at approximately the same energy deposition as for the zircaloy clad rods. Principal test results were as follows.

2.1.1 SPX Fuel Rods[15]. The initial failure threshold for stainless steel clad SPX rods was determined to be in the range of 244 to 276 cal/g UO_2, which is similar to that determined for the baseline fuel types. Initial cladding failure was apparently by cladding melting, and subsequent cladding failure was by cracking, probably occurring during the quenching or cooldown cycle. Cladding melting and cracking are clearly illustrated in Figure 7, which shows a posttest photograph of the central region of a SPX rod tested at 276 cal/g UO_2. Figure 8 shows a posttest photograph of the upper portion of this same rod, which clearly shows the boundary between melted and unmelted cladding, pellet slumping, and the preferential melting associated with the direction of pellet slumping. Higher energy deposition tests to 572 cal/g UO_2 had results similar to those observed for the zircaloy clad baseline fuels.

2.1.2 F-Type Fuel Rods[16]. The initial failure threshold for stainless steel clad F-type rods was in the range of 263 to 278 cal/g UO_2. Failure was observed in the form of a longitudinal cladding crack $\sim$ 1.3 cm long for the test at 278 cal/g UO_2, with some small patches of melted cladding, as shown in Figure 9. Cladding melting was somewhat less extensive than for the SPX stainless steel rod tested at approximately the same energy deposition. F-type rods were tested to only about 300 cal/g UO_2, for which significant cladding damage in the form of melting and circumferential cracking was observed, but fuel rod breakup did not occur. Circumferential ridging (bambooing) of the cladding at the pellet interfaces was also observed for F-type fuel rods, with the effect most pronounced at energy depositions slightly over 200 cal/g UO_2. Bambooing of the cladding was also observed for a similar type fuel following integral core tests in SPERT III[17].

2.2 Cladding Heat Treatment

Tests with annealed and cold-worked zircaloy clad SPX fuel rods were conducted in the CDC[13,18]. The initial failure threshold of the annealed clad rods was about 240 cal/g UO_2; cold-worked clad rods were only tested at energy depositions beyond the initial failure

Cladding
separation
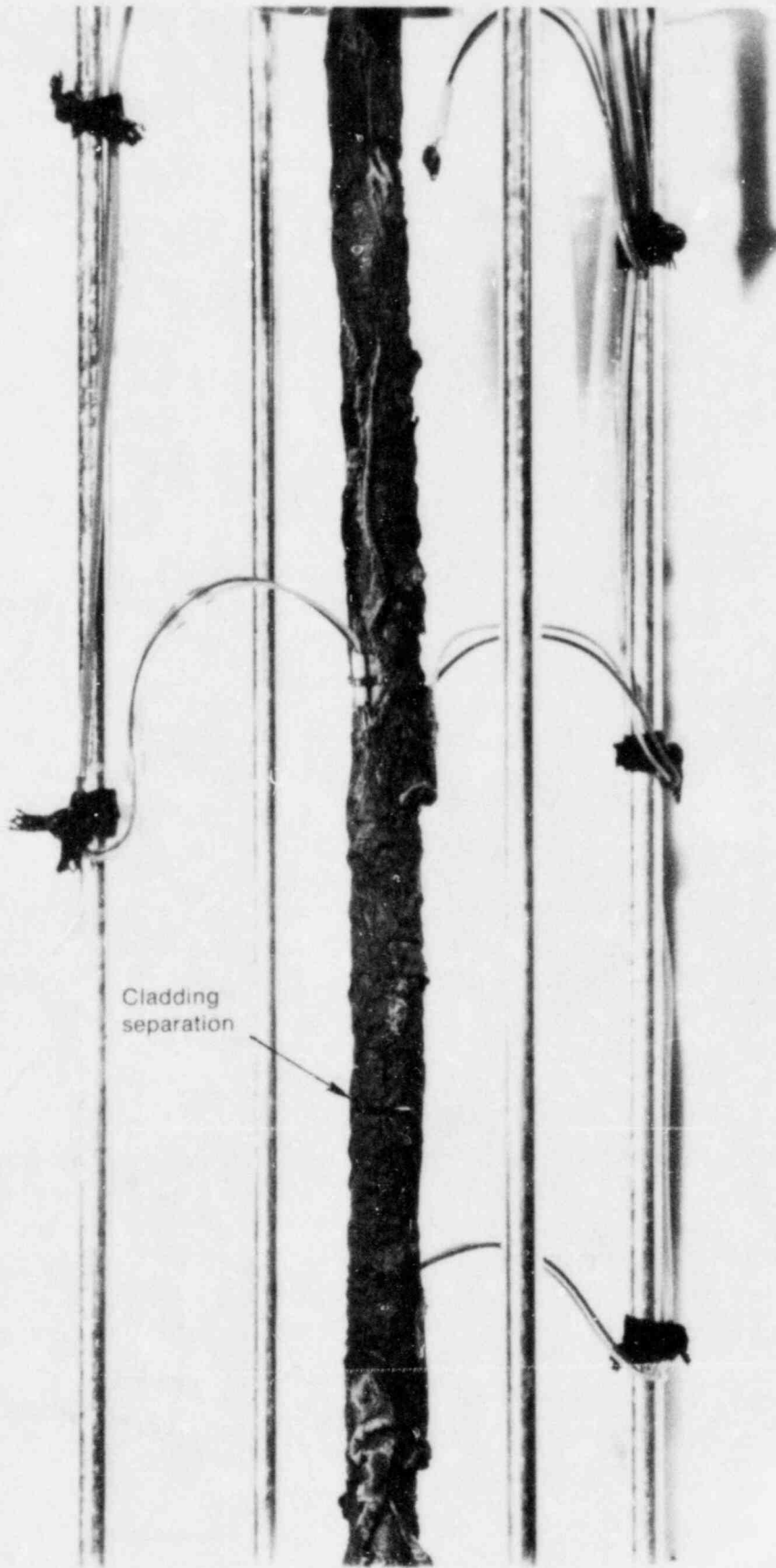
68-1255

Fig. 7 Central portion of stainless steel clad, 3% enriched SPX rod after Test 329 (276 cal/g UO_2) in the CDC.

20

Cladding melting-nonmelting boundary

Slumped pellets

68-1256
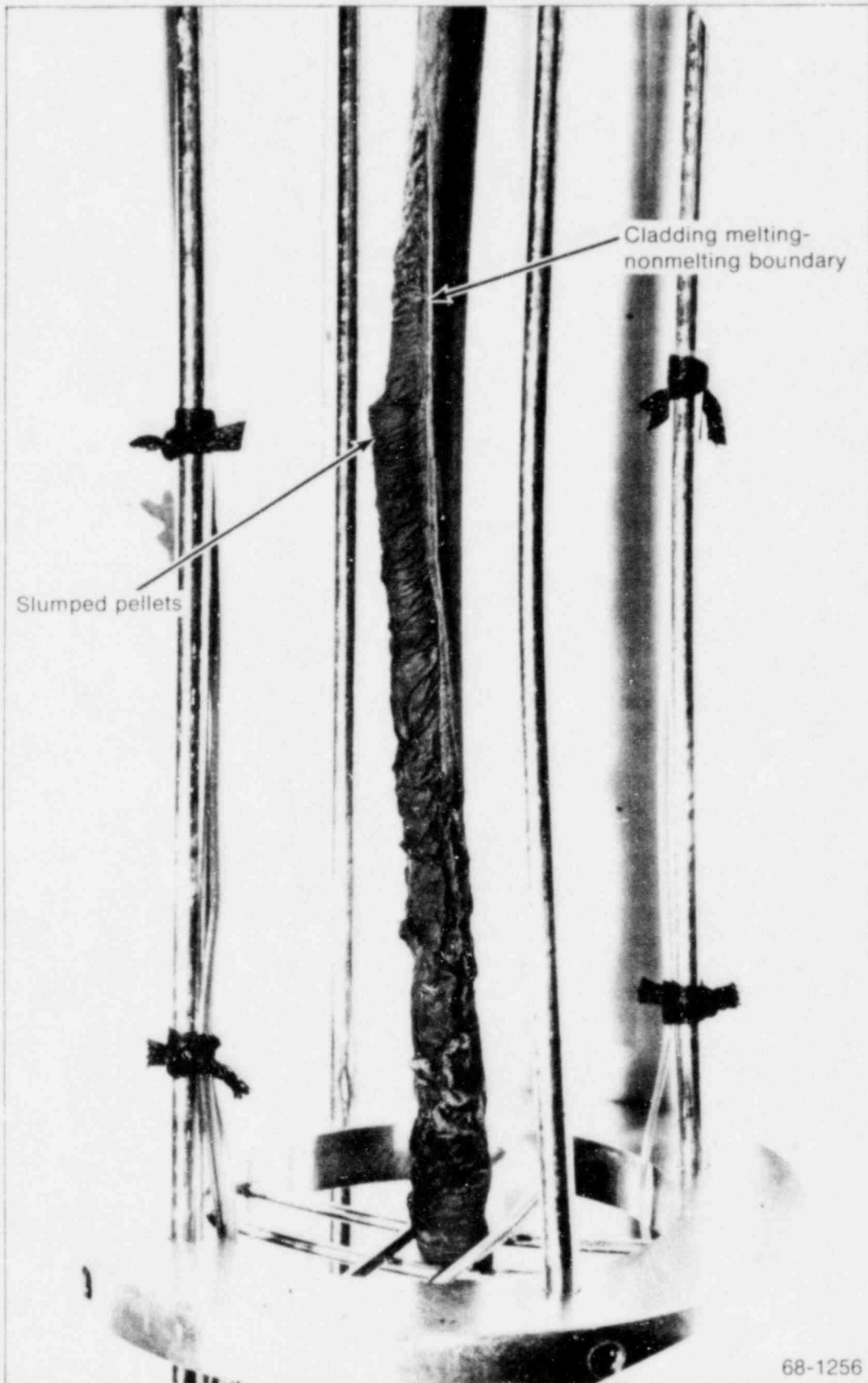
Fig. 8 Upper portion of stainless steel clad, 3% enriched SPX rod after Test 329 (276 cal/g UO_2) in the CDC.

21
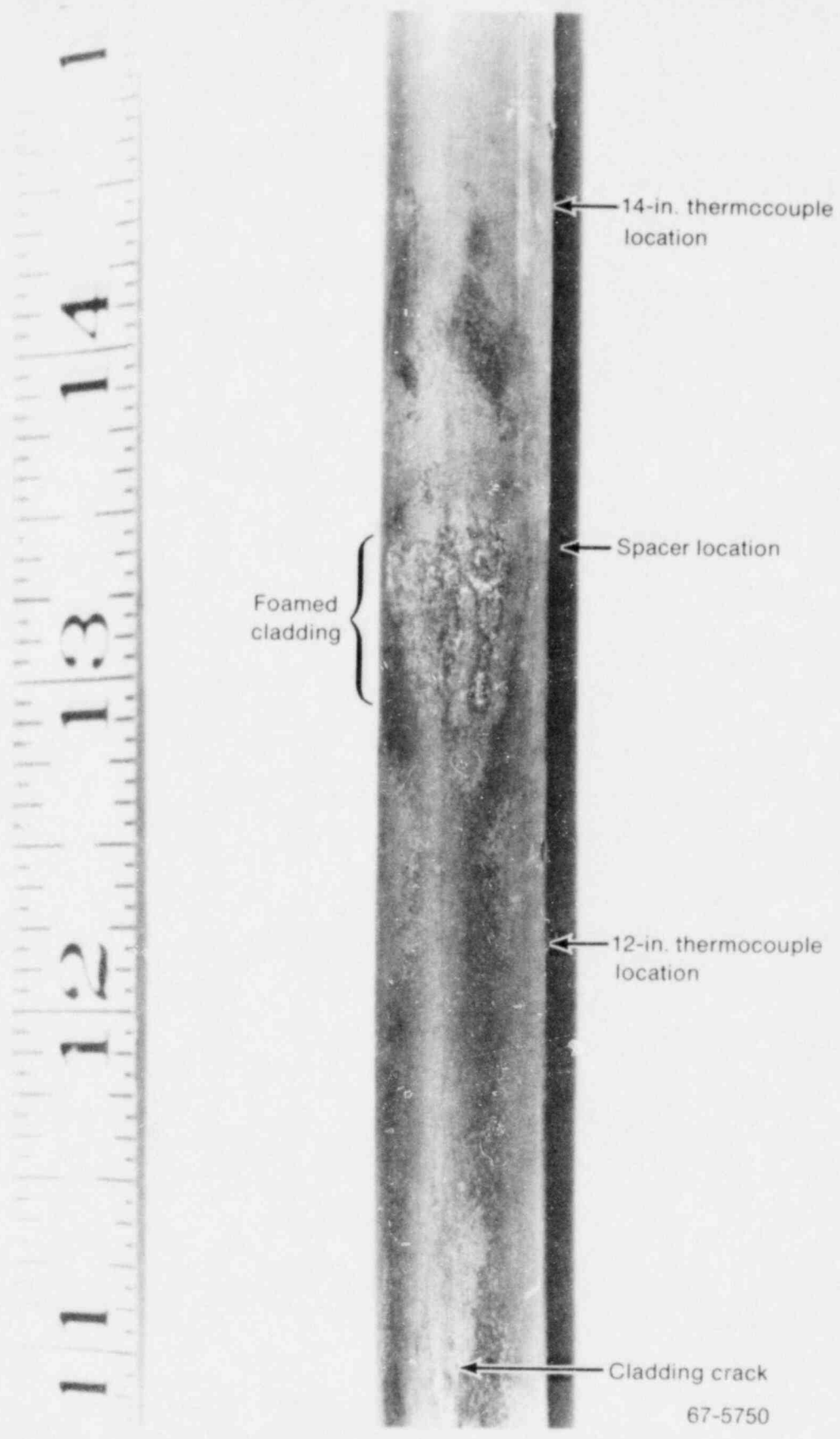
Fig. 9 Fuel rod following Test 193 (278 cal/g UO$_2$) in the CDC with stainless steel clad F-type rod.

threshold. The only significant difference in behavior due to cladding heat treatment occurred for energy depositions greater than about 400 cal/g UO_2, where the energy deposition at the time of cladding failure was appreciably greater for cold-worked clad rods than for annealed clad rods ($\sim$500 versus $\sim$400 cal/g UO_2). This behavior was attributed to the ability of the cold-worked cladding to withstand greater internal pressures prior to failure than the annealed cladding.

2.3 Gap Width

Tests with wide-gapped fuel (NSRR-WG)[8,19] were performed in the NSRR to evaluate the effects of gas gap width on cladding temperatures and failure modes. These tests employed rods with smaller pellet diameters than the NSRR-STD fuel, such that the gap width was twice as wide as the STD rod design. The wide-gapped rods had considerably lower cladding surface temperatures for energy depositions less than about 200 cal/g UO_2 compared with the STD rods. However, for energy depositions greater than 240 cal/g UO_2 where pellet expansion caused contact with the cladding for the wide-gapped fuel, maximum cladding temperatures were about the same for both the wide-gapped and STD fuel rods. Further, the initial failure threshold of the wide-gapped fuel design was approximately the same as for the STD fuel design.

2.4 Internal Pressure

The effects of rod internal pressure on the fuel behavior are discussed in the following two subsections. Included are the results of tests with prepressurized fuel rods and tests with fuel containing carbon impurities, which produced carbon monoxide and consequent pressure buildup during heating.

2.4.1 Prepressurized Fuel Tests. Tests have been conducted in the NSRR[11] with NSRR-STD fuel rods prepressurized from 0.25 to 4.9 MPa. Test results published to date indicate that increasing the initial internal pressure causes (a) a decrease in the initial cladding failure threshold, and (b) a change in the failure mode from cladding melting to cladding rutpure. Figure 10 graphically illustrates the decreasing initial failure threshold with increasing prepressurization. Initial internal pressures to 0.6 MPa had little, if any, influence on the threshold and mode of cladding failure. Initial pressures $\geqslant$ 1.2 MPa, however, resulted in a decrease in the failure threshold and failure by cladding rupture rather than by melting and embrittlement. At an initial internal pressure of 2.9 MPa, the failure threshold was in the range of 150 to 160 cal/g UO_2, compared with 244 to 264 cal/g UO_2 for initial pressures in the 0 to 0.6 MPa range.

Cladding swelling was minor for C to 0.6 MPa pressures, but for 1.2 to 2.0 MPa, significant swelling (60 to 100% circumferential strain) occurred over the active fuel length. Initial pressures of 2.9 to 4.9 MPa resulted in sizeable swelling localized near the position of cladding failure. Measured cladding surface temperatures at the time of cladding failure decreased with increasing initial internal pressure, as would be expected from out-of-pile tube burst data. Maximum cladding temperatures, however, were lower for intermediate
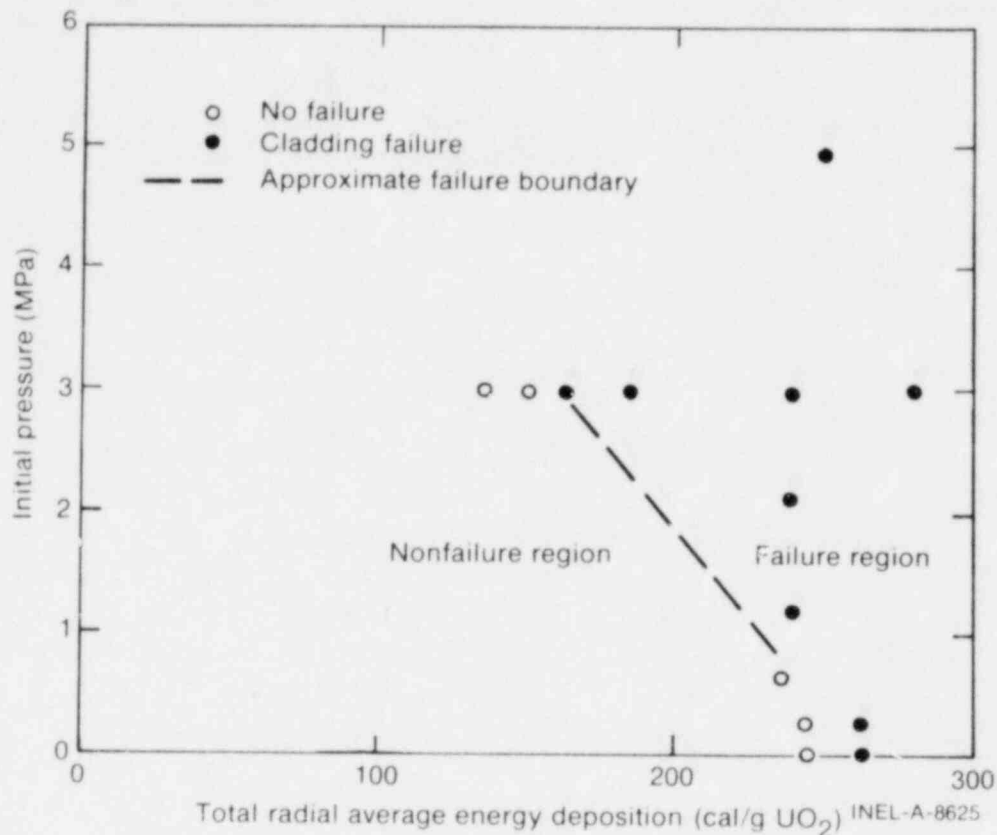
Fig. 10 Failure behavior of prepressurized NSRR-STD rods tested in the NSRR.

initial internal pressures where uniform cladding swelling was greatest. This behavior is illustrated in Figure 11, which shows cladding surface temperatures (maximum measured and at time of failure) as a function of initial internal pressure. These data were from a thermocouple located 3.3 cm below the test rod midplane for the series of seven tests performed at nominally 240 cal/g UO_2 (Figure 10).

2.4.2 Effects of Carbon Impurities. Unusually large cladding swelling was observed in some tests with GEP-pellet rods tested in the CDC[9]. In one test at 194 cal/g UO_2, a permanent diametral cladding deformation of 22% was measured. Posttest analysis of the internal gas from rods of this type showed significant amounts of carbon monoxide, apparently produced from carbon in the fuel matrix. The carbon in the fuel was subsequently determined to be the remains of a wax binder used during pellet fabrication. The maximum carbon concentration in the as-built pellets was about 51 ppm, which was within then-existing commercial specifications. Subsequent testing indicated that the degree of swelling was not highly reproducible due to an inability to accurately control all pertinent variables. However, simple calculations based on estimated internal gas temperatures showed that carbon monoxide evolution from the fuel could produce pressures of the magnitude required to initiate cladding deformation. Tests on similar rods containing pellets fabricated without the wax binder, and thus containing < 1 ppm carbon, exhibited little or no swelling.

24
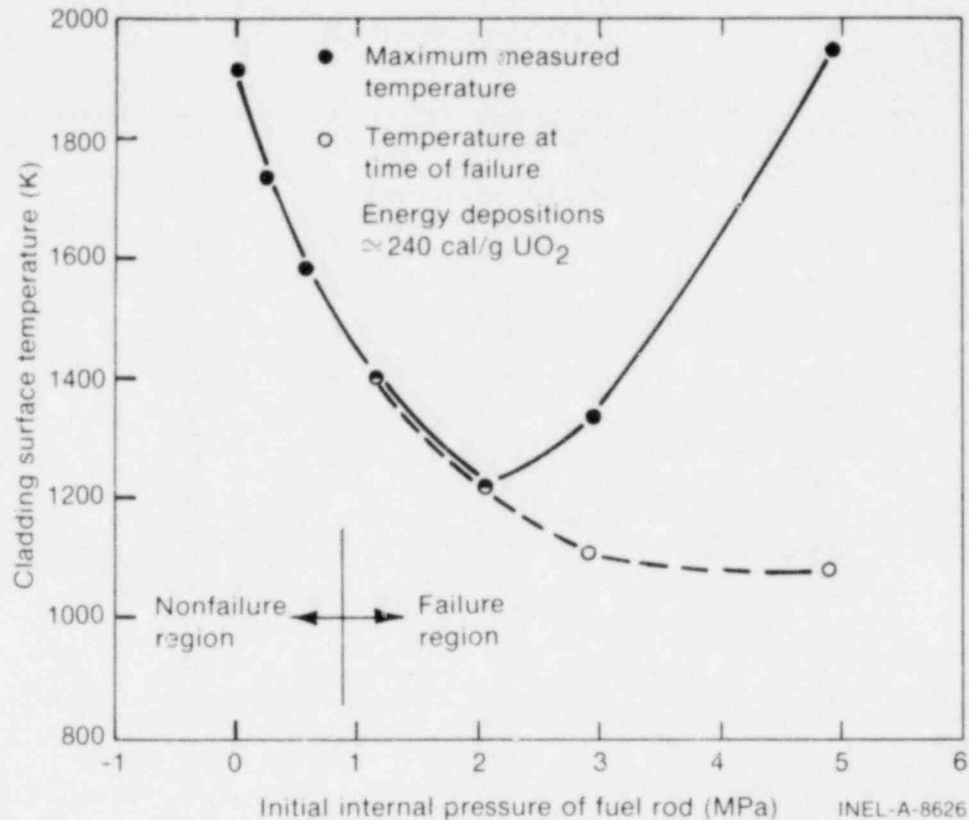
Fig. 11 Cladding surface temperatures as a function of initial internal pressure of NSRR-STD rods for tests at nominally 240 cal/g UO_2 in the NSRR.

2.5 Fuel Form

Tests with vibratory compacted powder-fueled rods were conducted in both the CDC[9] and TREAT[12]. The CDC tests used GEX and GEP powder-fueled rods. The initial failure threshold for the GEX powder rods was in the range of 266 to 292 cal/g UO_2 and was approximately 250 cal/g UO_2 for the GEP powder rods, both of which were slightly higher than for similar pellet-fueled rods. The initial failures were caused by melting of the cladding. The consequences of high energy deposition tests to 460 cal/g UO_2 with powder-fueled GEX rods showed pressures, nuclear-to-mechanical energy conversions, and cladding-water reaction extents similar to those observed for pellet-fueled GEX rods. Typical posttest photographs of GEX powder-fueled rods tested at various energy depositions are shown in Figure 12.

The initial failure threshold for the TREAT powder-fueled rods was determined to be approximately 270 cal/g UO_2, which was the same as that determined for similar pellet-fueled TREAT rods. Failure was by cladding melting, with indications of cladding penetration by molten UO_2.

25

Energy deposition
(cal/g UO$_2$)

440

343

314

292

266

69-3511

Fig. 12 Posttest photographs of GEX powder-fueled rods tested in the CDC.

2.6 Fuel Material

Plutonium recycle fuels, in the form of mixed oxides, were tested in the CDC[9]. The plutonium recycle test rods had a design similar to that of the GEX pellet UO_2 rods and were designated GEXPR and GEXPR-CH. The GEXPR rods contained solid pellets, whereas the GEXPR-CH rods contained pellets with a 0.292-cm-diameter hole through the axial center of each pellet. Test results showed the initial failure thresholds to be about the same as for the GEX UO_2 pellet rods; namely, 225 to 274 cal/g fuel for GEXPR rods and 223 to 275 cal/g fuel for the GEXPR-CH rods. Failure of the GEXPR rod at 274 cal/g fuel was apparently caused by cladding melting, which was also observed for GEX UO_2 rods tested slightly beyond the initial failure threshold. GEXPR-CH rods, however, showed no evidence of cladding melting in tests conducted at 275 and 277 cal/g fuel. Both of these rods failed by similar appearing longitudinal cladding splits, each about 0.5 cm long.

Cladding surface temperature measurements showed that at about 225 cal/g fuel, the maximum cladding surface temperature attained by the mixed oxide fuel rods was about 200 K less than that for a GEX pellet UO_2 rod. It was noted that the mixed oxide rods exhibited an initial short interval of nucleate boiling, whereas the UO_2 rods proceeded immediately into film boiling. It was postulated that this behavior may have been caused by heterogeneity of the mixed oxide fuel, which could have delayed the occurrence of DNB.

For energy depositions of about 275 cal/g fuel, maximum measured cladding surface temperatures were 200 to 300 K higher for the GEXPR rod than for the GEXPR-CH rods. This difference was postulated to be due to (a) the lower energy per unit length for a given specific energy deposition in the rods with a center hole, and (b) poorer fuel-cladding contact caused by lower thermal expansion of the center-hole fuel pellets.

The generally lower cladding temperatures for the mixed oxide rods resulted in slightly lower metal-water reaction extents than for GEX pellet UO_2 rods. Two higher energy deposition tests at 329 and 414 cal/g performed with the GEXPR-CH rods showed significantly lower pressure pulse generation and nuclear-to-mechanical energy conversion than was measured for GEX pellet UO_2 rods.

2.7 Fuel Enrichment

Test rods used in most single-rod experiments varied in enrichment from about 2.6 to 10.5%. To evaluate the effects of enrichment on test results, tests are being conducted in the NSRR[10,11] with 5, 10, and 20% enriched NSRR-STD rods; the radial power peaking factors for these enrichments are 1.16, 1.23, and 1.63, respectively. The initial failure thresholds, in terms of radial average energy depositions, decreased slightly with increasing enrichment, as illustrated in Figure 13. From these experimental data, the initial failure thresholds were determined to be 265 to 277 cal/g UO_2 for 5% enriched fuel, 254 to 264 cal/g UO_2 for 10% enriched fuel, and 232 to 246 cal/g UO_2 for 20% enriched fuel.
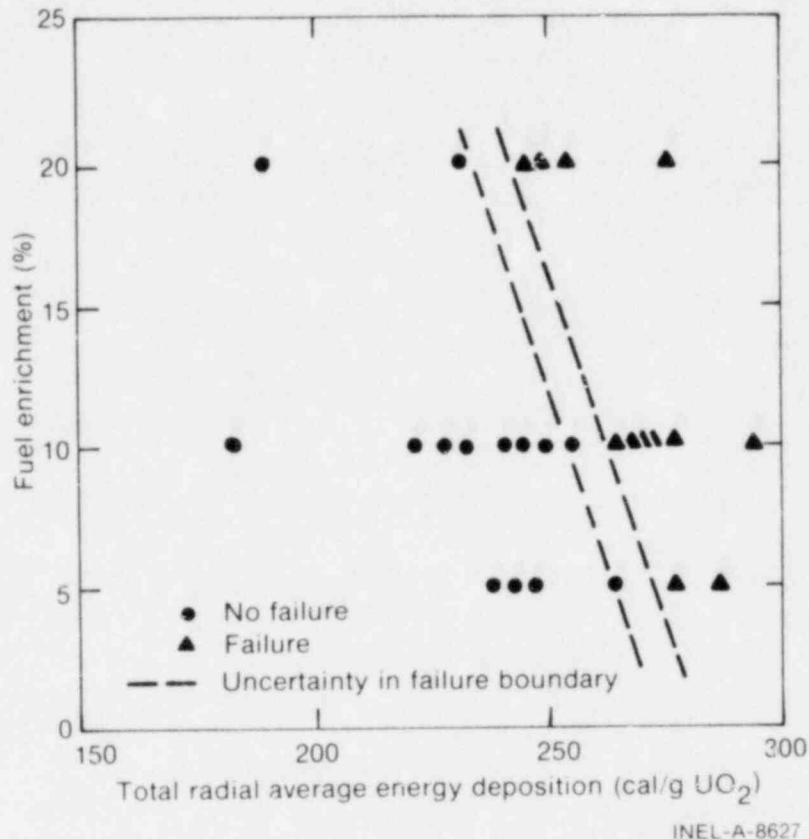
Fig. 13 Failure behavior of 5, 10, and 20% enriched NSRR-STD rods tested in the NSRR.

The lower failure threshold with increasing enrichment is believed to be caused by greater radial power peaking near the pellet surface for the higher enriched rods. The effects of such peaking are discussed further in Section III-3.2.

2.8 Axial Length

Most of the RIA fuel behavior data were obtained using relatively short test rods, usually about 13 cm long. Short rods were considered preferable to minimize axial flux variations, thus allowing experimental results to be easily related to the specific energy deposition. Several tests were conducted in the CDC[9] with 61-cm-long powder- and pellet-fueled GEX and GEP rods to determine whether the added length had any significant effect on the threshold or consequences of failure. On the basis of a limited number of tests, no unexpected or significantly different results were obtained for the longer rods, which was also confirmed by tests on 91-cm F-type rods and 46-cm SPX rods in the CDC.

3. EFFECTS OF ENVIRONMENTAL VARIATIONS

The effects of several selected environmental variations were investigated in tests performed in the CDC and NSRR. The scope of such testing was limited due to the inherent

capabilities of the driver cores and the types of capsules employed to contain test fuel rods. Thus, the only environmental variations investigated to date have included tests on small clusters of rods and variations in the amount of coolant locally available for heat transfer. The significant results of tests to evaluate these effects are summarized in this section.

3.1 Open-Lattice Fuel Rod Clusters

Open-lattice fuel rod cluster tests have been conducted in the NSRR and CDC. Fuel rod behavior during these tests is discussed in the following subsections.

3.1.1 **NSRR Test.** A single test has been performed in the NSRR with a five-rod open-lattice cluster of NSRR-STD fuel rods[11]. The test cluster was comprised of a 20% enriched central rod surrounded by four 10% enriched rods on a square pitch; the rods had a 14-mm center-to-center spacing. The test resulted in an energy deposition of about 180 cal/g UO_2 in the center rod and about 190 cal/g UO_2 in the outer rods. Each of the rods was uniformly discolored over its active length, but no cladding failure occurred. Cladding surface temperature histories at the same elevation (axial midplane of fuel) for the center rod and the inside and outside of an outer rod are shown in Figure 14. The maximum measured temperature, 1625 K, occurred on the outer surface of an outside rod, while the inner surface of the same rod attained a somewhat lower temperature due to the thermal flux depression (such depressions are created within rod clusters that are dependent on an external supply of neutrons from a driver core). Of particular interest was the behavior of the center rod cladding temperature, which reached a maximum value about the same as that observed for single rods at a similar energy deposition. However, the center rod
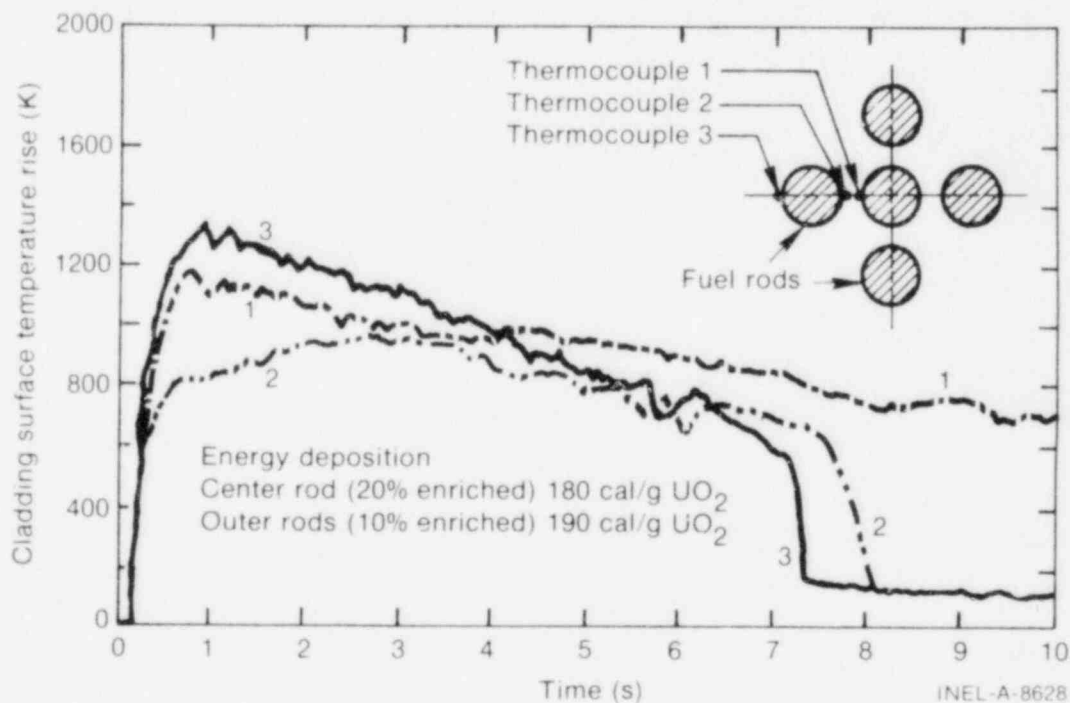
Fig. 14 Cladding surface temperature histories for an open-lattice five-rod cluster of NSRR-STD rods tested in the NSRR.

29

remained in film boiling for a significantly longer time prior to quenching than has been observed for single rods. Single rods at this energy deposition were observed to quench in about 5 s, whereas the cluster center rod remained in film boiling for a time exceeding 10 s.

3.1.2 CDC Tests. Tests with open-lattice, five-rod clusters of SPXM rods (zircaloy cladding, pelletized UO_2) were conducted in the CDC for energy depositions (center rod) in the range of 125 to 315 cal/g UO_2. The test clusters were comprised of 10.5% enriched fuel rods; a central rod was surrounded by four outer rods on a square pitch with an 8.3-mm center-to-center rod spacing. The primary results of these tests were:

(1)   The failure threshold of the center rod was essentially unchanged from that for single SPXM rods.

(2)   Maximum measured cladding surface temperatures were similar to those observed for single rods at comparable energy depositions.

(3)   The failure consequences of the test in which the center rod received 315 cal/g UO_2 and the outer rods received 383 cal/g UO_2 were more severe than for a test at 378 cal/g UO_2 on a single rod. The peak pressure and nuclear-to-mechanical energy conversion were 2.6 MPa and 0.10%, respectively, for the cluster, and 0.4 MPa and 0.06%, respectively, for the single rod. Metal-water reaction extent, however, was only 30% for the cluster compared with 47% for the single rod.

3.2   Reduced Local Coolant Inventory

Tests having a reduced local coolant inventory have been conducted in the NSRR and the CDC. Results from single-rod tests and cluster tests are presented in the following subsections.

3.2.1 Single-Rod Tests In NSRR. Tests have been conducted in the NSRR[10,11] in which NSRR-STD fuel rods were enclosed in open-ended aluminum tubes (flow shrouds) to restrict the water/fuel ratio to that more nearly equivalent to an LWR core lattice. Cross-section views of the flow shroud geometries used are shown in Figure 15.

Several tests performed with the 14-mm cylindrical shroud showed the initial failure threshold to be in the range of 211 to 247 cal/g UO_2, a decrease from the 244 to 264 cal/g UO_2 range determined for the unenclosed NSRR-STD rods. The reduced failure threshold was supported by test results with the other shroud geometries; failures occurred at 251 cal/g UO_2 with the 14-mm square shroud, at 237 cal/g UO_2 with the 16-mm cylindrical shroud, and at 240 cal/g UO_2 with the 20-mm cylindrical shroud.

The shrouds had little effect on the maximum cladding surface temperatures reached during the tests, but they did cause a significant increase in the duration of film boiling at
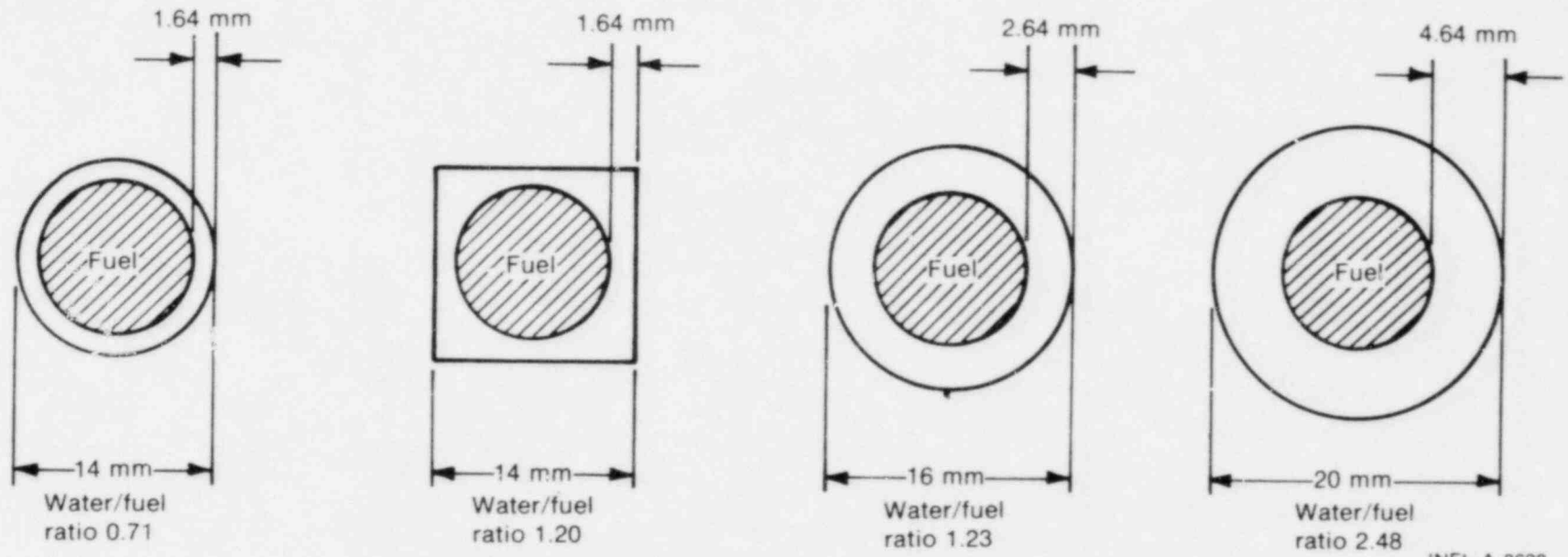
Fig. 15 Cross sections of flow shrouds used in NSRR tests.

the cladding surface. This effect is illustrated in the cladding surface temperature measurements shown in Figure 16. The test with no shroud quenched after about 5 s of film boiling, whereas the test with the 14-mm square shroud (water/fuel ratio of 1.20) did not quench until nearly 9 s, and the test with the 14-mm cylindrical shroud (water/fuel ratio of 0.71) quenched at over 10 s. Although not yet confirmed by metallurgical examinations, it is likely that the longer durations of film boiling for the tests with shrouds resulted in greater cladding embrittlement, which probably contributed to the occurrence of lower failure thresholds for the rods enclosed in shrouds.

Figure 17 illustrates the effects on temperature-related measurements of reducing the water/fuel ratio by the use of the various shroud geometries (Figure 15). The data shown were from five tests with energy depositions in the range of 237 to 251 cal/g UO_2, which are considered to be nominally the same for purposes of these comparisons. With decreasing water/fuel ratio (from 250 for no shroud to 0.71 for the smallest diameter shroud), the quenching time increased from about 5 to 15 s, the temperature of the cladding surface at time of quenching decreased from about 1170 to 570 K, the maximum measured cladding temperature remained approximately constant, and the maximum measured water temperature at the outlet of those rods with shrouds increased. Cladding failure occurred in each of the four tests with shrouds, but did not occur in the test with no shroud. As discussed previously, the long duration of film boiling for the tests with shrouds likely caused greater cladding embrittlement, which probably contributed to the failures.

3.2.2 Cluster Tests in the NSRR. Two tests have been performed in the NSRR[11] in which five-rod clusters of NSRR-STD fuel rods were enclosed in open-ended aluminum shrouds to effectively reduce the water/fuel ratio. The test clusters were comprised of a 20%
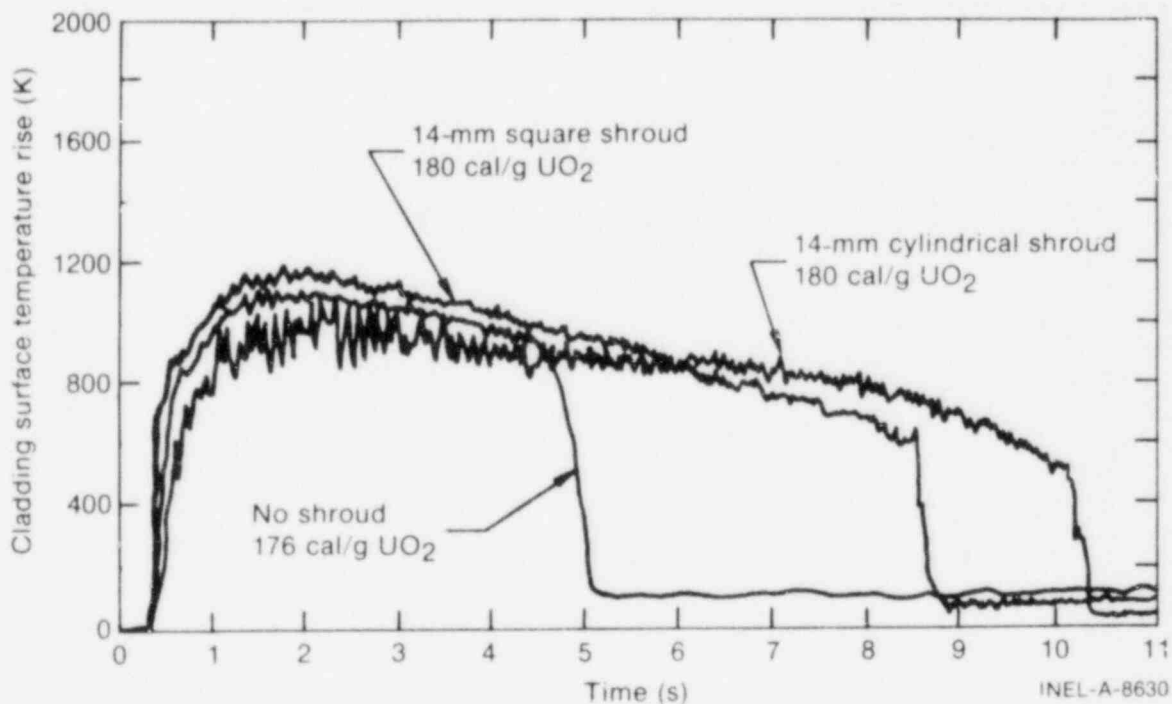
Fig. 16 Cladding surface temperature histories with and without shrouds for NSRR-STD rods tested in the NSRR.
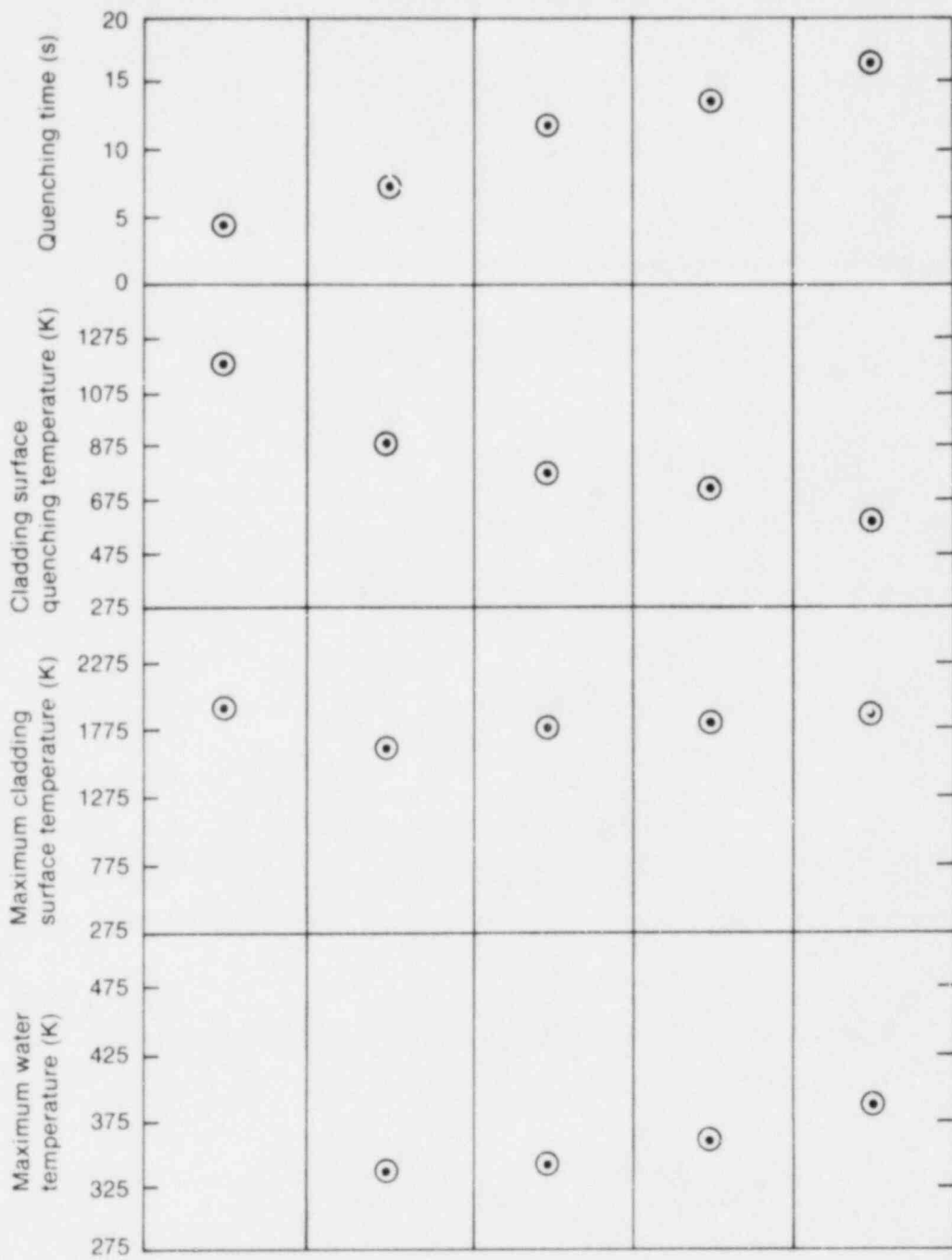
Fig. 17 Temperature-related data as a function of water/fuel ratio (shroud geometry) for energy depositions of 237 to 251 cal/g UO$_2$ with NSRR-STD rods tested in the NSRR.

enriched central rod surrounded by four 10% enriched rods on a square pitch of 14 mm. Figure 18 shows cross-section views of the clusters and flow shroud geometries.

The fuel rod cluster enclosed in the square shroud (water/fuel ratio of 2.91) was subjected to a test that deposited 200 cal/g UO_2 in the center rod and 190 cal/g UO_2 in the outer rods. This test was similar to the test performed on an open-lattice cluster (Section II-3.1.1, 180 cal/g UO_2 in center rod and 190 cal/g UO_2 in outer rods), and no significant differences in test results were observed.

The cluster enclosed in the cruciform shroud (water/fuel ratio of 1.17) was subjected to a test that deposited 225 cal/g UO_2 in the center rod and 240 cal/g UO_2 in the outer rods. This test caused failure of the center rod near the bottom of the active fuel length and evidence of cladding melting was apparent on the outer rods. The cladding melting on the outer rods was preferentially oriented on the side opposite the center rod (that is, where the local energy deposition was greatest). It has not been determined whether the melting was primarily a result of the asymmetric power distribution across these rods or whether the shroud influenced the behavior. The outer rods were also noted to be bowed away from the center rod. Only one thermocouple, located on an inner surface of an outside rod, survived throughout the test. This thermocouple indicated a maximum cladding temperature of 1570 K, a quenching temperature of 1070 K, and a quenching time of 11.3 s. These data would appear to be consistent with expectations based on the single rod tests performed with shrouds (Section II-3.2.1), but additional testing and analysis is required to better understand cluster behavior.
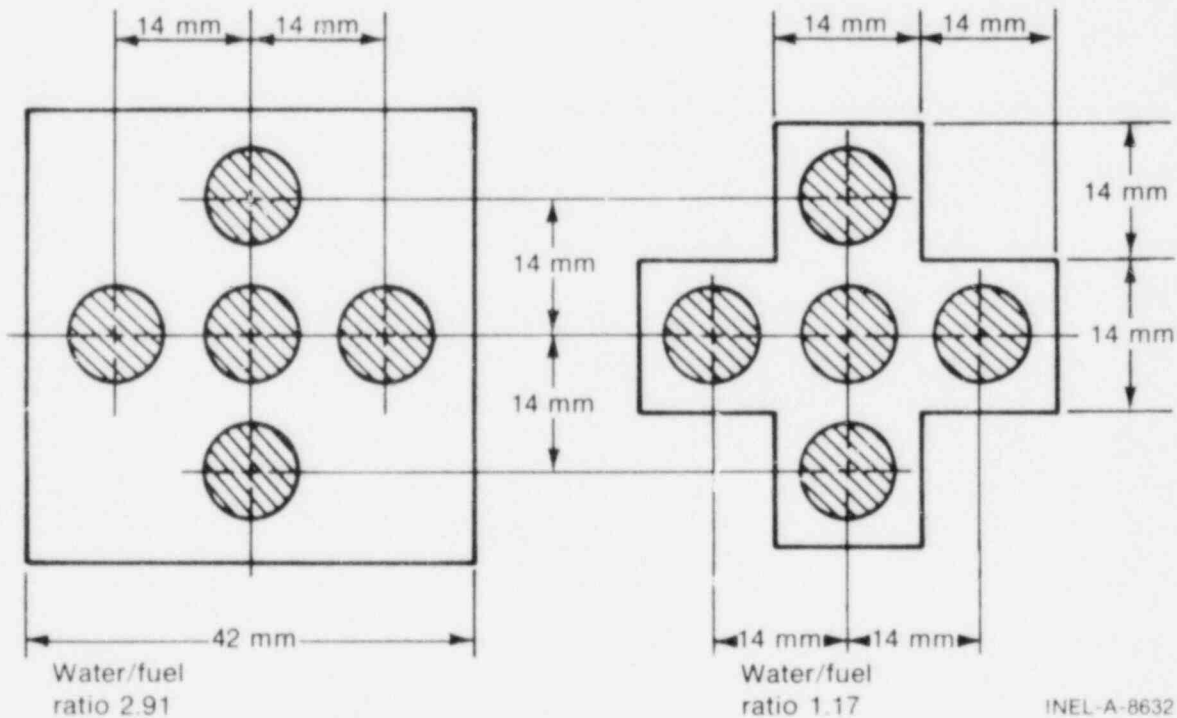
Fig. 18 Cross sections of clusters and flow shrouds used in NSRR tests.

34

3.2.3 Cluster Tests in the CDC. Tests with five-rod clusters of SPXM and GEX rods (zircaloy clad, pellet fuel) were conducted in the CDC with the clusters enclosed in both square and cylindrical flow shrouds (water/fuel ratios in the range of 1.2 to 2.11). The principal results of the few tests performed were as follows:

(1)   The failure threshold for SPXM clusters enclosed in canisters was reduced to less than 225 cal/g UO_2, compared with about 240 cal/g UO_2 for unenclosed single rods and for the center rod in open-lattice clusters

(2)   No failures occurred for a GEX cluster enclosed in a canister as a result of energy depositions of 197 cal/g UO_2 in the center rod (7% enriched) and 176 cal/g UO_2 in the outer rods (5% enriched).

4. EFFECTS OF FUEL BURNUP

Tests were conducted in the CDC[9,20] to scope the effects of burnup on the threshold and consequences of rod failure. Both GEP and GEX pellet-fueled rods were preirradiated in a pressurized water loop in the Engineering Test Reactor (ETR). Coolant conditions in the ETR loop simulated a BWR environment; that is, 6.9 MPa pressure, 511 K inlet temperature, and 561 K cladding surface temperature. Linear power densities were 55.8 to 65.6 kW/m. Atypical of BWRs was the slightly lower fast-to-thermal flux ratio (between 0.15 and 0.20), which resulted in a slightly less than typical fast neutron dose to the cladding.

Ten tests were performed in the CDC, two with GEP rods having burnups of ∿1000 megawatt-days per metric ton of uranium (MWd/t) and eight with GEX rods having burnups in the range of 3000 to 32 000 MWd/t. The principal results of the GEP rod tests were as follows:

(1)   The relatively low burnup (∿1000 MWd/t) of the GEP rods produced no significant differences in the initial failure threshold compared with similar tests on unirradiated rods at energy depositions of about 200 and 240 cal/g UO_2.

(2)   With regard to failure mode, the failure at 240 cal/g UO_2 for the unirradiated rod was in the form of cladding melting, whereas the preirradiated rod failed by cladding rupture. Thus, at 1000 MWd/t, a change in failure mode from passive meltdown to pressure-caused rupture was indicated.

Tests with the higher burnup GEX rods indicated that fuel burnup affected the initial failure threshold, failure mode, and consequences of failure. Specific findings were as follows:

(1) Failure thresholds: The test data indicated a reduction in the initial failure threshold for preirradiated rods compared with unirradiated rods. A 3000 MWd/t GEX rod subjected to a 200 cal/g UO_2 test failed at 147 cal/g UO_2, and a 32 000 MWd/t GEX rod subjected to a 190 cal/g UO_2 test failed at 85 cal/g UO_2. These two tests represent the lowest initial failure thresholds observed; other preirradiated rods either withstood higher energy depositions without failure, or failed at higher energy depositions than did comparable unirradiated rods.

(2) Failure modes: The failures of preirradiated GEX rods showed little or no evidence of cladding melting, which was evident in most unirradiated rods tested near the initial failure threshold. Failures of preirradiated rods were in the form of cladding ruptures or cracks, generally longitudinal, and, in some cases, extensive and multiple ruptures and cracks. While some failures appeared to have been ruptures induced by internal pressure, the 32 000 MWd/t GEX rod that failed at 85 cal/g UO_2 had three separate longitudinal fractures (cracks) that extended over the active length of the rod. The cracks appeared to be brittle fractures, although this was not confirmed by metallurgical examination. Based on available information, Miller[20] postulated that overpressure by internal gas was not the direct cause of the multiple cracking, but that the three fractures were probably caused by pellet-cladding interaction (PCI); namely, by the strain of thermally expanding fuel against embrittled cladding.

(3) Failure consequences: Measurable capsule pressure and mechanical energy generation occurred at lower energy depositions for preirradiated rods than for comparable unirradiated rods (200 cal/g UO_2 total energy deposition compared with over 300 cal/g UO_2). In the 200 to 300 cal/g UO_2 range, the pressure pulses were narrow, with magnitudes not exceeding about 2.4 MPa. Little fuel was expelled from the rods, and nuclear-to-mechanical energy conversions did not exceed 0.3% in the 200 to 300 cal/g UO_2 range.

One GEX rod with a burnup of ∿4140 MWd/t was tested at a total energy deposition of 348 cal/g UO_2. The rod failed at about 300 cal/g UO_2, producing a pressure pulse of 16.2 MPa and a nuclear-to-mechanical energy conversion of 0.21%. A

similar test on an unirradiated GEX rod also resulted in failure at about 300 cal/g UO_2, producing a much lower pressure pulse of 2.6 MPa, but a larger nuclear-to-mechanical energy conversion of 0.41%. These differences in behavior were conceivably directly related to the difference in failure modes for the two rods. The preirradiated rod ruptured near the bottom of the fuel stack, with the edges of the cladding showing evidence of cladding melting. The rod was completely severed at the point of rupture, but no other damage to the rod was noted and only a small amount of fuel was expelled into the coolant. The unirradiated rod, on the other hand, showed significant cladding melting over the entire active length, with a significantly greater quantity of fuel expelled into the coolant.

The failure behavior of the ten preirradiated rods tested in the CDC is illustrated in Figure 19. Compared with the initial failure threshold range determined for unirradiated GEX and GEP rods, seven of the ten preirradiated rods behaved in a manner that agrees with the findings for unirradiated fuel rods. Three of the preirradiated rods, however, failed at energy depositions somewhat below the failure threshold for unirradiated rods. The results of these few tests establish the need for additional experimental work to better understand and evaluate the effects of burnup on the threshold and consequences of failure under RIA conditions.
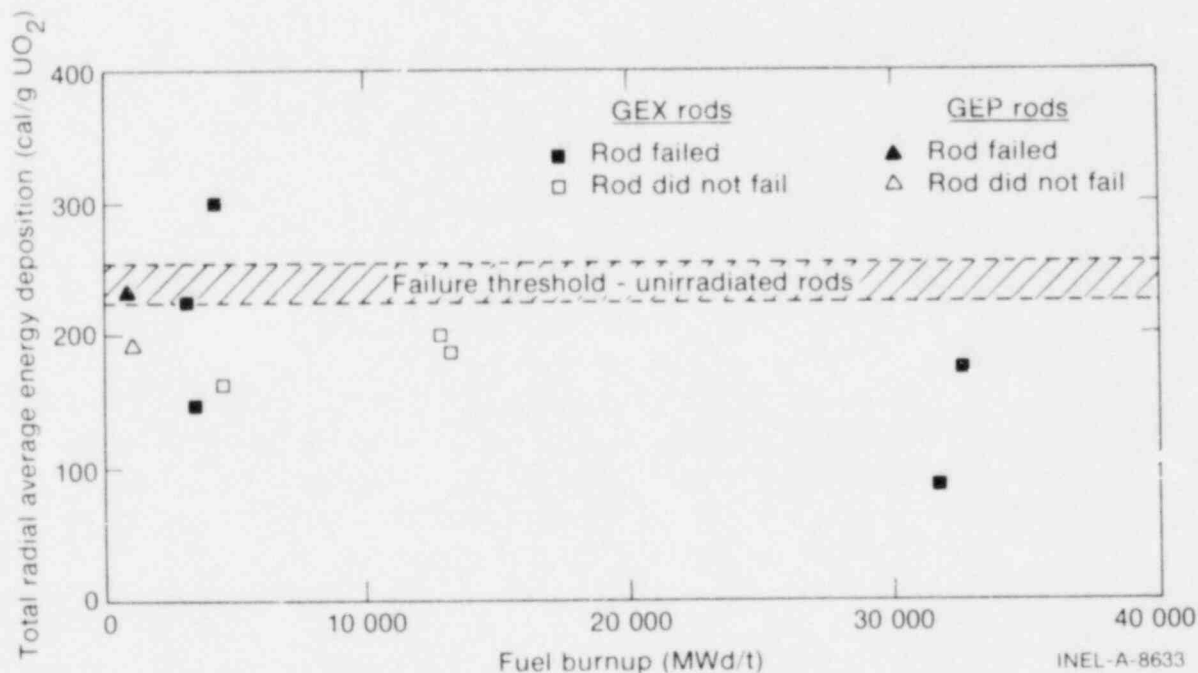
Fig. 19 Failure behavior of preirradiated GEX and GEP rods tested in the CDC.

5. EFFECTS OF WATERLOGGED FUEL

Tests with various waterlogged rod types have been conducted in both the CDC and NSRR. The CDC tests were performed on rods with pellet and powder fuel clad with both cold-worked and annealed zircaloy and stainless steel. The NSRR tests were performed on the NSRR-STD, NSRR-WG, and JPDR-II rod designs, all of which had pellet fuel clad with cold-worked zircaloy. The tests with waterlogged rods simulate the conditions of a startup accident in a power reactor in which previously failed fuel, which had become waterlogged during shutdown, is subjected to a sudden overpower transient. Most of the rods tested in the CDC were waterlogged by evacuating the rods and allowing water to enter the evacuated interior. This technique resulted in essentially complete waterlogging. Tests in the NSRR have investigated both fully and partially waterlogged rods, waterlogged rods with cladding defects, and the effects of reactor period on the failure threshold.

In general, waterlogged rods were found to fail at significantly lower energy depositions than nonwaterlogged rods (with the exception of annealed stainless steel clad rods). The initial failure threshold was found to be strongly dependent on cladding material and cladding heat treatment, and relatively independent of fuel form, rod design characteristics, and degree of waterlogging. Waterlogged rods failed almost exclusively by cladding rupture caused by internal pressure generated by water expansion. The consequences of failure, in terms of pressure pulse magnitudes and nuclear-to-mechanical energy conversion, were found to be greater for powder fuel rods than for pellet fuel rods.

The principal results of the waterlogged fuel rod tests are summarized in the following. Further details are provided in the referenced publications.

(1) Failure thresholds: The initial failure thresholds determined for various types of fully waterlogged fuel rods tested in the CDC and NSRR are shown in Table III. These data clearly indicate that the failure threshold is lower for zircaloy than for stainless steel cladding, and that cold-worked cladding fails at lower energy depositions than does annealed cladding. The cladding failures for stainless steel clad rods were generally in the form of splits, with little or no evidence of cladding oxidation or melting, whereas the zircaloy clad rods were, in some cases, discolored over the active region, indicating the attainment of higher temperatures. The discolored zircaloy clad rods were fragile and easily broken during handling, indicating some degree of cladding embrittlement.

(2) Failure consequences: Failure of waterlogged fuel rods produced high capsule pressures, but the pressure pulses were generally narrow and did not generate sufficient mechanical energy to damage adjacent rods. Waterlogged GEP powder rods generated pressure pulses as high as 41.4 MPa, which was two to

TABLE III

INITIAL FAILURE THRESHOLDS FOR WATERLOGGED FUEL RODS

Fuel Rod Type	Fuel Form	Cladding Material	Cladding Heat Treatment	Failure Threshold[a] $(cal/g\ UO_2)$
SPXM	Pellet	Zircaloy-2	Cold-worked	85 to 150[9]
SPXM	Pellet	Zircaloy-2	Annealed	157 to 164[9]
SPXM	Pellet	304 SS	Cold-worked	110 to 116[9]
SPXM	Pellet	304 SS	Annealed	330 to 352[9]
F-type	Pellet	304 SS	Annealed	240 to 245[b]
GEP	Pellet	Zircaloy-2	10% cold-worked	60[9]
GEP	Powder	Zircaloy-2	10% cold-worked	60 to 66[9]
NSRR-STD	Pellet	Zircaloy-4	Cold-worded	90 to 140[10,11]
JPDR-II	Pellet	Zircaloy-4	Cold-worked	100 to 130[10,11]
NSRR-WG	Pellet	Zircaloy-4	Cold-worked	90 to 140[10,11]

[a] Based on radial average energy deposition at axial flux peak at time of rod failure.

[b] Based on unpublished test results.

five times higher than comparable waterlogged pellet rods. The nuclear-to-mechanical energy conversions for the GEP powder rod that produced 41.4 MPa pressure was about 0.9%. Failure of waterlogged fuel rods generally resulted in all or most of the fuel being expelled into the coolant. The initial pressure pulses, however, were believed to have been caused by venting of the high-pressure water within the fuel rods, rather than by fuel-coolant interactions.

(3) Other effects: Tests have been performed in the NSRR[11] to investigate the effects of partial waterlogging, cladding defects, gap-width, and reactor period on the failure threshold and general behavior of waterlogged rods. Although variation of these parameters affected the detailed behavioral aspects of waterlogged rods, they were not found to significantly affect the thresholds and consequences of waterlogged rod failure.

III. CORRELATIONS AND INTERPRETATIONS

A part of the test results presented in Section II are correlated and interpreted in this section. The correlations are based primarily on data from the CDC program, supplemented with available data from the NSRR program. The TREAT data are not generally included because certain of the measurements required for correlation purposes were either not made or were not available in a usable form. It should be emphasized that only selected data correlations are presented. The selections were based both on relative importance to the understanding of the RIA and on the availability of data. The degree of detail included in the treatment of the various topics in this section varies depending on the type of measurements considered, measurement accuracy, range of tests considered, amount of data available, and current understanding of the physical phenomena involved. In several cases, the need for additional experiments or analysis, or both, is established.

Data from throughout Section II and Appendices B and C are used, where appropriate, in the correlations and interpretations presented in this section. Maximum measured cladding temperatures and deformations of the cladding and fuel are analyzed to determine the effects of test fuel design and initial parameter variations, to establish trends as a function of energy depositions, and to identify relevant mechanisms. Failure modes and mechanisms are examined in detail for both incipient and high energy failures, and a semi-quantitative model based on test fuel properties and characteristics is used to evaluate postulated failure mechanisms for high energy depositions.

1. ANALYSIS OF CLADDING TEMPERATURES

Cladding temperature data from tests with various rod types in the CDC and NSRR are correlated and analyzed in this section. Fuel design and initial parametric variations are evaluated to determine their effects on thermal response.

1.1 Maximum Cladding Temperature

Maximum cladding temperature data from the CDC and NSRR tests, in which the rods were not preirradiated, prepressurized, or enclosed within a shroud, are shown as a function of radial average energy deposition in Figure 20. These data indicate the following:

(1) With the exception of several waterlogged fuel tests, departure from nucleate boiling (DNB) was not observed for energy depositions less than about 130 cal/g of fuel. The occurrence of DNB at lower energy depositions for the waterlogged fuel tests resulted in cladding temperatures only about 50 K above the saturation temperature ($\sim$373 K).

CDC zircaloy cladding

CDC stainless
steel cladding

NSRR zircaloy cladding

- ● SPX-pellet
- ◔ SPXM-pellet
- ⊕ SPXM-pellet-bundle
- □ GEX-pellet
- ▨ GEX-powder

- ⊠ GEXPR
- ⊞ GEXPR-centerhole
- △ GEP-pellet
- ▲ GEP-powder

- ○ SPX-stainless steel
- ⊕ F-type

- ○ NSRR-STD
- ⊡ NSRR-WG
- ▽ JPDR-II
- ▼ JPDR-II-waterlogged
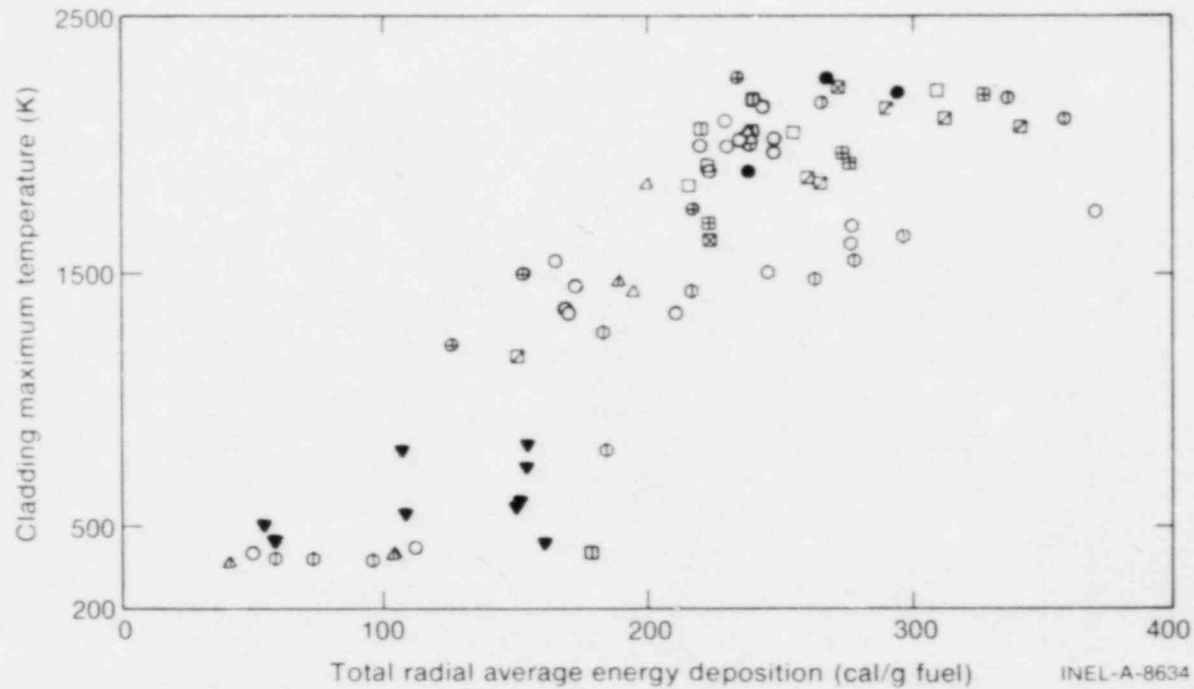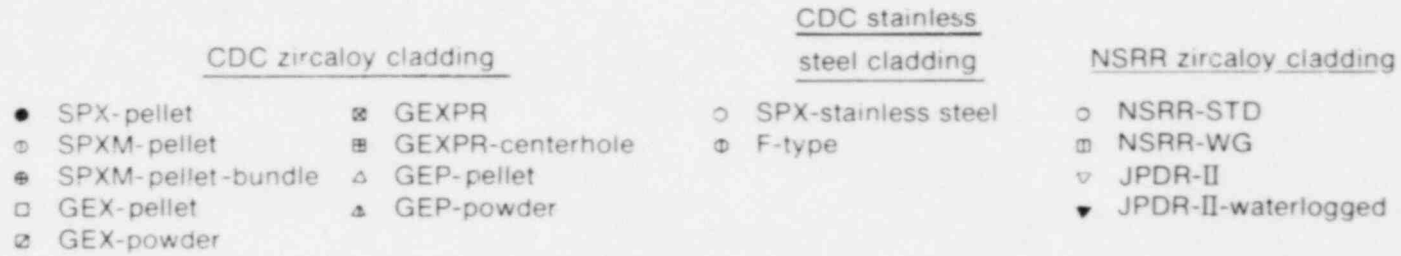
Fig. 20 Maximum cladding temperature plotted as a function of radial average energy deposition.

INEL-A-8634

(2) Between about 150 and 240 cal/g of fuel, maximum cladding temperatures increased significantly, indicating degradation of heat transfer from the cladding to the coolant caused by DNB and subsequent film boiling. Maximum cladding temperatures of stainless steel clad fuels were significantly lower than those of zircaloy clad fuels.

(3) For energy depositions greater than about 240 cal/g of fuel, maximum cladding temperatures reached the melting temperatures of 2073 K for zircaloy cladding and 1673 K for stainless steel cladding.

(4) Temperature differences among zircaloy clad fuel rods were not large; however, powder-fueled and mixed-oxide-fueled rods had lower temperatures than pellet-fueled rods. Further, the CDC test rods had generally lower temperatures than the NSRR test rods.

1.2 Effect of Pellet-to-Cladding Gap on the Onset of DNB

Fuel-cladding gap closure from fuel expansion causes a significant increase in gap conductance, with the resultant increased energy transfer leading to DNB at the cladding surface. Therefore, the minimum energy deposition necessary to cause DNB is dependent on the initial fuel-cladding gap; that is, DNB did not occur with NSRR wide-gapped fuel (NSRR-WG) below about 190 cal/g of fuel; however, it occurred at about 130 cal/g UO_2 for most other fuel types, and at even lower energy depositions for waterlogged rods. DNB is delayed to higher energy depositions for the wide-gapped fuel, because more fuel thermal expansion is required for gap closure. This effect is illustrated in Figure 21, where the calculated energy deposition required for gap closure in pellet-fueled rods is shown as a function of the ratio of initial gap width to fuel radius. Experimentally determined energy depositions near the onset of DNB, determined from both cladding temperature histories and cladding surface oxidation, are shown for comparison. The gap closure curve was calculated using the UO_2 heat capacity equations presented in Reference 21 and the UO_2 thermal expansion expression of Reference 22.

The calculated gap closure line in Figure 21 approximately coincides with the boundary between the DNB and non-DNB data. Therefore, gap closure is an apparent prerequisite for DNB in tests with pellet-fueled rods.

The existence of gap closure can also be determined using cladding deformation data. Cladding deformation is believed to be primarily caused by fuel thermal expansion when the test rods are not prepressurized and the energy depositions are such that the fuel rod internal gas pressure is below that required to cause cladding yield. In Figure 22, maximum cladding temperatures and cladding radial expansions are compared for zircaloy clad
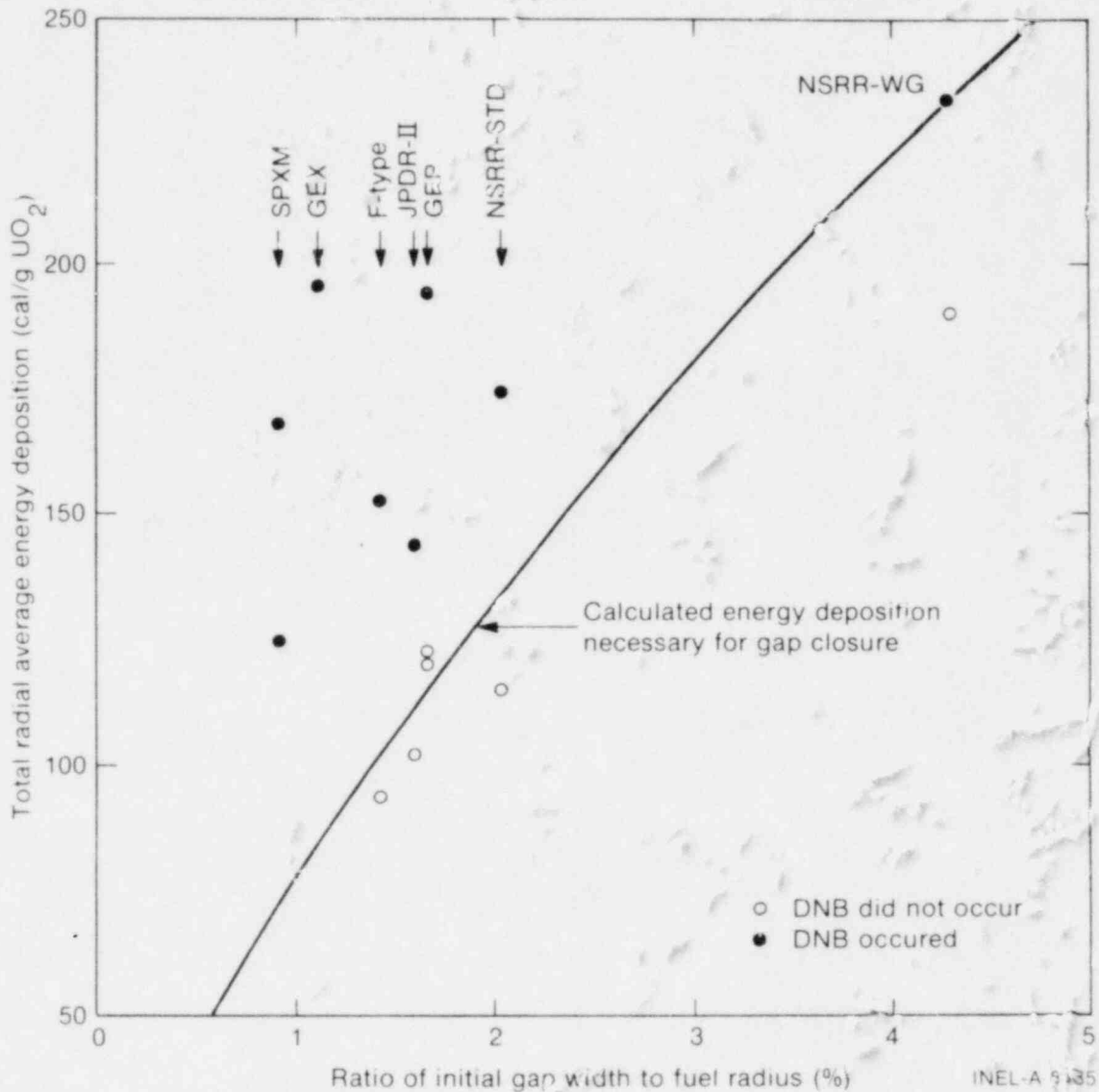
Fig. 21 Comparison between the energy depositions of DNB incidence and calculated energy deposition necessary for gap closure.

NSRR-STD and NSRR-WG fuels and stainless steel clad F-type fuels. The energy deposition thresholds for high cladding temperatures are in good agreement with the energy deposition thresholds for cladding expansion in each of the three fuel types.

Fuel cracking can also cause contact between fuel and cladding. However, soft contact of this type, with low interface pressure, apparently does not significantly improve heat transfer to the cladding; no apparent change in DNB occurrence was observed in sequential CDC testing of F-type rods which resulted in extensive fuel cracking[16].

At high energy depositions and subsequent early gap closure, initial gap width has an insignificant effect on maximum cladding temperatures (Figure 20).

43
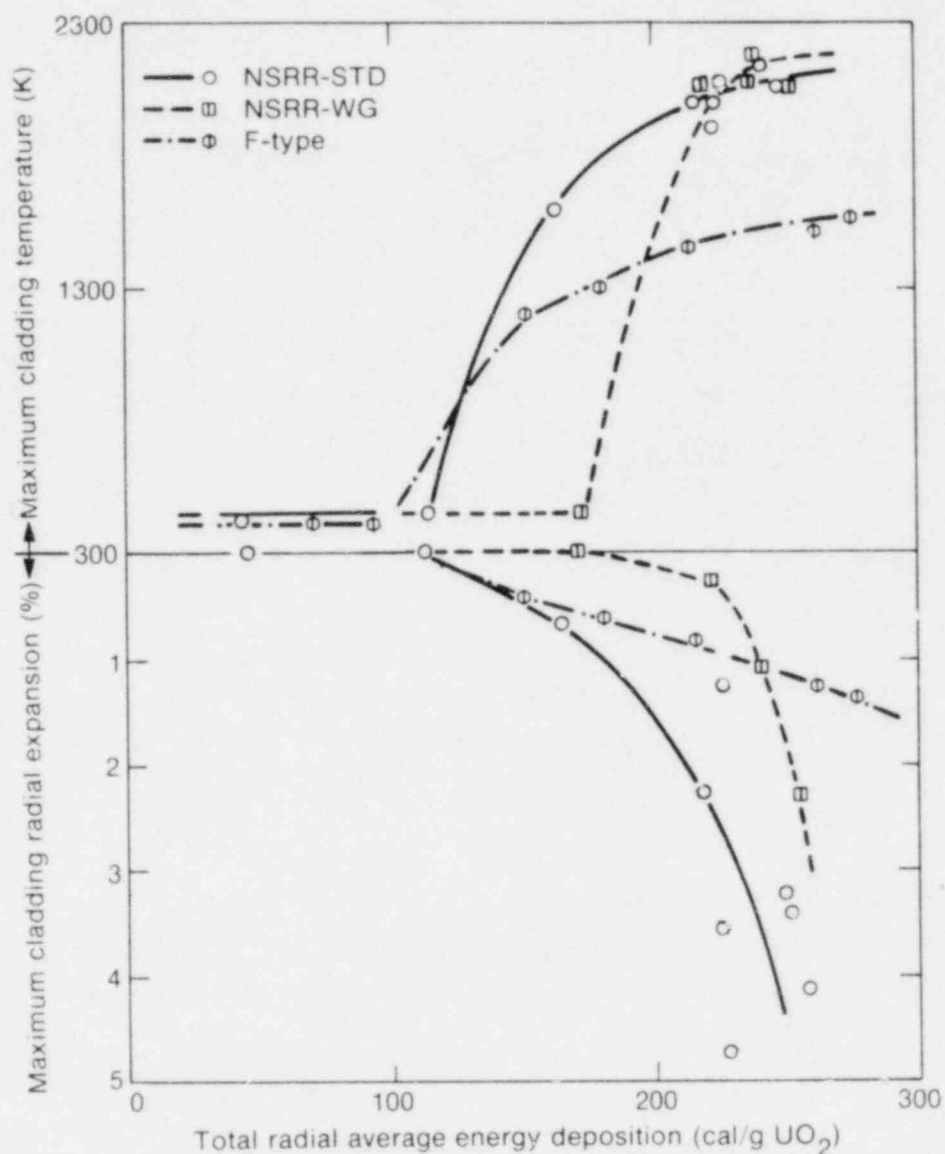
Fig. 22 Comparisons of maximum cladding temperature and cladding maximum radial expansion for different types of fuels.

For waterlogged rods, the incompressibility of water and large internal pressure generation tend to prevent gap closure. However, the higher thermal conductivity of water (about four times that of helium gas) promotes gap heat transfer. The test results exhibit improved heat transfer for waterlogged rods, in that DNB occurred at lower energy depositions for which gap closure was not predicted. High cladding temperatures and extensive cladding oxidation were not generally observed for waterlogged rods, since cladding failure and fuel expulsion typically occurred in the range of 90 to 165 cal/g UO_2.

1.3   Effects of Cladding Material

The cladding temperatures differed significantly between zircaloy and stainless steel clad fuel rods. Evaluation of the data indicates that differences in the thermal properties of

44

zircaloy and stainless steel are primarily responsible for the observed higher temperatures for zircaloy.

Thermal conductivities and heat capacities for zircaloy and stainless steel are presented and compared in Figures 23 and 24, respectively. In the temperature range of 200 to 1200 K, the thermal conductivities are nearly the same, whereas the heat capacity of Type 304 stainless steel is almost twice that of zircaloy-4 (except at the α-β phase transformation). Thus, the temperature increase of zircaloy-4 should be about twice that of stainless steel for the same heat input. At higher energy depositions, the melting temperature of stainless steel limits maximum cladding temperatures to approximately 1670 K.

Differences in the cladding temperature behavior of zircaloy and stainless steel clad rods with the same cladding thickness (0.508 mm), and both subjected to energy depositions of about 216 cal/g UO_2, are illustrated in Figure 25. During the initial 0.5 s of the temperature transient, the temperature increase of the zircaloy clad rod was about twice that of the stainless steel clad rod, as expected, based on their relative heat capacities. However, the maximum temperatures appear to be less dependent on differences in heat capacity, since the maximum temperature of the zircaloy cladding was only about 50% greater than that of the stainless steel cladding. The reasons for this behavior are not well understood.

1.4   Effects of Shrouds on Single Rods

Tests performed in the NSRR, in which NSRR-STD rods were enclosed in open-ended flow shrouds of various geometries, showed that such enclosures had little, if any, effect on maximum cladding surface temperatures. With regard to temperature behavior, the primary effect of such shrouds was to increase the time duration of film boiling during the tests from about 5 s to as much as 15 s.

1.5   Fuel Rod Clusters

Maximum cladding temperatures of rods tested in clusters of five, both with and without shrouds, were approximately the same as those for comparable tests with single rods. Cooling by the primary mechanisms of natural convection and radiation is reduced for clusters, particularly those with shrouds, when the fuel rod surfaces are in film boiling. The external heat transfer configuration, however, seemed to have a relatively small effect on maximum cladding temperatures for the CDC and NSRR tests in a stagnant coolant. The presence of a shroud around a five-rod cluster increased the time duration of film boiling as did a shroud in the single-rod tests.

1.6   Mixed Oxide Fuels

Maximum cladding temperatures for mixed-oxide-rod tests in the CDC were somewhat lower than for similar UO_2 rods (the mixed oxide fuel consisted of a mixture of PuO_2 particles and natural UO_2). Most of the fissions occurred in the PuO_2 particles and the
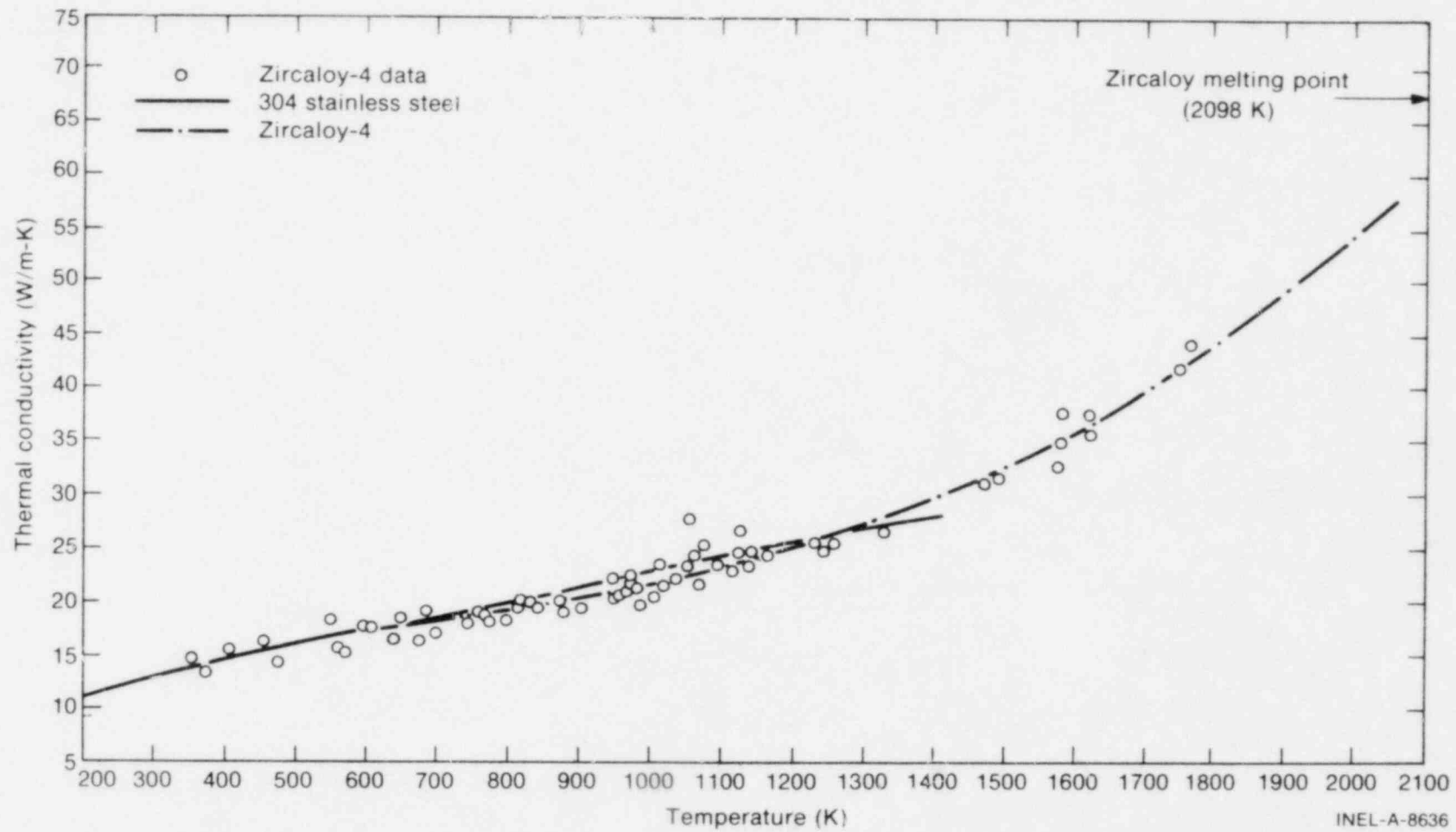
Fig. 23 Comparisons of thermal conductivities between zircaloy-4 and Type 304 stainless steel.
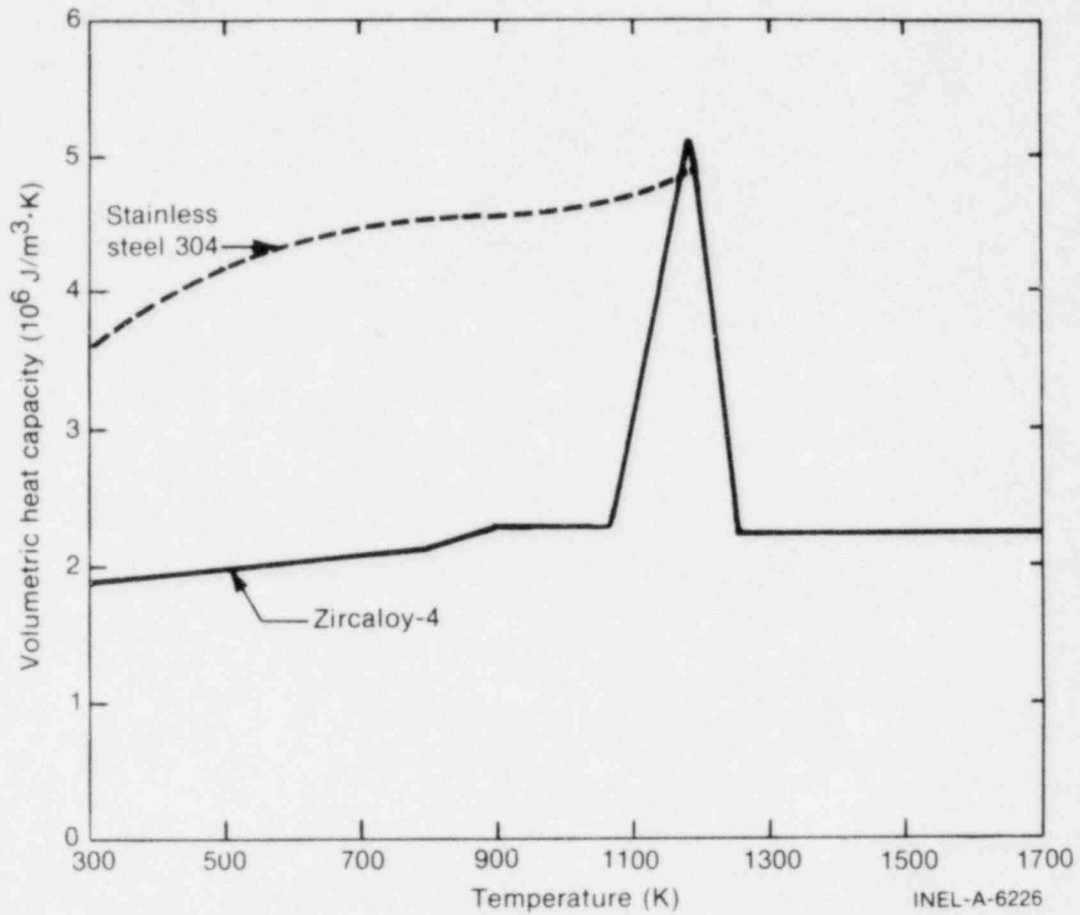
Fig. 24 Volumetric heat capacity of zircaloy-4 and Type 304 stainless steel.
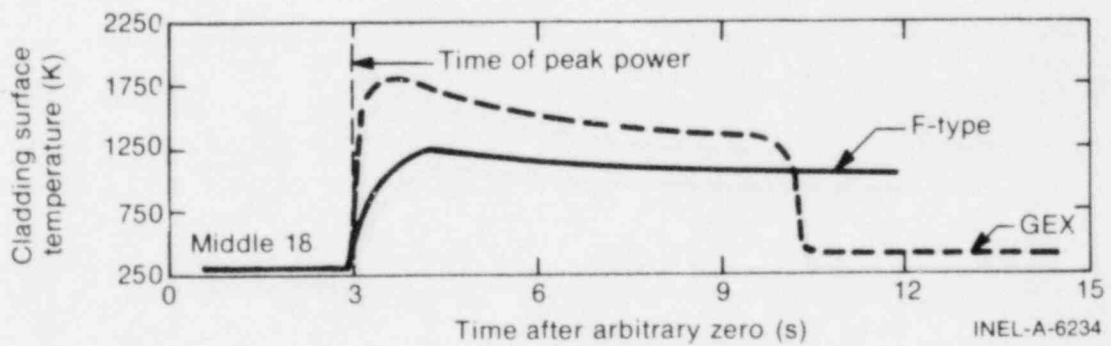
Fig. 25 Comparison of temperature histories of zircaloy clad fuel (GEX) and stainless steel clad fuel (F-type) at the same energy deposition of 216 cal/g UO_2 (tests in the CDC).

energy produced had to be transferred to the surrounding fuel matrix before being transferred to the cladding. This additional thermal resistance within the pellet appears to have decreased the effective pellet thermal conductivity, thus causing lower cladding temperatures than for UO_2 fuels tested at comparable energy depositions. Cladding surface temperature histories are compared in Figure 26 for mixed oxide and UO_2 fuel rods, each of which received energy depositions of about 225 cal/g of fuel. Both the GEXPR and GEXPR-CH mixed oxide rods exhibited a short interval of nucleate boiling prior to DNB, whereas the GEX UO_2 rod proceeded immediately into film boiling and attained the highest maximum temperature.
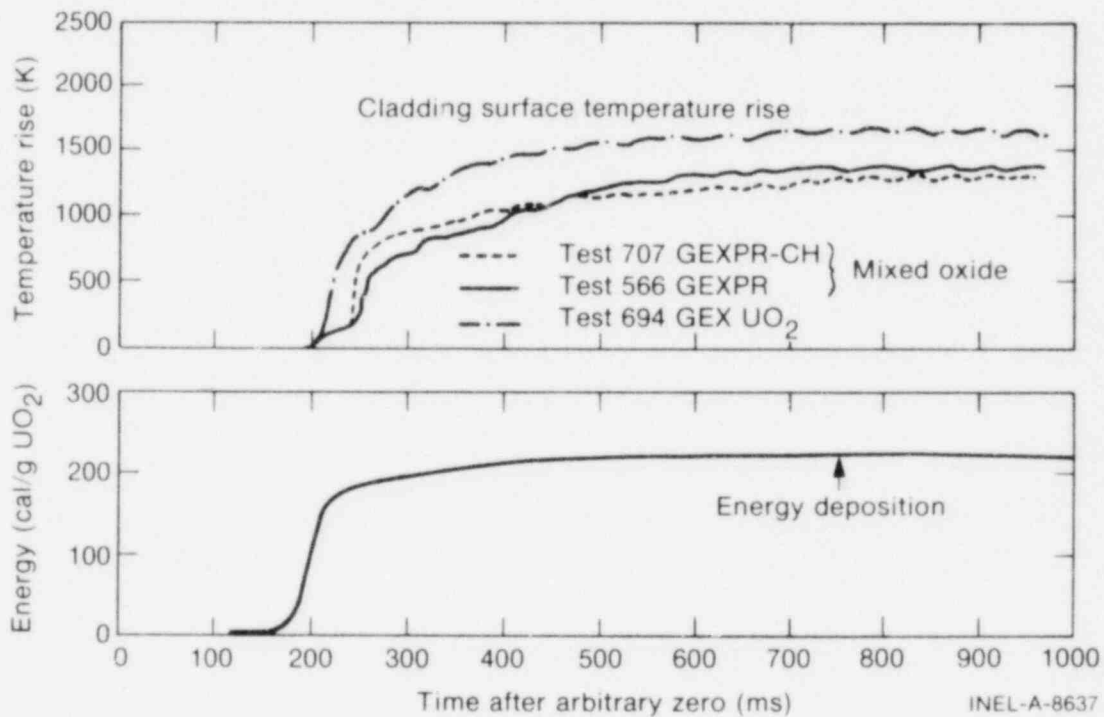
Fig. 26 Comparison of the cladding surface temperature rises in GEX, GEXPR, and GEXPR-CH rods during CDC tests in which energy depositions of about 225 cal/g of fuel were deposited at the axial flux peaks in the rods.

2. ANALYSIS OF CLADDING AND FUEL DEFORMATIONS

Cladding and fuel deformation data from tests with several rod types in the CDC and NSRR are correlated and analyzed in this section. Radial and axial elongations are discussed, with both transient and residual deformations evaluated to determine the relevant elongation mechanisms and the effects of fuel design and initial parametric variations on the radial and axial elongations. The data considered were obtained from rods that did not break up (that is, subjected to reactivity insertions generally below 300 cal/g UO_2).

2.1 General Trends

The residual radial and axial cladding deformation measurements for the CDC and NSRR experiments which used rods that were not prepressurized are shown as a function of radial average energy deposition in Figures 27 and 28, respectively. Both figures indicate a separation of the data into two groups (unirradiated and preirradiated or waterlogged), each of which exhibits distinct behavior with respect to energy deposition.

For unirradiated rods, the radial deformation data shown in Figure 27 began to increase in the range of 130 to 160 cal/g fuel. Maximum measured deformations of about 10% are observed at energy depositions greater than about 220 cal/g fuel. For preirradiated and waterlogged rods, cladding ballooning is observed at low energy depositions in the range of 50 to 70 cal/g fuel. Radial deformations in excess of 10% occur at energy depositions greater than about 160 cal/g fuel. The unirradiated rod axial elongation data of Figure 28 show trends similar to the radial deformation data for unirradiated rods, but the values are less than one-half of those for the radial deformations. The preirradiated and waterlogged rods axial elongation behavior is quite different from that of the unirradiated rods, however. Residual elongations of preirradiated and waterlogged rods were either negative or very small, with the exception of one GEX preirradiated rod that had a residual elongation of about 5% following a test at about 350 cal/g fuel.

2.2 Radial Deformation of Unirradiated Fuel Rods

For most of the unirradiated rods used in both the CDC and NSRR experients, the as-built internal gas pressure was one atmosphere (this is the data shown in Figures 27 and 28). On the basis of ideal gas law calculations, the internal pressure during these tests should not have exceeded ten atmospheres, which would not deform the cladding. Therefore, fuel pellet thermal expansion was the predominant cause of the cladding strain observed.

Calculations have been made to compare the cladding radial deformation with the fuel thermal expansion. Fuel-cladding gap width was taken into account for pellet fuels by assuming that the pellets would expand freely before contacting the cladding. After gap closure, the cladding radial deformation was assumed to be equal to the fuel pellet thermal expansion. Fuel pellet compression was assumed to be negligible. Powder fuels have no as-built fuel-cladding gap, but the lower density vipac fuel has voids that should be easily

49
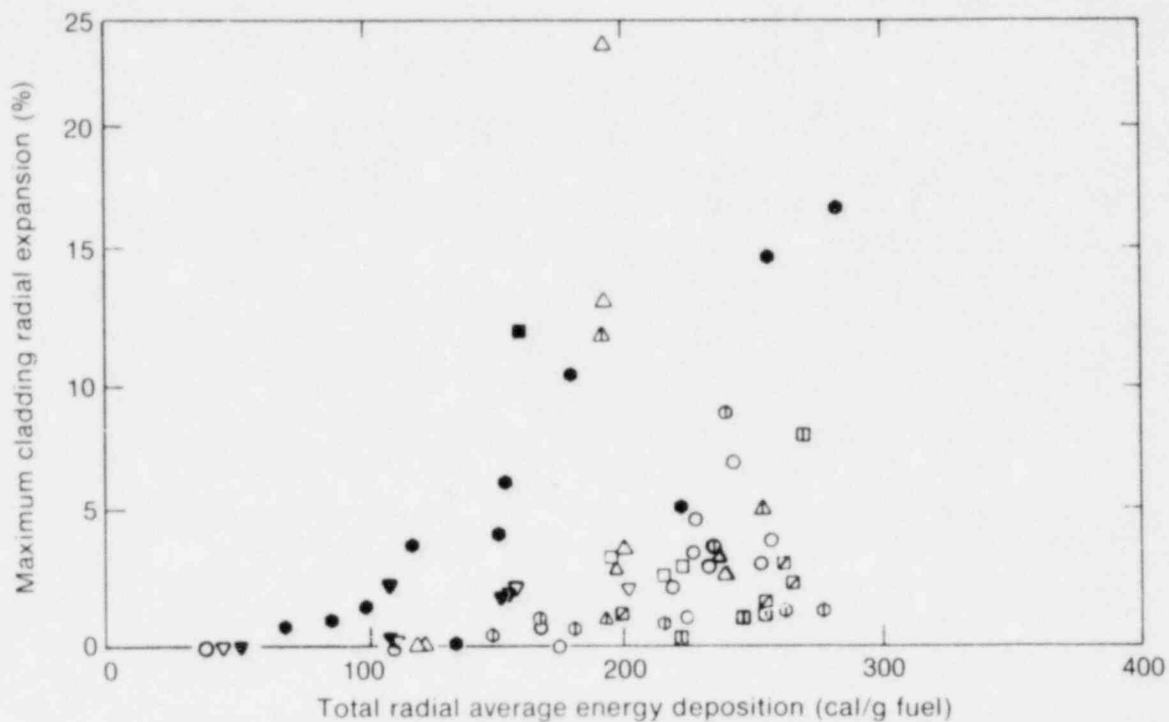
Fig. 27 Cladding radial expansion as a function of radial average energy deposition.

CDC zircaloy cladding

Φ SPXM
□ GEX-pellet
▨ GEX-powder
▧ GEXPR
■ GEX-preirradiated
△ GEP-pellet
▲ GEP-powder
▲ GEP-preirradiated

CDC stainless steel cladding

o SPX
Φ F-type
● F-type-waterlogged

NSRR zircaloy cladding

o NSRR-STD
⊞ NSRR-WG
▽ JPDR-II
▼ JPDR-II-waterlogged
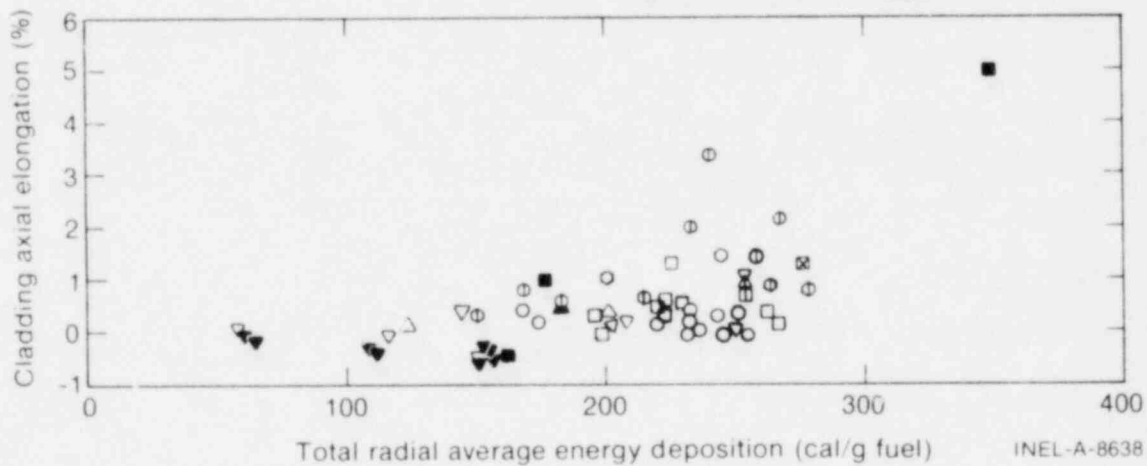
INEL-A-8638

Fig. 28 Cladding axial elongation as a function of radial average energy deposition.

50

deformed by compression forces. To estimate the effect of powder fuel expansion on cladding deformation, the fuel was assumed to be compressed to the same effective density as that of pellet fuel. No mechanical deformation of the cladding was assumed during the fuel compression period.

The sum of the unrestrained portion of fuel expansion and the observed cladding deformation, ϵ, was therefore calculated using the following equations:

Pellet Fuel

$$\epsilon = \epsilon_m + \frac{\Delta r}{r} \times 100 \tag{1}$$

Powder fuel

$$\epsilon = \epsilon_m + \frac{1}{3} \times \frac{\rho_o - \rho_p}{\rho_o} \times 100 \tag{2}$$

where

ϵ_m = measured cladding radial expansion (%)

Δr = gap width (mm)

r = pellet radius (mm)

ρ_p = powder fuel density

ρ_o = assumed density to which powder fuel is fully compressed (=94%).

The results of these calculations were compared with the thermal expansion curve of UO_2, as shown in Figure 29. Relatively good agreement is noted between the experimental data from several fuel types and the calculated UO_2 thermal expansion curve. The large increase in cladding deformations at approximately 230 cal/g UO_2 could be an indication of the effects of internal gas pressure acting on high temperature cladding or the effects of large fuel volume changes accompanying the beginning of fuel melting, or both.

The conclusion that can be reached from the previous discussion is that the radial cladding deformation of unirradiated rods which were not prepressurized was primarily caused by fuel thermal expansion. Further, the amount of deformation was comparable with the amount of fuel thermal expansion occurring after fuel-cladding contact for pellet fuels, and after full compression for powder fuels.

2.3 Axial Elongation of Unirradiated Fuel Rods

Cladding axial elongation is less dependent on fuel thermal expansion than the radial deformations because of axial slippage between the fuel and cladding during power

51
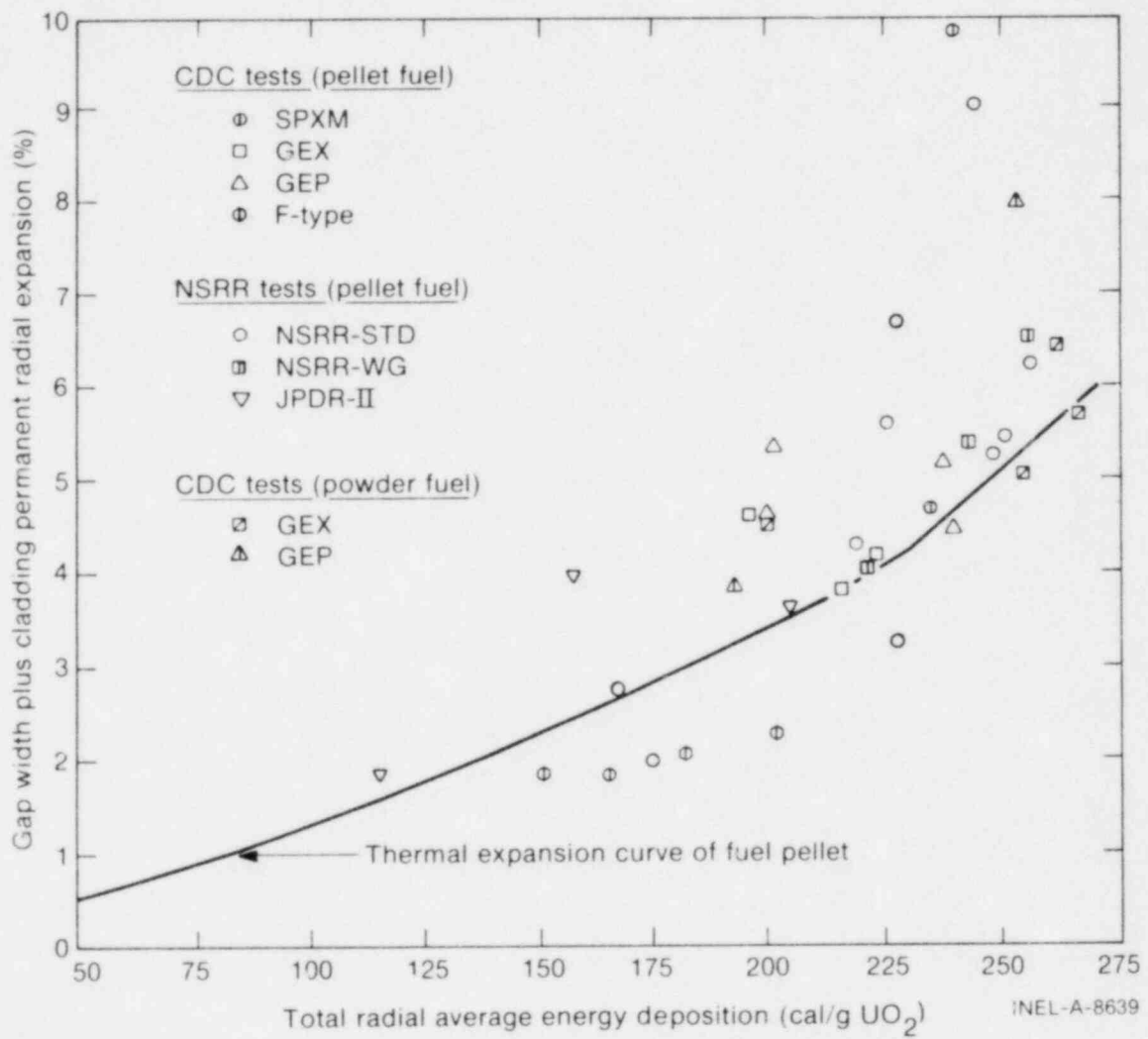
Fig. 29 Comparison of cladding radial expansion with thermal expansion of the fuel.

52

excursions. Figures 30 and 31 show the measured axial elongations of the fuel and cladding and other pertinent measured variables versus time for two different time scales during CDC Test 694 with a GEX pellet fuel rod. During the initial portion of the test, as shown in Figure 30, cladding elongation began about 50 ms after the initiation of fuel displacement; the delay is believed due primarily to the time required for gap closure. The slower rate of cladding elongation compared with fuel displacement indicates slippage of the fuel-cladding interface. The long-term behavior (Figure 31) shows that after reaching maximum displacements, both the fuel and cladding axial elongations decreased with decreasing cladding temperature (top and bottom thermocouples were 5.4 cm above and below the location of the middle thermocouples).

Residual and maximum axial elongations of the cladding were compared with the fuel expansion curve in the same manner as previously described for radial deformations
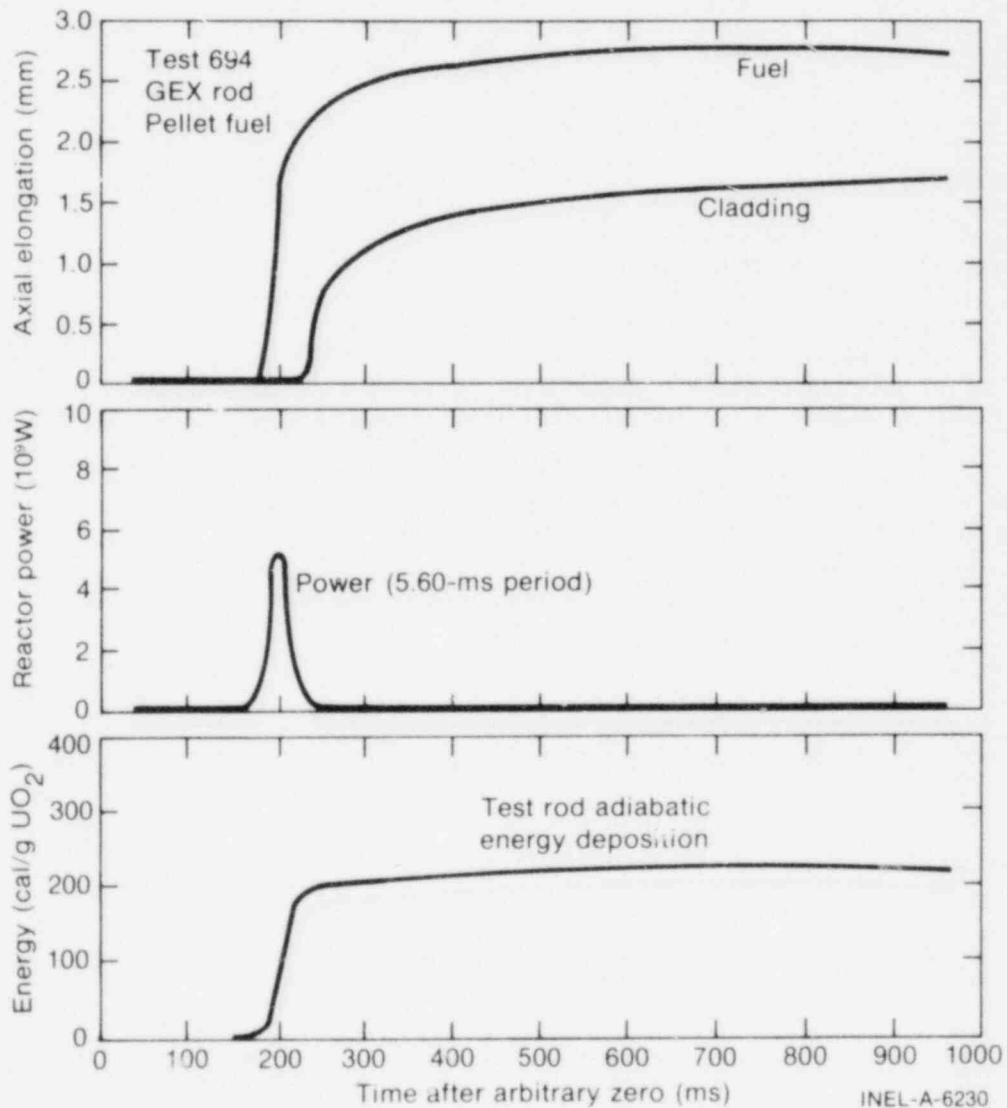
Fig. 30 Test rod energy deposition, reactor power, and axial displacement of the fuel and cladding during Test 694 (233 cal/g UO$_2$) with a GEX pellet rod in the CDC.
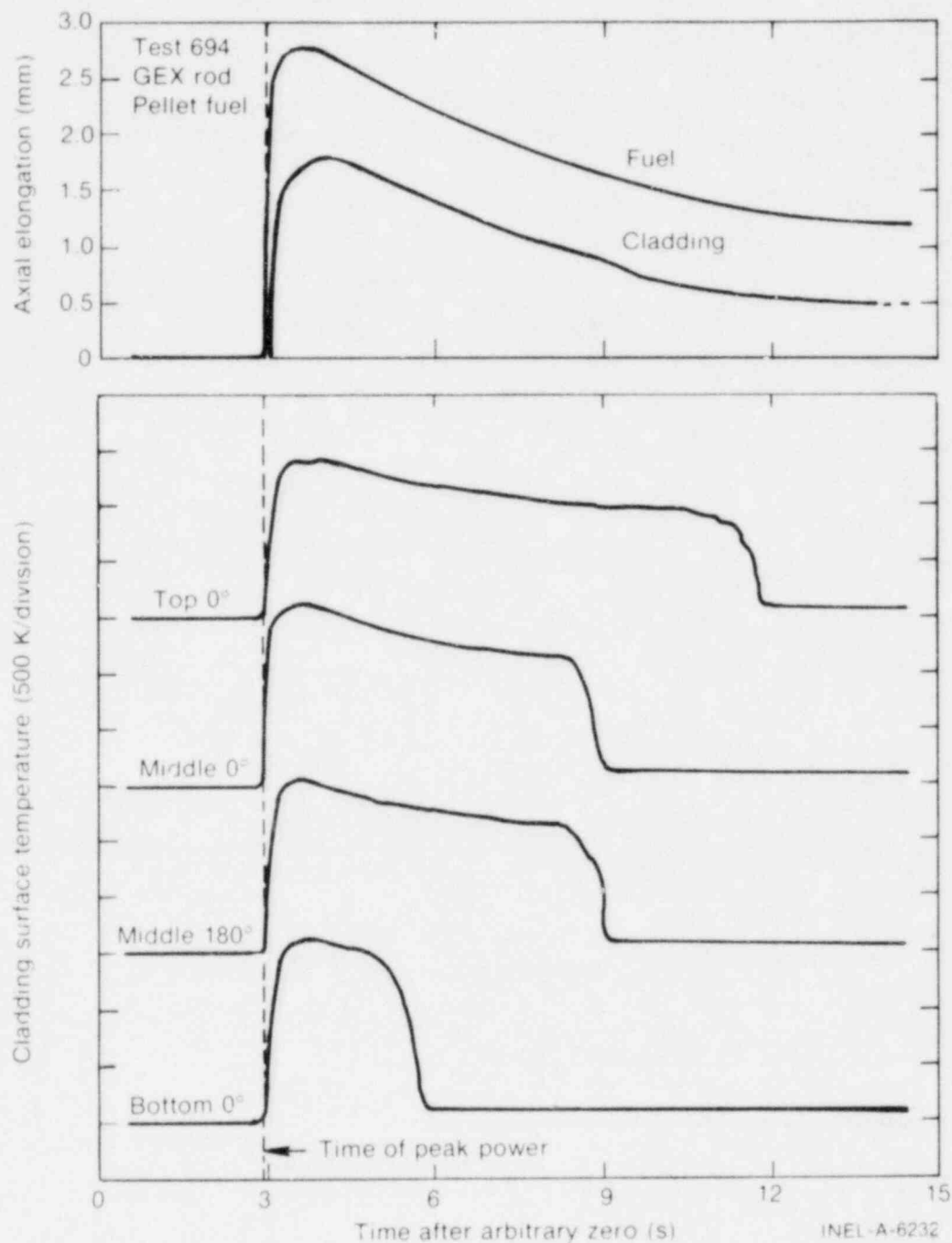
Fig. 31 Cladding surface temperature rise and axial displacement of the fuel and cladding during Test 694 (233 cal/g UO_2) with a GEX pellet rod in the CDC.

(Section III-2.2). Figure 32 shows the measured cladding elongation and the calculated free thermal expansion of the fuel as a function of energy deposition. The cladding elongations agree reasonably well with the total thermal expansion of the fuel stack for energy depositions less than about 150 cal/g UO_2. At higher energy depositions, the cladding elongations are generally less than the fuel stack axial elongation calculation, indicating the effect of fuel-cladding slippage.

54
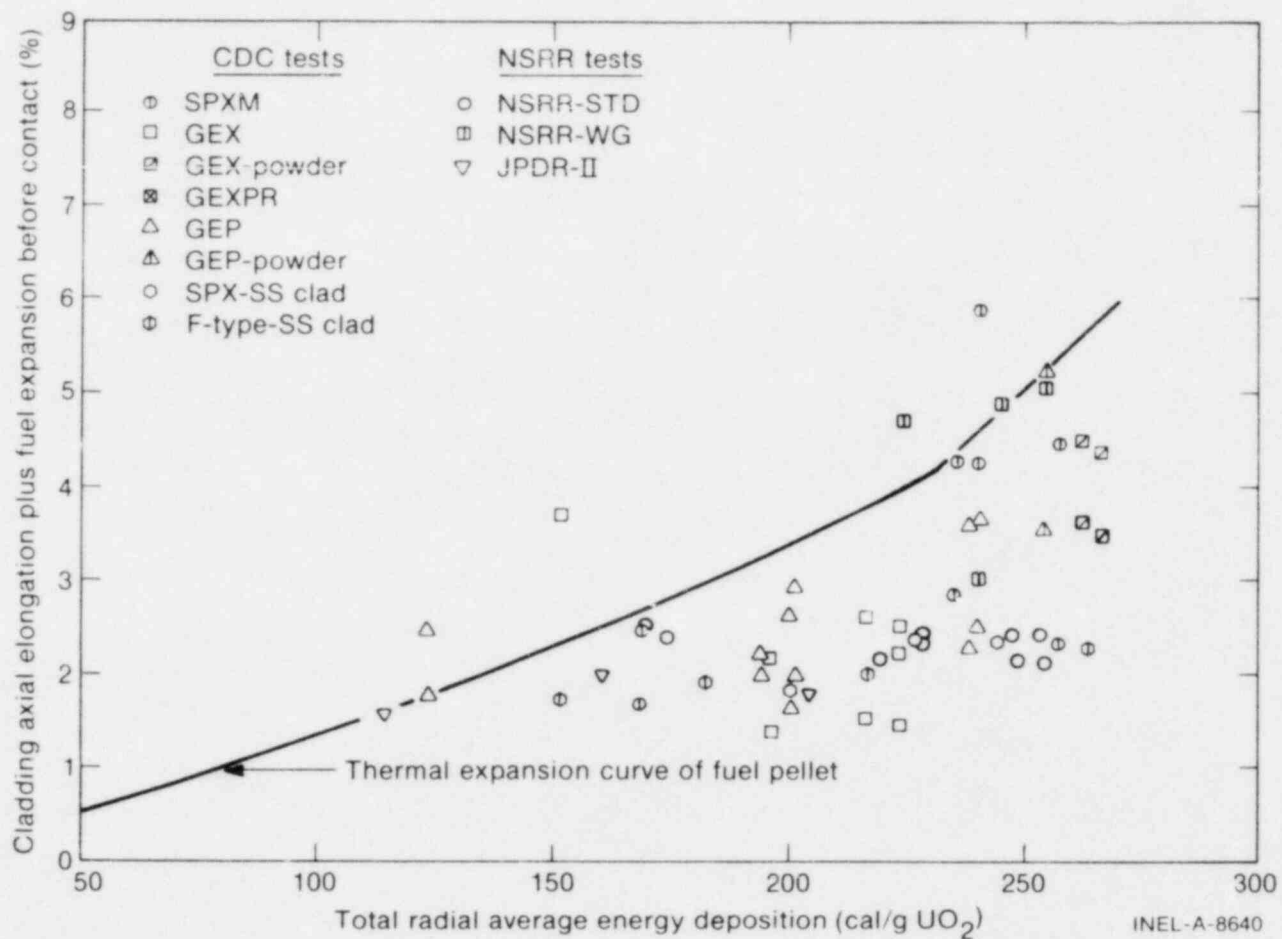
Fig. 32 Comparison of cladding elongation with fuel thermal expansion.

INEL-A-8640

55

2.4 Radial and Axial Deformations of Waterlogged and Preirradiated Rods

As discussed in Section III-2.1, waterlogged and preirradiated rods exhibited much larger radial cladding ballooning than did unirradiated rods. Also, axial elongations for waterlogged and preirradiated rods were either slightly positive or negative. These trends are believed to be a result of significantly higher internal rod pressures. For example, a maximum internal pressure of 54 MPa was measured in one NSRR waterlogged rod test at 150 cal/g UO_2. Both the waterlogged and preirradiated rods failed by cladding rupture, with no evidence of cladding melting. This failure mode differs from that observed for unirradiated rods, which failed by cladding melting or embrittlement. Radial cladding deformations at energy depositions greater than about 200 cal/g UO_2 exceeded 10%, which could not be attained by fuel thermal expansion alone. Therefore, these results indicate that internal pressure was more significant than fuel thermal expansion in causing cladding deformation of waterlogged and preirradiated rods for energy depositions greater than about 200 cal/g UO_2. Prompt and large pressure increases, particularly in waterlogged rods, may occur during the early stages of a transient. Increased pressure would prevent the pellet-cladding contact and resultant cladding axial elongation, which would explain the axial shrinkage and small positive elongations observed in waterlogged rod tests.

If the water or gas in the gap prevents fuel-cladding contact, the cladding will shrink axially according to Poisson's ratio for the material to compensate for the radial expansion. It should, therefore, be possible to correlate the negative axial elongations for waterlogged rods to their radial deformations through Poisson's ratio. Figure 33 shows cladding radial and axial deformation data for JPDR-II waterlogged fuels as a function of energy deposition. The amount of radial deformation is compared with the calculated radial thermal expansion of UO_2, with good agreement noted. The axial contraction data for JPDR-II fuels are compared with the calculated axial shrinkage based on a Poisson's ratio of 0.28 for zircaloy. The cladding axial contraction is overestimated, which is an expected
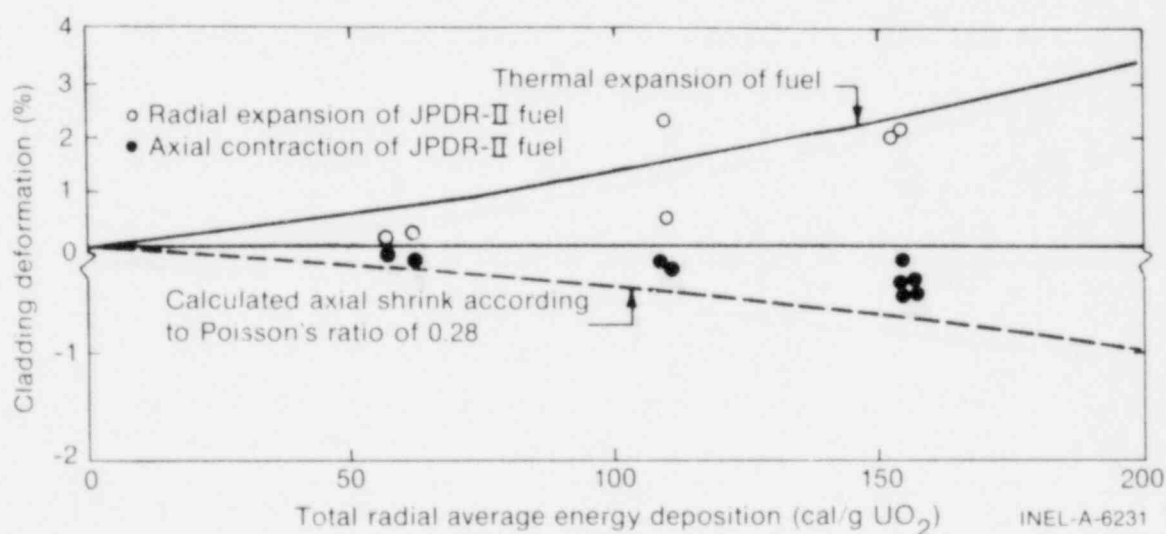
Fig. 33 Comparison of cladding radial expansion data with estimated thermal expansion of fuel (upper half), and comparison of cladding axial shrinkage data with estimated shrinkage curve (lower half) in waterlogged JPDR-II rod tests in the NSRR.

trend because the radial deformations (ballooning) were of a barrel shape. Uniform radial deformations over the active fuel length would have resulted in axial shrinkage of about twice that observed. Therefore, the comparisons shown in Figure 33 indicate that, for energy depositions below about 150 cal/g UO_2 in waterlogged rods, the cladding radial expansion was a direct result of fuel thermal expansion, and the axial elongation behavior can be related to the radial expansion through Poisson's ratio.

3. INCIPIENT FAILURE OF UNIRRADIATED UO_2 RODS

Observed failure modes and thresholds for unirradiated, zircaloy clad, UO_2 rods are discussed in this section, with differences and similarities examined and correlated for several fuel designs. All tests considered were performed in the CDC and NSRR test facilities on single, unpressurized rods without shrouds, in stagnant water at atmospheric pressure and ambient temperature. The discussion is confined primarily to the enthalpy region near the initial failure threshold. Certain aspects of the failure behavior described for the baseline fuels in Sections II-1.1 and II-1.2 are addressed in more detail and extended to other similar fuel designs.

3.1 Failure Modes

No apparent damage occurred to rods for energy depositions up to about 120 cal/g UO_2. For energy depositions greater than about 120 cal/g UO_2, DNB occurred at the cladding surface. DNB resulted in oxidation of the cladding surface, the extent of which increased with increasing energy depositions. The first evidence of cladding failure, termed incipient failure, generally occurred at about 240 cal/g UO_2. High energy depositions caused breakup of the test rods into progressively smaller pieces, and eventually into fine fragments. The behavior at high energy depositions is treated in detail in Section III-4.

Cladding melting, cracking, and low pressure rupture were all observed in varying degrees for tests conducted slightly beyond the incipient failure threshold with unirradiated, unpressurized zircaloy clad rods. Pellet-fueled SPX, SPXM, GEX, and NSRR rods appeared to have first failed by circumferential cracking of the cladding. Postirradiation examination (PIE) photographs showed the fractured cladding surfaces to be rugged and sharp-edged with no apparent decrease in thickness, even where cladding melting occurred. Extensive surface oxidation and at least partial melting of the inner cladding surface occurred in all cases. The condition of the cladding was such that additional cracks or breaks often occurred during posttest disassembly operations. The cladding metallurgical analyses discussed in Section II-1.2 show oxygen intrusion, and consequent cladding embrittlement, for tests performed near the failure threshold. Therefore, the incipient failure of these types of rods is postulated to have occurred by axial and bending forces acting on embrittled cladding, probably during the quenching or cooldown cycle of the transient. Forces were probably generated by fuel-cladding interactions, thermal shocks, or radial and axial temperature gradients during quenching.

57

Low pressure rupture (internal pressure coupled with high cladding temperature) appeared to be the prevalent cause of initial failure of the GEX-powder and the GEP-powder and -pellet-fueled rods. The cladding was locally swollen at the failure point, with the opening generally in the form of an axial split, as opposed to the melting and circumferential cracking typical of the other rod types. Low pressure rupture was also observed from high speed photography of the TREAT tests. Rods that failed by low pressure rupture also showed some evidence of circumferential cracking. Thus, the mechanisms for cladding embrittlement and low pressure rupture were both apparently active for tests with GEX-powder and GEP-powder and -pellet rods conducted at or slightly above the incipient failure threshold.

Both the powder-fueled GEX and GEP rods and the pellet-fueled GEP rods contained comparatively larger initial gas volumes within the fuel region than the pellet-fueled SPX, SPXM, GEX, and NSRR rods. The gas was distributed throughout the vipac powder fuel in the GEX and GEP rods and between the dished-end pellets used in the GEP rods. The pressure produced by heating the gas within the fuel in these rods (powder-fueled GEX and GEP rods and pellet-fueled GEP rods) may have produced comparatively higher internal pressure, thus causing the observed low pressure ruptures.

3.2 Failure Thresholds

Figure 34 illustrates the comparative failure behavior of several types of rods tested in the CDC and NSRR. The total energy deposition provide approximate bounds on the threshold of failure for each rod type. For rods that did not fail, the highest attained total energy deposition without failure is an approximate lower bound on the failure threshold. For rod that did fail, the lowest attained total energy deposition resulting in failure is an approximate upper bound on the threshold. Since there is no overlap of failures and nonfailures for tests on the same type of fuel rods, the minimum energy deposition difference between failures and nonfailures should be a low multiple of the uncertainty in the failure threshold.

For example, the GEX pellet rods failed during all tests with energy depositions greater than 256 cal/g UO_2 and did not fail in any test with energy depositions less than 233 cal/g UO_2. Assuming that σ is no larger than half the difference between these energies, the test data imply that the standard deviation of the energy deposition required for failure is no larger than 17 cal/g UO_2. The average of the standard deviations for GEX, SPX, and SPXM rods is 16 cal/g UO_2.

If the best value for the energy deposition at failure of a given rod type is taken to be halfway between the upper and lower bounds, established by the data presented in Figure 34, the energies at failure vary from 218 cal/g UO_2 for SPX pellet rods to 279 cal/g UO_2 for GEX powder rods. The difference, 61 cal/g UO_2, is considerably larger than the uncertainty for the individual rods.

The NSRR results also indicate a small uncertainty in threshold energy for two rod designs tested to date. Rods of standard design failed at 264 and 270 cal/g UO_2, but not at
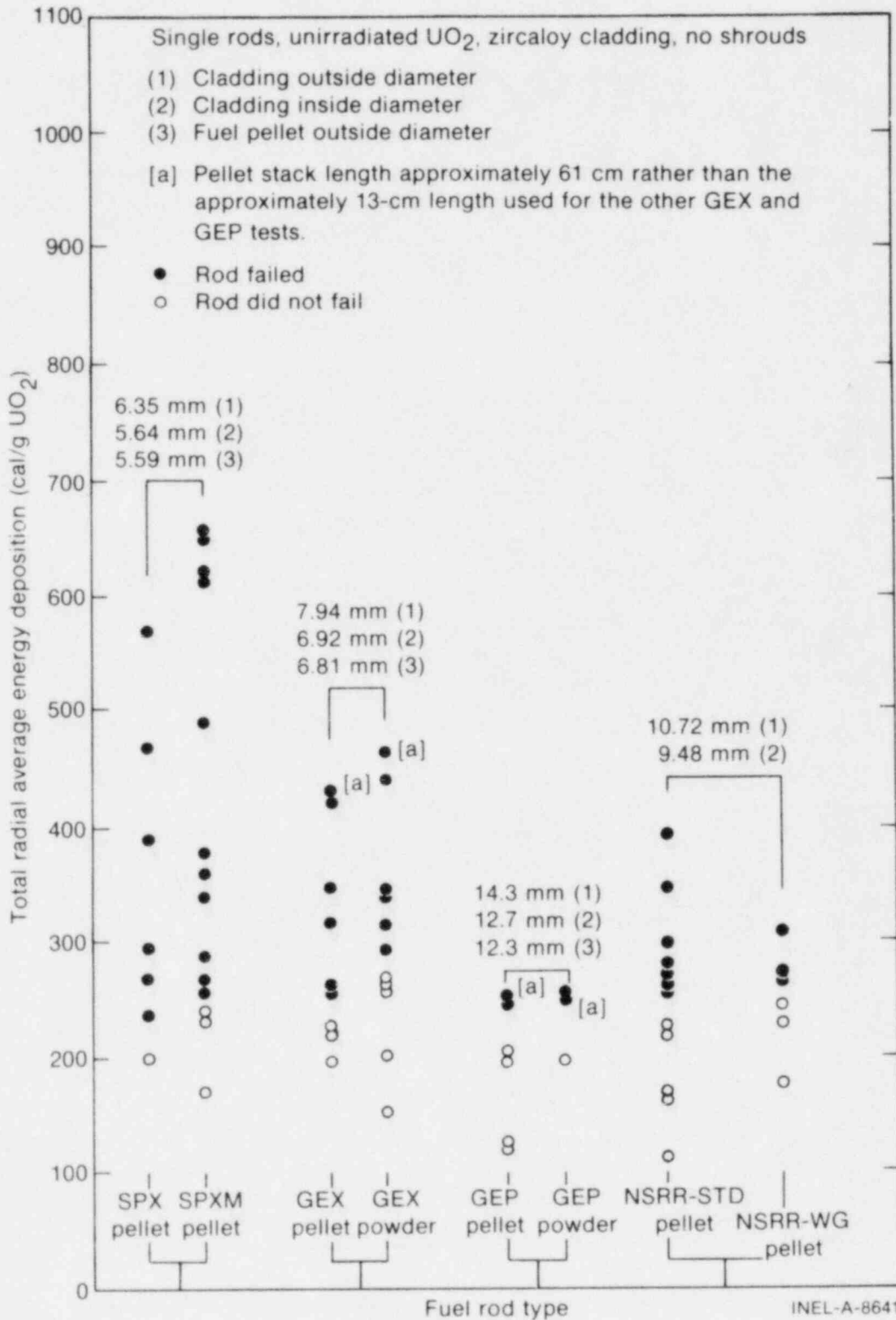
Fig. 34 Failure behavior of CDC and NSRR test fuels in terms of radially averaged total energy deposition.

244 cal/g UO_2. Rods of similar design but with a wider gap failed at 274 cal/g UO_2, but not at 261 cal/g UO_2.

Figure 35 shows the maximum cladding surface temperature as a function of the radial average energy deposition in the unirradiated, zircaloy clad CDC rods. With one exception (Test 432, in which fracture occurred about 25.4 cm above the bottom of a SPX fuel rod), rod failures in the energy deposition range up to 375 cal/g UO_2 occurred only when cladding temperatures exceeded 2008 K. Rods containing powder fuel exhibited lower cladding temperatures than pellet-fueled rods under the same conditions, and, consequently, had higher failure thresholds. For the static coolant CDC tests, the thermocouple measurements showed excellent correlation with cladding integrity in this energy deposition range.

If rod failure at low and moderate energy depositions is controlled by the cladding temperature, the radial average energy deposited per unit mass of fuel may not be the most appropriate independent parameter in all cases. Extensive computer calculations have shown that in RIA experiments of the type carried out in the CDC and NSRR, the energy deposited near the outside edge of the pellet is the primary heat source for cladding melting, whereas the energy deposited in the interior of the fuel is not conducted to the cladding surface until well after the maximum cladding temperature is reached. An estimate of the energy deposition at the fuel surface can be obtained by multiplying the average radial energy deposition by the peak-to-average radial power density (which is a function of pellet enrichment). The effects of differences in fuel density, which varied from about 83% theoretical density for vipac powder-fueled rods to about 95% theoretical density for pellet-fueled rods, can be taken into account by converting the energy deposition data to a
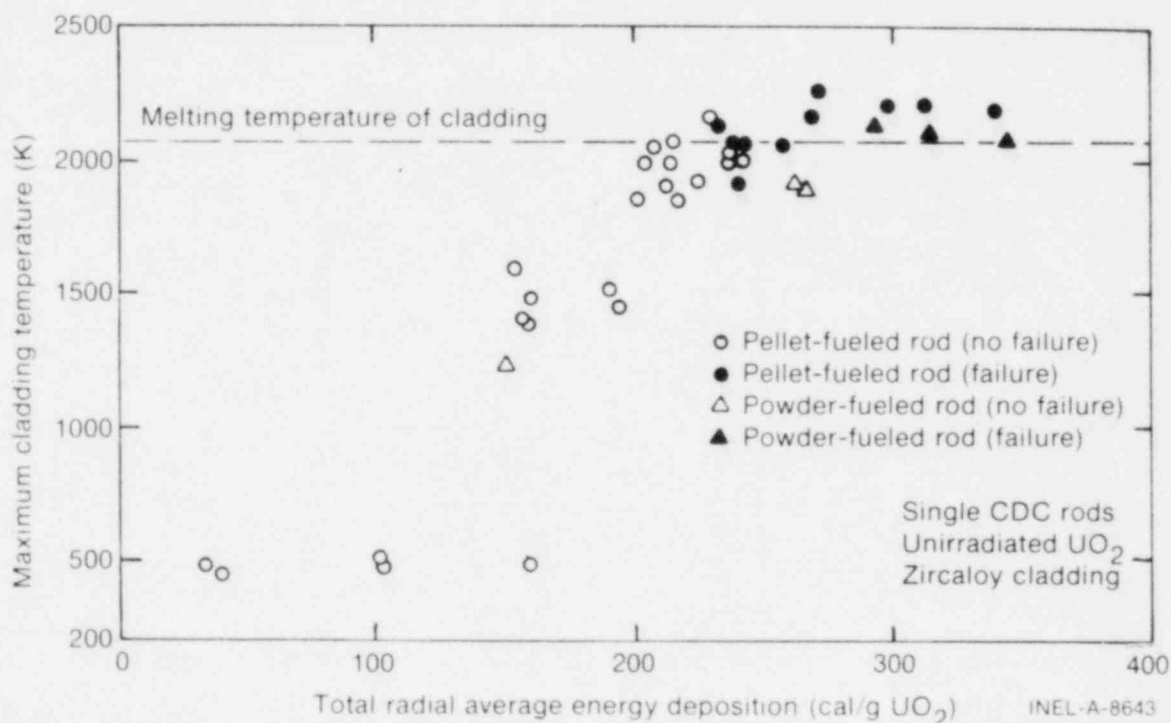
Fig. 35 Maximum cladding temperature as a function of radial average energy deposition (CDC tests rods).

volumetric basis. With these changes, the failure threshold behavior of the various test fuels can be considered in terms of peak energy deposition per unit volume of fuel near the pellet surface; a parameter that should be strongly related to cladding temperature.

Figure 36 shows the maximum cladding surface temperature data (from Figure 35) displayed as a function of peak energy deposition per unit volume at the fuel surface. The correlation is improved near the failure threshold, with no distinguishable differences between powder and pellet fuel. Subsequent correlations in Section III, therefore, use the parameter peak energy deposition at the fuel surface in terms of calories per unit volume (or unit mass), where considered appropriate.

Figure 37 shows the failure behavior data of Figure 34 replotted in terms of peak energy deposition per unit volume at the fuel surface. The high energy deposition data (above about 350 cal/g UO_2) have been deleted and the failure modes, cladding cracking or low pressure rupture, are shown. As illustrated, a peak energy deposition value of 2950 cal/cm^3 UO_2 is reasonably representative of the initial failure threshold for the various types of CDC test rods, whereas a value of 3350 cal/cm^3 UO_2 more nearly represents the initial failure threshold for NSRR test rods.

All 13-cm CDC rods, with the exception of GEP-pellet rods, failed when the peak energy deposition at the fuel surface exceeded 2950 cal/cm^3 UO_2, and no 13-cm rods failed below this value. Failure of GEP-pellet rods was first observed at about 3170 cal/cm^3 UO_2, with no failure occurring at 3080 cal/cm^3 UO_2. The only CDC rod that failed below 2950 cal/cm^3 UO_2 was a SPX test rod (46-cm active length), which failed at 2600 cal/cm^3 UO_2.

A higher initial failure threshold is indicated by the 13-cm NSRR-STD and NSRR-WG rods tested in the NSRR, in that all rods tested above 3350 cal/cm^3 UO_2 failed, whereas none failed below this value.

No apparent reason exists for the observed difference between the initial failure thresholds for rods tested in the CDC compared with rods tested in the NSRR. Similar energy deposition calibration methods (fission product analyses) were ostensibly used in each facility, but the test results indicate the possible presence of a systematic calibration error. The ±12% error band shown with each set of data in Figure 37 was determined to be the uncertainty in absolute energy deposition for CDC test rods. The illustrated overlap in error bands for the CDC and NSRR test results indicates that the noted differences may not be statistically significant.

The failure mode designations in Figure 37 illustrate that, with the exception of GEP-pellet rods, all other pellet rods first failed by cladding cracking (generally combined with partial cladding melting). With the exception of SPX rods, the failure mode for pellet rods changed to low pressure rupture at higher energy depositions.

All of the SPX rods tested failed by brittle fracture, including the previously mentioned failure at 2600 cal/cm^3 UO_2. The behavior of the SPX rods might have been
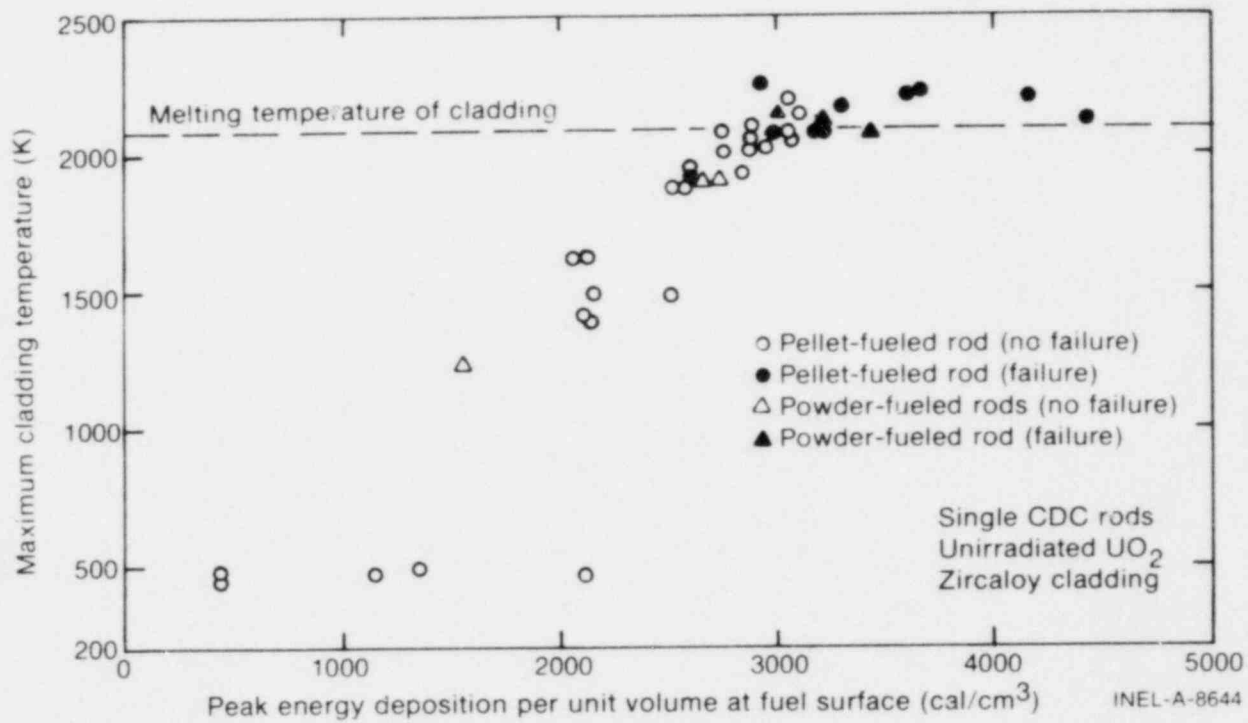
Fig. 36 Maximum cladding temperature as a function of peak energy deposition per unit volume (CDC test rods).
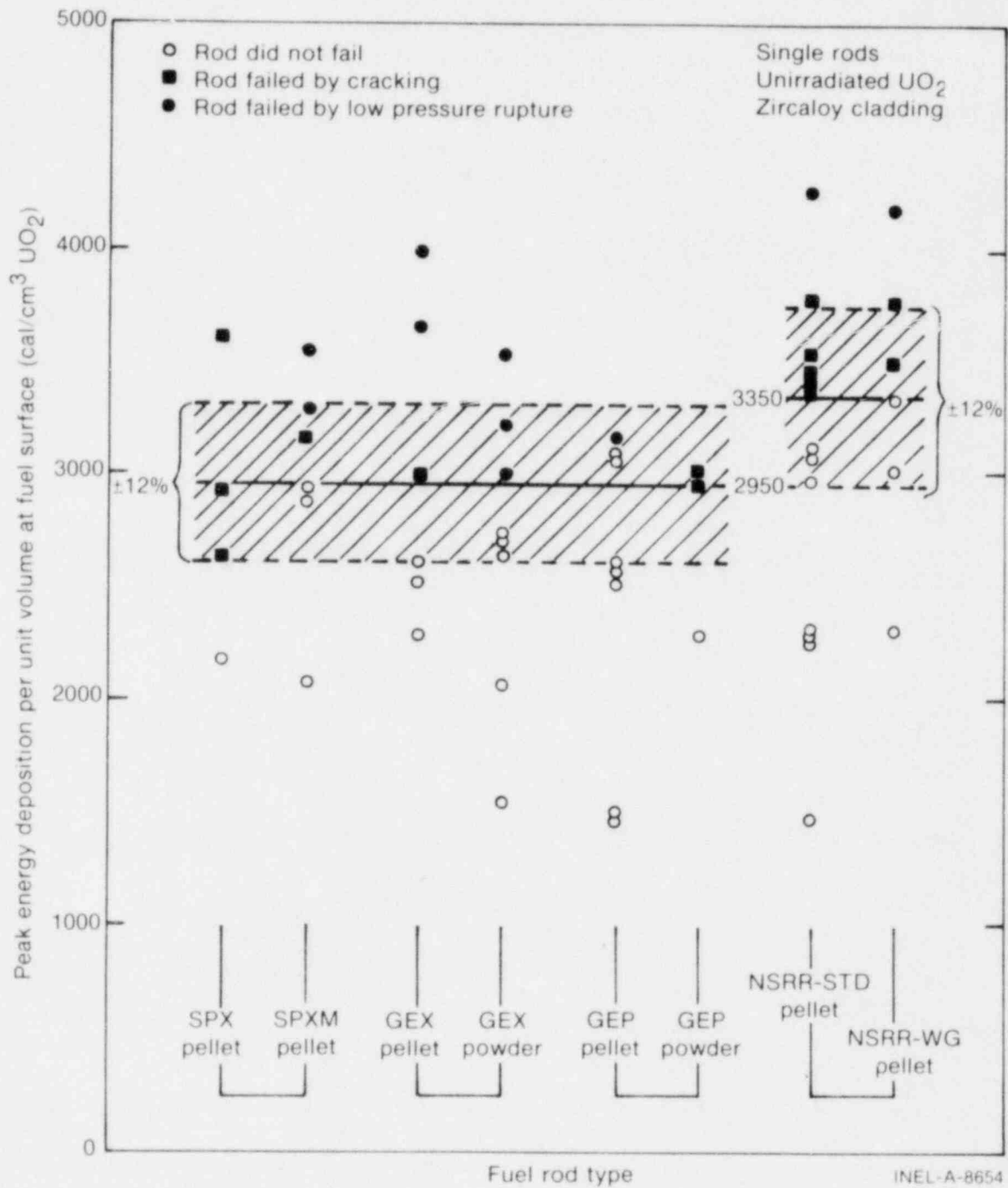
Fig. 37 Failure behavior of CDC and NSRR test fuels in terms of volumetric peak energy deposition at the fuel surface.

63

influenced by their radial and axial dimensions. Of the pellet-rod types tested near the failure threshold, the SPX rod had the smallest ratio of gap width to pellet radius (0.008) and the largest active length to diameter ratio (72). These dimensional characteristics would be expected to result in stronger pellet-cladding mechanical interaction and larger bending forces in the SPX rods under transient conditions than in the other rod types tested. Such effects may have contributed to the brittle failure (circumferential crack) of the SPX rod at the unusually low value of 2600 cal/cm^3 UO$_2$, and to the apparent preferential failure of SPX rods by brittle fracture at energy depositions well beyond the failure threshold.

No brittle fracture failures occurred in tests of powder-fueled rods and GEP-pellet rods. As discussed in Section III-3.1, the low pressure failures of these rods may be related to their larger initial gas volumes compared with the other test rod types.

4. HIGH ENERGY FAILURE BEHAVIOR OF UNIRRADIATED UO$_2$ RODS

Energy depositions beyond the initial failure threshold result in progressively greater breakup of the test rods, with fragmentation occurring for energy depositions greater than about 350 cal/g UO$_2$. Particle size distributions have been developed and analyzed for several rod types tested in the range of about 350 to 650 cal/g UO$_2$ in the CDC[14]. Correlation of these distributions with energy deposition has shown that the mean particle diameter decreases with increasing energy deposition and asymptotically approaches a lower limit of about 5 mils for energy depositions exceeding about 500 cal/g UO$_2$. Fuel fragmentation causes the development of transient pressure pulses and mechanical energy generation.

The modes and mechanisms of high energy failures are examined and analyzed in this section, primarily on the basis of the CDC test results (only a few NSRR tests have been conducted in the 400 to 500 cal/g UO$_2$ range, and none above 500 cal/g UO$_2$). The threshold of high energy cladding rupture is estimated on the basis of a simple cladding burst model, with UO$_2$ vapor pressure shown to be the primary contributor to such ruptures. Cladding surface temperatures at time of failure and pressure pulses generated by high energy failures are also examined and correlated.

4.1 High Energy Failure Modes and Mechanisms

The rod failure modes for energy depositions near the initial failure threshold were discussed in Section III-3.1. With increasing energy depositions to about 350 cal/g UO$_2$, the rods exhibited breakup into progressively smaller pieces. The failure mechanisms appeared to be similar to those near the initial failure threshold, with the occurrence of more severe surface oxidation, embrittlement, and complete cladding melting. The edge surfaces of the broken cladding were very sharp, in spite of complete melting, indicating that much of the rod breakup for energy depositions to about 350 cal/g UO$_2$ probably occurred after the melted cladding solidified. Rod breakup probably occurred during the quenching period,

when cladding temperatures typically decreased from about 900 to 400 K within about 0.1 s. Such a temperature decrease would result in a maximum thermal strain of about 0.2%, which would be adequate to cause breakup of previously melted, embrittled cladding.

Figure 38 shows the behavior of several CDC UO_2 fuels in terms of energy deposition at time of failure as a function of total energy deposition. The time of failure during tests with high energy depositions was indicated by the occurrence of pressure pulses within the containment capsules, thus allowing determination of the fuel energy deposition at time of failure. The solid line at $45°$ in Figure 38 defines the energy deposition at time of failure equal to the total energy deposition, which provides an upper bound for the failure data. Also shown in the figure is the UO_2 vapor pressure, calculated assuming adiabatic conditions, as a function of total energy deposition.

Cladding melting occurred for tests in which the total energy deposition exceeded about 240 cal/g UO_2 (Section III-1.1). The extent of melting generally increased with increasing energy deposition to about 350 cal/g UO_2. At 350 cal/g UO_2, which approximately corresponds to the point at which fuel rod fragmentation becomes noticeable, the rods begin to fail at energies less than the total energy deposition. The amount of internal pressure generated at these energy depositions is apparently sufficient to cause cladding near or at the melting temperature to break up.

With increasing energy depositions beyond 350 cal/g UO_2, cladding surface temperature measurements have shown that rod failure occurred prior to cladding melting. This behavior is illustrated in Figure 39, which shows measured cladding temperatures as a function of total energy deposition at the fuel surface. Solid lines are used to indicate the trends of the three types of data in the figure: maximum measured cladding temperatures for zircaloy clad rods, maximum measured cladding temperatures for stainless steel clad rods, and measured cladding temperatures at the time of rod failure. The decrease in the cladding surface temperature at the time of failure with increasing total energy deposition is believed to be due to the increase in UO_2 vapor pressure with increasing energy deposition, as shown in Figure 38.

The previous discussion suggests that UO_2 vapor pressure is a major variable affecting internal pressure rupture of the cladding. Such a failure mechanism could produce consequences consistent with experimental observations. Namely, the internal pressure produced by the UO_2 vapor pressure expels molten fuel into the coolant, and the fuel fragments by the combined effects of momentum at expulsion, turbulence caused by violent boiling of the coolant, and thermal stresses within fuel particles after solidification. UO_2 vapor condensation could further produce an additional amount of very fine fuel fragments.

4.2   Analysis of High Energy Failure Mechanisms

The previous section suggests that internal pressure rupture of the cladding UO_2 vapor pressure may be the primary failure mode at energy depositions sufficient to cause fuel fragmentation. An analysis using a simple cladding burst model is presented in this section to more quantitatively examine the failure mechanisms at high energy depositions.
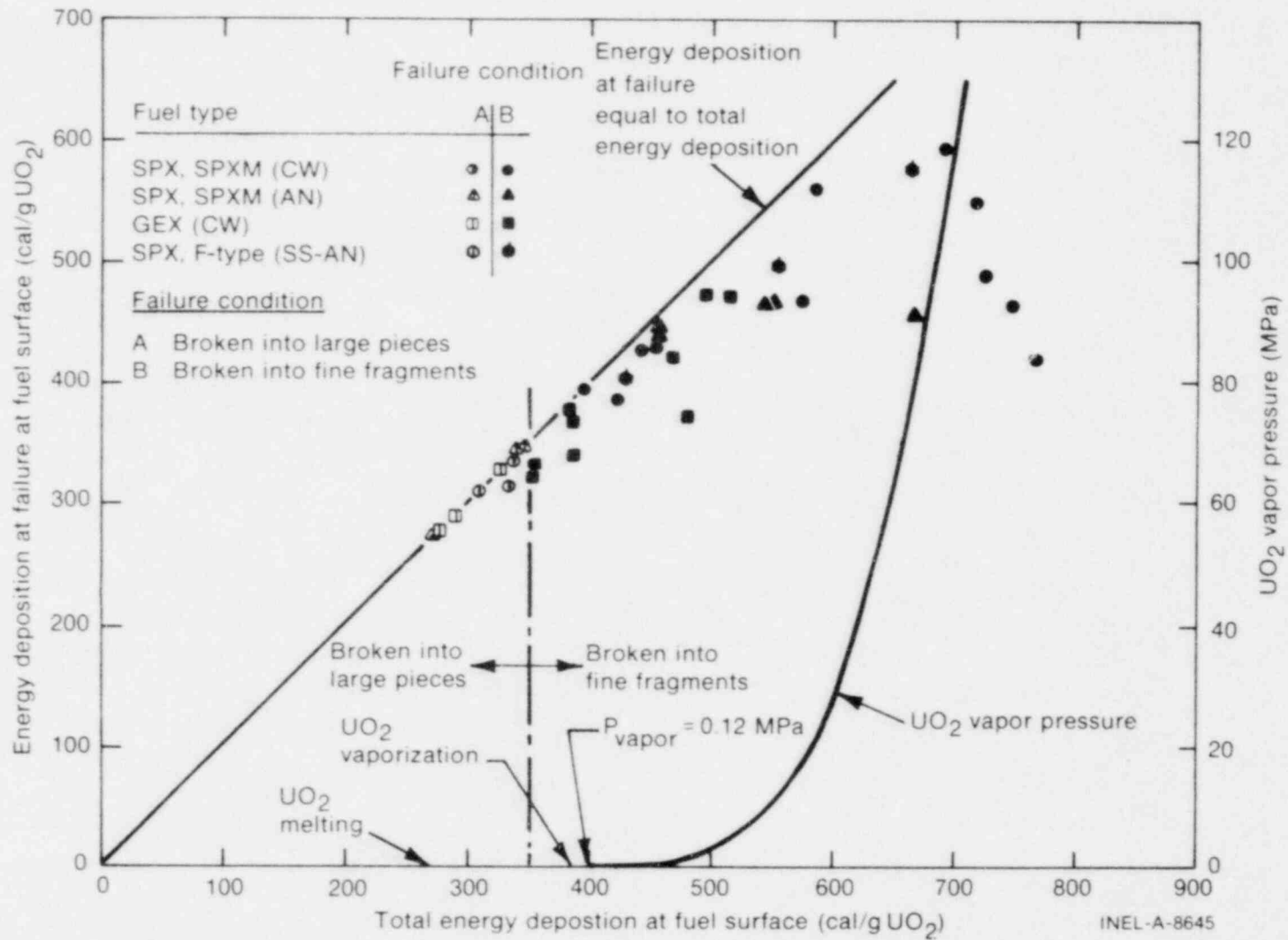
Fig. 38 UO$_2$ vapor pressure and fuel surface energy deposition at time of failure for CDC UO$_2$ test fuels versus total energy deposition at the fuel surface.
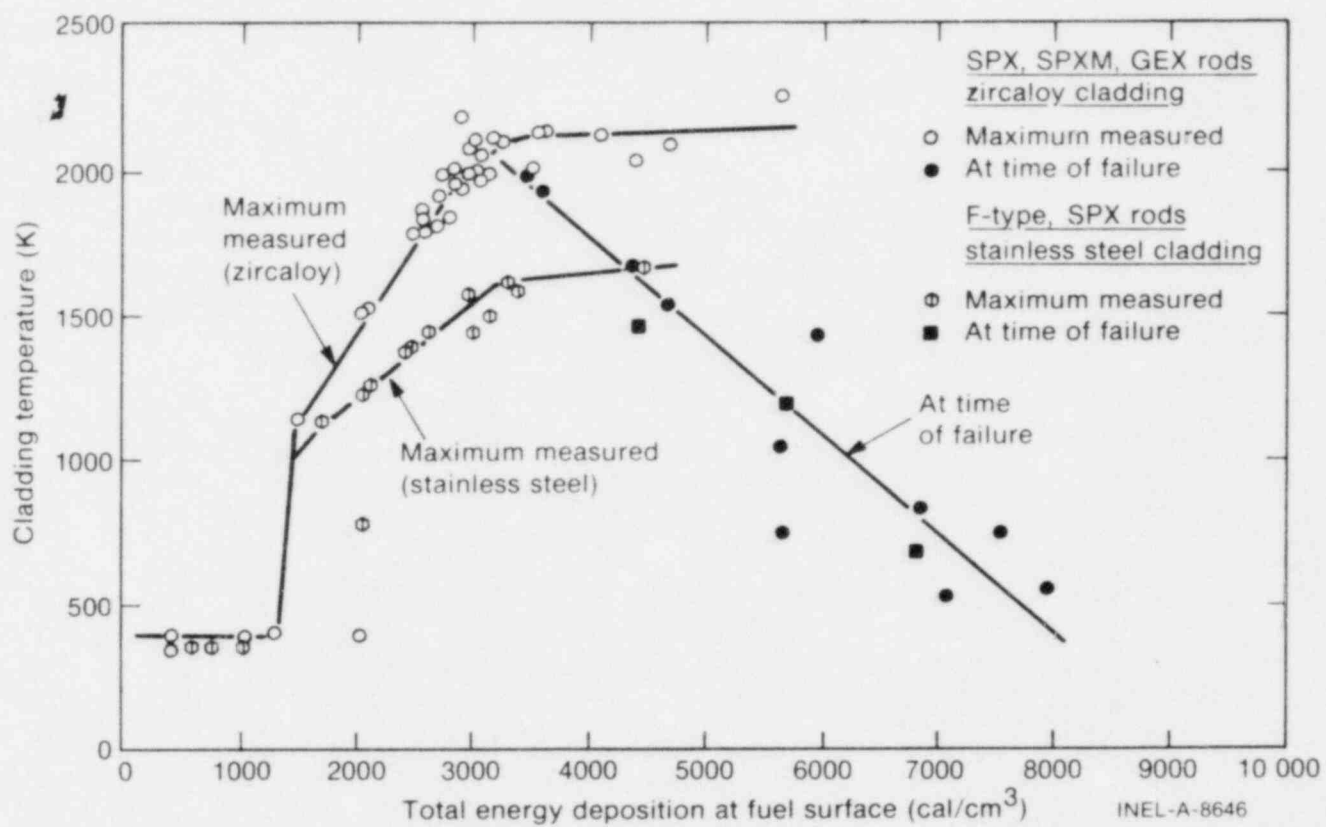
Fig. 39 Cladding temperatures (maximum measured and at time of failure) for CDC UO_2 test fuels versus energy deposition at fuel surface.

4.2.1 <u>Cladding Burst Pressure</u>. An exact determination of tube burst pressure during an RIA from the available ultimate tensile strength data is difficult, since the actual tube burst occurs under multiaxial stress conditions affected by ballooning and the axial tension generated at the tube ends. However, a simple calculation using the criteria that failure occurs when the hoop stress exceeds the ultimate tensile strength is assumed to be applicable as follows:

$$PB = \frac{2t \cdot \sigma_u}{D_i}$$

(3)

where

PB $=$ burst pressure (MPa)

t $=$ cladding wall thickness (mm)

D_i $=$ cladding inner diameter (mm)

σ_u $=$ ultimate tensile strength (MPa).

The cladding materials used in the CDC tests were cold-worked and annealed zircaloy for the SPX and SPXM rods, 10% cold-worked zircaloy for the GEP and GEX rods, and cold-worked and annealed stainless steel for the SPXM rods. Figure 40 shows a comparison of the ultimate tensile strength of the SPXM, GEP, and GEX cladding material with the correlations of Odekirk and Brassfield[22] for cold-worked and annealed zircaloy, respectively. These two correlations agree well with the data for the cold-worked and annealed SPX and SPXM zircaloy cladding. The data for the 10% cold-worked GEP and GEX rods are located between the two correlations as shown in Figure 40. Therefore, the two correlations referenced were used for zircaloy cladding.

For stainless steel cladding, both the yield and ultimate tensile strength of the CDC rods were compared with the correlation reported by Simmons and Cross[23] for annealed Type 304 stainless steel. As shown in Figure 41, good agreement was obtained. Therefore, the correlation of Simmons and Cross was used for stainless steel cladding.

The calculated burst pressures, using Equation (3) and the correlations of Figures 40 and 41, are shown in Figure 42 for CDC test rod claddings as a function of cladding temperature.

This calculation indicates the following:

(1) Differences in behavior between cold-worked and annealed clad rods would occur only at low cladding temperatures (less than about 800 K). These differences should occur at energy depositions greater than 6000 cal/cm^3 UO$_2$ as determined by

68
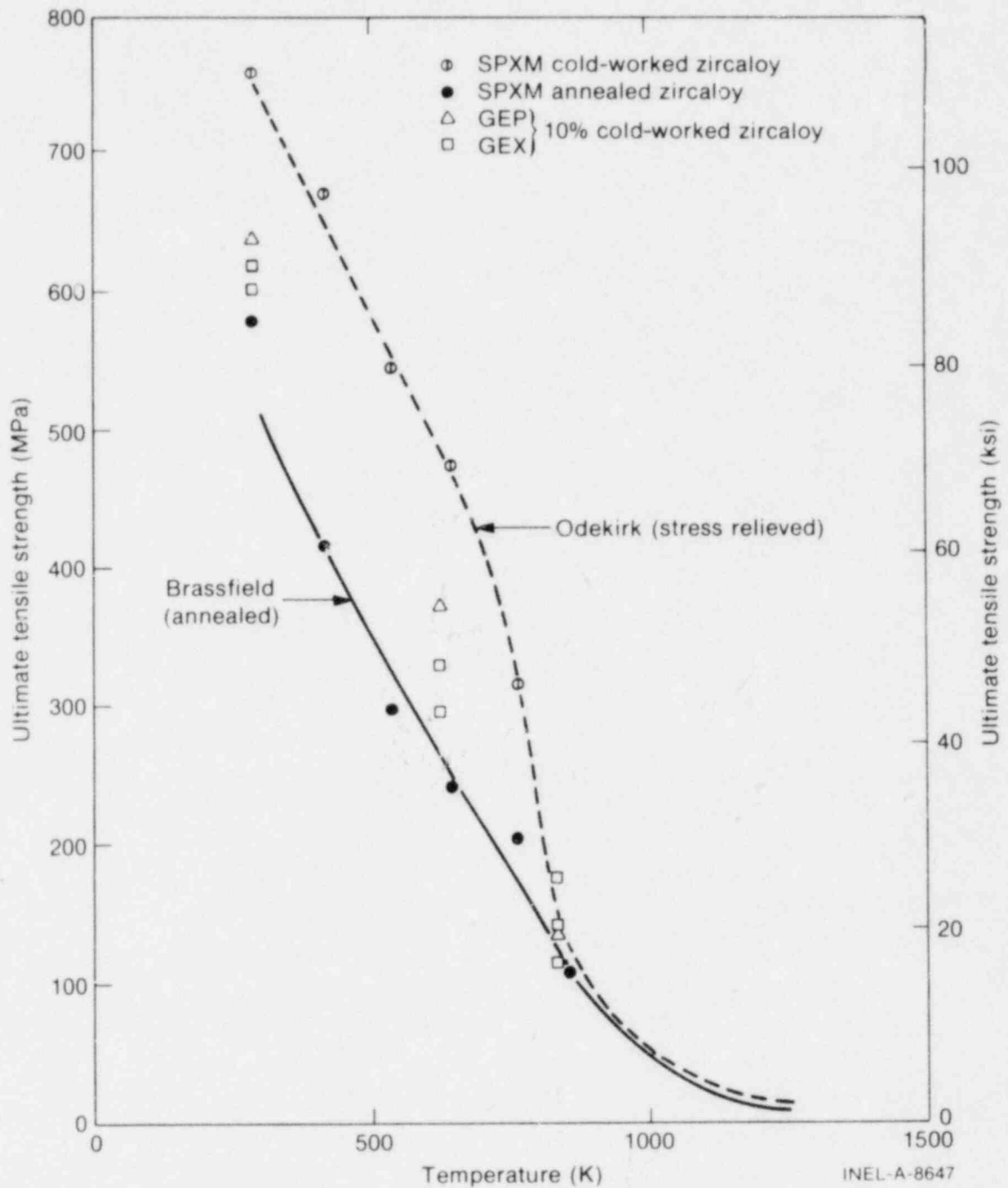
Fig. 40 Ultimate tensile strength as a function of temperature for SPXM, GEP, and GEX zircaloy cladding (Odekirk and Brassfield correlations).

the relationship shown in Figure 39 between energy deposition and cladding temperature at failure.

(2)　The burst pressure of annealed stainless steel cladding is greater than that for zircaloy cladding at cladding temperatures exceeding 800 K; that is, stainless steel clad rods would sustain higher energy depositions than zircaloy clad rods for the same
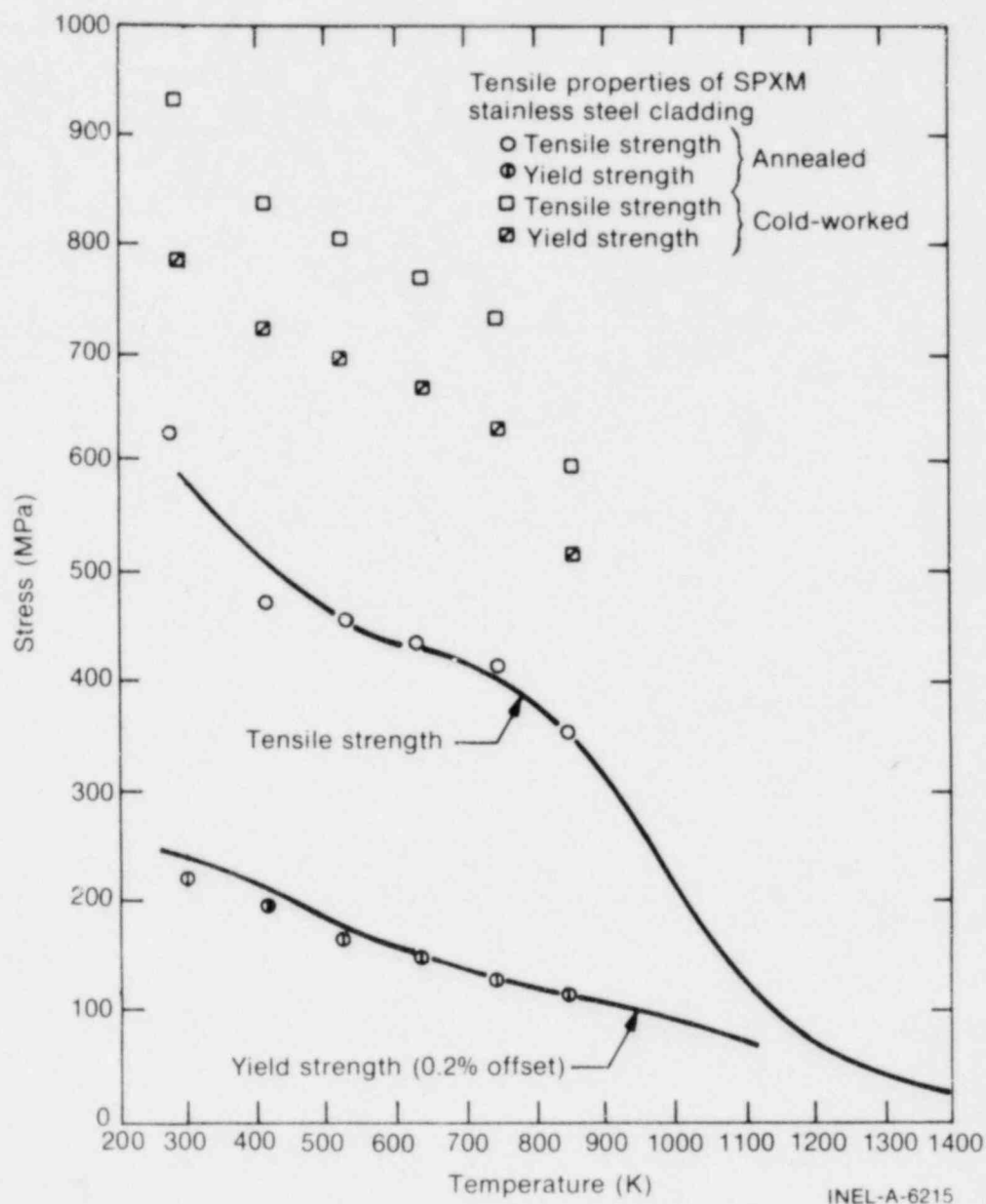
Fig. 41 Ultimate tensile and yield strengths as functions of tempertures for SPXM stainless steel cladding (Simmons and Cross correlation).

cladding temperatures. However, for a given energy deposition, stainless steel cladding reaches a lower maximum temperature than zircaloy cladding because of the larger heat capacity of stainless steel.

4.2.2 UO_2 Vapor Pressure. To obtain the UO_2 vapor pressure as a function of energy deposition, Equation (4) was first used to calculate the UO_2 temperature.

$$T = T_{melt} + \frac{1}{C_p} (q - q_m - L)$$

(4)
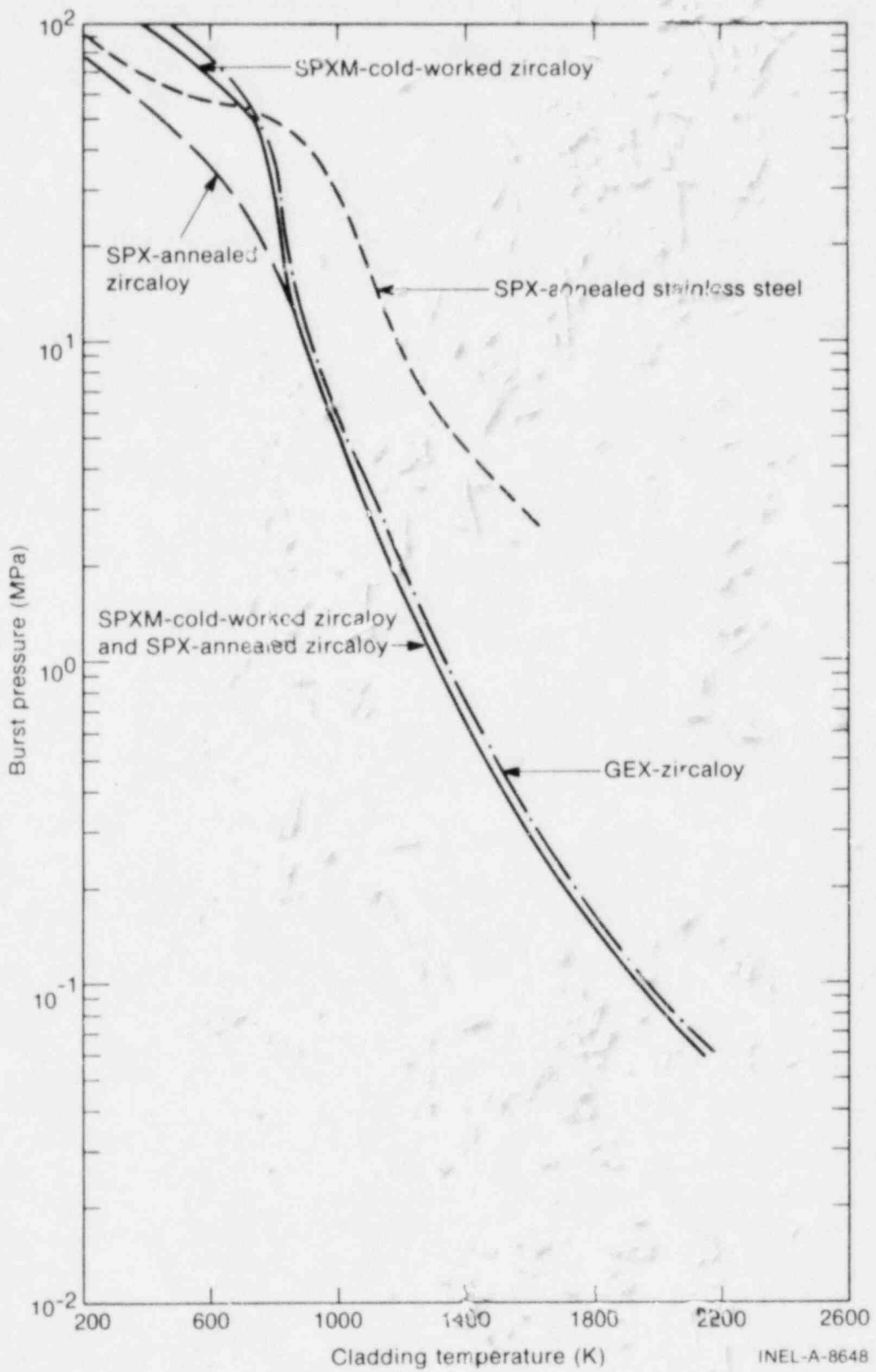
Fig. 42 Calculated cladding burst pressure as a function of cladding temperature for CDC test rods.

where

$$T \quad = \quad UO_2 \text{ temperature (K)}$$

$$T_{melt} \quad = \quad UO_2 \text{ melting temperature (K)} = 3115 [24]$$

$$C_p \quad = \quad \text{heat capacity for } UO_2 \text{ liquid (cal/g K)} = 0.120 [24]$$

$$q \quad = \quad \text{energy deposition (cal/g } UO_2)$$

$$q_m \quad = \quad \text{energy deposition necessary to increase fuel temperature to melting point (cal/g } UO_2) = 268 [24]$$

$$L \quad = \quad \text{latent heat of vaporization for } UO_2 \text{ (cal/g)} = 67 [24].$$

The UO_2 vapor pressure was then calculated by the following equation[25]:

$$\log P = 7.7 - \frac{27900}{T} \tag{5}$$

where

$$P \quad = \quad UO_2 \text{ vapor pressure (kg/cm}^2)$$

$$T \quad = \quad UO_2 \text{ temperature (K)}.$$

The calculated UO_2 vapor pressure (converted to MPa) as a function of energy deposition is shown in both Figures 38 and 43.

4.2.3 Comparison of Calculated Cladding Temperature at Failure with Measured Surface Cladding Temperatures at Failure. As described in Section III-4.1, the threshold energy deposition for internal pressure rupture is about 350 cal/g UO_2. For energy depositions greater than 350 cal/g UO_2, cladding rupture is assumed to occur when the cladding strength for a given temperature cannot withstand the UO_2 vapor pressure within the fuel rod. Thus the postulated rupture criterion is that rupture occurs when the UO_2 vapor pressure is equal to the cladding burst pressure.

Use of this rupture criterion based solely on UO_2 vapor pressure assume ...' other potential sources of fuel rod internal pressure can be neglected for high energy tests with unirradiated fuel rods. Gas gap expansion and gaseous fission products and impurities within the fuel matrix are two sources that could contribute to the internal pressure. Gas gap pressure in pellet-fueled rods which were not prepressurized should be insignificant, since the initial internal pressure was one atmosphere in the CDC and NSRR test rods, and almost all of the gap gas would have been expelled from the gap into the plenum by gap closure (shown in Section III-1.2 to occur at a relatively low energy deposition of about 120 cal/g UO_2). Only minor pressures would be expected from gaseous fission products and

72
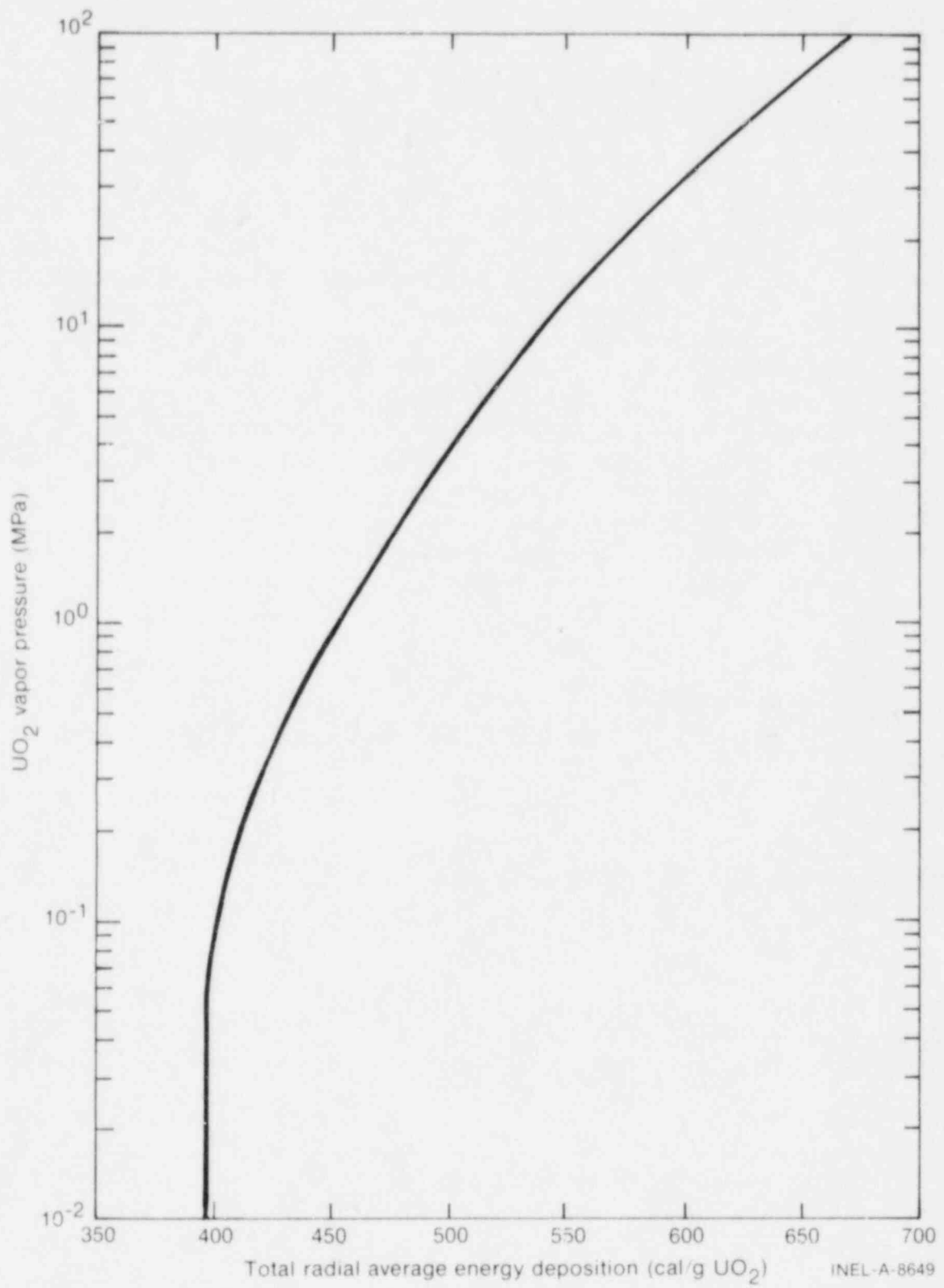
Fig. 43 Calculated UO_2 vapor pressure as a function of energy deposition.

impurities in unirradiated fuel rods. Therefore, the effects of pressure generated by gas gap expansion and by gaseous fission products and impurities were assumed negligible and were not included in the cladding burst model calculations.

Cladding temperatures at failure (that is, for equal cladding burst and UO_2 vapor pressures) can be determined as a function of energy deposition at failure from the correlations shown in Figures 42 and 43. The correlation curves obtained in this manner are shown in Figure 44 for the cladding of several rod types. Measured cladding surface temperatures at failure are also shown for high energy deposition tests, which is the applicable region of the cladding burst model. Comparison of the correlations with the measured data indicate the following:

(1) The threshold energy deposition for rod rupture (fragmentation threshold) can be defined as that value at which the cladding temperature at failure drops below the cladding melting temperature. The calculations show these points to be at energy depositions of about 360 cal/g UO_2 for zircaloy cladding and about 450 cal/g UO_2 for stainless steel cladding. The data shown in Figure 44 are in reasonable agreement with the calculated curves in these regions.
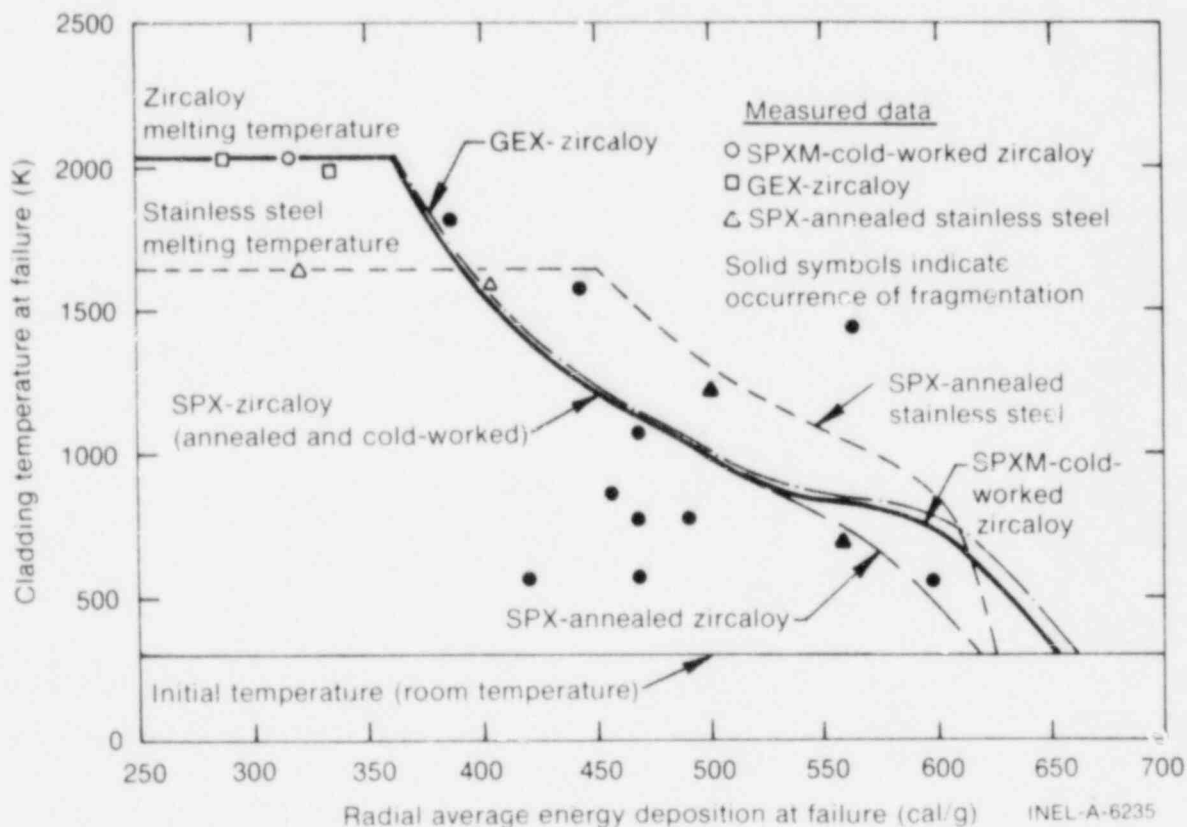
Fig. 44 Calculated and measured cladding temperatures at failure as a function of calculated and measured energy depositions at failure for several CDC test rod types.

(2)   Most of the measured cladding temperatues at time of failure for
        zircaloy clad rods in the failure energy deposition range of 450
        to 500 cal/g UO_2 were somewhat lower than predicted by the
        calculational model. The single data point for a stainless steel
        clad rod in this region, however, agrees well with the calculated
        curve.

(3)   Two of the three measured temperature data points for failure
        energy depositions greater than 500 cal/g UO_2 are lower than
        predicted, and one value is somewhat higher than expected.

Measurement errors associated with the cladding surface thermocouples could have
contributed to the observed differences between the experimental data and calculated
curves in Figure 44. Experience with the small-mass thermocouples used in these
experiments, however, would indicate that such errors would be much less than required to
explain the observed differences. A more likely explanation is that the measurements were
of the cladding surface temperature, whereas the calculated behavior is more indicative of
the average cladding temperature. A method for estimating average cladding temperatures
based on analysis of measured surface temperatures has been developed, as described in the
following subsection.

4.2.4 Comparison of Calculated Cladding Temperature at Failure with Estimated
Average Cladding Temperature at Failure. To develop a method for determining average
cladding temperatures at time of failure, it was postulated that measured cladding surface
temperatures at failure are related to the time of failure during a test. Such a postulate was
evaluated by examination of the time of failure following power excursion peak power.
Measured time of failure after peak power is plotted versus total energy deposition in
Figure 45. The time of failure decreases exponentially as the total energy deposition is
increased. As the cladding surface temperature increase lags the fuel temperature increase,
the decrease of failure time at higher energy should result in a decrease of the cladding
temperature. In Figure 46, the measured temperatures at failure are plotted versus time of
failure after peak power. The calculated curves shown in the figure were developed as
follows. If the temperature at time of failure is mainly controlled by the failure time, the
data would coincide with the history of cladding temperature rise versus time. A transient
heat transfer calculation was performed to examine this assumption using the simplified
model described in the following:

(1)   Power-time history was approximated by a delta function; that
        is, the heat deposition versus time was assumed to be a step
        function.

(2)   It was assumed that the cladding inner surface temperature
        remained at the melting point during the transient. The initial
        condition was, therefore, melting temperature at the cladding
        inner surface, and room temperature in the rest of the cladding.
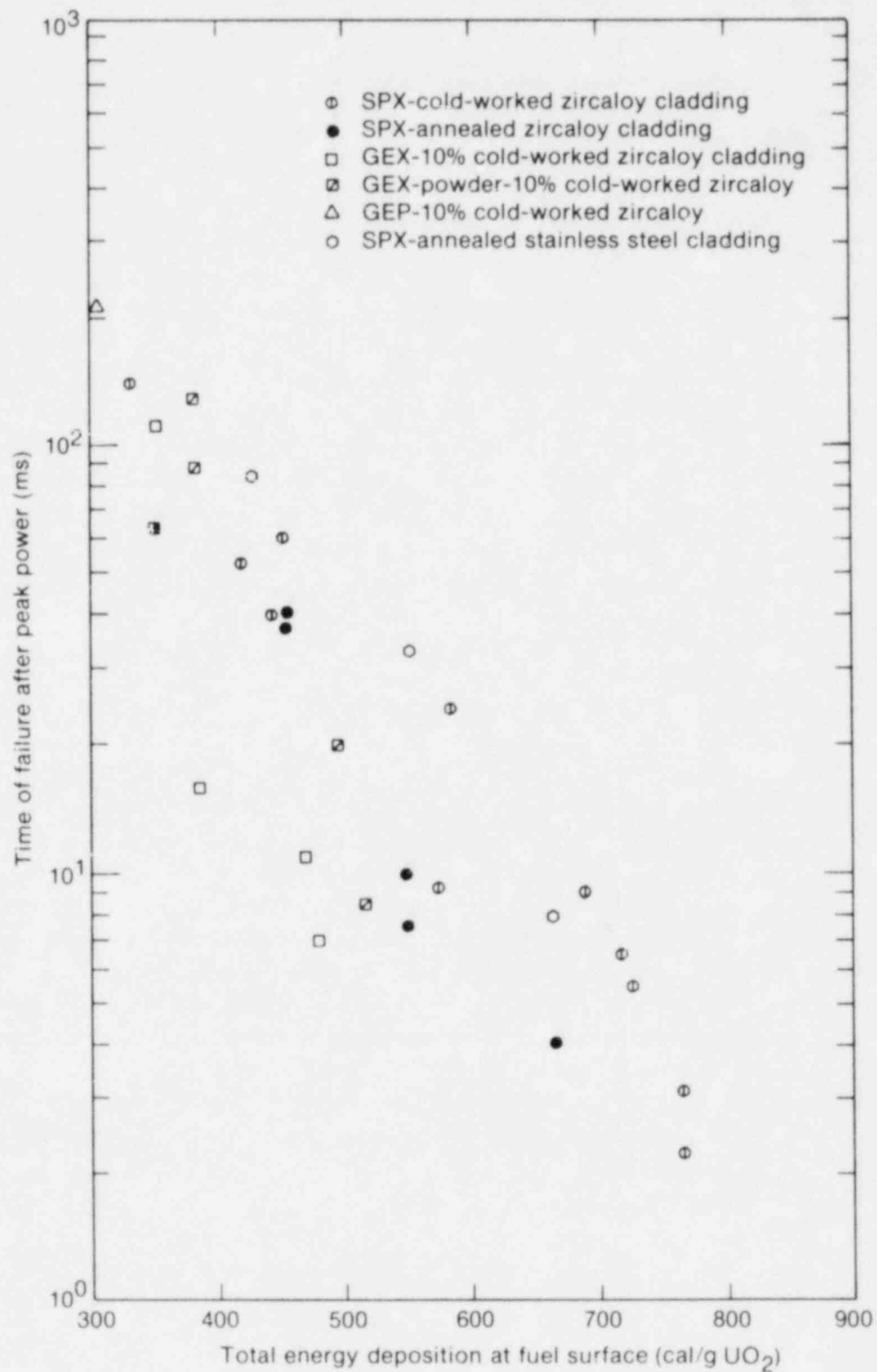
Fig. 45 Time of failure after peak power versus total energy deposition at fuel surface for several CDC rod designs.

INEL-A-8651
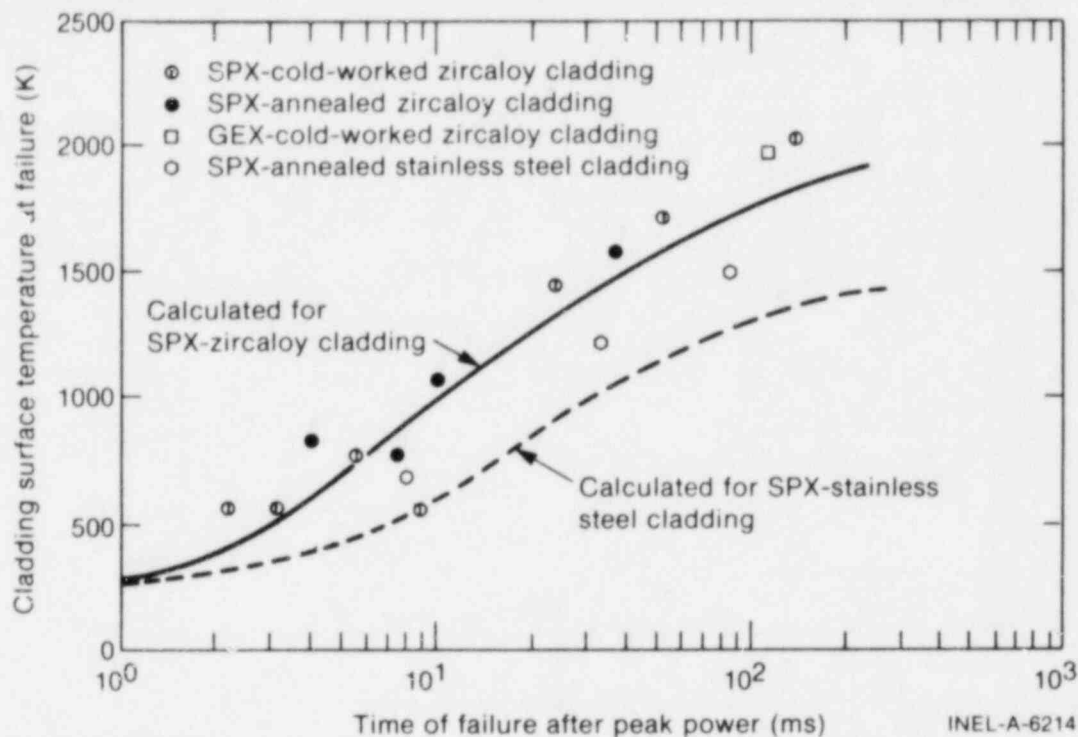
Fig. 46 Calculated and measured cladding surface temperatures versus time of failure after peak power for zircaloy and stainless steel clad CDC rods.

(3) Heat transfer in the cladding was calculated as heat conduction in a semi-infinite body, the interface of which was the cladding inner surface. The temperature at the cladding outer surface was then calculated as a temperature at the depth of the cladding wall thickness as shown in Figure 47. Calculated results for zircaloy and stainless steel cladding are indicated in Figure 46 for comparison with the measured data. This calculation implies that the cladding surface temperature rise is strongly controlled by the heat conduction across the cladding wall, and that the decrease in cladding temperature at failure (at higher energy depositions) results from the decrease in failure time. The calculation also implies a large temperature drop across the cladding (approximate maximum of 1000 K). Therefore, the effect of this temperature drop on cladding rupture should be taken into account.

Based on the agreement obtained between the measured and calculated values in Figure 46, the cladding average temperature may probably be defined as the average of the measured cladding surface temperature and the cladding melting temperature. Therefore, the calculated average temperatures for several fuel rod types are compared with the calculated temperature curves as a function of energy deposition at failure in Figure 48. Better agreement, especially for stainless steel clad rods, is shown than in the comparison of Figure 44.
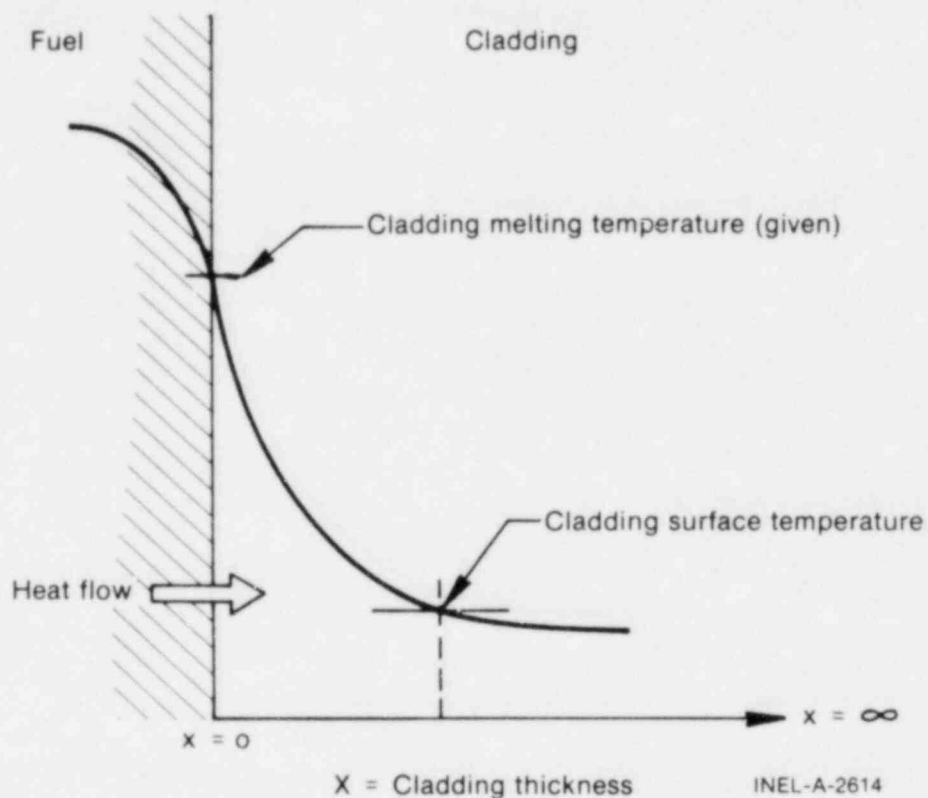
Fig. 47 Cladding heat transfer model.

The calculated curve in Figure 48 is, however, less than most of the calculated data points which may be a result of the following.

(1) UO_2 vapor pressure is overestimated by neglecting the heat loss from the fuel surface. If the heat loss is considered, the temperature curve of Figure 48 will shift toward the higher energy depositions by the amount of the heat loss.

(2) The effect of large strain rates on cladding rupture strength was neglected. If a circumferential elongation at rupture of 0.2 is assumed, and if this value is divided by the time of failure after peak power, the strain rate is 1 to $100\ s^{-1}$ for energy depositions of 350 to 750 cal/g UO_2. Thus, strain rates may affect the cladding strength. The burst pressure of the cladding increases with strain rate, and, therefore, the temperature curve would shift upwards toward higher cladding temperatures.

4.3 Analysis of Pressure Pulses Generated by the High Energy Failure of Unirradiated Rods

Unirradiated rod failures for energy depositions greater than approximately 300 cal/g UO_2 produced pressure pulses within the experiment containment capsules. The measured

78
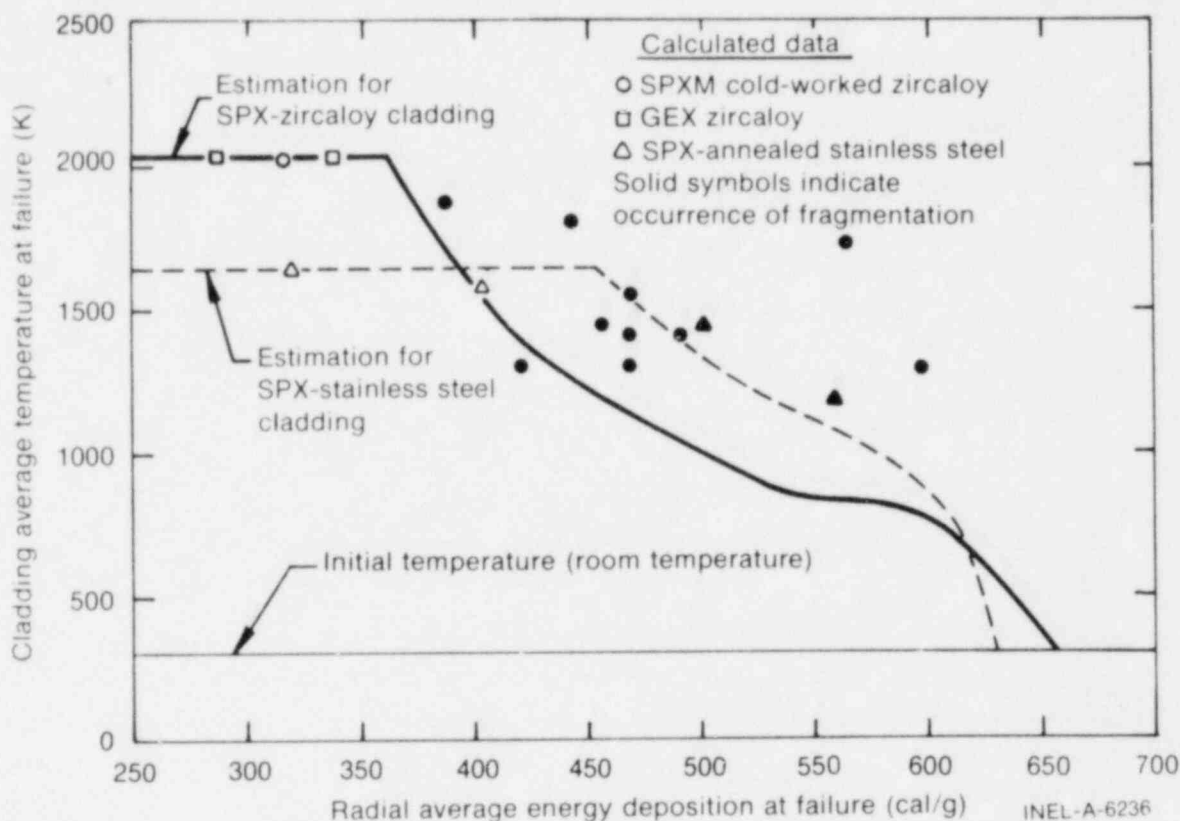
Fig. 48 Calculated cladding average temperatures at failure as a function of energy depositions at failure for several CDC test rod types.

pressure histories were generally characterized by an initial pulse, followed by several less severe additional pulses of varying frequency and magnitude. Such pressure histories are strongly coupled to both the degree of fuel fragmentation and capsule geometry.

The initial pressure pulse is postulated to be directly related to the internal pressure of the fuel rod at the time of cladding rupture, and would, therefore, be essentially independent of fuel dispersal and heat transfer effects. Figure 49 shows initial pressure pulse data from the CDC tests as a function of the energy deposition at time of failure. The pressure data shown are only one-half the measured values, because the measurements in the CDC tests were made by a transducer located at the bottom of the capsule, which caused pressure magnitude doubling. (Pressure transducer characteristics are described in Appendix A and the doubling effect is discussed in Section II-1.3.) Also shown in Figure 49 is the estimated fuel rod internal pressure based on UO_2 vapor pressure alone and with the addition of gap gas pressure. The UO_2 vapor pressure curve was determined by the method described in Section III-4.2.2. The pressure from gap gas expansion was determined by assuming the gap gas temperature was the average of the pellet surface and cladding temperatures. Comparison of the measured initial pressure pulses with the calculated internal fuel rod pressure indicates a correlation, particularly for the UO_2 vapor pressure alone. The addition of the estimated gap gas pressure provides better agreement with some data, but not with the majority of the data. On the other hand, the curve defined by the sum of the gap gas pressure and UO_2 vapor pressure provides an approximate upper bound on the measured pressures.
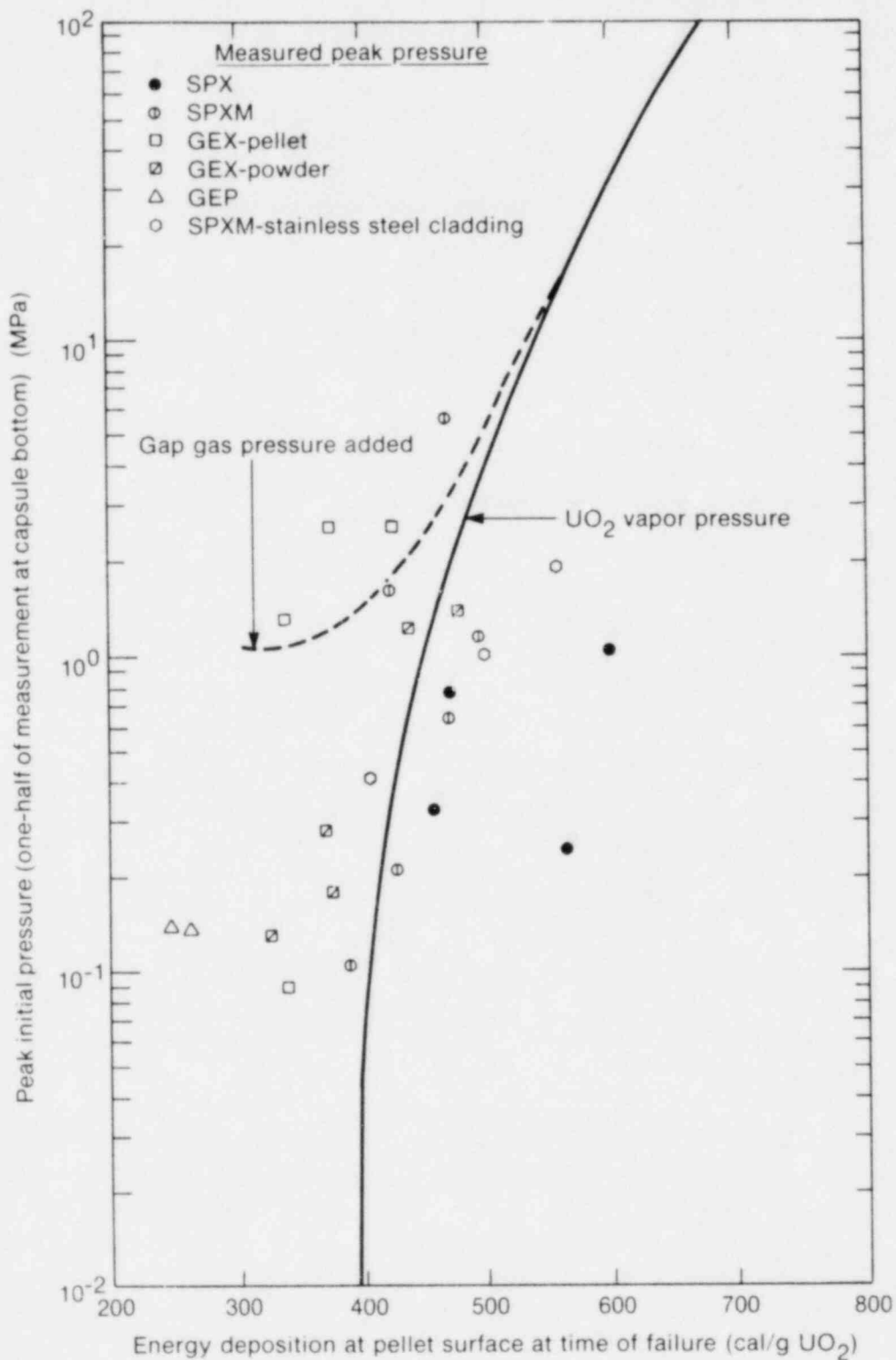
Fig. 49 Comparison of peak pressure at failure and estimated UO_2 vapor pressure in the rod.

INEL-A-6213

Cladding temperatures at time of failure were shown, in Section III-4.2.4, to be strongly related to the time of failure after peak power. The correlations of Figures 42 through 46 may be used to estimate cladding burst pressures as a function of time of failure after peak power. These calculated curves (based on surface and estimated average cladding temperatures) are shown in Figure 50 along with peak initial pressure pulse data. Comparison indicates the initial pressure pulses are related to the internal pressure of the rods at time of failure.
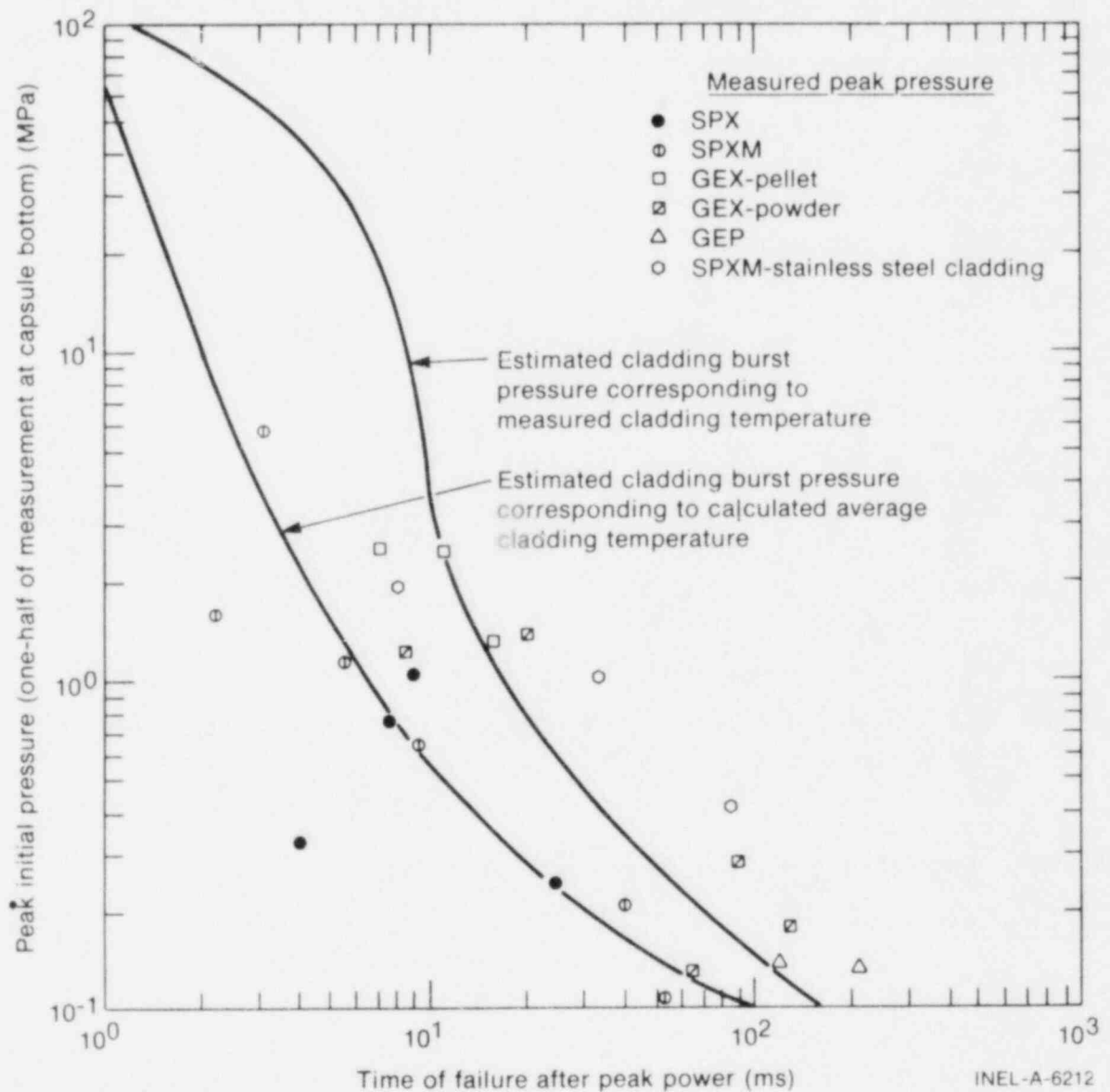
Fig. 50 Trend of peak pressure versus time of failure after peak power compared with estimated cladding burst pressure curves.

The CDC, TREAT, and NSRR programs have provided significant information germane to the understanding of fuel behavior under RIA conditions. Most of the results, however, were acquired from tests with single, unirradiated fuel rods at zero initial power in stagnant water at ambient temperature and atmospheric pressure. Only a few tests were performed to investigate the effects of fuel burnup and environmental variations. To further develop and verify fuel behavior analytical models, additional experimental data are required with preirradiated fuel under conditions more nearly typical of power reactor environments (high temperature, pressure, flow, and initial power).

The following principal conclusions have been formulated regarding the current understanding of fuel behavior under RIA conditions. These conclusions are based primarily on test data obtained from the CDC and NSRR programs and on the correlations and interpretations of those data.

1. MAXIMUM CLADDING TEMPERATURES

Cladding surface temperature data correlations for unirradiated UO_2 rods showed that cladding melting temperatures were generally attained at time of failure for energy depositions to about 350 cal/g UO_2. Beyond 350 cal/g UO_2, which was the approximate threshold for rod fragmentation, cladding temperatures at time of failure decreased inversely proportional to the energy deposition. The cladding temperature at time of failure was shown to be directly related to the UO_2 vapor pressure and cladding strength at time of failure.

Shroud enclosures about the NSRR-STD rods were found to have no detectable effect on maximum measured cladding surface temperatures, but did significantly extend the duration of film boiling at the cladding surface prior to quenching. This extended film boiling time may have caused additional cladding embrittlement, thus contributing to the observed lower failure thresholds for shroud-enclosed rods.

2. CLADDING AND FUEL DEFORMATIONS

Cladding radial deformation of unpressurized, unirradiated rods was shown to be directly related to fuel thermal expansion. Larger expansions were noted for preirradiated and waterlogged rods, apparently due to internal pressure generation.

Cladding axial deformation was apparently caused primarily by fuel stack growth after gas gap closure. Slipping at the fuel-cladding interface resulted in less elongation of the cladding than occurred for the fuel stack. Small or negative cladding elongations occurred

for waterlogged and preirradiated rods, apparently because prompt and large radial deformation of the cladding prevented gap closures.

3. INCIPIENT FAILURE THRESHOLD OF UNIRRADIATED RODS

The incipient failure threshold of unirradiated rods was generally in the range of about 240 to 265 cal/g UO_2. Rods failed by cladding melting or cracking or apparently embrittled cladding, or both. The GEX rods had slightly lower thresholds, 223 to 256 cal/g UO_2, and the TREAT rods slightly higher thresholds, $\sim$270 cal/g UO_2. The incipient failure threshold was found to be relatively insensitive to cladding material, cladding heat treatment, fuel form, fuel material, and gap width. However, correlation of the cladding temperature and failure behavior data for several test rod designs indicates that the incipient failure threshold has a stronger dependence on the energy deposition near the fuel surface than on the radial average energy deposition.

Single NSRR-STD rods enclosed in shrouds failed at lower energy depositions. The incipient failure threshold for rods enclosed in a 14-mm cylindrical shroud (water/fuel ratio of 0.71) was determined to be in the range of 211 to 247 cal/g UO_2, compared with 244 to 264 cal/g UO_2 for unenclosed rods. Similar scoping tests with five-rod clusters (both with and without shrouds) also indicated a reduction in the incipient failure threshold when a shroud was present.

Tests with prepressurized NSRR-STD fuel rods showed that initial internal pressures $\geqslant$1.2 MPa resulted in a decrease in the failure threshold; at 2.9 MPa, the failure threshold was 150 to 160 cal/g UO_2.

Tests with 5, 10, and 20% enriched NSRR-STD rods showed that the failure threshold decreased slightly with increasing enrichment, apparently due to the increased radial power peaking near the fuel surface.

Zircaloy clad waterlogged rods were found to fail by cladding rupture at energy depositions as low as 60 cal/g UO_2. The failure threshold was strongly dependent on cladding heat treatment and cladding material; work-hardened cladding failed at lower energy depositions than annealed cladding, and zircaloy cladding failed at lower energy depositions than stainless steel cladding. Fuel rod dimensional variations, degree of waterlogging, and cladding defects did not significantly affect the failure threshold of waterlogged rods.

4. HIGH ENERGY FAILURE BEHAVIOR OF UNIRRADIATED RODS

For energy depositions to about 350 cal/g UO_2, unirradiated UO_2 rods failed as a result of cladding heatup to the approximate melting temperature, which caused

embrittlement and loss of strength. Some cladding perforation probably occurred while the cladding was molten, but much of the rod breakup appeared to have occurred during the cooldown cycle. For energy depositions in excess of about 350 cal/g UO_2, failures occurred by cladding rupture caused by internal pressure, the likely source of which was shown to be UO_2 vapor pressure, prior to the attainment of cladding melting.

The failure consequences of unirradiated UO_2 rods were insignificant below about 300 cal/g UO_2. In the 300 to 500 cal/g UO_2 range, rods were broken up and fragmented, but the maximum measured pressures did not exceed a few MPa, and nuclear-to-mechanical energy conversions did not exceed 1%. Metal-water reaction extents increased with energy deposition, reaching as much as 50% at about 500 cal/g UO_2. Tests at over 600 cal/g UO_2 had more severe consequences, with pressures up to 12 MPa, energy conversions to near 3%, and metal-water reaction extents to near 100% being observed.

Failure of waterlogged rods often produced capsule pressures in the tens of MPa, but the pressure pulses did not contain sufficient energy to produce failure of adjacent rods. Fuel rod dimensional variations, degree of waterlogging, and cladding defects did not significantly affect the failure consequences of waterlogged rods.

5. BEHAVIOR OF IRRADIATED RODS

Preirradiated rods tested in the CDC with burnups to 32 000 MWd/t were observed to fail, in some cases, at lower energy depositions than unirradiated rods, with little sensitivity attributable to the degree of burnup. Only a few preirradiated rods were tested, with relatively large scatter in the data; thus, the lower failure threshold was not statistically established.

The initial failure of preirradiated rods was in the form of cladding rupture or cracking, generally longitudinal, and in some cases, extensive and multiple fractures occurred. The cause of failure appeared to be internal pressure or fuel-cladding interaction, or both. Little or no evidence of cladding melting was detected. Pressure and mechanical energy generation were detected at lower energy depositions (≥ 200 cal/g UO_2) for preirradiated rods; however, the observed magnitudes were relatively insignificant.

V. REFERENCES

1. United States Nuclear Regulatory Commission, Reactor Safety Program, *A Description of Current and Planned Reactor Safety Research Sponsored by the Nuclear Regulatory Commission's Division of Reactor Safety Research*, NUREG-75/058 (June 1975).

2. T. E. Murley et al, "Summary of LWR Safety Research in the USA," *International Conference on Nuclear Power and Its Fuel Cycle, Salzburg, Austria*, NUREG-0234 (May 1977).

3. *Code of Federal Regulations*, Title 10, Part 50, Appendix A, Criterion 28, "Reactivity Limits".

4. "Assumptions Used for Evaluating a Control Rod Ejection Accident for Pressurized Water Reactors," *NRC Regulatory Guide 1.77* (May 1974).

5. D. H. Risher, Jr., *An Evaluation of the Rod Ejection Accident in Westinghouse Pressurized Water Reactors Using Spatial Kinetics Methods*, WCAP-7588 (December 1971), and Rev. 1-A (January 1975).

6. C. J. Paone et al, *Rod Drop Accident Analysis for Large Boiling Water Reactors*, NEDO-10527 (March 1972).

7. J. A. Dearien et al, *FRAP-T2: A Computer Code for the Transient Analysis of Oxide Fuel Rods, Volume I – FRAP-T2 Analytical Models and Input Manual*, TREE-NUREG-1040 (March 1977).

8. M. Ishikawa et al, "NSRR Experiments of LWR Fuel Behavior Under Reactivity Initiated Accident Conditions," *Proceedings of Topical Meeting on Thermal Reactivity Safety, Sun Valley, Idaho, July 31-August 4, 1977*, CONF-770708.

9. T. G. Taxelius (ed.), *Annual Report, SPERT Project, October 1968–September 1969*, IN-1370 (June 1970).

10. M. Ishikawa and K. Tomii (ed.), *Quarterly Progress Report on the NSRR Experiments (3); Combined, July – December 1976*, JAERI-M 7051 (March 1977).

11. M. Ishikawa and K. Tomii (ed.). *Quarterly Progress Report on the NSRR Experiments (4); Combined, January – June 1977*, JAREI-M 7304 (August 1977).

12. M. D. Freshley and L. J. Harrison, "The Transient Behavior of Vipac and Pellet Thermal Reactor Oxide Fuels," *Nuclear Technology*, 15 (August 1972).

13. T. G. Taxelius (ed.), *Quarterly Technical Report, SPERT Project — July, August, September 1968*, IDO-17294 (February 1969).

14. J. A. McClure, *Particle Size Distributions from Fuel Rods Fragmented During Power Burst Tests in the Capsule Driver Core*, IN-1428 (October 1970).

15. T. G. Taxelius (ed.), *Quarterly Technical Report, SPERT Project — January, February, March 1968*, IDO-17287 (November 1968).

16. T. G. Taxelius (ed.), *Quarterly Technical Report, SPERT Project — July, August, September 1967*, IDO-17271 (July 1968).

17. R. K. McCardell et al, *Reactivity Accident Test Results and Analyses for the SPERT III E-Core — A Small, Oxide-Fueled, Pressurized-Water Reactor*, IDO-17281 (March 1969).

18. T. G. Taxelius (ed.) *Quarterly Technical Report, SPERT Project — April, May, June 1968*, IDO-17289 (January 1969).

19. M. Ishikawa and K. Tomii (ed.), *Quarterly Progress Report on the NSRR Experiments (1); Combined, October 1975 — March 1976*, JAERI-M 6635 (June 1976).

20. R. W. Miller, *The Effects of Burnup on Fuel Failure — Power Burst Tests on Fuel Rods with 13,000 and 32,000 MWd/MTU Burnup*, ANCR-1280 (January 1976).

21. J. Belle (ed.), *Uranium Dioxide: Properties and Nuclear Applications*, U.S. Government Printing Office (1961).

22. P. E. MacDonald and L. B. Thompson (eds.), *MATPRO, A Handbook of Materials Properties For Use in the Analysis of Light Water Reactor Fuel Rod Behavior*, ANCR-1263 (February 1976).

23. W. F. Simons and H. C. Cross, *Report on the Elevated-Temperature Properties of Stainless Steels*, ASTM Special Technical Publication 124 (1952).

24. D. Miller, *The Effect of Melting on UO_2 Thermodynamic Properties*, ANL-7610 (1970).

25. R. W. Ohse et al, "Measurement of Vapor Pressure of $(U, Pu)O_2$ and UO_2 to 5000 K for Fast Reactor Safety Analysis and the Contribution of the Radial Cs Distribution to Fuel Pin Behavior," *Symposium on Thermodynamics of Nuclear Materials, Vienna, Austria, October 21, 1974*, STI/PUB-380 (Vol. I), CONF-741030-P1.

APPENDIX A

TEST METHODS

APPENDIX A

TESTS METHODS

Similar methods were used in the CDC, NSRR, and TREAT programs to obtain fuel behavior data under reactivity initiated accident (RIA) conditions. In each program, encapsulated rods were positioned in the central flux trap region of a driver core and subjected to rapid power excursions. Numerous pretest, dynamic, and posttest measurements were made to obtain pertinent information. This appendix summarizes the characteristics and design features of the facilities, test environments, test fuels, instrumentation, measurements, and examinations. Additional detailed information is available in referenced publications.

1. TEST FACILITIES

The characteristics and design features of the test facilities are discussed in the following subsections.

1.1 Capsule Driver Core (CDC)

The CDC[A-1] was an oxide-fueled, pool-type reactor located in the SPERT-IV Facility at the Idaho National Engineering Laboratory (INEL). The core rods were comprised of 3% enriched UO_2 powder, swage-compressed within Type 304 stainless steel cladding. Reactor control was accomplished by the use of eight cruciform-shaped blades. Four banked transient rods were ejected by compressed air to provide step insertions of reactivity. A 8.64-cm inside diameter cylindrical, stainless steel experiment tube, which extended the length of the core, was centrally located in the core to provide a flux-trap irradiation space for experimental rods. The CDC was capable of power excursions with minimum reactor periods of about 3 ms.

1.2 Nuclear Safety Research Reactor (NSRR)

The NSRR[A-2] is a modified TRIGA Annular Core Pulse Reactor located at the Japan Atomic Energy Research Institute. The core is comprised of stainless steel clad, uranium-zirconium hydride fuel moderator elements in an open-pool vessel. Normal control is provided by eight fuel-follower control rods with power excursions initiated by rapid withdrawal of three transient rods. A 22-cm inside diameter experiment tube passes axially through the center of the core to provide a flux trap space for fuel testing. The NSRR is capable of power excursions with minimum initial periods of about 2 ms.

1.3 Transient Reactor Test Facility (TREAT)

TREAT[A-3] is an air-cooled, graphite-moderated reactor located at the INEL. Core fuel elements are extruded U_3O_8 and are graphite clad with zircaloy. Twenty-four control rods are used for both normal operation and power excursion initiation. A centrally located test space, approximately 10 cm square, with horizontal access slots provides an experimental irradiation space. TREAT is capable of power excursions with minimum reactor periods of about 35 ms.

2. CONTAINMENT CAPSULES AND ENVIRONMENTS

In CDC, NSRR, and TREAT experimental fuel rods were positioned in containment capsules that were located in the central test space of the respective facilities. In both the CDC[A-4] and NSRR[A-2], cylindrical stainless steel capsules with inside diameters of about 7.3 and 12 cm, respectively, were used. The TREAT tests used stainless steel rectangular capsules, approximately 10 x 10 cm, some of which had a quartz window[A-5] to allow high speed photography during tests. Capsule lengths were in the range of 120 to 180 cm.

The capsules normally contained stagnant, deionized water at room temperature and atmospheric pressure. Capsules were normally filled to within about 25 cm of the top, with the upper volume containing atmospheric pressure air. The NSRR capsules had the capability of heating the capsule water to about 363 K.

Internal capsule hardware radially centered the test rods at the approximate axial flux peak. Rods were rigidly supported only at their bottom ends, allowing free growth or contraction in response to power excursions. Intermediate spacers were normally used for relatively long (> 25 cm) test rods. The rod mounting hardware was generally connected via a support tube to the upper capsule head, resulting in an easily insertable and removable test train. Figure A-1 shows a typical test train and capsule used in the NSRR program. The instruments shown in the figure are discussed in Section 4.

3. TEST FUEL

The characteristics of the test rods used in the fuel behavior tests discussed in this report are summarized in Table A-I. The information presented in the table was obtained primarily from References A-2, A-4, A-6, and A-7. These publications also include additional detailed information on the fabrication techniques and physical properties of the fuel and cladding for each of the test rod designs.

200 mm

Water level sensor

Water level

Cladding and fuel
displacement sensor

Test fuel

Thermocouple

120 mm

Fuel pressure sensor

Capsule pressure
sensor

Grip flange

1200 mm

800 mm

135 mm

7 mm

INEL-A-8621
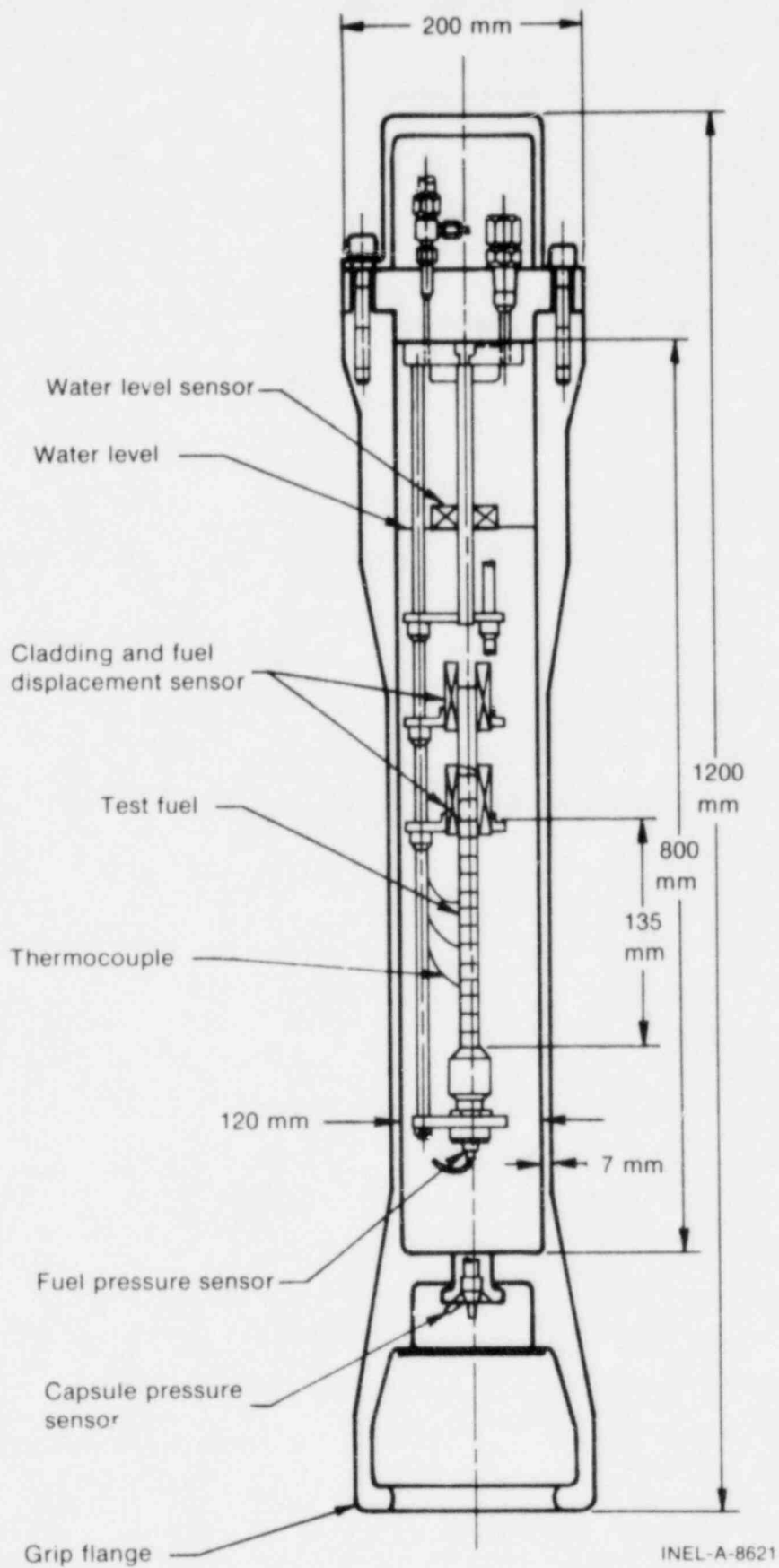
Fig. A-1 Standard capsule and internal hardware used in the NSRR tests.

TABLE A-I

NOMINAL CHARACTERISTICS OF TEST FUEL RODS[a]

Fuel Rod Type	F-type	SPX	SPXM	GEX	GEP	GEXPR	GEXPR-CH	TREAT	NSRR-STD	NSRR-WG	JPDR-II
Overall length (cm)	106	53	19.5	22.6/71	22.1/71	21.1	21.1	21.1	26.5	26.5	26.5
Active length (cm)	91	46	12.7	13.2/61	13.2/61	12.7	13.0	14.0	13.5	13.5	13.5
Cladding material	304-SS	304-SS/Zr-2	304-SS/Zr-2	Zr-2	Zr-2	Zr-2	Zr-2	Zr-2	Zr-4	Zr-4	Zr-4
Cladding heat treatment	AN	AN/CW	AN/CW	10% CW	10% CW	10% CW	10% CW	--	CW	CW	CW
Cladding outside diameter (cm)	1.184	0.635	0.635	0.794	1.43	0.794	0.794	1.422	1.072	1.072	1.223
Cladding thickness (mm)	0.508	0.356	0.356	0.508	0.313	0.508	0.508	0.71	0.62	0.62	0.70
Fuel material	UO_2	UO_2	UO_2	UO_2	UO_2	PuO_2-UO_2	PuO_2-UO_2	UO_2	UO_2	UO_2	UO_2
Fuel form	PL	PL	PL	PL/PW	PL/PW	PL	PL[b]	PL/PW	PL	PL	PL
Fuel density (% TD)	92	95	95	94/84	94/84	91	92	95/82	95	95	95
Enrichment (%)	4.8	3/5/10.5	5/10.5	5/7	5/7	7(wt% Pu)	7(wt% Pu)	5	5/10/20	10	2.6
Pellet diameter (cm)	1.067	0.559	0.559	0.681	1.23	0.683	0.688	1.260	0.929	0.909	1.066
Pellet length (cm)	1.52	1.14	1.14	1.20	2.20	0.711	0.615	--	1.0	1.0	1.5
Pellet end shape	FL	FL	FL	FL/D	FL/D	FL	FL	FL	CH	CH	FL
Radial gas gap (mm)[c]	0.076	0.025	0.025	0.038	0.102	0.051	0.051	0.102	0.095	0.195	0.085
Peak-to-average radial power density[d]	1.136	1.05/1.07/1.17	1.07/1.17	-/1.13(PL) -/1.12(PW)	1.19/1.27(PL) -/1.24(PW)	1.20	1.20	--	1.16/1.23/ 1.63	1.23	1.08

[a] Abbreviations used in this table are are follows:

AN - annealed	D - dished	PW - powder
CH - chamfered	FL - flat	SS - stainless steel
CW - cold-worked	PL - pellet	Zr - zircaloy

[b] GEXPR-CH rods had a 2.92-mm hole axially through the center of the fuel pellets.

[c] Gas gap and plenum fill gas was helium at one atmosphere for all test rods.

[d] Multiple values correspond to enrichment or fuel form variations, or both.

The GEP and TREAT rod designs were typical of boiling water reactor (BWR) rod technology of the mid-1960s, while the JPDR-II design is representative of current BWR designs. The GEX rods were radially-scaled versions of the GEP design. The SPX and SPXM test rods were radially scaled to approximate pressurized water reactor (PWR) designs of the mid-1960s while the NSRR-STD and NSRR-WG test rods more nearly typify current PWR design. the GEXPR and GEXPR-CH test rod designs were scaled versions of plutonium recycle rod designs that were under development. The F-type test rod was representative of oxide rod designs used in early generation commercial power reactors.

Radial scaling to smaller diameters and the use of higher enrichments than typical of commercial practice were necessary to allow investigations of fuel behavior at high energy depositions in the CDC. Test rods were necessarily scaled down to shorter lengths than are typical of commercial plants, due to the axial dimensions of the driver cores. As a general rule, it was determined that if the length-to-diameter ratio of the test rods was 10 or greater and end effects in the form of flux peaking were eliminated, short rods would provide representative transient data. The use of short rods with active lengths of 13 to 14 cm was also preferable to minimize the effects of axial flux variations inherent in the driver cores, thus allowing experimental results to be easily related to the specific energy depositions. Flux peaking at the ends of the fuel stacks were minimized, as necessary, by the use of poison discs or sleeves.

Some of the test rods were designed and fabricated with special features to permit dynamic measurements to be made during transients. For example, the GEX, GEP, GEXPR, GEXPR-CH, NSRR-STD, NSRR-WG, and JPDR-II fuel rods contained an iron-alloy piston in the upper plenum that served as the core of a linear variable differential transformer (LVDT) mounted on the outside of the rod during testing. This feature permitted continuous measurement of the axial fuel movement during tests. These rod types, with the exception of the GEXPR and GEXPR-CH, also had a specially designed bottom end plug that served as an adapter to a pressure transducer to allow measurement of the internal rod pressure during tests.

4. INSTRUMENTATION

Numerous instruments were used to measure dynamic variables during transient tests. All available instruments were not installed or used in all tests. Instrument selection for any given test or group of tests was dependent on specific test objectives, test fuel design, and reliability of certain instruments, depending on their state of development. Variables frequently measured in the CDC, TREAT, and NSRR programs, and the methods used to make such measurements are given in the following sections.

4.1 Fuel Rod Axial Elongation [A-2,A-4]

In the CDC and NSRR tests a small slug of iron alloy was contained within an extension piece attached to the upper end of the fuel rods. The slug formed the magnetic

core of a LVDT. Growth or contraction of the fuel rod length changed the position of the slug and the coupling between the primary and secondary windings in the LVDT. The signal from the LVDT, which was proportional to the slug position, was recorded. The accuracy of the measurement was $\sim 5\%$, with the response time estimated to be less than 1 ms.

4.2 Fuel Stack Axial Elongation[A-2,A-4]

The GEX, GEP, NSRR-STD, NSRR-WG, and JPDR-II rods were fabricated with an iron alloy piston in the upper plenum. LVDTs positioned about the upper part of the fuel rods provided a measurement of fuel stack growth or contraction during tests, with an accuracy of $\sim 5\%$ and a response time less than 1 ms.

4.3 Fuel Rod Internal Gas Pressure[A-2,A-4]

The GEX, GEP, NSRR-STD, NSRR-WG, and JPDR-II rods were designed with a lower end plug that would allow installation of a fast-response pressure transducer to measure fuel rod internal pressure. Pressure transducers were also attached to the bottom end plug of waterlogged SPXM rods. In the CDC, internal pressure measurements were generally unsatisfactory due to differential heating of the transducer diaphragm from fuel particles and blockage of the pressure transmission path.

4.4 Capsule Pressure[A-2,A-4,A-8]

A fast-response pressure transducer was positioned in the bottom of the CDC and NSRR capsules to measure dynamic pressure pulses in the capsule water surrounding the rods. Transducers with ranges up to 140 MPa were used, which had response times of $\sim 20~\mu s$ and precisions of about $\pm 20\%$. Similar transducers were located at various positions within the capsules in some NSRR tests.

4.5 Water Column Velocity[A-2,A-4]

Capsule water column velocity following rod failure was measured in the CDC and NSRR tests using a device (termed a velocity transducer) comprised of a polyethylene float, sensing coils, and two permanent magnets. The sensing coils were wound around an extension rod, with the direction of the coil winding periodically reversed. The permanent magnets, diametrically opposed, were embedded in the float. The float had about the same density as water, and when positioned in the capsule, the surface of the water was at about the top of the float. As the float moved upward with the water column, the output of the sensing coil approximated a sine wave. This system was capable of measuring water velocity to within $\pm 10\%$.

4.6 Cladding Surface Temperature[A-2,A-4,A-7]

Cladding surface temperatures were measured in the CDC, TREAT, and NSRR tests by thermocouples, resistance welded to the cladding surface. In the CDC, the most reliable method developed to measure surface temperatures of zircaloy cladding was by the use of

0.013-cm (tungsten/3% rhenium) versus (tungsten/25% rhenium) thermocouple junctions. The thermocouples were of the intrinsic type; that is, each wire was separately attached to the cladding, with the cladding completing the thermoelectric junction. Similar thermocouples were used in the TREAT tests, whereas good success has been obtained in the NSRR with platinum versus (platinum/26% rhodium) thermocouples. Chromel-Alumel thermocouples were used in the CDC tests with stainless steel clad rods.

4.7   High Speed Photography[A-5,A-7]

Some TREAT tests were conducted in capsules having a transparent quartz window to allow high speed (304 m/s) color motion pictures to be taken of rods undergoing power excursions. The film assisted in the evaluation of rod behavior during tests.

5.   PRETEST AND POSTTEST MEASUREMENTS AND INSPECTIONS

Pretest and posttest measurements and inspections generally consisted of those given in the following sections[A-2,A-4,A-7,A-8].

5.1   Neutron Radiography

All of the CDC rods were neutron radiographed and inspected prior to testing to determine if flaws existed and to verify proper construction. Neutron radiographs were taken of some intact or partially intact rods after testing, to detect changes in fuel configuration. Similar radiography was performed in some cases for the TREAT and NSRR rods.

5.2   Weights, Dimensions, and Profiles

Measurements were made of the weights and dimensions of rod components during fabrication and of the as-built rods prior to testing. Some rods were passed through a profilometer to obtain a pretest diametral profile of the cladding. Similar posttest measurements of weights, dimensions, and profiles were made on intact rods in some cases.

5.3   Particle-Size Analysis[A-9]

In some of the CDC tests in which rod failure occurred and fragmented UO_2 was released into the capsule, the fragments were collected and sized by sieve-screen methods to establish particle size distributions. These distributions were analyzed and related to energy depositions. Similar analyses were performed for some of the TREAT and NSRR tests.

5.4   Photography

Fuel rods and hardware were normally photographed following the completion of each test.

5.5   Metallurgical Examinations

Posttest metallurgical examinations of various types have been carried out on selected CDC and TREAT fuel rods. These examinations have provided detailed metallographic information on the effects of rapid power excursions on rod materials.

6.   INDIRECT MEASUREMENTS

Several measurements of importance to the evaluation of fuel behavior under RIA conditions were determined indirectly; that is, on the basis of calibration experiments and other direct measurements. These direct measurements included fuel energy deposition, energy conversion ratio, and metal-water reaction extent, which were determined as described in the following.

6.1   Energy Deposition[A-4,A-7,A-8]

Energy deposition data for tests in the CDC, TREAT, and NSRR were all derived from radiochemical determination of fission product concentrations. While destructive analysis of rods following fuel behavior tests were performed in isolated cases, most energy deposition data were based on calibration tests for specific rod types. The calibration tests in the CDC subjected a specific rod design to a nondestructive steady state or transient test; flux wires or foils were also activated during the test. Following radiochemical analysis of the fuel at the axial hot spot of the rod and scanning of the flux wire or foil, a ratio of fuel energy deposition to flux detector activation was established. Energy depositions for subsequent fuel behavior tests on the "calibrated" fuel type could then be determined from flux wires or foils activated during each test in conjunction with the reactor power history. Energy depositions determined in this way in the CDC had about a ± 12% uncertainty in absolute value and a relative precision of about ± 2%. Calibrations described in Reference A-10 indicate that uncertainties in energy deposition for most NSRR fuel types are on the order of ± 3%.

6.2   Energy Conversion Ratio

The energy conversion ratio measured in the CDC and NSRR tests was defined as the ratio of the mechanical energy generated by a rod to the fission energy deposited within the rod. The principal components of the mechanical energy were (a) kinetic energy of the water column within the capsule, and (b) enthalpy increase of the air at the top of the capsule due to adiabatic compression by the upward movement of the water column. These components were evaluated from measured water column velocities for tests with fuel failure. The reported energy conversion ratios were estimated to be within 10% of the maximum energy conversion ratios that could have been produced under the test conditions. The approach provides a meaningful relative comparison of energy conversion data as a function of energy deposition. In this way, the effects of fuel rod design,

environmental conditions, and burnup on the conversion efficiency can be determined. Further details on the methods used to determine the energy conversion ratio are provided in Reference A-4.

6.3 Metal-Water Reaction Extent[A-4,A-7]

The extent of chemical reaction between the metal rod cladding and the capsule water was experimentally determined for the CDC and TREAT tests. The reaction extent was calculated on the basis of posttest measurements of the volume of hydrogen present in the capsules. CDC data were corrected for hydrogen produced by radiolysis of the capsule water and, in cases where fuel spillage from failed rods to the capsule water occurred, for hydrogen produced by the fuel-water reaction. The extent of the fuel-water reaction was determined from the results of tests performed in the CDC with glass clad rods. Further details are provided in Reference A-4.

7. REFERENCES

A-1. J. E. Grund et al, *Subassembly Test Program Outline for FY 1969 and 1970*, IN-1313 (IDO-17277) (August 1969).

A-2. M. Ishikawa and K. Tomii (ed.), *Quarterly Progress Report on the NSRR Experiments (1); Combined, October 1975 – March 1976*, JAERI-M 6635 (June 1976).

A-3. G. A. Freund et al, "TREAT, A Pulsed Graphite-Moderated Reactor for Kinetic Experiments," *Proceedings of 2nd Conference on the Peaceful Uses of Atomic Energy, Geneva, Switzerland, 1958*, Conference Proceedings, 10.

A-4. T. G. Taxelius (ed.), *Annual Report, SPERT Project, October 1968 – September 1969*, IN-1370 (June 1970).

A-5. G. H. Golden et al, *Facility for Photographing In-Pile Meltdown Experiments in TREAT*, ANL-6457 (1962).

A-6. T. G. Taxelius (ed.), *Quarterly Technical Report, SPERT Project – July, August, Septempber 1967*, IDO-17271 (July 1968).

A-7. M. D. Freshley and L. J. Harrison, "The Transient Behavior of Vipac and Pellet Thermal Reactor Oxide Fuels," *Nuclear Technology, 15* (August 1972).

A-8. M. Ishikawa and K. Tomii (ed.), *Quarterly Progress Report on the NSRR Experiments (3); Combined, July – December 1976*, JAERI-M 7051 (March 1977).

A-9.   J. A. McClure, *Particle Size Distributions from Fuel Rods Fragmented During Power Burst Tests in the Capsule Driver Core*, IN-1428 (October 1970).

A-10. M. Ishikawa and K. Tomii (ed.), *Quarterly Progress Report on the NSRR Experiments (4); Combined, January – June 1977*, JAERI-M 7304 (August 1977).

APPENDIX B

SUMMARY OF EXPERIMENTS CONDUCTED IN THE CDC AND NSRR

APPENDIX B

SUMMARY OF EXPERIMENTS CONDUCTED IN THE CDC AND NSRR

Experiments conducted in the CDC and NSRR are categorized in terms of test numbers, fuel rod designs, transient measurements, and postirradiation examinations. Data specific to each of the experiments are summarized in Appendix C.

The information is organized into tables, which include the following for the CDC tests:

Table B-I – CDC, Unirradiated, Zircaloy Clad, Single Rod Tests
Table B-II – CDC, Unirradiated, Zircaloy Clad, Cluster Tests
Table B-III – CDC, Unirradiated, Zircaloy Clad, Mixed Oxide Tests
Table B-IV – CDC, Preirradiated, Zircaloy Clad, Single Rod Tests
Table B-V – CDC, Unirradiated, Stainless Steel Clad, Single Rod Tests
Table B-VI – CDC, Unirradiated, Zircaloy Clad Waterlogged Tests
Table B-VII – CDC, Unirradiated, Stainless Steel Clad, Waterlogged Tests.

The following tables are included for the NSRR tests[a]:

Table B-VIII – NSRR, Unirradiated, Zircaloy Clad, Single Rod Tests (NSRR-STD Fuel Rods)
Table B-IX – NSRR, Unirradiated, Zircaloy Clad, Single Rod Tests (NSRR-WG and JPDR-II Fuel Rods)
Table B-X – NSRR, Unirradiated, Zircaloy Clad, Waterlogged Tests (JPDR-II Fuel Rods).

_____

[a]   Not all NSRR tests considered in the text of this report are included in these tables. For a complete listing of NSRR tests, see Appendix C of Reference B-1.

101

TABLE B-I

CDC, UNIRRADIATED, ZIRCALOY CLAD, SINGLE ROD TESTS

Parameter	Test									
	431	432	433	434	437	438	439	454	455	456
Rod type	SPX	SPX	SPX	SPX	SPX	SPX	SPX	SPX	SPX	SPX
Fuel type	Pellet	Pellet	Pellet	Pellet	Pellet	Pellet	Pellet	Pellet	Pellet	Pellet
Cladding material[a]	An. Zr-2	An. Zr-2	An. Zr-2	An. Zr-2	An. Zr-2	An. Zr-2	An. Zr-2	CW. Zr-2	CW. Zr-2	CW. Zr-2
Energy deposition (cal/g UO_2)	197	239	269	296	388	469	569	286	388	498
Enrichment (%)	3	3	3	10	10	10	10	10	10	10
Transient measurement[b]										
Cladding elongation	N	N	N	N	N	N	N	N	N	N
Fuel elongation	N	N	N	N	N	N	N	N	N	N
Capsule pressure	N	N	N	N	N	N	0	--	X	0
Rod internal pressure	N	N	N	N	N	N	N	N	N	N
Cladding surface temperature	X	0	0	0	0	0	0	0	0	0
Water velocity	N	N	N	N	N	0	0	--	0	0
Postirradiation examination[b]										
Radiograph	N	N	N	N	N	N	N	N	N	N
Photograph	0	0	0	0	0	0	0	0	0	0
Cladding elongation	0	N	N	N	N	N	N	N	N	N
Cladding profile	N	N	N	N	N	N	N	N	N	N
Fuel weight	N	N	N	N	N	N	N	N	N	N
Metal-water reaction	0	0	0	0	0	0	0	0	0	0
Flux wire	0	0	0	0	0	0	0	0	0	0
Fuel particle size	N	N	N	N	0	0	0	N	N	0
Reference	B-2	B-2	B-2	B-2	B-2	B-2	B-2	B-2	B-2	B-2

TABLE B-I (continued)

Parameter	Test									
	457	452	458	510	537	539	503	545	504	541
Rod type	SPX	SPX-B[c]	SPX-B[c]	SPXM	SPXM	SPXM	SPXM	SPXM	SPXM	SPXM
Fuel type	Pellet	Pellet	Pellet	Pellet	Pellet	Pellet	Pellet	Pellet	Pellet	Pellet
Cladding material[a]	CW. Z-2	An. Zr-2	An. Zr-2	CW. Zr-2	CW. Zr-2	CW. Zr-2	CW. Zr-2	CW. Zr-2	CW. Zr-2	CW. Zr-2
Energy deposition (cal/g UO_2)	590	390	471	168	235	240	257	267	287	338
Enrichment (%)	10	10	10	10.5	10.5	10.5	10.5	10.5	10.5	10.5
Transient measurement[b]										
Cladding elongation	N	N	N	O	O	O	O	O	O	O
Fuel elongation	N	N	N	N	N	N	N	N	N	N
Capsule pressure	O	N	O	N	N	--	--	--	N	N
Rod internal pressure	N	N	N	N	N	N	N	N	N	N
Cladding surface temperature	O	N	O	N	O	O	N	O	N	O
Water velocity	O	O	O	N	N	--	--	--	N	N
Postirradiation examination[b]										
Radiograph	N	N	N	N	O	O	O	N	N	N
Photograph	O	O	O	O	O	O	O	O	O	O
Cladding elongation	N	N	N	O	O	O	O	N	N	N
Cladding profile	N	N	N	O	O	O	O	O	O	N
Fuel weight	N	N	N	N	N	N	N	N	N	N
Metal-water reaction	O	O	O	O	O	O	O	O	O	O
Flux wire	O	O	O	O	O	O	O	O	O	O
Fuel particle size	O	N	N	N	N	N	N	N	N	N
Reference	B-2	B-2	B-2	B-3	B-3	B-3	B-3	B-3	B-3	B-3

TABLE B-I (continued)

Parameter	Test 543	506	507	505	536	551	549	471	476	478
Rod type	SPXM	SPXM	SPXM	SPXM	SPXM	SPXM	SPXM	GEX	GEX	GEX
Fuel type	Pellet	Pellet	Pellet	Pellet	Pellet	Pellet	Pellet	Pellet	Pellet	Pellet
Cladding material[a]	CW. Zr-2	CW. Zr-2	CW.Zr-2	CW. Zr-2	CW. Zr-2	CW. Zr-2	CW. Zr-2	CW. Zr-2	CW. Zr-2	CW. Zr-2
Energy deposition (cal/g UO_2)	360	378	490	613	620	653	655	196	257	342
Enrichment (%)	10.5	10.5	10.5	10.5	10.5	10.5	10.5	7	7	7
Transient measurement[b]										
Cladding elongation	0	0	0	0	0	0	0	0	0	0
Fuel elongation	N	N	N	N	N	N	N	0	0	0
Capsule pressure	0	0	0	X	0	0	0	--	--	0
Rod internal pressure	N	N	N	N	N	N	N	N	N	N
Cladding surface temperature	0	N	N	N	0	0	0	N	N	N
Water velocity	0	0	0	0	0	0	0	--	--	0
Postirradiation examination[b]										
Radiograph	N	N	N	N	N	N	N	0	0	0
Photograph	0	0	0	0	0	0	0	0	0	0
Cladding elongation	N	N	N	N	N	N	N	0	N	N
Cladding profile	N	N	N	N	N	N	N	0	N	N
Fuel weight	N	N	N	N	N	N	N	N	N	N
Metal-water reaction	0	0	0	0	0	0	0	N	0	0
Flux wire	0	0	0	0	0	0	0	0	0	0
Fuel particle size	N	0	0	0	0	N	0	N	N	0
Reference	B-3	B-3	B-3	B-3	B-3	B-3	B-3	B-4	B-4	B-4

105

Parameter	Test									
	479	692	694	690	693	491	523	518	520	519
Rod type	GEX	GEX	GEX	GEX	GEX	GEX-L[d]	GEX	GEX	GEX	GEX
Fuel type	Pellet	Pellet	Pellet	Pellet	Pellet	Pellet	Powder	Powder	Powder	Powder
Cladding material[a]	CW. Zr-2	CW. Zr-2	CW. Zr-2	CW. Zr-2	CW. Zr-2	CW. Zr-2	CW. Zr-2	CW. Zr-2	CW. Zr-2	CW. Zr-2
Energy deposition (cal/g UO_2)	414	216	223	256	313	425	151	262	266	292
Enrichment (%)	7	7	7	7	7	7	7	7	7	7
Transient measurement[b]										
Cladding elongation	0	0	0	0	0	0	0	0	0	0
Fuel elongation	0	0	0	0	0	X	0	0	0	0
Capsule pressure	0	--	--	--	0	0	--	--	--	--
Rod internal pressure	N	N	N	N	N	N	N	N	N	N
Cladding surface temperature	N	0	0	0	0	N	0	0	0	0
Water velocity	0	--	--	--	--	0	--	--	--	--
Postirradiation examination[b]										
Radiograph	N	0	0	0	0	N	N	0	0	0
Photograph	0	0	0	0	0	0	0	0	0	0
Cladding elongation	N	0	0	0	0	N	--	0	0	0
Cladding profile	N	0	0	0	0	N	N	N	N	N
Fuel weight	N	N	N	N	N	0	N	N	N	N
Metal-water reaction	0	0	0	0	0	0	--	0	0	0
Flux wire	0	0	0	0	0	0	0	0	0	0
Fuel particle size	0	N	N	N	N	0	N	N	N	N
Reference	B-4	B-5	B-5	B-5	B-5	B-6	B-7	B-7	B-7	B-7

TABLE B-I (continued)

Parameter	Test									
	525	524	472	477	480	483	492	490	501	484
Rod type	GEX	GEX	GEX	GEX	GEX	GEX	GEX-L[d]	GEP	GEP	GEP[e]
Fuel type	Powder	Powder	Powder	Powder	Powder	Powder	Powder	Pellet	Pellet	Pellet
Cladding material[a]	CW. Zr-2	CW. Zr-2	CW. Zr-2	CW. Zr-2	CW. Zr-2	CW. Zr-2	CW. Zr-2	CW. Zr-2	CW. Zr-2	CW. Zr-2
Energy deposition (cal/g UO_2)	314	343	200	255	342	440	460	123	120	194
Enrichment (%)	7	7	7	7	7	7	7	4.95	4.95	7
Transient measurement[b]										
Cladding elongation	0	0	0	0	0	0	0	N	0	0
Fuel elongation	0	0	N	0	0	0	N	N	N	0
Capsule pressure	0	0	--	--	0	0	0	--	--	--
Rod internal pressure	N	N	N	N	N	N	N	N	N	0
Cladding surface temperature	0	0	N	N	N	N	N	N	N	N
Water velocity	--	0	--	--	0	0	0	--	--	--
Postirradiation examination[b]										
Radiograph	0	0	0	0	0	N	N	0	0	0
Photograph	0	0	0	0	0	0	0	0	0	0
Cladding elongation	N	N	0	0	N	N	N	N	0	0
Cladding profile	N	N	N	N	N	N	N	0	0	0
Fuel weight	N	N	N	N	N	N	0	N	N	N
Metal-water reaction	0	0	0	0	0	0	0	N	N	0
Flux wire	0	0	0	0	0	0	0	0	0	0
Fuel particle size	N	N	N	N	0	N	0	N	N	N
Reference	B-7	B-7	B-4	B-4	B-4	B-4	B-6	B-8	B-8	B-8

TABLE B-I (continued)

Parameter	Test 489	487	740	741	743	742	682	485	488	509
Rod type	GEP[e]	GEP[e]	GEP[e]	GEP	GEP	GEP	GEP-L[d]	GEP	GEP	GEP[d]
Fuel type	Pellet	Pellet	Pellet	Pellet	Pellet	Pellet	Pellet	Powder	Powder	Powder
Cladding material[a]	CW. Zr-2	CW. Zr-2	CW. Zr-2	CW. Zr-2	CW. Zr-2	CW. Zr-2	CW. Zr-2	CW. Zr-2	CW. Zr-2	CW. Zr-2
Energy deposition (cal/g UO_2)	201	243	194	200	238	240	245	193	254	250
Enrichment (%)	7	7	7	6.8	6.8	6.8	7	7	7	7
Transient measurement[b]										
Cladding elongation	0	0	0	0	0	0	0	0	0	0
Fuel elongation	0	0	0	0	0	0	0	N	0	0
Capsule pressure	--	0	--	--	--	--	0	--	--	--
Rod internal pressure	N	0	N	N	N	N	N	N	N	N
Cladding surface temperature	N	N	0	0	0	0	N	N	N	N
Water velocity	--	0	--	--	--	--	--	--	--	--
Postirradiation examination[b]										
Radiograph	0	0	N	N	N	N	N	0	0	N
Photograph	0	0[f]	0	0	0	0	0	0[f]	0[f]	0
Cladding elongation	0	N	0	0	0	0	N	N	N	N
Cladding profile	0	N	0	0	0	0	N	0	0	N
Fuel weight	N	N	N	N	N	N	0	N	N	0
Metal-water reaction	0	0	0	0	0	0	0	0	0	0
Flux wire	0	0	0	0	0	0	0	0	0	0
Fuel particle size	N	N	N	N	N	N	N	N	N	N
Reference	B-8	B-8	B-9	B-9	B-9	B-9	B-6	B-8	B-8	B-6

[a] An. = annealed, CW. = cold-worked.

[b] 0 = measured, - = not detected, X = instrument failure, N = no measurement.

[c] A single fuel rod was positioned in the center of a 5 x 5 square array of water filled aluminum tubes.

[d] Long rod with 0.61 m of active length.

[e] Contained 51 ppm carbon impurity.

[f] Include photomicrographs.

TABLE B-II

CDC, UNIRRADIATED, ZIRCALOY CLAD, CLUSTER TESTS

Parameter	Test						
	678	691	706	710	736	752	755
Rod type	SPXM-5[a]	SPXM-5[a]	SPXM-5[a]	SPXM-5[a]	SPXM-5[b]	SPXM-5[c]	GEX-5[c]
Fuel type	Pellet	Pellet	Pellet	Pellet	Pellet	Pellet	Pellet
Cladding material[d]	CW. Zr-2	CW. Zr-2	CW. Zr-2	CW. Zr-2	CW. Zr-2	CW. Zr-2	CW. Zr-2
Energy deposition (cal/g UO_2)[e]	125/152	218/265	236/287	315/383	225/273	226/275	197/176
Enrichment (%)	10.5	10.5	10.5	10.5	10.5	10.5	7 and 5
Transient measurement[f]							
Cladding elongation	N	N	N	N	N	N	N
Fuel elongation	N	N	N	N	N	N	N
Capsule pressure	N	N	O	O	O	O	O
Rod internal pressure	N	N	N	N	N	N	N
Cladding surface temperature	O	O	O	N	O	O	O
Water velocity	N	N	N	O	N	N	N
Postirradiation examination[f]							
Radiograph	N	N	N	N	N	N	N
Photograph	O	O	O	O	O	O	O
Cladding elongation	N	N	N	N	N	N	N
Cladding profile	N	N	N	N	N	N	O
Fuel weight	N	N	N	N	N	N	N
Metal-water reaction	N	O	O	O	O	O	N
Flux wire	O	O	O	O	O	O	O
Fuel particle size	N	N	N	O	N	N	N
Reference	B-10	B-10	B-10	B-10	B-10	B-10	B-10

[a] Five-rod lattice tests.

[b] Five-rod test with cylindrical canister, top vent.

[c] Five-rod test with four dummy rods and a square canister.

[d] CW. = cold-worked.

[e] A/B = Energy deposited in center rod/energy deposited in outside rods.

[f] O = measured, N = not measured.

TABLE B-III

CDC, UNIRRADIATED, ZIRCALOY CLAD, MIXED OXIDE TESTS

Parameter	Test						
	566	562	707	744	731	745	753
Rod type	GEXPR	GEXPR	GEXPR-CH[a]	GEXPR-CH	GEXPR-CH	GEXPR-CH	GEXPR-CH
Fuel type	Pellet[b]	Pellet[b]	Pellet[c]	Pellet[c]	Pellet[c]	Pellet[c]	Pellet[c]
Cladding material[d]	CW. Zr-2	CW. Zr-2	CW. Zr-2	CW. Zr-2	CW. Zr-2	CW. Zr-2	CW. Zr-2
Energy Deposition (cal/g UO_2)	225	274	223	275	277	329	414
Enrichment (%)	7.2	7.2	6.8	6.8	6.8	6.8	6.8
Transient measurement[e]							
Cladding elongation	0	0	0	0	0	0	0
Fuel elongation	N	N	N	0	N	0	0
Capsule pressure	N	N	N	N	N	--	0
Fuel/Internal pressure	N	N	N	N	N	N	N
Cladding surface temperature	0	0	0	0	0	0	0
Water velocity	N	N	N	N	N	--	0
Postirradiation examination[e]							
Radiograph	N	N	N	N	N	N	N
Photograph	0	0	0	0	0	0	0
Cladding elongation	0	0	0	0	0	N	N
Cladding profile	N	N	N	N	N	N	N
Fuel weight	N	N	N	N	N	N	N
Metal-water reaction	0	0	0	0	0	0	0
Flux wire	0	0	0	0	0	0	0
Fuel particle size	N	N	N	N	N	N	N
Reference	B-11	B-11	B-11	B-11	B-11	B-11	B-11

[a] CH denotes center hole.

[b] 7.2 wt% plutonium was mixed with natural uranium.

[c] 6.8 wt% plutonium was mixed with natural uranium.

[d] CW. = cold worked.

[e] 0 = measured, - = not detected, N = no measurement.

TABLE B-IV

CDC, PREIRRADIATED, ZIRCALOY CLAD, SINGLE ROD TESTS

Parameter	Test									
	759	568	567	569	703	709	685	684	756	859
Rod type	GEX 4550 MWd/t	GEX 3480 MWd/t	GEX 3100 MWd/t	GEX 4140 MWd/t	GEP 1140 MWd/t	GEP 990 MWd/t	GEX 13 100 MWd/t	GEX 12 900 MWd/t	GEX 32 700 MWd/t	GEX 31 800 MWd/t
Fuel type	Pellet	Pellet	Pellet	Pellet	Pellet	Pellet	Pellet	Pellet	Pellet	Pellet
Cladding material[a]	CW. Zr-2	CW. Zr-2	CW. Zr-2	CW. Zr-2	CW. Zr-2	CW. Zr-2	CW. Zr-2	CW. Zr-2	CW. Zr-2	CW. Zr-2
Energy Deposition (cal/g UO_2)	161	199	264	348	192	238	186	200	176	190
Enrichment (%)	7	7	7	7	7	7	7	7	7	7
Transient measurement[b]										
Cladding elongation	0	0	0	0	0	0	0	0	0	0
Fuel elongation	0	0	0	0	0	0	0	0	0	0
Capsule pressure	0	0	0	0	0	0	0	0	0	0
Fuel/Internal pressure	0	0	0	0	N	N	N	N	N	N
Cladding surface temperature	N	N	N	N	N	N	N	N	N	N
Water velocity	--	0	0	0	--	0	--	--	--	0
Postirradiation examination[b]										
Radiograph	0	0	0	0	0	0	N	N	N	N
Photograph	0[c]	0[c]	0[c]	0[c]	0	0	0	0	0	0
Cladding elongation	0	0	0	0	0	0	N	N	0	N
Cladding profile	0	0	0	0	0	0	N	N	0	N
Fuel weight	N	N	N	N	N	N	N	N	N	N
Metal-water reaction	0	0	0	0	0	0	0	0	0	0
Flux wire	0	0	0	0	0	0	0	0	0	0
Fuel particle size	N	N	N	N	N	N	N	N	N	N
Reference	B-12	B-12	B-12	B-12	B-12	B-12	B-13	B-13	B-13	B-13

[a] CW. = cold worked.

[b] 0 = measured, - = not detected, N = not measured.

[c] Include photomicrographs.

110

TABLE B-V

CDC, UNIRRADIATED, STAINLESS STEEL CLAD, SINGLE ROD TESTS

	Test									
Parameter	182	183	184	185	186	187	188	189	190	191
Rod type	F type	[a]	[a]	[a]	[a]	[a]	[a]	F type	F type	F type
Fuel type	Pellet							Pellet	Pellet	Pellet
Cladding material	Type 304							Type 304	Type 304	Type 304
Energy Deposition (cal/g UO_2)	57	71	94	153	184	220	257	151	182	216
Enrichment (%)	4.8							4.8	4.8	4.8
Transient measurement[b]										
Cladding elongation	N	N	N	N	N	N	N	N	N	N
Fuel elongation	N	N	N	N	N	N	N	N	N	N
Capsule pressure	--	--	--	--	--	--	--	--	--	--
Fuel/Internal pressure	N	N	N	N	N	N	N	N	N	N
Cladding surface temperature	0[c]	0[c]	0[c]	0[c]	0[c]	N	N	0	0	0
Water velocity	N	N	N	N	N	N	N	N	N	N
Postirradiation examination[b]										
Radiograph	N	N	N	N	N	N	N	N	N	N
Photograph	N	N	N	N	N	N	0	N	N	0[d]
Cladding elongation	0	0	0	0	0	0	0	0	0	0
Cladding profile	N	N	N	N	N	N	N	N	N	N
Fuel weight	N	N	N	N	N	N	N	N	N	N
Metal-water reaction	N	N	N	N	N	N	N	N	N	N
Flux wire	0	0	0	0	0	0	0	0	0	0
Fuel particle size	N	N	N	N	N	N	N	N	N	N
Reference	B-14	B-14	B-14	B-14	B-14	B-14	B-14	B-14	B-14	B-14

TABLE B-V (continued)

Parameter	Test 192	193	203	246-287[e]	288-301[f]	302-325[g]	319
Rod type	F type	F type	F type	F type	F type	F type	SPX
Fuel type	Pellet	Pellet	Pellet	Pellet	Pellet	Pellet	Pellet
Cladding material	Type 304	Type 304	Type 304	Type 304	Type 304	Type 304	Type 304
Energy Deposition (cal/g UO$_2$)	263	278	299	200	100	150	200
Enrichment (%)	4.8	4.8	4.8	4.8	4.8	4.8	3
Transient measurement							
Cladding elongation	N	N	N	N	N	N	N
Fuel elongation	N	N	N	N	N	N	N
Capsule pressure	--	--	--	--	--	--	--
Fuel/Internal pressure	N	N	N	N	N	N	N
Cladding surface temperature	O	O	O	N	N	N	N
Water velocity	N	N	N	N	N	N	--
Postirradiation examination							
Radiograph	N	N	N	N	N	N	N
Photograph	N	O[d]	O[d]	N	N	N	O
Cladding elongation	O	O	O	O	O	O	O
Cladding profile	N	N	N	N	N	N	N
Fuel weight	N	N	N	N	N	N	N
Metal-water reaction	N	N	N	N	N	N	--
Flux wire	O	O	O	O	O	O	O
Fuel particle size	N	N	N	N	N	N	N
Reference	B-14	B-14	B-14	B-14	B-14	B-14	B-15

TABLE B-V (continued)

Parameter	Test 322	Test 329	Test 323	Test 326	Test 327	Test 328
Rod type	SPX	SPX	SPX	SPX	SPX	SPX
Fuel type	Pellet	Pellet	Pellet	Pellet	Pellet	Pellet
Cladding material[a]	Type 304	Type 304	Type 304	Type 304	Type 304	Type 304
Energy Deposition (cal/g UO_2)	244	276	277	370	477	572
Enrichment (%)	3	3	10	10	10	10
Transient measurement						
Cladding elongation	N	N	N	N	N	N
Fuel elongation	N	N	N	N	N	N
Capsule pressure	--	--	--	0	0	0
Fuel/Internal pressure	N	N	N	N	N	N
Cladding surface temperature	0	0	0	0	0	0
Water velocity	--	--	--	0	0	0
Postirradiation examination						
Radiograph	N	N	N	N	N	N
Photograph	0	0	0	0	0	0
Cladding elongation	0	N	N	N	N	N
Cladding profile	N	N	N	N	N	N
Fuel weight	N	N	N	N	N	N
Metal-water reaction	--	0	0	0	0	0
Flux wire	0	0	0	0	0	0
Fuel particle size	N	N	N	0	0	0
Reference	B-15	B-15	B-15	B-15	B-15	B-15

[a] Sequential test on a single rod (Test 182).

[b] 0 = measured, - = not detected, N = not measured.

[c] Not accurate.

[d] Include photomicrographs.

[e] 13 tests repeated on a single rod.

[f] 14 tests repeated on a single rod.

[g] 7 tests repeated on a single rod.

TABLE B-VI

CDC, UNIRRADIATED, ZIRCALOY CLAD, WATERLOGGED TESTS

Parameter	Test									
	496	514	494	511	552	555	558	547	556	559
Rod type	GEP	GEP	GEP	GEP	SPXM-B	SPXM-B	SPXM-B	SPXM-B	SPXM-B	SPXM-B
Fuel type	Pellet	Pellet	Powder	Powder	Pellet	Pellet	Pellet	Pellet	Pellet	Pellet
Cladding material[a]	CW. Zr-2	CW. Zr-2	CW. Zr-2	CW. Zr-2	CW. Zr-2	CW. Zr-2	CW. Zr-2	CW. Zr-2	CW. Zr-2	CW. Zr-2
Energy deposition (cal/g UO_2)	220	220	265	265	430	225	225	430	225	225
Enrichment (%)	5	5	7	7	5	5	5	5	5	5
Transient measurement[b]										
Cladding elongation	0	0	0	0	0	0	0	0	0	0
Fuel elongation	N	N	N	N	N	N	N	N	N	N
Capsule pressure	0	0	0	0	0	0	0	0	0	0
Fuel/Internal pressure	N	0	0	0	0	0	0	0	0	0
Cladding surface temperature	N	N	N	N	N	N	N	N	N	N
Water velocity	0	0	0	0	0	0	0	0	0	0
Postirradiation examination[b]										
Radiograph	N	N	N	N	N	N	N	N	N	N
Photograph	0	0	0	0	0	0	0	0	0	0
Cladding elongation	N	N	N	N	N	N	N	N	N	N
Cladding profile	N	N	N	N	N	N	N	N	N	N
Fuel weight	N	N	N	N	N	N	N	N	N	N
Metal-water reaction	N	N	N	N	N	N	N	N	N	N
Flux wire	0	0	0	0	0	0	0	0	0	0
Fuel particle size	N	N	N	N	N	N	N	N	N	N
Reference	B-16	B-16	B-16	B-16	B-17	B-17	B-17	B-17	B-17	B-17

[a] CW. = cold-worked.

[b] 0 = measured, N = not measured.

TABLE B-VII

CDC, UNIRRADIATED, STAINLESS STEEL CLAD, WATERLOGGED TESTS

					Test					
Parameter	194	195	196	197	198	199	200	201	202	205
Rod type	F type	[a]	[a]	[a]	[a]	[a]	[a]	[a]	F type	F type
Fuel type	Pellet								Pellet	Pellet
Cladding material[b]	An. Type 304								An. Type 304	An. Type 304
Energy Deposition (cal/g UO_2)	54	70	71	89	101	119	136	155	153	181
Enrichment (%)	4.8								4.8	4.8
Transient measurement[c]										
Cladding elongation	N	N	N	N	N	N	N	N	N	N
Fuel elongation	N	N	N	N	N	N	N	N	N	N
Capsule pressure	--	--	--	--	--	--	--	--	--	--
Fuel/Internal pressure	N	N	N	N	N	N	N	N	N	N
Cladding surface temperature	N	N	N	N	N	N	N	N	N	N
Water velocity	N	N	N	N	N	N	N	N	N	N
Postirradiation examination[c]										
Radiograph	N	N	N	N	N	N	N	N	N	N
Photograph	N	N	N	N	N	N	N	N	N	N
Cladding elongation	--	--	0	0	0	0	0	0	0	0
Cladding profile	N	N	N	N	N	N	N	N	N	N
Fuel weight	N	N	N	N	N	N	N	N	N	N
Metal-water reaction	N	N	N	N	N	N	N	N	N	N
Flux wire	0	0	0	0	0	0	0	0	0	0
Fuel particle size	N	N	N	N	N	N	N	N	N	N
Reference	B-14	B-14	B-14	B-14	B-14	B-14	B-14	B-14	B-14	B-14

TABLE B-VII (continued)

Parameter	Test 206	217	218	521	527	538	546	540	544
Rod type	F type	F type	F type	F type	F type[d]	SPXM-B	SPXM-B	SPXM-B	SPXM-B
Fuel type	Pellet	Pellet	Pellet	Pellet	Pellet	Pellet	Pellet	Pellet	Pellet
Cladding material[a]	An. Type 304	An. Type 304	An. Type 304	An. Type 304	An. Type 304	An. Type 304	An. Type 304	An. Type 304	An. Type 304
Energy deposition (cal/g UO_2)	223	257	283	300	300	380	380	380	380
Enrichment (%)	4.8	4.8	4.8	4.8	4.8	5	5	5	5
Transient measurement									
Cladding elongation	N	N	N	N	N	0	0	0	0
Fuel elongation	N	N	N	N	N	N	N	N	N
Capsule pressure	--	--	--	0	0	0	0	0	0
Fuel/Internal pressure	N	N	N	0	0	0	0	0	0
Cladding surface temperature	N	N	N	N	N	N	N	N	N
Water velocity	N	N	N	0	0	0	0	0	0
Postirradiation examination									
Radiograph	N	N	N	N	N	N	N	N	N
Photograph	N	N	N	0	0	0	0	0	0
Cladding elongation	0	0	0	N	N	N	N	N	N
Cladding profile	N	N	N	N	N	N	N	N	N
Fuel weight	N	N	N	N	N	N	N	N	N
Metal-water reaction	N	N	N	N	N	N	N	N	N
Flux wire	0	0	0	0	0	0	0	0	0
Fuel particle size	N	N	0	N	N	N	N	N	N
Reference	B-14	B-14	B-14	B-14	B-14	B-17	B-17	B-17	B-17

[a] Sequential tests on a single rod.

[b] An. = annealed.

[c] 0 = measured, - = not detected, N = not measured.

[d] Rod was partially filled with water, 0.36 m of 0.91 m active length.

TABLE B-VIII

NSRR, UNIRRADIATED, ZIRCALOY CLAD, SINGLE ROD TESTS (NSRR-STD rods)

Parameter	Test									
	200-1-1	200-2-1	200-3	111-3	200-4	200-1-2[a]	111-4	201-1	200-5	200-5b
Rod type	NS-STD	NS-STD	NS-STD	NS-STD	NS-STD	NS-STD	NS-STD	NS-STD	NS-STD	NS-STD
Fuel type	Pellet	Pellet	Pellet	Pellet	Pellet	Pellet	Pellet	Pellet	Pellet	Pellet
Cladding material	Zr-4	Zr-4	Zr-4	Zr-4	Zr-4	Zr-4	Zr-4	Zr-4	Zr-4	Zr-4
Energy deposition (cal/g UO_2)	39	116	176	189	233	241	244	244	264	267
Enrichment (%)	10	10	10	10	10	10	10	10	10	10
Transient measurement[b]										
Cladding elongation	N	N	N	N	N	N	N	N	N	N
Fuel elongation	N	N	N	N	N	N	N	N	N	N
Capsule pressure	N	N	N	N	N	N	N	N	N	N
Fuel/Internal pressure	N	N	N	N	N	N	N	N	N	N
Cladding surface temperature	0	0	0	X	0	0	0	0	0	0
Water velocity	N	N	N	N	N	N	N	N	N	N
Postirradiation Examination[b]										
Radiograph	N	N	N	N	N	N	N	N	N	N
Photograph	N	N	0	0	0	0	0	0	0	0
Cladding elongation	N	N	0	0	0	0	0	0	0	0
Cladding profile	N	N	0	0	0	0	0	0	0	0
Fuel weight	N	N	N	N	N	N	N	N	N	N
Metal-water reaction	N	N	N	N	N	N	N	N	N	N
Flux wire	N	N	N	N	N	N	N	N	N	N
Fuel particle size	N	N	N	N	N	N	N	N	N	N
Reference	B-18	B-18	B-18	B-18	B-18	B-18	B-18	B-19	B-18	B-19

	Test									
Parameter	111-5	200-2-2	200-6	200-6b	200-7	111-6	111-7	111-8	209-1-1	209-1-5
Rod type	NS-STD	NS-STD	NS-STD	NS-STD	NS-STD	NS-STD	NS-STD	NS-STD	NS-STD[c]	NS-STD[c]
Fuel type	Pellet	Pellet	Pellet	Pellet	Pellet	Pellet	Pellet	Pellet	Pellet	
Cladding material	Zr-4	Zr-4	Zr-4	Zr-4	Zr-4	Zr-4	Zr-4	Zr-4	Zr-4	
Energy deposition (cal/g UO_2)	270	271	271	276	295	333	376	433	177	179
Enrichment (%)	10	10	10	10	10	10	10	10	10	10
Transient measurement[b]										
Cladding elongation	N	N	N	N	N	N	N	N	N	N
Fuel elongation	N	N	N	N	N	N	N	N	N	N
Capsule pressure	N	N	N	N	N	N	N	N	N	N
Fuel/Internal pressure	N	N	N	N	N	N	N	N	N	N
Cladding surface temperature	O	O	O	O	O	O	O	X	O	O
Water velocity	N	N	N	N	N	N	N	N	N	N
Postirradiation examination[b]										
Radiograph	N	N	N	N	N	N	N	N	N	N
Photograph	O	O	O	O	O	O	O	O	N	O
Cladding elongation	O	O	O	N	N	N	N	N	N	O
Cladding profile	O	O	O	N	N	N	N	N	N	O
Fuel weight	N	N	N	N	N	N	N	N	N	N
Metal-water reaction	N	N	N	N	N	N	N	N	N	N
Flux wire	N	N	N	N	N	N	N	N	N	N
Fuel particle size	N	N	N	N	N	N	N	N	N	N
Reference	B-18	B-18	B-18	B-19	B-18	B-18	B-18	B-19	B-19	B-19

[a] Long run-out power period test.

[b] O = measured, X = instrument failure, N = not measured.

[c] Five sequential tests on a single rod (Tests 209-1-1 through 209-1-5).

TABLE B-IX

NSRR, UNIRRADIATED, ZIRCALOY CLAD, SINGLE ROD TESTS (NSRR-WG, and JPDR-II rods)

Parameter	Test									
	232-1	232-2	232-3	232-4	232-6	232-5	111-1	111-2	111-9	111-10
Rod type	NS-WG	NS-WG	NS-WG	NS-WG	NS-WG	NS-WG	JPDR-II	JPDR-II	JPDR-II	JPDR-II
Fuel type	Pellet	Pellet	Pellet	Pellet	Pellet	Pellet	Pellet	Pellet	Pellet	Pellet
Cladding material	Zr-4	Zr-4	Zr-4	Zr-4	Zr-4	Zr-4	Zr-4	Zr-4	Zr-4	Zr-4
Energy deposition (cal/g UO_2)	181	236	261	274	294	326	44	112	158	204
Enrichment (%)	10	10	10	10	10	10	2.6	2.6	2.6	2.6
Transient measurement[a]										
Cladding elongation	N	N	N	N	N	N	N	N	N	N
Fuel elongation	N	N	N	N	N	N	N	N	N	N
Capsule pressure	N	N	N	N	N	N	N	N	N	N
Fuel/Internal pressure	N	N	N	N	N	N	N	N	N	N
Cladding surface temperature	O	O	O	O	O	X	O	O	X	O
Water velocity	N	N	N	N	N	N	N	N	N	N
Postirradiation examination[a]										
Radiograph	N	N	N	N	N	N	N	N	N	N
Photograph	O	O	O	O	O	O	O	O	O	O
Cladding elongation	--	O	O	O	O	N	O	O	O	O
Cladding profile	--	O	O	O	O	N	O	O	O	O
Fuel weight	N	N	N	N	N	N	N	N	N	N
Metal-water reaction	N	N	N	N	N	N	N	N	N	N
Flux wire	N	N	N	N	N	N	N	N	N	N
Fuel particle size	N	N	N	N	N	N	N	N	N	N
Reference	B-18	B-18	B-18	B-18	B-18	B-18	B-18	B-18	B-19	B-19

[a] O = measured, X = instrument failure, N = not measured.

NSRR, UNIRRADIATED, ZIRCALOY CLAD, WATERLOGGED TESTS (JPDR-II rods)

Parameter	401-1	401-2	401-3	401-3b	402-1[a]	402-2[a]	402-3[a]	411-3[b]	421-3[c]
					Test				
Rod type	JPDR-II	JPDR-II	JPDR-II	JPDR-II	JPDR-II	JPDR-II	JPDR-II	JPDR-II	JPDR-II
Fuel type	Pellet	Pellet	Pellet	Pellet	Pellet	Pellet	Pellet	Pellet	Pellet
Cladding Material	Zr-2	Zr-2	Zr-2	Zr-2	Zr-2	Zr-2	Zr-2	Zr-2	Zr-2
Energy deposition (cal/g UO_2)	53	106	154	150	47	104	154	152	152
Enrichment (%)	2.6	2.6	2.6	2.6	2.6	2.6	2.6	2.6	2.6
Transient measurement[d]									
Cladding elongation	N	N	N	N	N	N	N	N	N
Fuel elongation	N	N	N	N	N	N	N	N	N
Capsule pressure	O	O	O	O	O	O	X	O	O
Fuel/Internal pressure	O	O	X	O	O	X	O	O	O
Cladding surface temperature	O	O	O	O	O	O	O	O	O
Water velocity	--	--	O	O	--	--	--	O	--
Postirradiation examination[d]									
Radiograph	N	N	N	N	N	N	N	N	N
Photograph	N	N	O	O	N	N	N	O	O
Cladding elongation	O	O	O	O	O	O	O	O	O
Cladding profile	O	O	O	O	O	O	O	O	O
Fuel weight	N	N	N	N	N	N	N	N	N
Metal-water reaction	N	N	N	N	N	N	N	N	N
Flux wire	N	N	N	N	N	N	N	N	N
Fuel particle size	N	N	N	N	N	N	N	N	N
Reference	B-18	B-18	B-18	B-19	B-18	B-18	B-18	B-19	B-19

[a] Rod was partially filled with water.

[b] Cladding had a small hole drilled at the center of active region.

[c] Cladding had a small hole drilled at the upper plenum region.

[d] O = measured, X = instrument failure, N = not measured.

REFERENCES

B-1.   M. Ishikawa and K. Tomii (ed.), *Quarterly Progress Report on the NSRR Experiments (4); Combined, January – June 1977*, JAERI-M 7304 (August 1977).

B-2.   Z. R. Martinson and R. L. Johnson, *Transient Irradiation of 1/4-Inch OD Zircaloy-2 Clad Oxide Fuel Rods to 590 cal/g UO_2*, IDO-ITR-102 (November 1968).

B-3.   Z. R. Martinson, *Behavior of 5-Inch Long, 1/4-Inch OD, Zircaloy-2 Clad Oxide Fuel Rods Subjected to High Energy Power Bursts*, IN-ITR-107 (August 1969).

B-4.   R. W. Miller and W. G. Lussie, *The Response of UO_2 Fuel Rods to Power Bursts – 5/16-Inch OD, Pellet and Powder Fuel, Zircaloy Clad*, IDO-ITR-103 (January 1969).

B-5.   W. G. Lussie, *The Response of UO_2 Fuel Rods to Power Bursts – Detailed Tests on 5/16-Inch OD, Pellet Fuel, Zircaloy Clad Rods*, IN-ITR-112 (January 1970).

B-6.   L. J. Siefken, *The Effects of Axial Length on the Response of Zircaloy Clad, UO_2 Fuel Rods to Power Bursts*, IN-ITR-109 (December 1969).

B-7.   W. G. Lussie and R. W. Miller, *The Response of UO_2 Fuel Rods to Power Bursts – Detailed Tests on 5/16-Inch OD, Powder Fuel, Zircaloy Clad Rods*, IN-1302, (IDO-ITR-106) (June 1969).

B-8.   R. W. Miller and W. G. Lussie, *The Response of UO_2 Fuel Rods to Power Bursts – 9/16-Inch OD, Pellet and Powder Fuel, Zircaloy Clad*, IDO-ITR-104 (April 1969).

B-9.   W. G. Lussie and R. W. Miller, *Carbon Impurity in UO_2 and Its Effects on Cladding Swelling During Power Bursts*, IN-ITR 115 (July 1970).

B-10.   L. J. Siefken, *The Response of Fuel Rod Clusters to Power Bursts*, IN-ITR-116 (May 1970).

B-11.   W. G. Lussie, *The Response of Mixed Oxide Fuel Rods to Power Bursts*, IN-ITR-114 (April 1970).

B-12.   R. W. Miller, *The Effects of Burnup on Fuel Failure: I. Power Burst Tests on Low Burnup UO_2 Fuel Rods*, IN-ITR-113 (July 1970).

B-13.   R. W. Miller, *The Effects of Burnup on Fuel Failure – Power Burst Tests on Fuel Rods with 13,000 and 32,000 MWd/MTU Burnup*, ANCR-1280 (January 1976).

B-14.   L. A. Stephan and C. S. Olsen, *Transient Irradiation of 0.466-Inch OD Stainless Steel Clad Oxide Fuel Rods to 300 cal/g UO_2*, IDO-ITR-101 (November 1968).

B-15. J. A. McClure and L. J. Siefken, *Transient Irradiation of 1/4-Inch OD Stainless Steel Clad Oxide Fuel Rods to 570 cal/g UO$_2$*, IDO-ITR-100 (October 1968).

B-16. L. A. Stephan, *The Response of Waterlogged UO$_2$ Fuel Rods to Power Bursts*, IDO-ITR-105 (April 1969).

B-17. L. A. Stephan, *The Effects of Cladding Material and Heat Treatment on the Response of Waterlogged UO$_2$ Fuel Rods to Power Bursts*, IN-ITR-111 (January 1970).

B-18. M. Ishikawa and K. Tomii (ed.), *Quarterly Progress Report on the NSRR Experiments (1); Combined, October 1975 — March 1976*, JAERI-M 6635 (June 1976).

B-19. M. Ishikawa and K. Tomii (ed.), *Quarterly Progress Report on the NSRR Experiments (2), April — June 1976*, JAERI-M 6790 (October 1976).

The following two interim technical reports (ITR) are included to provide a literature source for those readers in search of additional information.

1. C. S. Olsen, *Measurements of the Reaction of UO$_2$ With Water for Transient Energy Depositions to 550 cal/g of UO$_2$*, IN-ITR-108 (November 1969).

2. W. G. Lussie, *The Response of Heterogeneous Mixed-Oxide Fuel Rods to Power Bursts*, IN-ITR-117 (September 1970).

APPENDIX C

SUMMARY OF DATA FROM THE CDC AND NSRR EXPERIMENTS

APPENDIX C

SUMMARY OF DATA FROM THE CDC AND NSRR EXPERIMENTS

Data from tests conducted in the CDC and NSRR are summarized in this appendix. The data are contained in tables that parallel those presented in Appendix B (fuel rod and experiment design) and include the following for the CDC:

Table C-I – CDC, Unirradiated, Zircaloy Clad, Single Rod Test Data
Table C-II – CDC, Unirradiated, Zircaloy Clad, Cluster Test Data
Table C-III – CDC, Unirradiated, Zircaloy Clad, Mixed Oxide Test Data
Table C-IV – CDC, Preirradiated, Zircaloy Clad, Single Rod Test Data
Table C-V – CDC, Unirradiated, Stainless Steel Clad, Single Rod Test Data
Table C-VI – CDC, Unirradiated, Zircaloy Clad, Waterlogged Test Data
Table C-VII – CDC, Unirradiated, Stainless Steel Clad, Waterlogged Test Data.

The following data tables are included for the NSRR[a]:

Table C-VIII – NSRR, Unirradiated, Zircaloy Clad, Single Rod Test Data (NSRR-STD Fuel Rods)
Table C-IX – NSRR, Unirradiated, Zircaloy Clad, Single Rod Test Data (NSRR-WG and JPDR-II Fuel Rods)
Table C-X – NSRR, Unirradiated, Zircaloy Clad, Waterlogged Test Data (JPDR-II Fuel Rods).

---

[a] Not all NSRR data considered in the text of this report are included in these tables. Most additional data may be found in Reference C-1.

TABLE C-I

CDC, UNIRRADIATED, ZIRCALOY CLAD, SINGLE ROD TEST DATA

Parameter	Test 431	432	433	434	437
Rod type[a]	SPX-PL	SPX-PL	SPX-PL	SPX-PL	SPX-PL
Average energy Deposition (cal/g UO_2):					
Total	197	239	269	296	388
At failure	--	--	--	--	--
Pellet surface energy Deposition (cal/cm^3 UO_2):					
Total	2141	2597	2923	3602	4721
At failure	--	--	--	--	--
Reactor period (ms)	4.3	3.6	3.15	6.7	5.0
Peaking factor:					
Radial	1.045	1.045	1.045	1.17	1.17
Axial	1.08	1.08	1.08	1.09	1.09
Cladding temperature (°C):					
Maximum	--	1600	1950	1900	--
At failure	--	--	--	--	1300
Cladding radial expansion (%):					
Maximum	--	--	--	--	--
Average	--	--	--	--	--
Cladding elongation (%):					
Transient maximum	--	--	--	--	--
Residual	1.79	--	--	--	--
Fuel elongation, maximum (%)	--	--	--	--	--
Capsule pressure (MPa)	0	0	0	0	0
Nuclear-to-mechanical energy conversion (%)	--	--	--	--	--
Cladding surface oxidation[b]	2	2	2	2	--
Failure mode and extent[c]	No-B	Crack-I	Melt-II	Melt-II	Melt-III
Fuel enrichment (%)[d]	3	3	3	10	10
Fuel density (g/cm^3)[d]	10.4	10.4	10.4	10.4	10.4
Fuel diameter (mm)[d]	5.59	5.59	5.59	5.59	5.59
Cladding (mm)[d]					
Outside diameter	6.35	6.35	6.35	6.35	6.35
Thickness	0.356	0.356	0.356	0.356	0.356
Gas gap width (mm)[d]	0.025	0.025	0.025	0.025	0.025
Active UO_2 length (mm)[d]	457	457	457	457	457

TABLE C-I (continued)

Parameter	Test 438	Test 439	Test 454	Test 455	Test 456
Rod type[a]	SPX-PL	SPX-PL	SPX-PL	SPX-PL	SPX-PL
Average energy					
Deposition (cal/g UO_2):					
Total	469	569	286	388	498
At failure	400	390	--	370	480
Pellet surface energy					
Deposition (cal/cm^3 UO_2):					
Total	5707	6926	3480	4721	6060
At failure	4867	4746	--	4502	5841
Reactor period (ms)	4.1	3.4	6.9	5.1	4.0
Peaking factor:					
Radial	1.17	1.17	1.17	1.17	1.17
Axial	1.09	1.09	1.09	1.09	1.09
Cladding temperature (°C):					
Maximum	2060	--	--	--	--
At failure	800	580	1750	~1860	1170
Cladding radial expansion (%):					
Maximum	--	--	--	--	--
Average	--	--	--	--	--
Cladding elongation (%):					
Transient maximum	--	--	--	--	--
Residual	--	--	--	--	--
Fuel elongation, maximum (%)	--	--	--	--	--
Capsule pressure (MPa)	--	0.82	0	--	0.48
Nuclear-to-mechanical energy conversion (%)	0.04	0.21	--	0.01	0.02
Cladding surface oxidation[b]	--	--	--	--	--
Failure mode and extent[c]	Melt-III	Melt-III	Melt-II	Melt-III	Melt-III
Fuel Enrichment (%)[d]	10	10	10	10	10
Fuel density (g/cm^3)[d]	10.4	10.4	10.4	10.4	10.4
Fuel diameter (mm)[d]	5.59	5.59	5.59	5.59	5.59
Cladding (mm)[d]					
Outside diameter	6.35	6.35	6.35	6.35	6.35
Thickness	0.356	0.356	0.356	0.356	0.356
Gas gap width (mm)[d]	0.025	0.025	0.025	0.025	0.025
Active UO_2 length (mm)[d]	457	457	457	457	457

TABLE C-I (continued)

Parameter	Test 457	452	458	510	537
Rod type[a]	SPX-PL	SPXB-PL	SPXB-PL	SPXM-PL	SPXM-PL
Average energy					
Deposition (cal/g UO_2):					
Total	590	390	471	168	235
At failure	510	380	400	--	--
Pellet surface energy					
Deposition (cal/cm^3 UO_2):					
Total	7179	4746	5751	2063	7987
At failure	6206	4624	4867	--	--
Reactor period (ms)	3.3	4.2	3.4	11.7	8.25
Peaking factor:					
Radial	1.17	1.17	1.17	1.17	1.17
Axial	1.09	1.09	1.09	1.08	1.08
Cladding temperature (°C):					
Maximum	--	--	--	--	1720
At failure	280	--	500	--	--
Cladding radial expansion (%):					
Maximum	--	--	--	1.04	3.79
Average	--	--	--	0.76	3.19
Cladding elongation (%):					
Transient maximum	--	--	--	1.6	3.4
Residual	--	--	--	0.8	2.0
Fuel elongation, maximum (%)	--	--	--	--	--
Capsule pressure (MPa)	2.76	--	1.48	0	0
Nuclear-to-mechanical					
energy conversion (%)	0.19	0.0	0.05	0	0
Cladding surface oxidation[b]	--	--	--	2	2
Failure mode and extent[c]	Melt-III	Melt-III	Melt-III	No-B	No-B
Fuel enrichment (%)[d]	10	10	10	10.5	10.5
Fuel density (g/cm^3)[d]	10.4	10.4	10.4	10.4	10.4
Fuel diameter (mm)[d]	5.59	5.59	5.59	5.59	5.59
Cladding (mm)[d]					
Outside diameter	6.35	6.35	6.35	6.35	6.35
Thickness	0.356	0.356	0.356	0.356	0.356
Gas gap width (mm)[d]	0.025	0.025	0.025	0.025	0.025
Active UO_2 length (mm)[d]	457	457	457	127	127

TABLE C-I (continued)

Parameter	Test				
	539	503	545	504	541
Rod type[a]	SPXM-PL	SPXM-PL	SPXM-PL	SPXM-PL	SPXM-PL
Average energy					
Deposition (cal/g UO_2):					
Total	240	247	267	287	338
At failure	--	--	--	--	--
Pellet surface energy					
Deposition (cal/cm^3 UO_2):					
Total	2948	3157	3280	3526	4152
At failure	--	--	--	--	--
Reactor period (ms)	8.11	7.60	7.26	6.86	5.59
Peaking factor:					
Radial	1.17	1.17	1.17	1.17	1.17
Axial	1.08	1.08	1.08	1.08	1.08
Cladding temperature (°C):					
Maximum	1700	--	1806	--	1880
At failure	--	--	--	--	--
Cladding radial expansion (%):					
Maximum		--	--	--	--
Average	3.11	--	--	--	--
Cladding elongation (%):					
Transient maximum	5.0	3.6	3.6	3.6	2.2
Residual	3.4	1.46	2.2	--	--
Fuel elongation, maximum (%)	--	--	--	--	--
Capsule pressure (MPa)	0	3	0	0	0
Nuclear-to-mechanical					
energy conversion (%)	0	0	0	0	0
Cladding surface oxidation[b]	2	2	2	2	2
Failure mode and extent[c]	No-B	Crack-I	Melt-II	Melt-II	Melt-II-III
Fuel enrichment (%)[d]	10.5	10.5	10.5	10.5	10.5
Fuel density (g/cm^3)[d]	10.4	10.4	10.4	10.4	10.4
Fuel diameter (mm)[d]	5.59	5.59	5.59	5.59	5.59
Cladding (mm)[d]					
Outside diameter	6.35	6.35	6.35	6.35	6.35
Thickness	0.356	0.356	0.356	0.356	0.356
Gas gap width (mm)[d]	0.025	0.025	0.025	0.025	0.025
Active UO_2 length (mm)[d]	127	127	127	127	127

TABLE C-I (continued)

Parameter	Test				
	543	506	507	505	536
Rod type[a]	SPXM-PL	SPXM-PL	SPXM-PL	SPXM-PL	SPXM-PL
Average energy					
Deposition (cal/g UO_2):					
Total	360	378	410	613	620
At failure	330	365	403	470	420
Pellet surface energy					
Deposition (cal/cm^3 UO_2):					
Total	4423	4644	6020	7531	7617
At failure	4054	4494	4914	5774	5160
Reactor period (ms)	5.2	4.93	4.10	3.27	3.28
Peaking factor:					
Radial	1.17	1.17	1.17	1.17	1.17
Axial	1.08	1.08	1.08	1.08	1.08
Cladding temperature (°C):					
Maximum	1680	--	--	--	--
At failure	1440	--	--	--	500
Cladding radial expansion (%):					
Maximum	--	--	--	--	--
Average	--	--	--	--	--
Cladding elongation (%):					
Transient maximum	2.0	1.8	1.3	2.9	0.8
Residual	--	--	--	--	--
Fuel elongation, maximum (%)	--	--	--	--	--
Capsule pressure (MPa)	0.21	0.41	1.25	--	2.62
Nuclear-to-mechanical					
energy conversion (%)	0.01	0.02	0.2	1.3	1.4
Cladding surface oxidation[b]	--	--	--	--	--
Failure mode and extent[c]	Melt-III	Melt-III	Melt-III	Melt-III	Melt-III
Fuel enrichment (%)[d]	10.5	10.5	10.5	10.5	10.5
Fuel density (g/cm^3)[d]	10.5	10.5	10.5	10.5	10.5
Fuel diameter (mm)[d]	5.59	5.59	5.59	5.59	5.59
Cladding (mm)[d]					
Outside diameter	6.35	6.35	6.35	6.35	6.35
Thickness	0.356	0.356	0.356	0.356	0.356
Gas gap width (mm)	0.025[d]	0.025[e]	0.025[e]	0.025[e]	0.025[e]
Active UO_2 length (mm)[d]	127	127	127	127	127

TABLE C-I (continued)

Parameter	Test				
	551	549	471	476	478
Rod type[a]	SPXM-PL	SPXM-PL	GEX-PL	GEX-PL	GEX-PL
Average energy Deposition (cal/g UO_2):					
Total	653	665	196	257	342
At failure	600	360	--	--	300
Pellet surface energy Deposition (cal/cm^3 UO_2):					
Total	8022	8047	2281	2991	3981
At failure	4914	4423	--	--	3492
Reactor period (ms)	2.99	3.01	6.44	4.80	3.66
Peaking factor:					
Radial	1.17	1.17	1.13	1.13	1.13
Axial	1.08	1.08	1.08	1.08	1.08
Cladding temperature (°C):					
Maximum	--	--	--	--	--
At failure	300	300	--	--	--
Cladding radial expansion (%):					
Maximum	--	--	3.52	--	--
Average	--	--	1.76	--	--
Cladding elongation (%):					
Transient maximum	1.0	1.0	1..	2.72	0.26
Residual	--	--	0.36	--	--
Fuel elongation, maximum (%)	--	--	1.24	2.94	1.1
Capsule pressure (MPa)	11.03	12.07	--	0	2.59
Nuclear-to-mechanical energy conversion (%)	2.2	2.8	0	0	0.19
Cladding surface oxidation[b]	--	--	2	2	2
Failure mode and extent[c]	Melt-III	Melt-III	No-B	Melt-II	Melt-III
Fuel enrichment (%)[d]	10.5	10.5	7	7	7
Fuel density (g/cm^3)[d]	10.5	10.5	10.3	10.3	10.3
Fuel diameter (mm)	5.59[d]	5.59[d]	6.82[e]	6.82[e]	6.82[e]
Cladding (mm)					
Outside diameter	6.35[d]	6.35[d]	7.86[e]	7.87[e]	7.85[e]
Thickness[d]	0.365	0.365	0.490	0.491	0.481
Gas gap width (mm)	0.025[e]	0.025[e]	0.033[e]	0.032[e]	0.033[e]
Active UO_2 length (mm)	127[d]	127[d]	131[e]	131[e]	131[e]

TABLE C-I (continued)

Parameter	479	692	694	690	693
			Test		
Rod type[a]	GEX-PL	GEX-PL	GEX-PL	GEX-PL	GEX-PL
Average energy					
Deposition (cal/g UO_2):					
Total	414	216	223	256	313
At failure	375	--	--	--	298
Pellet surface energy					
Deposition (cal/cm^3 UO_2):					
Total	4819	2514	2595	2980	3643
At failure	4365	--	--	--	3468
Reactor period (ms)	3.00	5.58	5.60	4.90	4.23
Peaking factor:					
Radial	1.13	1.13	1.13	1.13	1.13
Axial	1.08	1.08	1.08	1.08	1.08
Cladding temperature (°C):					
Maximum	--	1550	1625	1750	1900
At failure	--	--	--	--	1700
Cladding radial expansion (%):					
Maximum	--	2.72	3.10	--	--
Average	--	1.89	1.76	--	--
Cladding elongation (%):					
Transient maximum	14.0	1.52	1.42	1.56	1.26
Residual	--	0.44	0.38	--	--
Fuel elongation, maximum (%)	5	1.92	2.2	1.22	2.00
Capsule pressure (MPa)	4.96	0	0	0	0.18
Nuclear-to-mechanical					
energy conversion (%)	0.19	0	0	0	0
Cladding surface oxidation[h]	2	2	2	2	2
Failure mode and extent[c]	Melt-III	No	No-B	Crack-I	Melt-II-III
Fuel enrichment (%)[d]	7	7	7	7	7
Fuel density (g/cm^3)	10.3	10.33[e]	10.22[e]	10.31[e]	10.38[e]
Fuel diameter (mm)	6.82[e]	6.81[d]	6.81[d]	6.81[d]	6.81[d]
Cladding (mm)[d]					
Outside diameter	7.87	7.84	7.86	7.86	7.84
Thickness	0.491	0.491	0.486	0.487	0.486
Gas gap width (mm)	0.032[e]	0.038[d]	0.038[d]	0.038[d]	0.038[d]
Active UO_2 length (mm)[d]	128	128	128	128	128

TABLE C-I (continued)

Parameter	Test 491	523	518	520	519
Rod type[a]	GEXL-PL	GEX-PW	HRC-PW	GEX-PW	GEX-PW
Average energy Deposition (cal/g UO_2):					
Total	425	151	262	266	292
At failure	330	--	--	--	--
Pellet surface energy Deposition (cal/cm^3 UO_2):					
Total	4903	1546	2697	2735	2996
At failure	3807	--	--	--	--
Reactor period (ms)	3.0	8.53	5.13	4.96	4.62
Peaking factor:					
Radial	1.12	1.12	1.12	1.12	1.12
Axial	1.2	1.08	1.08	1.08	1.08
Cladding temperature (°C):					
Maximum	--	900	1575	1570	1850
At failure	--	--	--	--	--
Cladding radial expansion (%):					
Maximum	--	--	3.16	2.42	--
Average	--	--	1.90	1.61	--
Cladding elongation (%):					
Transient maximum	1.80	0.44	1.26	1.12	2.24
Residual	--	--	0.40	0.20	--
Fuel elongation, maximum (%)	--	1.56	4.40	4.40	1.32
Capsule pressure (MPa)	4.93	0	0	0	0
Nuclear-to-mechanical energy conversion (%)	0.19	0	0	0	0
Cladding surface oxidation[b]	--	2	2	2	2
Failure mode and extent[c]	Melt-III	No-B	No-B	No	Melt-II
Fuel enrichment (%)[d]	7	7	7	7	7
Fuel density (g/cm^3)[d]	10.30	9.14	9.19	9.18	9.16
Fuel diameter (mm)	6.97[d]	6.97[d]	6.96[e]	6.97[e]	6.97[e]
Cladding (mm)[d]					
Outside diameter	7.94	7.88	7.89	7.88	7.89
Thickness	0.483	0.453	0.465	0.455	0.458
Gas gap width (mm)	0.038[d]	0[e]	0[e]	0[e]	0[e]
Active UO_2 length (mm)[d]	612	130	130	130	130

TABLE C-I (continued)

Parameter	Test				
	525	524	472	477	480
Rod type[a]	GEX-PW	GEX-PW	GEX-PW	GEX-PW	GEX-PW
Average energy					
Deposition (cal/g UO$_2$):					
Total	314	343	200	255	342
At failure	290	330	--	--	--
Pellet surface energy					
Deposition (cal/cm^3 UO$_2$):					
Total	3221	3538	2063	2630	3528
At failure	2975	3404	--	--	3456
Reactor period (ms)	4.22	3.93	6.65	5.02	3.88
Peaking factor:					
Radial	1.12	1.12	1.12	1.12	1.12
Axial	1.08	1.08	1.08	1.08	1.08
Cladding temperature (°C):					
Maximum	1875	1775	--	--	--
At failure	~1300	600 to 1000	--	--	--
Cladding radial expansion (%):					
Maximum	--	--	1.25	1.79	--
Average	--	--	0.74	1.18	--
Cladding elongation (%):					
Transient maximum	0.60	0.90	0.72	1.56	1.12
Residual	--	--	--	--	--
Fuel elongation, maximum (%)	3.9	5.6	--	2.28	5.28
Capsule pressure (MPa)	0.25	0.55	0	0	0.34
Nuclear-to-mechanical					
energy conversion (%)	0	0.07	0	0	0.03
Cladding surface oxidation[b]	2	2	2	2	--
Failure mode and extent[c]	Melt-II-III	Melt-III	No-B	No-B	Melt-III
Fuel enrichment (%)[d]	7	7	7	7	7
Fuel density (g/cm^3)[d]	9.16	9.13	9.11	9.11	9.16
Fuel diameter (mm)[d]	6.96	6.97	6.88	6.88	6.88
Cladding (mm)[d]					
Outside diameter	7.88	7.87	7.85	7.85	7.85
Thickness	0.453	0.453	0.483	0.483	0.483
Gas gap width (mm)[d]	0	0	0	0	0
Active UO$_2$ length (mm)[d]	130	131	130	130	130

134

TABLE C-I (continued)

Parameter	Test				
	483	492	490	501	484
Rod type[a]	GEX-PW	GEXL-PW	GEP-PL	GEP-PL	GEP-PL
Average energy					
Deposition (cal/g UO_2):					
Total	440	460	123	120	196
At failure	425	390	--	--	--
Pellet surface energy					
Deposition (cal/cm³ UO_2):					
Total	4539	4704	1505	1469	2516
At failure	4384	3988	--	--	--
Reactor period (ms)	3.0	3.0	5.26	5.17	3.76
Peaking factor:					
Radial	1.12	1.12	1.19	1.19	1.27
Axial	1.08	1.2	1.08	1.08	1.08
Cladding temperature (°C):					
Maximum	--	--	--	--	--
At failure	--	--	--	--	--
Cladding radial expansion (%):					
Maximum	--	--	0	0	23.08
Average	--	--	0	0	15.08
Cladding elongation (%):					
Transient maximum	0.20	0.50	0.84	--	0.80
Residual	--	--	0.14	--	--
Fuel elongation, maximum (%)	4.8	--	--	--	5.94
Capsule pressure (MPa)	2.76	3.96	0	0	0
Nuclear-to-mechanical					
energy conversion (%)	0.11	0.16	0	0	0
Cladding surface oxidation[b]	--	--	0	0	0
Failure mode and extent[c]	Melt-III	Melt-III	No	No	No-B
Fuel enrichment (%)[d]	7	7	4.95	4.95	7
Fuel density (g/cm³)[d]	8.95	9.13	10.29	10.30	10.22
Fuel diameter (mm)	6.88[e]	6.97[d]	12.30[e]	12.30[e]	12.30[e]
Cladding (mm)					
Outside diameter	7.85[e]	7.94[d]	14.3[e]	14.4[e]	14.3[e]
Thickness[d]	0.483	0.483	0.904	0.927	0.902
Gas gap width (mm)	0[e]	0[e]	0.102[d]	0.102[e]	0.102[d]
Active UO_2 length (mm)[d]	130	615	142	141	131

TABLE C-I (continued)

Parameter	Test 489	487	740	741	743
Rod type[a]	GEP-PL	GEP-PL	GEP-PL	GEP-PL	GEP-PL
Average energy Deposition (cal/g UO_2):					
Total	201	243	194	200	238
At failure	--	205	--	--	--
Pellet surface energy Deposition (cal/cm^3 UO_2):					
Total	2611	3166	2511	2568	3056
At failure	--	2671	--	--	--
Reactor period (ms)	3.84	3.00	3.79	3.67	3.04
Peaking factor:					
Radial	1.27	1.27	1.27	1.26	1.26
Axial	1.08	1.08	1.08	1.08	1.08
Cladding temperature (°C):					
Maximum	--	--	1150	1550	1750
At failure	--	--	--	--	--
Cladding radial expansion (%):					
Maximum	3.73	--	13.3	3.02	3.56
Average	3.02	--	9.78	1.74	1.88
Cladding elongation (%):					
Transient Maximum	1.30	0.30	0.62	1.02	1.98
Residual	0.38	--	0.38	0.03	0.64
Fuel elongation, maximum (%)	5.60	6.20	6.2	2.0	6.0
Capsule pressure (MPa)	0	0.26	0	0	0
Nuclear-to-mechanical energy conversion (%)	0	0.006	0	0	0
Cladding surface oxidation[b]	2	2	2	2	2
Failure mode and extent[c]	No-B	Melt-II	No	No	No-B
Fuel enrichment (%)[d]	7	7	7	6.8	6.8
Fuel density (g/cm^3)[d]	10.24	10.27	10.24	10.22	10.25
Fuel diameter (mm)[d]	12.30	12.30	12.29	12.30	12.30
Cladding (mm)[d]					
Outside diameter	14.3	14.4	14.4	14.3	14.3
Thickness	0.899	0.904	0.939	0.909	0.907
Gas gap width (mm)[d]	0.102	0.102	0.102	0.114	0.114
Active UO_2 length (mm)[d]	129	130	130	136	136

TABLE C-I (continued)

Parameter	Test 742	682	485	488	509
Rod type[a]	GEP-PL	GEP-PL	GEP-PW	GEP-PW	GEPL-PW
Average energy					
Deposition (cal/g UO_2):					
Total	240	245	193	254	250
At failure	--	--	--	--	200
Pellet surface energy					
Deposition (cal/cm^3 UO_2):					
Total	3081	3049	2284	3006	2824
At failure	--	--	--	--	2260
Reactor period (ms)	3.03	3.0	3.99	3.00	3.0
Peaking factor:					
Radial	1.26	1.26	1.27	1.27	1.22
Axial	1.08	1.2	1.08	1.08	1.2
Cladding temperature (°C):					
Maximum	1725	--	--	--	--
At failure	--	--	--	--	--
Cladding radial expansion (%):					
Maximum	2.84	--	1.21	5.34	--
Average	1.96	--	0.71	3.38	--
Cladding elongation (%):					
Transient maximum	2.06	1.06	0.36	2.60	0.57
Residual	0.88	--	--	0.92	--
Fuel elongation, maximum (%)	4.24	1.49	--	7.6	0.51
Capusle pressure (MPa)	0	0.27	0	0	0.27
Nuclear-to-mechanical					
energy conversion (%)	0	0	0	0	0
Cladding surface oxidation[b]	2	2	2	2	2
Failure mode and extent[c]	No-B	No-B	No-B	Crack	Melt-II
Fuel enrichment (%)	6.8[d]	6.8[e]	7[d]	7[d]	7[e]
Fuel density (g/cm^3)[d]	10.24	10.2	9.32	9.32	9.27
Fuel diameter (mm)[d]	12.30	12.3	12.49	12.49	12.5
Cladding (mm)					
Outside diameter	14.3[e]	14.3[d]	14.3[e]	14.3[e]	14.3[d]
Thickness[d]	0.904	0.508	0.89	0.89	0.508
Gas gap width (mm)	0.114[d]	0.114[e]	0[e]	0[e]	0[e]
Active UO_2 length (mm)[d]	136	623	134	134	625

[a] PL = pellet fuel, PW = powder fuel.

[b] Cladding surface oxidation; 0 = no oxidation, 1 = partial oxidation, 2 = full oxidation.

[c] Failure mode; No = no failure, Crack = crack or split was formed but no disintegration of rod, Melt = failure by cladding melting, Split = cladding was split open, B = bowing observed.

  Failure extent; I = broken while disassembling, II = broken into several large pieces, III = broken into fine fragments.

[d] Nominal value.

[e] Actual value.

TABLE C-II

CDC, UNIRRADIATED, ZIRCALOY CLAD, CLUSTER TEST DATA

Parameter	Test				
	678	678	691	691	706
Rod type[a]	SPXM5-PL Center	SPXM5-PL Outside	SPXM5-PL Center	SPXM5-PL Outside	SPXM5-PL Center
Average energy Deposition (cal/g UO_2):					
Total	125	152	218	265	236
At failure	--	--	--	--	--
Pellet surface energy Deposition (cal/cm^3 UO_2):					
Total	1521	1850	2653	3225	2872
At failure	--	--	--	--	--
Reactor period (ms)	8.37	--	4.41	--	3.94
Peaking factor:					
Radial	1.17	--	1.17	--	1.17
Axial	1.08	1.08	1.08	1.08	1.08
Cladding temperature (°C):					
Maximum	940	1210	1460	Above melting point	1960
At fail.	--	--	--	--	--
Cladding radial expansion (%):					
Maximum	--	--	--	--	--
Average	--	--	--	--	--
Cladding elongation (%):					
Transient maximum	--	--	--	--	--
Residual	--	--	--	--	--
Fuel elongation, maximum (%)	--	--	--	--	--
Capsule pressure (MPa)	0	--	0.34	0	0.38
Nuclear-to-mechanical energy conversion (%)	0	--	0	--	0
Cladding surface oxidation[b]	2	2	2	2	2
Failure mode and extent[c]	No	No-8	No	Melt-11	No
Fuel enrichment (%)[d]	10.5	10.5	10.5	10.5	10.5
Fuel density (g/cm^3)[d]	10.4	10.4	10.4	10.4	10.4
Fuel diameter (mm)[d]	5.59	5.59	5.59	5.59	5.59
Cladding (mm)[d]					
Outside diameter	6.35	6.35	6.35	6.35	6.35
Thickness	0.356	0.356	0.356	0.356	0.356
Gas gap width (mm)[d]	0.025	0.025	0.025	0.025	0.025
Active UO_2 length (mm)[d]	127	127	127	127	127

TABLE C-II (continued)

Parameter	Test				
	706	710	710	736	736
Rod type[a]	SPXM5-PL Outside	SPXM5-PL Center	SPXM5-PL Outside	SPXM5-PL Center	SPXM5-PL Outside
Average energy					
Deposition (cal/g UO_2):					
Total	287	315	383	225	273
At failure	--	--	--	--	--
Pellet surface energy					
Deposition (cal/cm^3 UO_2):					
Total	3492	3833	4660	2738	3322
At failure	--	--	--	--	--
Reactor period (ms)	--	3.04	--	4.43	--
Peaking factor:					
Radial	--	1.17	--	1.17	--
Axial	1.08	1.08	1.08	1.08	1.08
Cladding temperature (°C):					
Maximum	Above melting point	--	--	--	--
At failure	--	--	--	--	--
Cladding radial expansion (%):					
Maximum	--	--	--	--	--
Average	--	--	--	--	--
Cladding elongation (%):					
Transient maximum	--	--	--	--	--
Residual	--	--	--	--	--
Fuel elongation, maximum (%)	--	--	--	--	--
Capsule pressure (MPa)	--	2.59	--	0.79	--
Nuclear-to-mechanical					
energy conversion (%)	--	0.10	--	0	--
Cladding surface oxidation[b]	2	--	--	2	2
Failure mode and extent[c]	Melt-II	Melt-II	Melt-II	Melt-II	Melt-II
Fuel enrichment (%)[d]	10.5	10.5	10.5	10.5	10.5
Fuel density (g/cm^3)[d]	10.4	10.4	10.4	10.4	10.4
Fuel diameter (mm)[d]	5.59	5.59	5.59	5.59	5.59
Cladding (mm)[d]					
Outside diameter	6.35	6.35	6.35	6.35	6.35
Thickness	0.356	0.356	0.356	0.356	0.356
Gas gap width (mm)[d]	0.025	0.025	0.025	0.025	0.025
Active UO_2 length (mm)[d]	127	127	127	127	127

TABLE C-II (continued)

Parameter	Test			
	752	752	755	755
Rod type[a]	SPXM5-PL Center	SPXM5-PL Outside	SPXM5-PL Center	SPXM5-PL Outside
Average energy Deposition (cal/g UO_2):				
Total	226	275	197	176
At failure	--	--	--	--
Pellet surface energy Deposition (cal/cm^3 UO_2):				
Total	2750	3346	2331	2082
At failure	--	--	--	--
Reactor period (ms)	4.45	--	3.97	--
Peaking factor:				
Radial	1.17	--	1.16	--
Axial	1.08	1.08	1.08	1.08
Cladding temperature (°C):				
Maximum	--	--	1150	1410
At failure	--	--	--	--
Cladding radial expansion (%):				
Maximum	--	--	9	1
Average	--	--	--	--
Cladding elongation (%):				
Transient maximum	--	--	--	--
Residual	--	--	--	--
Fuel elongation, maximum (%)	--	--	--	--
Capsule pressure (MPa)	0.57	--	0.04	--
Nuclear-to-mechanical energy conversion (%)	0	--	0	--
Cladding surface oxidation[b]	2	2	2	2
Failure mode and extent [c]	Melt-II	Melt-II	No	No
Fuel enrichment (%)[d]	10.5	10.5	7	5
Fuel density (g/cm^3)[d]	10.4	10.4	10.2	10.2
Fuel diameter (mm)[d]	5.59	5.59	6.81	6.81
Cladding (mm)[d]				
Outside diameter	6.35	6.35	6.35	6.35
Thickness	0.356	0.356	0.356	0.356
Gas gap width (mm)[d]	0.025	0.025	0.025	0.025
Active UO_2 length (mm)[d]	127	127	127	127

[a] PL = pellet fuel, PW = powder fuel.

[b] Cladding surface oxidation; 0 = no oxidation, 1 = partial oxidation, 2 = full oxidation.

[c] Failure mode, No = no failure, Crack = crack or split was formed but no disintegration of rod, Melt = failure by cladding melting, Split = cladding was split open, B = bowing observed.

Failure extent; I = broken while disassembling, II = broken into several large pieces, III = broken into fine fragments.

[d] Nominal value.

140

TABLE C-III

CDC, UNIRRADIATED, ZIRCALOY CLAD, MIXED OXIDE TEST DATA

Parameter	Test 566	Test 562	Test 707	Test 744	Test 731
Rod type[a]	GEXPR-PL	GEXPR-PR	GEXPRCH-PL	GEXPRCH-PL	GEXPRCH-PL
Average energy					
Deposition (cal/g fuel):					
Total	225	274	223	275	277
At failure	--	< 260	--	--	--
Pellet surface energy					
Deposition (cal/cm^3 fuel):					
Total	2716	3230	2606	3185	3208
At failure	--	< 3070	--	--	--
Reactor period (ms)	7.37	5.69	8.28	6.57	6.59
Peaking factor:					
Radial	1.20	1.20	1.15	1.15	1.15
Axial	1.08	1.08	1.08	1.08	1.08
Cladding temperature (°C):					
Maximum	1350	1925	1400	1675	1625
At failure	--	1700	--	--	--
Cladding radial expansion (%):					
Maximum	--	--	--	--	--
Average	--	--	--	--	--
Cladding elongation (%):					
Transient maximum	2.28	3.8	1.45	2.61	1.14
Residual	1.34	--	0.61	1.33	--
Fuel elongation, maximum (%)	--	--	--	--	--
Capsule pressure (MPa)	0	0	0	0	0
Nuclear-to-mechanical					
energy conversion (%)	0	0	0	0	0
Cladding surface oxidation[b]	2	2	2	2	2
Failure mode and extent[c]	No	Melt-II	No	Crack	Crack-I
Fuel enrichment (%)[d]	7.2	7.2	6.8	6.8	6.8
Fuel density (g/cm^3)[e]	10.06	9.83	10.16	10.07	10.07
Fuel diameter (mm)[d]	6.88	6.88	6.88	6.88	6.88
Cladding (mm)[d]					
Outside diameter	7.89	7.89	7.94	7.95	7.95
Thickness	0.483	0.483	0.483	0.483	0.463
Gas gap width (mm)[d]	0.069-0.124	0.066-0.124	0.097-0.124	0.104-0.137	0.097-0.137
Active fuel length (mm)[d]	128	128	129	131	131

TABLE C-III (continued)

Parameter	Test 745	Test 753
Rod type[a]	GEXPRCH-PL	GEXPRCH-PL
Average energy		
Deposition (cal/g fuel):		
Total	329	414
At failure	~ 315	398
Pellet surface energy		
Deposition (cal/cm^3 fuel):		
Total	3806	4790
At failure	< 3644	4604
Reactor period (ms)	5.30	4.30
Peaking factor:		
Radial	1.15	1.15
Axial	1.08	1.08
Cladding temperature (°C):		
Maximum	1900	1950
At failure	1675	1600
Cladding radial expansion (%):		
Maximum	--	--
Average	--	--
Cladding elongation (%):		
Transient maximum	~ 1.57	1.12
Residual	--	--
Fuel elongation, maximum (%):	_	_
Capsule pressure (MPa)	0	0.09
Nuclear-to-mechanical		
energy conversion (%)	0	0.0002
Cladding surface oxidation[b]	2	--
Failure mode and extent[c]	Melt-III	Melt-III
Fuel enrichment (%)[d]	6.8	6.8
Fuel density (g/cm^3)[d]	10.06	10.06
Fuel diameter (mm)[d]	6.88	6.88
Cladding (mm)[d]		
Outside diameter	7.95	7.92
Thickness	0.483	0.483
Gas gap width (mm)[d]	0.104-0.132	0.074-0.127
Active fuel length (mm)[d]	137	131

[a] PL = pellet fuel, PW = powder fuel.

[b] Cladding surface oxidation; 0 = no oxidation, 1 = partial oxidation, 2 = full oxidation.

[c] Failure mode; No = no failure, Crack = crack or split was formed but no disintegration of rod, Melt = failure by cladding melting, Split = cladding was split open, B = bowing observed.

Failure extent; I = broken while disassembling, II = broken into several large pieces, III = broken into fine fragments.

[d] Nominal value.

TABLE C-IV

CDC, PREIRRADIATED, ZIRCALOY CLAD, SINGLE ROD TEST DATA

Parameter	Test				
	571	568	567	569	703
Rod type[a]	GEX-PL 4550 MWd/t	GEX-PL 3480 MWd/t	GEX-PL 3100 MWd/t	GEX-PL 4140 MWd/t	GEX-PL 1140 MWd/t
Average energy					
Deposition (cal/g UO_2):					
Total	161	199	264	348	192
At failure	--	147	225	300	--
Pellet surface energy					
Deposition (cal/cm³ UO_2):					
Total	1874	2316	3073	4050	2235
At failure	--	1711	2619	3493	--
Reactor period (ms)	7.80	6.06	4.53	3.55	3.68
Peaking factor:					
Radial	1.1x	1.13	1.13	1.13	1.13
Axial	1.08	1.08	1.08	1.08	1.08
Cladding temperature (°C):					
Maximum	--	--	--	--	--
At failure	--	--	--	--	--
Cladding radial expansion (%):					
Maximum	12.16	--	--	--	12
Average	--	--	--	--	--
Cladding elongation (%):					
Transient maximum	0.8	0.6	2.0	8.3	1.8
Residual	-0.44	0	1.04	5.02	0.5
Fuel elongation, maximum (%)	1	4	2.8	6	7.0
Capsule pressure (MPa)	0.14	1.14	2.41	16.21	0
Nuclear-to-mechanical					
energy conversion (%)	0	--	0.05	--	0
Cladding surface oxidation[b]	--	--	--	--	--
Failure mode and extent[c]	No	Crack	Crack	Crack	No
Fuel enrichment (%)[d]	7	7	7	7	7
Fuel density (g/cm³)[d]	10.3	10.26	10.3	10.37	10.30
Fuel diameter (mm)[d]	6.82	6.82	6.82	6.82	12.31
Cladding (mm)[d]					
Outside diameter	7.87	7.85	7.87	7.85	14.31
Thickness	0.494	0.484	0.493	0.481	0.899
Gas gap width (mm)[d]	0.032	0.033	0.033	0.033	0.102
Active UO_2 length (mm)[d]	130	130	132	131	129

TABLE C-IV (continued)

Parameter	Test				
	709	685	684	756	859
Rod type[a]	GEP-PL 990 MWd/t	GEX-PL 13,000 MWd/t	GEX-PL 12,900 MWd/t	GEX-PL 32,700 MWd/t	GEX-PL 31,800 MWd/t
Average energy					
Deposition (cal/g UO_2):					
Total	238	186	200	176	190
At failure	238	--	--	--	--
Pellet surface energy					
Deposition (cal/cm^3 UO_2):					
Total	2770	2167	2330	2050	2214
At failure	2770	--	--	--	--
Reactor period (ms)	3.10	5.75	5.12	4.42	3.94
Peaking factor:					
Radial	1.27	1.13	1.13	1.13	1.13
Axial	1.08	1.08	1.08	1.08	1.08
Cladding temperature (°C):					
Maximum	--	--	--	--	--
At failure	--	--	--	--	--
Cladding radial expansion (%):					
Maximum	--	0	--	3	--
Average	--	0	--	--	--
Cladding elongation (%):					
Transient maximum	1.1	0.8	1.2	1.4	0.6
Residual	0.26	0	--	1.0	--
Fuel elongation, maximum (%)	5.6	0.6	0.9	1.5	1.5
Capsule pressure (MPa)	0.39	0.52	0.52	1.03	0.48
Nuclear-to-mechanical					
energy conversion (%)	0.06	0	0	0	0.014
Cladding surface oxidation[b]	--	--	--	--	--
Failure mode and extent[c]	Crack	No	No	Crack	Split
Fuel enrichment (%)[d]	7	7	7	7	7
Fuel density (g/cm^3)	10.22[e]	10.31[d]	10.31[d]	10.31[d]	10.31[d]
Fuel diameter (mm)	12.28[e]	6.81[d]	6.81[d]	6.81[d]	6.81[d]
Cladding (mm)					
Outside diameter	14.37[e]	7.94[d]	7.94[d]	7.94[d]	7.94[d]
Thickness	0.940[e]	0.508[e]	0.508[e]	0.508[e]	0.508[e]
Gas gap width (mm)	0.102[e]	0.032[d]	0.032[d]	0.032[d]	0.032[d]
Active UO_2 length (mm)	131[e]	130[d]	130[d]	130[d]	130[d]

[a] PL = pellet fuel, PW = powder fuel.

[b] Cladding surface oxidation; 0 = no oxidation, 1 = partial oxidation, 2 = full oxidation.

[c] Failure mode; No = no failure, Crack = crack or split was formed but no disintegration of rod, Melt = failure by cladding melting, Split = cladding was split open, B = bowing observed.

Failure extent; I = broken while disassembling, II = broken into several large pieces, III = broken into fine fragments.

[d] Nominal value.

[e] Actual value.

TABLE C-V

CDC, UNIRRDIATED, STAINLESS STEEL CLAD, SINGLE ROD TEST DATA

Parameter	Test				
	182[a]	183	184	185	186
Rod type [b]	F-type PL	F-type PL	F-type PL	F-type PL	F-type PL
Average energy Deposition (cal/g UO$_2$):					
Total	57	71	94	153	184
At failure	--	--	--	--	--
Pellet surface energy Deposition (cal/cm^3 UO$_2$):					
Total	653	813	1076	1752	2107
At failure	--	--	--	--	--
Reactor period (ms)	25	15	11.7	6.5	5.2
Peaking factor:					
Radial	1.136	1.136	1.136	1.136	1.136
Axial	--	--	--	--	--
Cladding temperature (°C):					
Maximum	~100	~100	~100	~550	~530
At failure	--	--	--	--	--
Cladding radial expansion (%):					
Maximum	0	0	0	0	0
Average	--	--	--	--	--
Cladding elongation (%):					
Transient maximum	--	--	--	--	--
Residual	--	--	--	--	--
Fuel elongation, maximum (%)					
Capsule pressure (MPa)	--	--	--	--	--
Nuclear-to-mechanical energy conversion (%)	--	--	--	--	--
Cladding surface oxidation[c]	0	0	0	1	2
Failure mode and extent[d]	No	No	No	No-B	No-B
Fuel enrichment (%)[e]	4.8	4.8	4.8	4.8	4.8
Fuel density (g/cm^3)[e]	10.08	10.08	10.08	10.08	10.08
Fuel diameter (mm)[e]	10.67	10.67	10.67	10.67	10.67
Cladding (mm)[e]					
Outside diameter	11.83	11.83	11.83	11.83	11.83
Thickness	0.508	0.508	0.508	0.508	0.508
Gas gap width (mm)[e]	0.076	0.076	0.076	0.076	0.076
Active UO$_2$ length (mm)[e]	914	914	914	914	914

TABLE C-V (continued)

	Test				
Parameter	187	188[a]	189	190	191
Rod type[b]	F-type PL	F-type PL	F-type PL	F-type PL	F-type PL
Average energy					
Deposition (cal/g UO_2):					
Total	200	257	151	182	216
At failure	--	--	--	--	--
Pellet surface energy					
Deposition (cal/cm^3 UO_2):					
Total	2519	2943	1729	2084	2473
At failure	--	--	--	--	--
Reactor period (ms)	4.3	3.5	6.8	5.2	4.0
Peaking factor:					
Radial	1.136	1.136	1.136	1.136	1.136
Axial	--	--	--	--	--
Cladding temperature (°C):					
Maximum	--	--	890	984	1140
At failure	--	--	--	--	--
Cladding radial expansion (%):					
Maximum	Slight	--	0.43	0.64	0.86
Average	--	--	--	--	--
Cladding elongation (%):					
Transient maximum	--	--	--	--	--
Residual	--	--	0.32	0.51	0.61
Fuel elongation, maximum (%)	--	--	--	--	--
Capsule pressure (MPa)	--	--	--	--	--
Nuclear-to-mechanical					
energy conversion (%)	--	--	--	--	--
Cladding surface oxidation[c]	2	2	2	2	2
Failure mode and extent[d]	No-B	Crack	No-B	No-B	No
Fuel enrichment (%)[e]	4.8	4.8	4.8	4.8	4.8
Fuel density (g/cm^3)[e]	10.08	10.08	10.08	10.08	10.08
Fuel diameter (mm)[e]	10.67	10.67	10.67	10.67	10.67
Cladding (mm)[e]					
Outside diameter	11.83	11.83	11.83	11.83	11.83
Thickness	0.508	0.508	0.508	0.508	0.508
Gas gap width (mm)[e]	0.076	0.076	0.076	0.076	0.076
Active UO_2 length (mm)[e]	914	914	914	914	914

TABLE C-V (continued)

Parameter	Test				
	192	193	203	246[f]	247
Rod type[b]	F-type PL	F-type PL	F-type PL	F-type PL	F-type PL
Average energy					
Deposition (cal/g UO_2):					
Total	263	276	299	200	200
At failure	--	--	--	--	--
Pellet surface energy					
Deposition (cal/cm^3 UO_2):					
Total	30/2	3/82	3424	2290	2290
At failure	--	--	--	--	--
Reactor period (ms)	3.4	3.2	2.93	4.3	4.3
Peaking factor:					
Radial	1.136	1.136	1.136	1.136	1.136
Axial	--	--	--	--	--
Cladding temperature (°C):					
Maximum	1195	1255	1355	--	--
At failure	--	--	--	--	--
Cladding radial expansion (%):					
Maximum	1.29	1.39	2.15	--	--
Average	--	--	--	--	--
Cladding elongation (%):					
Transient maximum	--	--	--	--	--
Residual	0.88	0.84	--	0.36/0.36[g]	0.72/1.08[g]
Fuel elongation, maximum (%)	--	--	--	--	--
Capsule pressure (MPa)	--	--	--	--	--
Nuclear-to-mechanical					
energy conversion (%)	--	--	--	--	--
Cladding surface oxidation[c]	2	2	2	--	--
Failure mode and extent[d]	No-B	Crack	Melt-I	No-B	No-B
Fuel enrichment (%)[e]	4.8	4.8	4.8	4.8	4.8
Fuel density (g/cm^3)[e]	10.08	10.08	10.08	10.08	10.08
Fuel diameter (mm)[e]	10.67	10.67	10.67	10.67	10.67
Cladding (mm)[e]					
Outside diameter	11.83	11.83	11.83	11.83	11.83
Thickness	0.508	0.508	0.508	0.508	0.508
Gas gap width (mm)[e]	0.076	0.076	0.076	0.076	0.076
Active UO_2 length (mm)[e]	914	914	914	914	914

TABLE C-V (continued)

Parameter	Test 248	Test 249	Test 250	Test 251	Test 2ผ1
Rod type[b]	F-type PL	F-type PL	F-type PL	F-type PL	F-type PL
Average energy					
Deposition (cal/g UO_2):					
Total	200	200	200	200	200
At failure	--	--	--	--	--
Pellet surface energy					
Deposition (cal/cm^3 UO_2):					
Total	2290	2290	2290	2290	2290
At failure	--	--	--	--	--
Reactor period (ms)	4.3	4.3	4.3	4.3	4.3
Peaking factor:					
Radial	1.136	1.136	1.136	1.136	1.136
Axial	--	--	--	--	--
Cladding temperature (°C):					
Maximum	--	--	--	--	--
At failure	--	--	--	--	--
Cladding radial expansion (%):					
Maximum	--	--	--	--	--
Average	--	--	--	--	--
Cladding elongation (%):					
Transient maximum	--	--	--	--	--
Residual[g]	0.52/1.60	0.51/2.11	0.50/2.69	0.48/3.17	0.35/3.53
Fuel elongation, maximum (%)	--	--	--	--	--
Capsule pressure (MPa)	--	--	--	--	--
Nuclear-to-mechanical					
energy conversion (%)	--	--	--	--	--
Cladding surface oxidation[c]	--	--	--	--	--
Failure mode and extent[d]	No-B	No-B	No-B	No-B	No-B
Fuel enrichment (%)[e]	4.8	4.8	4.8	4.8	4.8
Fuel density (g/cm^3)[e]	10.08	10.08	10.08	10.08	10.08
Fuel diameter (mm)[e]	10.67	10.67	10.67	10.67	10.67
Cladding (mm)[e]					
Outside diameter	11.83	11.83	11.83	11.83	11.83
Thickness	0.508	0.508	0.508	0.508	0.508
Gas gap width (mm)[e]	0.076	0.076	0.076	0.076	0.076
Active UO_2 length (mm)[e]	914	914	914	914	914

TABLE C-V (continued)

Parameter	Test				
	282	283	284	285	286
Rod type[b]	F-type PL	F-type PL	F-type PL	F-type PL	F-type PL
Average energy					
Deposition (cal/g UO_2):					
Total	200	200	200	200	200
At failure	--	--	--	--	--
Pellet surface energy					
Deposition (cal/cm^3 UO_2):					
Total	2290	2290	2290	2290	2290
At failure	--	--	--	--	--
Reactor period (ms)	4.3	4.3	4.3	4.3	4.3
Peaking factor:					
Radial	1.136	1.136	1.136	1.136	1.136
Axial	--	--	--	--	--
Cladding temperature (°C):					
Maximum	--	--	--	--	--
At failure	--	--	--	--	--
Cladding radial expansion (%):					
Maximum	--	--	--	--	--
Average	--	--	--	--	--
Cladding elongation (%):					
Transient maximum	--	--	--	--	--
Residual[g]	0.48/4.01	0.39/4.40	0.49/4.89	0.37/5.26	0.34/5.60
Fuel elongation, maximum (%)	--	--	--	--	--
Capsule pressure (MPa)	--	--	--	--	--
Nuclear-to-mechanical					
energy conversion (%)	--	--	--	--	--
Cladding surface oxidation[c]	--	--	--	--	--
Failure mode and extent[d]	No-B	No-B	No-B	No-B	No-B
Fuel enrichment (%)[e]	4.8	4.8	4.8	4.8	4.8
Fuel density (g/cm^3)[e]	10.08	10.08	10.08	10.08	10.08
Fuel diameter (mm)[e]	10.67	10.67	10.67	10.67	10.67
Cladding (mm)[e]					
Outside diameter	11.83	11.83	11.83	11.83	11.83
Thickness	0.508	0.508	0.508	0.508	0.508
Gas gap width (mm)[e]	0.076	0.076	0.076	0.076	0.076
Active UO_2 length (mm)[e]	914	914	914	914	914

TABLE C-V (continued)

Parameter	287	288[h]	289	290	291
Rod type[b]	F-type PL	F-type PL	F-type PL	F-type PL	F-type PL
Average energy Deposition (cal/g UO_2):					
Total	200	100	100	100	100
At failure	--	--	--	--	--
Pellet surface energy Deposition (cal/cm^3 UO_2):					
Total	2290	1145	1145	1145	1145
At failure	--	--	--	--	--
Reactor period (ms)	4.3	11	11	11	11
Peaking factor:					
Radial	1.136	1.136	1.136	1.136	1.136
Axial	--	--	--	--	--
Cladding temperature (°C):					
Maximum	--	--	--	--	--
At failure	--	--	--	--	--
Cladding radial expansion (%):					
Maximum	--	--	--	--	--
Average	--	--	--	--	--
Cladding elongation (%):					
Transient maximum	--	--	--	--	--
Residual	0.38/5.99[g]	--	--	--	0.21/0.21[i]
Fuel elongation, maximum (%)	--	--	--	--	--
Capsule pressure (MPa)	--	--	--	--	--
Nuclear-to-mechanical energy conversion (%)	--	--	--	--	--
Cladding surface oxidation[c]	--	--	--	--	--
Failure mode and extent[d]	No-B	No-B	No-B	No-B	No-B
Fuel enrichment (%)[e]	4.8	4.8	4.8	4.8	4.8
Fuel density (g/cm^3)[e]	10.08	10.08	10.08	10.08	10.08
Fuel diameter (mm)[e]	10.67	10.67	10.67	10.67	10.67
Cladding (mm)[e]					
Outside diameter	11.83	11.83	11.83	11.83	11.83
Thickness	0.508	0.508	0.508	0.508	0.508
Gas gap width (mm)[e]	0.076	0.076	0.076	0.076	0.076
Active UO_2 length (mm)[e]	914	914	914	914	914

TABLE C-V (continued)

Parameter	Test 292	Test 293	Test 294	Test 295	Test 296
Rod type[b]	F-type PL	F-type PL	F-type PL	F-type PL	F-type PL
Average energy					
Deposition (cal/g UO_2):					
Total	100	100	100	100	100
At failure	--	--	--	--	--
Pellet surface energy					
Deposition (cal/cm^3 UO_2):					
Total	1145	1145	1145	1145	1145
At failure	--	--	--	--	--
Reactor period (ms)	11	11	11	11	11
Peaking factor:					
Radial	1.136	1.136	1.136	1.136	1.136
Axial	--	--	--	--	--
Cladding temperature (°C):					
Maximum	--	--	--	--	--
At failure	--	--	--	--	--
Cladding radial expansion (%):					
Maximum	--	--	--	--	--
Average	--	--	--	--	--
Cladding elongation (%):					
Transient maximum	--	--	--	--	--
Residual	--	0.12/0.33[i]	--	--	0.12/0.45[i]
Fuel elongation, maximum (%)	--	--	--	--	--
Capsule pressure (MPa)	--	--	--	--	--
Nuclear-to-mechanical					
energy conversion (%)	--	--	--	--	--
Cladding surface Oxidation[c]	0	0	0	0	0
Failure mode and extent[d]	No-B	No-B	No-B	No-B	No-B
Fuel enrichment (%)[e]	4.8	4.8	4.8	4.8	4.8
Fuel density (g/cm^3)[e]	10.08	10.08	10.08	10.08	10.08
Fuel diameter (mm)[e]	10.67	10.67	10.67	10.67	10.67
Cladding (mm)[e]					
Outside diameter	11.83	11.83	11.83	11.83	11.83
Thickness	0.508	0.508	0.508	0.508	0.508
Gas gap width (mm)[e]	0.076	0.076	0.076	0.076	0.076
Active UO_2 length (mm)[e]	914	914	914	914	914

TABLE C-V (continued)

Parameter	Test				
	297	298	299	300	301
Rod type[b]	F-type PL	F-type PL	F-type PL	F-type PL	F-type PL
Average energy					
Deposition (cal/g UO_2):					
Total	100	100	100	100	100
At failure	--	--	--	--	--
Pellet surface energy					
Deposition (cal/cm^3 UO_2):					
Total	1145	1145	1145	1145	1145
At failure	--	--	--	--	--
Reactor period (ms)	11	11	11	11	11
Peaking factor:					
Radial	1.136	1.136	1.136	1.136	1.136
Axial	--	--	--	--	--
Cladding temperature (°C):					
Maximum	--	--	--	--	--
At failure	--	--	--	--	--
Cladding radial expansion (%):					
Maximum	--	--	--	--	--
Average	--	--	--	--	--
Cladding elongation (%):					
Transient maximum	--	--	--	--	--
Residual	--	--	0.15/0.59[i]	--	0.13/0.72[i]
Fuel elongation, maximum (%)	--	--	--	--	--
Capsule pressure (MPa)	--	--	--	--	--
Nuclear-to-mechanical					
energy conversion (%)	--	--	--	--	--
Cladding surface oxidation[c]	0	0	0	0	0
Failure mode and extent[d]	No-B	No-B	No-B	No-B	No-B
Fuel enrichment (%)[e]	4.8	4.8	4.8	4.8	4.8
Fuel density (g/cm^3)[e]	10.08	10.08	10.08	10.08	10.08
Fuel diameter (mm)[e]	10.67	10.67	10.67	10.67	10.67
Cladding (mm)[e]					
Outside diameter	11.83	11.83	11.83	11.83	11.83
Thickness	0.508	0.508	0.508	0.508	0.508
Gas gap width (mm)[e]	0.076	0.076	0.076	0.076	0.076
Active UO_2 length (mm)[e]	914	914	914	914	914

TABLE C-V (continued)

Parameter	302[j]	303	304	320	321
			Test		
Rod type[b]	F-type PL	F-type PL	F-type PL	F-type PL	F-type PL
Average energy					
Deposition (cal/g UO_2):					
Total	150	150	150	150	150
At failure	--	--	--	--	--
Pellet surface energy					
Deposition (cal/cm³ UO_2):					
Total	1718	1718	1718	1718	1718
At failure	--	--	--	--	--
Reactor period (ms)	6.8	6.8	6.8	6.8	6.8
Peaking factor:					
Radial	1.136	1.136	1.136	1.136	1.136
Axial	--	--	--	--	--
Cladding temperature (°C):					
Maximum	--	--	--	--	--
At failure	--	--	--	--	--
Cladding radial expansion (%):					
Maximum	--	--	--	--	--
Average	--	--	--	--	--
Cladding elongation (%):					
Transient maximum	--	--	--	--	--
Residual	--	--	0.42/0.42[k]	--	0.31/0.73[k]
Fuel elongation, maximum (%)	--	--	--	--	--
Capsule pressure (MPa)	--	--	--	--	--
Nuclear-to-mechanical					
energy conversion (%)	--	--	--	--	--
Cladding surface oxidation[c]	1	1	1	1	1
Failure mode and extent[d]	No-B	No-B	No-B	No-B	No-B
Fuel enrichment (%)[e]	4.8	4.8	4.8	4.8	4.8
Fuel density (g/cm³)[e]	10.08	10.08	10.08	10.08	10.08
Fuel diameter (mm)[e]	10.67	10.67	10.67	10.67	10.67
Cladding (mm)[e]					
Outside diameter	11.83	11.83	11.83	11.83	11.83
Thickness	0.508	0.508	0.508	0.508	0.508
Gas gap width (mm)[e]	0.076	0.076	0.076	0.076	0.076
Active UO_2 length (mm)[e]	914	914	914	914	914

TABLE C-V (continued)

Parameter	324	325	319	322	329
Rod type[b]	F-type PL	F-type PL	F-type PL	F-type PL	F-type PL
Average energy					
Deposition (cal/g UO_2):					
Total	150	150	200	244	276
At failure	--	--	--	--	--
Pellet surface energy					
Deposition (cal/cm³ UO_2):					
Total	1718	1718	2163	2639	2985
At failure	--	--	--	--	--
Reactor period (ms)	6.8	6.8	4.2	3.5	3.05
Peaking factor:					
Radial	1.136	1.136	1.04	1.04	1.04
Axial	--	--	1.09	1.09	1.09
Cladding temperature (°C):					
Maximum	--	--	1040	1210	1330
At failure	--	--	--	--	--
Cladding radial expansion (%)					
Maximum	--	--	--	--	--
Average	--	--	--	--	--
Cladding elongation (%):					
Transient maximum	--	--	--	--	--
Residual	--	0.28/1.01[*]	1.04	1.44	--
Fuel elongation, maximum (%):	--	--	--	--	--
Capsule pressure (MPa)	--	--	0	0	0
Nuclear-to-mechanical					
Energy conversion (%)	--	--	0	0	0
Cladding surface oxidation[c]	1	1	2	2	2
Failure mode and extent[d]	No-B	No-B	No-B	No-B	No-B
Fuel enrichment (%)[e]	4.6	4.6	3	3	3
Fuel density (g/cm³)[e]	10.08	10.08	10.4	10.4	10.4
Fuel diameter (mm)[e]	10.67	10.67	5.59	5.59	5.59
Cladding (mm)[e]					
Outside diameter	11.63	11.63	6.35	6.35	6.35
Thickness	0.508	0.508	0.356	0.356	0.356
Gas gap width (mm)[e]	0.076	0.076	0.076	0.076	0.076
Active UO_2 length (mm)[e]	914	914	457	457	457

TABLE C-V (continued)

Parameter	Test			
	323	326	327	328
Rod type[b]	SPX-PL	SPX-PL	SPX-PL	SPX-PL
Average energy				
Deposition (cal/g UO_2):				
Total	277	370	477	572
At failure	--	350	430	480
Pellet surface energy				
Deposition (cal/cm^3 UO_2):				
Total	3342	4464	5755	6901
At failure	--	4222	5188	5791
Reactor period (ms)	6.4	4.6	3.76	3.15
Peaking factor:				
Radial	1.16	1.16	1.16	1.16
Axial	1.10	1.10	1.10	1.10
Cladding temperature (°C):				
Maximum	1380	~1440	--	--
At failure	--	1220	950	420
Cladding radial expansion (%):				
Maximum	--	--	--	--
Average	--	--	--	--
Cladding elongation (%):				
Transient maximum	--	--	--	--
Residual	--	--	--	--
Fuel elongation, maximum (%):	--	--	--	--
Capsule pressure (MPa)	0	1.03	2.00	3.80
Nuclear-to-mechanical				
energy conversion (%)	0	0.01	0.06	0.35
Cladding surface oxidation[c]	2	2	2	--
Failure mode and extent[d]	Melt-I	Melt-II, -III	Melt-III	Melt-III
Fuel enrichment (%)[e]	10	10	10	10
Fuel density (g/cm^3)[d]	10.4	10.4	10.4	10.4
Fuel diameter (mm)[e]	5.59	5.59	5.59	5.59
Cladding (mm)[e]				
Outside diameter	6.35	6.35	6.35	6.35
Thickness	0.356	0.356	0.356	0.356
Gas gap width (mm)[e]	0.025	0.025	0.025	0.025
Active UO_2 length (mm)[e]	457	457	457	457

[a] Sequential tests, from 182 through 188.

[b] PL = pellet fuel, PW = powder fuel.

[c] Cladding surface oxidation; 0 = no oxidation, 1 = partial oxidation, 2 = full oxidation.

[d] Failure mode; No = no failure, Crack = crack split was formed but no disintegration of rod,
Melt = failure by cladding melting, Split = cladding was split open, B = bowing observed.

Failure extent; I = broken while disassembling, II = broken into several large pieces,
III = broken into fine fragments.

[e] Nominal value.

[f] Same test repeated, from Tests 246 through 287.

[g] Per test/cumulative (beginning with Test 246).

[h] Same test repeated, from Tests 288 through 301.

[i] Per group of tests/cumulative (beginning with Test 288).

[j] Same test repeated, from Tests 302 through 325.

[k] Per group of tests/cumulative (beginning with Test 302).

TABLE C-VI

CDC, UNIRRADIATED, ZIRCALOY CLAD, WATERLOGGED TEST DATA

Parameter	Test 496	514	494	511	552
Rod type[a]	GEP-PL	GEP-PL	GEP-PW	GEP-PW	SPXM}-PL
Average energy Deposition (cal/g UO_2):					
Total	220	220	265	265	430
At failure	60	33	65	60	165
Pellet surface energy Deposition (cal/cm^3 UO_2):					
Total	2697	2697	3100	3100	4785
At failure	735	404	772	702	1836
Reactor period (ms)	3.0	3.0	3.0	3.0	3.0
Peaking factor:					
Radial	1.19	1.19	1.27	1.27	1.07
Axial	1.08	1.08	1.08	1.08	1.08
Cladding temperature (°C):					
Maximum	--	--	--	--	--
At failure	--	--	--	--	--
Cladding radial expansion (%):					
Maximum	--	--	--	--	--
Average	--	--	--	--	--
Cladding elongation (%):					
Transient maximum	+0.18 -0.34	+0.28	+0.14 -0.70	+0.36 -0.10	0.18
Residual	--	--	--	-	--
Fuel elongation, maximum (%)	--	--	--	--	--
Capsule pressure (MPa)	8.24	11.6	41.4	2.7	0.96
Nuclear-to-mechanical energy conversion (%)	0.2	--	1.8	1.4	0.18
Cladding surface oxidation[b]	0	--	0	0	3
Failure mode and extent[c]	Split-III	Broken-III	Split-III	Split-III	Split-III
Fuel enrichment (%)[d]	5	5	7	7	5
Fuel density (g/cm^3)[d]	10.30	10.30	9.21	9.21	9.21
Fuel diameter (mm)	12.44[e]	12.44[e]	12.67[e]	12.67[e]	5.59[d]
Cladding (mm)[d]					
Outside diameter	14.27	14.27	14.27	14.27	6.35
Thickness	0.813	0.813	0.813	0.813	0.356
Gas gap width (mm)	0.102[d]	0.102[d]	0[e]	0[e]	0.025[d]
Active UO_2 length (mm)[d]	132	132	132	132	127

TABLE C-VI (continued)

Parameter	Test				
	555	558	547	556	559
Rod type[a]	SPXMB-PL	SPXMB-PL	SPXMB-PL	SPXMB-PL	SPXMB-PL
Average energy					
Deposition (cal/g UO_2):					
Total	225	225	430	225	225
At failure	160	160	85	150	120
Pellet surface energy					
Deposition (cal/cm³ UO_2):					
Total	2504	2504	4785	2504	2504
At failure	1780	1780	946	1669	1335
Reactor period (ms)	5.5	5.5	3.0	5.5	5.5
Peaking factor:					
Radial	1.07	1.07	1.07	1.07	1.07
Axial	1.04	1.04	1.04	1.04	1.04
Cladding temperature (°C):					
Maximum	--	--	--	--	--
At failure	--	--	--	--	--
Cladding radial expansion (%):					
Maximum	--	--	--	--	--
Average	--	--	--	--	--
Cladding elongation (%):					
Transient maximum (%):	0.20	0.30	0.24	0.34	0.18
Residual	--	--	--	--	--
Fuel elongation, maximum (%)	--	--	--	--	--
Capsule pressure (MPa)	3.03	3.66	1.18	3.66	2.84
Nuclear-to-mechanical					
energy conversion (%)	0.038	0.059	0.25	0.031	0.022
Cladding surface oxidation[b]	2	2	2	2	2
Failure mode and extent[c]	Split-III	Split-III	Split-III	Split-III	Split-III
Fuel enrichment (%)[d]	5	5	5	5	5
Fuel density (g/cm³)[d]	10.4	10.4	10.4	10.4	10.4
Fuel diameter (mm)[d]	5.59	5.59	5.59	5.59	5.59
Cladding (mm)[d]					
Outside diameter	6.35	6.35	6.35	6.35	6.35
Thickness	0.356	0.356	0.356	0.356	0.356
Gas gap width (mm)[d]	0.025	0.025	0.025	0.025	0.025
Active UO_2 length (mm)[e]	127	127	127	127	127

[a] PL = pellet fuel, PW = powder fuel.

[b] Cladding surface oxidation: 0 = no oxidation, 1 = partial oxidation, 2 = full oxidation.

[c] Failure mode: No = no failure, Crack = crack or split was formed but no disintegration, Melt = failure by cladding melting, Split = cladding was split open, B = bowing observed.

Failure extent: I = broken while disassembling, II = broken into several pieces, III = broken into fine fragments.

[d] Nominal value.

[e] Actual value.

TABLE C-VII

CDC, UNIRRADIATED, STAINLESS STEEL CLAD, WATERLOGGED TEST DATA

Parameter	Test 194[a]	195	196	197	198
Rod type[b]	F-type PL	F-type PL	F-type PL	F-type PL	F-type PL
Average energy Deposition (cal/g UO_2):					
Total	54	70	71	89	101
At failure	--	--	--	--	--
Pellet surface energy Deposition (cal/cm^3 UO_2):					
Total	613	801	813	1019	1157
At failure	--	--	--	--	--
Reactor period (ms)	32	20	15.5	12.4	11.3
Peaking factor:					
Radial	1.136	1.136	1.136	1.136	1.136
Axial	--	--	--	--	--
Cladding temperature (°C):					
Maximum	--	--	--	--	--
At failure	--	--	--	--	--
Cladding radial expansion (%):			0.86[c]	1.07[c]	1.50[c]
Maximum	0	0	0.64	1.29	1.72
Average	--	--	--	--	--
Cladding elongation (%):					
Transient maximum	--	--	--	--	--
Residual	--	--	--	--	--
Fuel elongation, maximum (%)	--	--	--	--	--
Capsule pressure (MPa)	--	--	--	--	--
Nuclear-to-mechanical energy conversion (%)	--	--	--	--	--
Cladding surface oxidation[d]	0	0	0	0	0
Failure mode and extent[e]	No	No	No	No	No
Fuel enrichment (%)[f]	4.8	4.8	4.8	4.8	4.8
Fuel density (g/cm^3)[f]	10.08	10.08	10.08	10.08	10.08
Fuel diameter (mm)[f]	10.67	10.67	10.67	10.67	10.67
Cladding (mm)[f]					
Outside diameter	11.83	11.83	11.83	11.83	11.83
Thickness	0.508	0.508	0.508	0.508	0.508
Gas gap width (mm)[f]	0.076	0.076	0.076	0.076	0.076
Active UO_2 length (mm)[f]	194	914	914	914	914

TABLE C-VII (continued)

Parameter	Test 199	Test 200	Test 201[a]	Test 202	Test 205
Rod type[b]	F-type PL	F-type PL	F-type PL	F-type PL	F-type PL
Average energy Deposition (cal/g UO_2):					
Total	119	136	155	153	181
At failure	--	--	--	--	--
Pellet surface energy Deposition (cal/cm^3 UO_2):					
Total	1563	1557	1775	1752	2073
At failure	--	--	--	--	--
Reactor period (ms)	9.1	7.7	6.7	6.8	4.9
Peaking factor:					
Radial	1.136	1.136	1.136	1.136	1.136
Axial	--	--	--	--	--
Cladding temperature (°C):					
Maximum	--	--	--	--	--
At failure	--	--	--	--	--
Cladding radial expansion (%):	3.87[c]	0.21[c]	6.22[c]		
Maximum	3.65	0.0	7.20	4.29	10.51
Average	--	--	--	--	--
Cladding elongation (%):					
Transient maximum	--	--	--	--	--
Residual	--	--	--	--	--
Fuel elongation, maximum (%)	--	--	--	--	--
Capsule pressure (MPa)	--	--	--	--	--
Nuclear-to-mechanical energy conversion (%)	--	--	--	--	--
Cladding surface oxidation[d]	0	0	1	1	1
Failure mode and extent[e]	No-B	No-B	No-B	No-B	No-B
Fuel enrichment (%)[f]	4.8	4.8	4.8	4.8	4.8
Fuel density (g/cm^3)[f]	10.8	10.8	10.8	10.8	10.8
Fuel diameter (mm)[f]	11.83	11.83	11.83	11.83	11.83
Cladding (mm)[f]					
Outside diameter	10.67	10.67	10.67	10.67	10.67
Thickness	0.508	0.508	0.508	0.508	0.508
Gas gap width (mm)[f]	0.076	0.076	0.076	0.076	0.076
Active UO_2 length (mm)[f]	194	194	194	194	194

TABLE C-VII (continued)

Parameter	Test				
	206	217	218	521	527
Rod type[b]	F-type PL	F-type PL	F-type PL	F-type PL	F-type PL
Average energy					
Deposition (cal/g UO_2):					
Total	223	257	283	300	300
At failure	--	--	--	246	240
Pellet surface energy					
Deposition (cal/cm^3 UO_2):					
Total	2554	2943	3241	3435	⁺3435
At failure	--	--	--	2805	2748
Reactor period (ms)	4.2	3.7	3.2	3.0	3.0
Peaking factor:					
Radial	1.136	1.136	1.136	1.136	1.136
Axial	--	--	--	--	--
Cladding temperature (°C):					
Maximum	--	--	--	--	--
At failure	--	--	--	--	--
Cladding radial expansion (%):					
Maximum	5.6	16.02	16.95	--	--
Average	--	--	--	--	--
Cladding elongation (%):					
Transient maximum	--	--	--	--	--
Residual	--	--	--	--	--
Fuel elongation, maximum (%)	--	--	--	--	--
Capsule pressure (MPa)	--	--	--	12.7	12.7
Nuclear-to-mechanical					
energy conversion (%)	--	--	--	0.17	0.25
Cladding surface oxidation[d]	1	2	0	1	0
Failure mode and extent[e]	No-B	No-B	Split-III	Split-III	Split-III
Fuel enrichment (%)[f]	4.8	4.8	4.8	4.8	4.8
Fuel density (g/cm^3)[f]	10.08	10.08	10.08	10.08	10.08
Fuel diameter (mm)[f]	10.67	10.67	10.67	10.67	10.67
Cladding (mm)[f]					
Outside diameter	11.83	11.83	11.83	11.83	11.83
Thickness	0.508	0.508	0.508	0.508	0.508
Gas gap width (mm)[f]	0.076	0.076	0.076	0.076	0.076
Active UO_2 length (mm)[f]	914	914	914	914	914

TABLE C-VII (continued)

Parameter	Test 538	546	540	544
Rod type[b]	SPXMB-PL	SPXMB-PL	SPXMB-PL	SPXMB-PL
Average energy Deposition (cal/g UO_2):				
Total	380	380	380	380
At failure	330	350	110	115
Pellet surface energy Deposition (cal/cm^3 UO_2):				
Total	4189	4189	4189	4189
At failure	3638	3858	1213	1268
Reactor period (ms)	3.0	3.0	3.0	3.0
Peaking factor:				
Radial	1.06	1.06	1.06	1.06
Axial	--	--	--	--
Cladding temperature (°C):				
Maximum	--	--	--	--
At failure	--	--	--	--
Cladding radial expansion (%):				
Maximum	--	--	--	--
Average	--	--	--	--
Cladding elongation (%):				
Transient maximum	0.58	0.26	0.30	0.44
Residual	--	--	--	--
Fuel elongation, maximum (%)	--	--	--	--
Capsule pressure (MPa)	9.02	11.7	3.53	2.26
Nuclear-to-mechanical energy conversion (%)	1.2	1.1	0.20	0.18
Cladding surface oxidation[d]	2	0	1	1
Failure mode and extent[e]	Split-III	Split-III	Split-III	Split-III
Fuel enrichment (%)[f]	5	5	5	5
Fuel density (g/cm^3)[f]	10.4	10.4	10.4	10.4
Fuel diameter (mm)[f]	5.59	5.59	5.59	5.59
Cladding (mm)[f]				
Outside diameter	6.35	6.35	6.35	6.35
Thickness	0.356	0.356	0.356	0.356
Gas gap width (mm)[f]	0.025	0.025	0.025	0.025
Active UO_2 length (mm)[f]	127	127	127	127

[a] Sequential tests, from Tests 194 through 201.

[b] PL = pellet fuel, PW = powder fuel.

[c] Diameter increases, at 90° apart.

[d] Cladding surface oxidation; 0 = no oxidation, 1 = partial oxidation, 2 = full oxidation.

[e] Failure mode; No = no failure, Crack = crack or split was formed but no disintegration of rod, Melt = failure by cladding melting, Split = cladding was split open, B = bowing observed.

Failure extent; I = broken while disassembling, II = broken into several large pieces, III = broken into fine fragments.

[f] Nominal value.

TABLE C-VIII

NSRR, UNIRRADIATED, ZIRCALOY CLAD, SINGLE ROD TEST DATA
(NSRR-STD rods)

Parameter	Test				
	200-1-1	200-2-1	200-3	111-3	200-4
Rod type[a]	NSRR-STD-PL	NSRR-STD-PL	NSRR-STD-PL	NSRR-STD-PL	NSRR-STD-PL
Average energy					
Deposition (cal/g UO_2):					
Total	39	116	176	189	233
At failure	--	--	--	--	--
Pellet surface energy					
Deposition (cal/cm^3 UO_2):					
Total	521	1546	2357	2433	3122
At failure	--	--	--	--	--
Reactor period (ms)	28.63	5.96	3.44	3.29	2.36
Peaking factor:					
Radial	1.29	1.29	1.29	1.29	1.29
Axial	1.03	1.03	1.03	1.03	1.03
Cladding temperature (°C):					
Maximum	134	153	1278	--	1680
At failure	--	--	--	--	--
Cladding radial expansion (%):					
Maximum	0	0	0.70	-0.09	2.28
Average	0	0	0.31	-0.06	2.05
Cladding elongation (%):					
Transient maximum	--	--	--	--	--
Residual	--	--	0.52	0.30	0.17
Fuel elongation, maximum (%)	--	--	--	--	--
Capsule pressure (MPa)	--	--	--	--	--
Nuclear-to-mechanical					
energy conversion (%)	--	--	--	--	--
Cladding surface oxidation[h]	--	--	1	2	2
Failure mode and extent[c]	No	No	No	No-B	No-B
Fuel enrichment (%)[d]	10	10	10	10	10
Fuel density (g/cm^3)[d]	10.41	10.41	10.41	10.41	10.41
Fuel diameter (mm)[d]	9.29	9.29	9.29	9.29	9.29
Cladding (mm)[d]					5
Outside diameter	10.72	10.72	10.72	10.72	10.72
Thickness	0.62	0.62	0.62	0.62	0.62
Gas gap width (mm)[d]	0.095	0.095	0.095	0.095	0.095
Active UO_2 length (mm)[d]	135	135	135	135	135

TABLE C-VIII (continued)

Parameter	Test				
	200-1-2	111-4	201-1	200-5	200-5b
Rod type[a]	NS-STD-PL	NS-STD-PL	NS-STD-PL	NS-STD-PL	NS-STD-PL
Average energy					
Deposition (cal/g UO₂):					
Total	241	244	244	264	267
At failure	--	--	--	--	--
Pellet surface energy					
Deposition (cal/cm³ UO₂):					
Total	3230	2706	3276	2412	3582
At failure	--	--	--	--	--
Reactor period (ms)	2.36	2.41	2.25	2.09	2.03
Peaking factor:					
Radial	1.29	1.29	1.29	1.29	1.29
Axial	1.03	1.03	1.03	1.03	1.03
Cladding temperature (°C):					
Maximum	1600	1690	1775	1825	> 1700
At failure	--	--	--	--	--
Cladding radial expansion (%):					
Maximum	3.54	1.21	4.75	1.07	3.26
Average	2.25	1.01	2.84	4.38	1.24
Cladding elongation (%):					
Transient maximum	--	--	--	--	--
Residual	0.37	0.49	0.37	0.44	0.15
Fuel elongation, maximum (%)	--	--	--	--	--
Capsule pressure (MPa)	--	--	--	--	--
Nuclear-to-mechanical					
energy conversion (%)	--	--	--	--	--
Cladding surface oxidation[b]	2	2	2	2	2
Failure mode and extent[c]	No-B	No-B	No-B	Crack-I	Crack
Fuel enrichment (%)[d]	10	10	10	10	10
Fuel density (g/cm³)[d]	10.41	10.41	10.41	10.41	10.41
Fuel diameter (mm)[d]	9.29	9.29	9.29	9.29	9.29
Cladding (mm)[d]					
Outside diameter	10.72	10.72	10.72	10.72	10.72
Thickness	0.62	0.62	0.62	0.62	0.62
Gas gap width (mm)[d]	0.095	0.095	0.095	0.095	0.095
Active UO₂ length (mm)[d]	135	135	135	135	135

TABLE C-VIII (continued)

Parameter	Test				
	111-5	200-2-2	200-6	200-6b	200-7
Rod type[a]	NS-STD-PL	NS-STD-PL	NS-STD-PL	NS-STD-PL	NS-STD-PL
Average energy					
Deposition (cal/g UO₂):					
Total	270	271	271	276	295
At failure	--	--	--	--	--
Pellet surface energy					
Deposition (cal/cm³ UO₂):					
Total	3629	3643	3643	3705	3965
At failure	--	--	--	--	--
Reactor period (ms)	1.91	2.00	2.00	1.95	1.83
Peaking factor:					
Radial	1.29	1.29	1.29	1.29	1.29
Axial	1.03	1.03	1.03	1.03	1.03
Cladding temperature (°C):					
Maximum	1750	> 1660	> 1780	> 1800	> 1800
At failure	--	--	--	--	--
Cladding radial expansion (%):					
Maximum	3.43	--	--	4.19	--
Average	1.48	--	--	1.86	--
Cladding elongation (%):					
Transient maximum	--	--	--	--	--
Residual	0.45	--	0.22	--	--
Fuel elongation, maximum (%)	--	--	--	--	--
Capsule pressure (MPa)	--	--	--	--	--
Nuclear-to-mechanical					
energy conversion (%)	--	--	--	--	--
Cladding surface oxidation[b]	2	2	2	2	2
Failure mode and extent[c]	Crack	Crack-I	Crack-I	Crack-I	Melt-II
Fuel enrichment (%)[d]	10	10	10	10	10
Fuel density (g/cm³)[d]	10.41	10.41	10.41	10.41	10.41
Fuel diameter (mm)[d]	9.29	9.29	9.29	9.29	9.29
Cladding (mm)[d]					
Outside diameter	10.72	10.72	10.72	10.72	10.72
Thickness	0.62	0.62	0.62	0.62	0.62
Gas gap width (mm)[d]	0.095	0.095	0.095	0.095	0.095
Active UO₂ length (mm)[d]	135	135	135	135	135

TABLE C-VIII (continued)

Parameter	Test				
	111-6	111-7	111-8	209-1-1[e]	209-1-2
Rod type[a]	NS-STD-PL	NS-STD-PL	NS-STD-PL	NS-STD-PL	NS-STD-PL
Average energy					
Deposition (cal/g UO_2):					
Total	333	376	433	177	179
At failure	--	--	--	--	--
Pellet surface energy					
Deposition (cal/cm^3 UO_2):					
Total	4470	5053	5817	2372	2403
At failure	--	--	--	--	--
Reactor period (ms)	1.61	1.43	1.32	1.38	1.38
Peaking factor:					
Radial	1.29	1.29	1.29	1.29	1.29
Axial	1.03	1.03	1.03	1.03	1.03
Cladding temperature (°C):					
Maximum	> 1720	> 1720	--	--	--
At failure	--	--	--	--	--
Cladding radial expansion (%):					
Maximum	--	--	--	--	--
Average	--	--	--	--	--
Cladding elongation (%):					
Transient maximum	--	--	--	--	--
Residual	--	--	--	--	--
Fuel elongation, maximum (%)	--	--	--	--	--
Capsule pressure (MPa)	--	--	--	--	--
Nuclear-to-mechanical energy conversion (%)	--	--	--	--	--
Cladding surface oxidation[b]	--	--	--	--	--
Failure mode and extent[c]	Melt-II	Melt-III	Melt-III	--	--
Fuel enrichment (%)[d]	10	10	10	10	10
Fuel density (g/cm^3)[d]	10.41	10.41	10.41	10.41	10.41
Fuel diameter (mm)[d]	9.29	9.29	9.29	9.29	9.29
Cladding (mm)[d]					
Outside diameter	10.72	10.72	10.72	10.72	10.72
Thickness	0.62	0.62	0.62	0.62	0.62
Gas gap width (mm)[d]	0.095	0.095	0.095	0.095	0.095
Active UO_2 length (mm)[d]	135	135	135	135	135

TABLE C-VIII (continued)

Parameter	Test 209-1-3	Test 209-1-4	Test 209-1-5
Rod type[a]	NS-STD-PL	NS-STD-PL	NS-STD-PL
Average energy Deposition (cal/g UO_2):			
Total	179	180	183
At failure	--	--	--
Pellet surface energy Deposition [cal/cm³ UO_2]:			
Total	2403	2419	2450
At failure	--	--	--
Reactor period (ms)	3.38	3.38	3.38
Peaking factor:			
Radial	1.29	1.29	1.29
Axial	1.03	1.03	1.03
Cladding temperature (°C):			
Maximum	1080	1060	1160
At failure	--	--	--
Cladding radial expansion (%):			
Maximum	--	--	6.15[f]
Average	--	--	2.07[f]
Cladding elongation (%):			
Transient maximum	--	--	--
Residual	--	--	0.70[f]
Fuel elongation, maximum (%)	--	--	--
Capsule pressure (MPa)			
Nuclear-to-mechanical energy conversion (%)	--	--	--
Cladding surface oxidation[b]	--	--	2
Failure mode and extent[c]	--	--	No-B
Fuel enrichment (%)[d]	10	10	10
Fuel density (g/cm³)[d]	10.41	10.41	10.41
Fuel diameter (mm)[d]	9.29	9.29	9.29
Cladding (mm)[d]			
Outside diameter	10.72	10.72	10.72
Thickness	0.62	0.62	0.62
Gas gap width (mm)[d]	0.095	0.095	0.095
Active UO_2 length (mm)[d]	135	135	135

[a] PL = pellet fuel, PW = powder fuel.

[b] Cladding surface oxidation; 0 = no oxidation, 1 = partial oxidation, 2 = fuel oxidation.

[c] Failure mode: No = no failure, Crack = crack or split was formed but no disintegration of rod, Melt = failure by cladding melting, Split = cladding was split open, B = bowing observed.

Failure extent; I = broken while disassembling, II = broken into several large pieces, III = broken into fine fragments.

[d] Nominal value.

[e] Sequential tests, from Tests 209-1-1 through 209-1-5.

[f] Cumulative in the five tests.

TABLE C-IX

NSRR, UNIRRADIATED, ZIRCALOY CLAD, SINGLE ROD TEST DATA
(NSRR-WG and JPDR-II rods)

Parameter	Test					
	232-1	232-2	232-3	232-4	232-6	232-5
Rod type[a]	NSWG-PL	NSWG-PL	NSWG-PL	NSWG-PL	NSWG-PL	NSWG-PL
Average energy						
Deposition (cal/g UO_2):						
Total	181	236	261	274	294	326
At failure	--	--	--	--	--	--
Pellet surface energy						
Deposition (cal/cm^3 UO_2):						
Total	2416	3144	3478	3646	3919	4345
At failure	--	--	--	--	--	--
Reactor period (ms)	3.46	2.50	2.22	2.00	1.83	1.68
Peaking factor:						
Radial	1.28	1.28	1.28	1.28	1.28	1.28
Axial	1.03	1.03	1.03	1.03	1.03	1.03
Cladding temperature (°C):						
Maximum	136	1750	1870	1750	--	--
At failure	--	--	--	--	--	--
Cladding radial expansion (%):						
Maximum	0	0.28	1.16	2.29	9.14	--
Average	0	0.03	0.92	1.49	5.64	--
Cladding elongation (%):						
Transient maximum	--	--	--	--	--	--
Residual	0	0.52	0.59	0.81	--	--
Fuel elongation, maximum (%)	--	--	--	--	--	--
Capsule pressure (MPa)	--	--	--	--	--	--
Nuclear-to-mechanical						
energy conversion (%)	--	--	--	--	--	--
Cladding surface oxidation[b]	0	2	2	2	2	2
Failure mode and extent[c]	No	No-B	No-B	No-B	No-B	Melt-II
Fuel enrichment (%)[d]	10	10	10	10	10	10
Fuel density (g/cm^3)[d]	10.41	10.41	10.41	10.41	10.41	10.41
Fuel diameter (mm)[d]	9.09	9.09	9.09	9.09	9.09	9.09
Cladding (mm)[d]						
Outside diameter	10.72	10.72	10.72	10.72	10.72	10.72
Thickness	0.62	0.62	0.62	0.62	0.62	0.62
Gas gap width (mm)[d]	0.195	0.195	0.195	0.195	0.195	0.195
Active UO_2 length (mm)[d]	135	135	135	135	135	135

TABLE C-IX (continued)

Parameter	Test 111-1	Test 111-2	Test 111-9	Test 111-10
Rod type[a]	JPDR-II PL	JPDR-II PL	JPDR-II PL	JPDR-II PL
Average energy				
Deposition (cal/g UO_2):				
Total	44	112	158	204
At failure	--	--	--	--
Pellet surface energy				
Deposition (cal/cm^3 UO_2):				
Total	495	1260	1780	2350
At failure	--	--	--	--
Reactor period (ms)	9.14	2.29	1.59	1.23
Peaking factor:				
Radial	1.08	1.08	1.08	1.08
Axial	1.03	1.03	1.03	1.03
Cladding temperature (°C):				
Maximum	90	140	--	1290
At failure	--	--	--	--
Cladding radial expansion (%):				
Maximum	-0.08	0.024	2.37	2.05
Average	-0.04	0.13	2.01	1.80
Cladding elongation (%):				
Transient maximum	--	--	--	--
Residual	0.07	0.07	0.44	0.26
Fuel elongation, maximum (%)	--	--	--	--
Capsule pressure (MPa)	--	--	--	--
Nuclear-to-mechanical				
energy conversion (%)	--	--	--	--
Cladding surface oxidation[b]	0	0	2	2
Failure mode and extent[c]	No	No	No-B	No
Fuel enrichment (%)[d]	2.6	2.6	2.6	2.6
Fuel density (g/cm^3)[d]	10.41	10.41	10.41	10.41
Fuel diameter (mm)[d]	10.66	10.66	10.66	10.66
Cladding (mm)[d]				
Outside diameter	12.33	12.33	12.33	12.33
Thickness	0.70	0.70	0.70	0.70
Gas gap width (mm)[d]	0.085	0.085	0.085	0.085
Active UO_2 length (mm)[d]	126	126	126	126

[a] PL = pellet fuel, PW = powder fuel.

[b] Cladding surface oxidation; 0 = no oxidation, 1 = partial oxidation, 2 = full oxidation.

[c] Failure mode; No = no failure, Crack = crack or split was formed but no disintegration of rod, Melt = failure by cladding melting, Split = cladding was split open, B = bowing observed.

    Failure extent; I = broken while disassembling, II = broken into several large pieces. III = broken into fine fragments.

[d] Nominal value.

TABLE C-X

NSRR, UNIRRADIATED, ZIRCALOY CLAD, WATERLOGGED TEST DATA
(JPDR-II rods)

Parameter	Test				
	401-1	401-2	401-3	401-3b	402-1
Rod type[a]	JPDR-II FW	JPDR-II FW	JPDR-II FW	JPDR-II FW	JPDR-II FW
Average energy					
Deposition (cal/g UO_2):					
Total	53	106	154	150	47
At failure	--	--	101	130	--
Pellet surface energy					
Deposition (cal/cm^3 UO_2):					
Total	594	1200	1744	1694	531
At failure	--	--	1136	1462	--
Reactor period (ms)	5.24	2.32	1.56	1.53	5.58
Peaking factor:					
Radial	1.08	1.08	1.08	1.08	1.08
Axial	1.03	1.03	1.03	1.03	1.03
Cladding temperature (°C):					
Maximum	180	270	170	310	240
At failure	--	--	120	305	0
Cladding radial expansion (%):					
Maximum	0.16	0.57	--	--	0.06
Average	0	0.41	--	--	0.03
Cladding elongation (%):					
Transient maximum	--	--	--	--	--
Residual	0.05	-0.20	-0.03	-0.37	-0.07
Fuel elongation, maximum (%)	--	--	--	--	--
Capsule Pressure (MPa)	0.49	0.98	5.39	5.49	0.78
Nuclear-to-mechanical					
energy conversion (%)	0	0	0.015	0.013	0
Cladding surface oxidation[b]	0	0	0	0	0
Failure mode and extent[c]	No	No	Split-III	Split-III	No
Fuel enrichment (%)[d]	2.6	2.6	2.6	2.6	2.6
Fuel density (g/cm^3)[d]	10.41	10.41	10.41	10.41	10.41
Fuel diameter (mm)[d]	10.66	10.66	10.66	10.66	10.66
Cladding (mm)[d]					
Ourside diameter	12.33	1.233	12.33	12.33	12.33
Thickness	0.70	0.70	0.70	0.70	0.70
Gas gap width (mm)[d]	0.085	0.085	0.085	0.085	0.085
Active UO_2 length (mm)[d]	126	126	126	126	126

TABLE C-X (continued)

Parameter	Test			
	402-2	402-2	411-3	421-3
Rod type[a]	JPDR-II PW	JPDR-II PW	JPDR-II[e] PW	JPDR-II[e] PW
Average energy				
Deposition (cal/g UO_2):				
Total	104	154	152	152
At failure	--	--	112	--
Pellet surface energy				
Deposition (cal/cm^3 UO_2):				
Total	1175	1744	1720	1720
At failure	--	--	--	--
Reactor period (ms)	2.27	1.53	1.53	1.53
Peaking factor:				
Radial	1.08	1.08	1.08	1.08
Axial	1.03	1.03	1.03	1.03
Cladding temperature (°C):				
Maximum	540	560	481	325
At failure	--	--	215	--
Cladding radial expansion (%):				
Maximum	237	2.21	--	2.13
Average	1.28	1.72	--	0.44
Cladding elongation (%):				
Transient maximum	--	--	--	--
Residual	-0.15	-0.41	-0.31	-0.15
Fuel elongation, maximum (%)	--	--	--	--
Capsule pressure (MPa)	1.47	--	6.37	0.32
Nuclear-to-mechanical				
energy conversion (%)	0	0	0.046	0
Cladding surface oxidation[b]	1	1	--	--
Failure mode and extent[c]	No	No-B	Split-III	No-B
Fuel enrichment (%)[d]	2.6	2.6	2.6	2.6
Fuel density (g/cm^3)[d]	10.41	10.41	10.41	10.41
Fuel diameter (mm)[d]	10.66	10.66	10.66	10.66
Cladding (mm)[d]				
Outside diameter	12.23	12.23	12.23	12.23
Thickness	0.70	0.70	0.70	0.70
Gas gap width (mm)[d]	0.085	0.085	0.085	0.085
Active UO_2 length (mm)[d]	126	126	126	126

[a] FW = fully waterlogged, PW = partially waterlogged.

[b] Cladding surface oxidation: 0 = no oxidation, 1 = partial oxidation, 2 = full oxidation.

[c] Failure mode: No = no failure, Crack = crack or split was formed but no distintegration of rod, Melt = failure by cladding melting, Split = cladding was split open, B = bowing observed.

  Failure extent: I = broken while disassembling, II = broken into several large pieces, III = broken into fine fragments.

[d] Nominal value.

REFERENCE

C-1. M. Ishikawa and K. Tomii (ed.), *Quarterly Progress Report on the NSRR Experiments (4); Combined, January – June 1977*, JAERI-M 7304 (August 1977).

DISTRIBUTION RECORD FOR NUREG/CR-0269 (TREE-1237)

Internal Distribution

1 - Chicago Patent Group - DOE
    9800 South Cass
    Argonne, IL 60439

2 - R. L. Blackledge
    Idaho Operations Office - DOE
    Idaho Falls, ID 83401

3 - R. J. Beers, ID

4 - P. E. Litteneker, ID

5 - R. E. Tiller, ID

6 - H. P. Pearson
    Information Management, EG&G

7-16 - INEL Technical Library

17-36 - Authors

37-117 - Special Internal

External Distribution

118-119 - Saul Levine, Director
          Office of Nuclear Regulatory Research, NRC
          Washington, D.C. 20555

120-121 - Special External

122-502 - Distribution under R3, Water Reactor Safety Research -
          Fuel Behavior